RHODES UNIVERSITY
Where leaders learn

Petrographic and geochemical characterisation of the hangingwall and the footwall rocks (the Dipeta and R.A.T. stratigraphic units) to the Kinsevere and Nambulwa copper ore deposits of the Lufilian Arc, southern Democratic Republic of Congo.

By

Robert Kankomba Nkulu

A thesis submitted in fulfilment of the requirements for the degree of
MASTER OF SCIENCE
(Exploration Geology Coursework and Thesis)

Supervisor: Professor Dr. Stephen A. Prevec
MSc Exploration Geology Program in 2016
Geology Department
Rhodes University
P.O. Box 94
Grahamstown 6140
South Africa

October 2018

Declaration

I, Robert Kankomba, declare that this thesis is my own work and any authors have been acknowledged accordingly. It is being submitted in fulfilment of the Degree of Master of Science in Exploration Geology at Rhodes University, Grahamstown, and has not been submitted before for the examination of any degree through any other tertiary institution or university.

Signature of the candidate

Mr. Robert Kankomba

Signed on the 10th day of March 2019.

Dedication

I would want to take a great privilege to dedicate this work to my wife Mireille Banze Kankomba, my children Davina Kankomba, Dan Kankomba and Darnel Kankomba for their infallible support and encouragement during my study on the MSc Exploration Geology course program at Rhodes University.

Acknowledgements

This scientific study was made possible by the great encouragement and support of MMG Kinsevere Ltd Company and the gracious authorization of the DRC exploration Manager Mr. Dan Olberg without its implication no study would be possible. In the same way, I would like to acknowledge the Africa Exploration Manager Mr. James McMaster and the head of Geology Mr. Steve Ryan for their humble approbation of this MSc study project.

I would also like to address my special thanks to the principal geologist Toby Dawborn and Senior geochemist Takalani M. for their important contribution to this output, their stimulating discussions, encouragement and their availability despite the multiple preoccupations.

To Professor Steve Prevec, my supervisor, I would like to express my deep gratitude for your guidance, advice, remarks and suggestions, professional mentoring and comments. Your constructive criticism has greatly improved the quality of this dissertation.

I would also like to thank the following people for their support towards the successful achievement of this thesis:

Mrs. Ashley Goddard for her administrative and logistical supports during the period of our study at Rhodes University. She was ready to help whenever I needed help.

The entire academic staff of the Geology Department, MSc program at Rhodes University for their high quality and standard of lectures during the whole coursework program;

All my colleagues of MMG Kinsevere Exploration Geologists: – Mr. Levi Wani, Mr. Prosper Mwamba, Mr Alain Mukulu, Mr Herve Ilongo, Mr Girma and Mr Joel Kurita for the encouragements and geoscientific exchange;

My lovely wife Mireille Banze Kankomba for her affection, great encouragement and deep prayers and keeping me under the god spirit during my academic activities;

My children Davina Kankomba, Dan Kankomba and Darnel Kankomba for your precious affection, may this work become a good stimulus for your further activities study? I thank you for your support and appreciate your sacrifices;

My family in particular my father Joseph Kankomba and my mother Alim Kayumba for their education and gave me the key of instruction. Thanks for all.

Abstract

The Kinsevere and Nambulwa copper deposits in the Democratic Republic of Congo (D.R.C.) are set in the eastern side of the Neoproterozoic Katanga Supergroup, forming the Lufilian Arc, resulting from a cratonic collision between the Congo and the Kalahari Cratons (ca.620-570_Ma). The Katanga Supergroup was deposited in an extensional rift setting with a sedimentary thickness succession ranging between 7 to 10 km, sub-divided into: – the Roan, the Nguba and the Kundelungu Groups. The stratigraphic column of the Roan Group consists of the R.A.T. (Roche Argilo Talqueuse), the Mines, the Dipeta and the Mwashya Subgroups.

Three major deformation phases have been described characterised by complex multiphase tectonics related to a curved superposition of folded, thrust and sheared blocks. The rocks of the R.A.T., Mines and Dipeta Subgroups are recognised as blocks that occur within a stratiform to discordant and diapiritic megabreccia. The blocks were rafted upward with salt tectonics, resulting in the juxtaposition with the hangingwall and the footwall terranes. Therefore, in that context it has been found that the Dipeta may appear overlying the R.A.T. Subgroup through the unconformity decollement surface of heterogeneous breccia.

The petrographic observations made of the R.A.T. and Dipeta samples indicates in both units the presence of detrital quartz and feldspar that have been altered and replaced by sericite and muscovite minerals. Gypsum is intimately associated with magnesite, showing an evaporitic environment domain, while magnesite is common as alteration phase both in the R.A.T. and Dipeta Subgroups. Pyrophyllite has been observed in the Dipeta, resulting from reaction of silica with the Kaolinite at low temperature. Accessory detrital minerals include zircon, as well as xenotime intergrown with altered Fe-Ti-oxide hematite, forming complex textures with disseminated Ti-oxides both in R.A.T. and Dipeta units.

Major and trace element geochemistry indicates that the Dipeta is more dolomitic and magnesite while the R.A.T. is clay-rich. The Ti_2O value of Dipeta and R.A.T samples is relatively low, ranging between 0.36 and 0.69 wt.% respectively, which suggest highly evolved felsic material in the protolith. This is consistent with interpretation based on the Al_2O_3/TiO_2 ratio, which ranges between 18 and 23 for the R.A.T. and Dipeta respectively, indicating an intermediate to felsic granitoids as the protolith of R.A.T. and Dipeta siltstones.

The Ti/Zr ratio of R.A.T. and Dipeta samples of less than 10, while, the higher La/Sc ratio of between 2.6 and 5.5 (for the R.A.T. and Dipeta respectively) indicate that both the R.A.T. and Dipeta are active continental and passive margin tectonic setting.

Based on the geochemical variation with depth across the R.A.T. and Dipeta and their contact zone, a geochemical fingerprinting suggests that the ratio TiO_2/Al_2O_3 appears to be useful and could be considered as a stratigraphic geochemical maker able to discriminate the R.A.T. and the Dipeta Subgroups during the geological mapping.

Table of Contents

List of figures

List of Tables

Chapter 1: General Introduction

1.1 Introduction

The Neoproterozoic Katangan sedimentary rock succession, located in Zambia and Democratic Republic of Congo (D.R.C.), hosts the rich copper-cobalt ore mineralisation of the Central African Copper Belt (C.A.C.B.), which constitutes the most economically important Pan-African belt in the continent (Cailteux et al., 2007).

The Central African Copper Belt forms a northward convex structure, straddling the Congo-Zambia border called the "Lufilian Arc" made during the Lufilian orogeny (ca.620-570 Ma). It extends over a 700 km long and 50 km wide region from the Mwinilunga district in north western Zambia (Steven, 2000), east-north-eastwards through Kolwezi and Likasi (D.R.C.), and south-eastwards to Itawa (Zambia) (Figure 1).

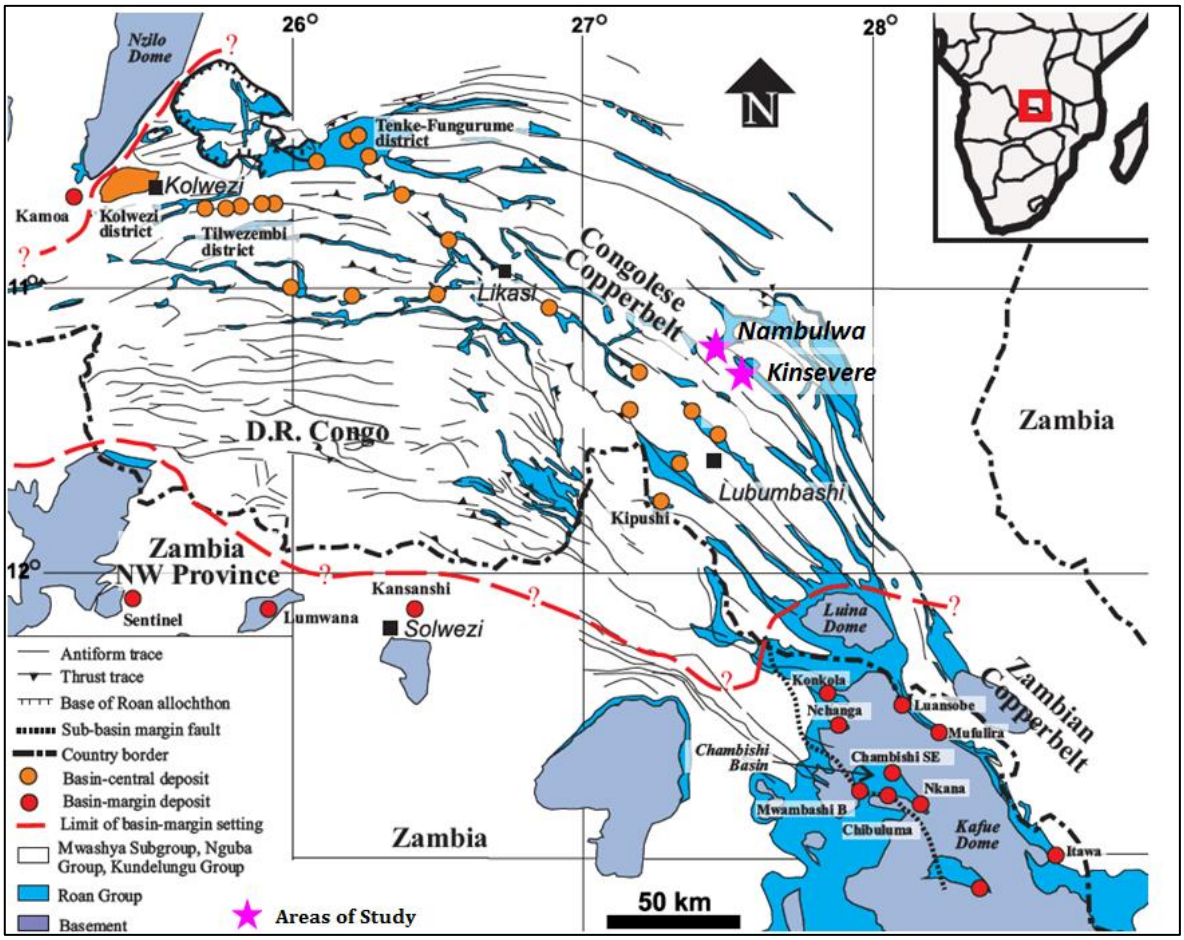

Figure 1: Map of the Central African Copperbelt with location of the main ore deposits including the Kinsevere and Nambulwa (modified after Francois, 1974; Cailteux, 1994; and Broughton, 2014).

Approximately half of the world's cobalt reserves are found in the Central African Copper Belt (Jackson et al., 2003) which offers a good opportunity for exploration within that area. The mineralization style of the central African Copper Belt is classically understood to be both sedimentary stratabound and vein-hosted, with varieties of copper, cobalt, lead, zinc and uranium mineralisation present (Kampunzu and Cailteux, 1999). Several geologists recognized significant post-folding ore remobilization (Haest and Muchez, 2011), either as due to supergene weathering enrichment (De Putter et al., 2010) or formed as disseminated and vein-hosted coarse-grained sulphides (Brems et al., 2009).

The tectonic evolution and metallogenesis are relatively well known, especially for the Neoproterozoic to early Paleozoic Katangan sedimentary sequences that have been folded, thrusted and faulted during the Lufilian orogeny (François, 1973, Kampunzu and Cailteux, 1999; Jackson et al., 2003). The Lufilian Arc is a result of the interaction between the Kalahari and the Congo-Tanzania cratons related to an event of the Pan-African amalgamation of Gondwana (Porada and Behorst, 2000). Three orogenic phases, D1 to D3, have been described by Kampunzu and Cailteux (1999).

The Neoproterozoic Katangan R.A.T. (Roches Argilo Talqueuse) Subgroup is a sedimentary sequence characterised by deposition of massive to irregularly laminated silty dolomitic units located at the base of the Katanga Supergroup (Cailteux, et al., 2005) (Figure 6). Thrusting of tectonic nappes derived from the Lufilian orogeny led to the decollement of R.A.T. Subgroup from its pre-Katangan basement (Francois 1973, Cailteux, 1994), facilitated by the presence of evaporite units underneath the R.A.T. Despite, the tectonic complexity resulting from the three phases of deformation, the relationship, between the R.A.T. Subgroup and other overlying units, especially those hosting ore such as the Mines Subgroup, are thoroughly documented (Cailteux, 1994), while the contact with the Dipeta stratigraphic units remains debatable. The macroscopic facies of the R.A.T. and Dipeta Subgroups are similar as each sequence units are characterised predominantly as comprising argillaceous and siliclastic beds with a dolomitic matrix (Cailteux, 1994).

Therefore, macroscopic identification of both stratigraphic unit succession during the mapping or core description is still confusing and questionable as blocks of R.A.T., Mines and Dipeta Subgroup have been rafted upwards accompanied by evaporitic salts, resulting in their juxtaposition with younger stratigraphic units (Broughton, 2014). It appears that, the geological map established in the Kinsevere and/or Nambulwa areas may be imperfect due to the mix up of the two distinct stratigraphic units being misrepresented as one main unit (R.A.T.) and as such the situation needs to be redefined. Consequently, the structural interpretation model has become incoherent and this has the potential to impact negatively on the mineral exploration program. The rare occurrences of stratigraphic markers facilitate the distinction of these two units locally, such as the presence of a mafic unit in the Dipeta intersected in the drill hole KHLSS274 and the heterogeneous breccia as a footwall of the R.A.T. unit described in the Kinsevere drill hole SM59016. However, it appears that those markers are not sufficiently persistent to serve as regional index markers.

1.2 Lufilian Arc

The Lufilian Arc is located in Central Africa between the Congo and Kalahari Cratons. It belongs to the late Neoproterozoic to early Cambrian Panafrican orogenic belts including the Mozambique, Lurio, Zambezi, Damara and West-Congo belts (Frimmel et al., 2006) which are a result of the amalgamation of Gondwana of three Pan-African lithospheric plates (East-, West and South-Gondwana). The Katangan rocks were deposited within a series of intracratonic extensional basin associated with the breakup of Rhodinia (Urung, 1988; Kampunzu et al., 2000; Hitzman et al., 2012). The rifting may have started at 880 Ma by separating the Congo-Tanzania and the Angola-Kalahari blocks, (Padora and Berhorst, 2000), leading to the formation of a passive continental margin on the southern side of the Congo craton (Figure 2). The initial rift-stage of the basin includes the basal Roan Group forms by a clastic and evaporitic carbonate rocks while the second rifting stage includes the clastic rocks, mafic igneous flows and sills. The Nguba and Kundelungu Groups dominated with siliclastic sedimentary rocks (Francois 1973; Selley 2005; Cailteux et al., 2005). The Lufilian Arc, together with the Zambezi and Damara belts resulted from a cratonic collision between the Congo and Kalahari cratons 650-600 Ma to 530 Ma (Frimmel et al., 2011). The

Katangan rocks were variably metamorphosed and deformed during 590 to 500 Ma Pan-African Lufilian orogeny (Hitzman, 2012).

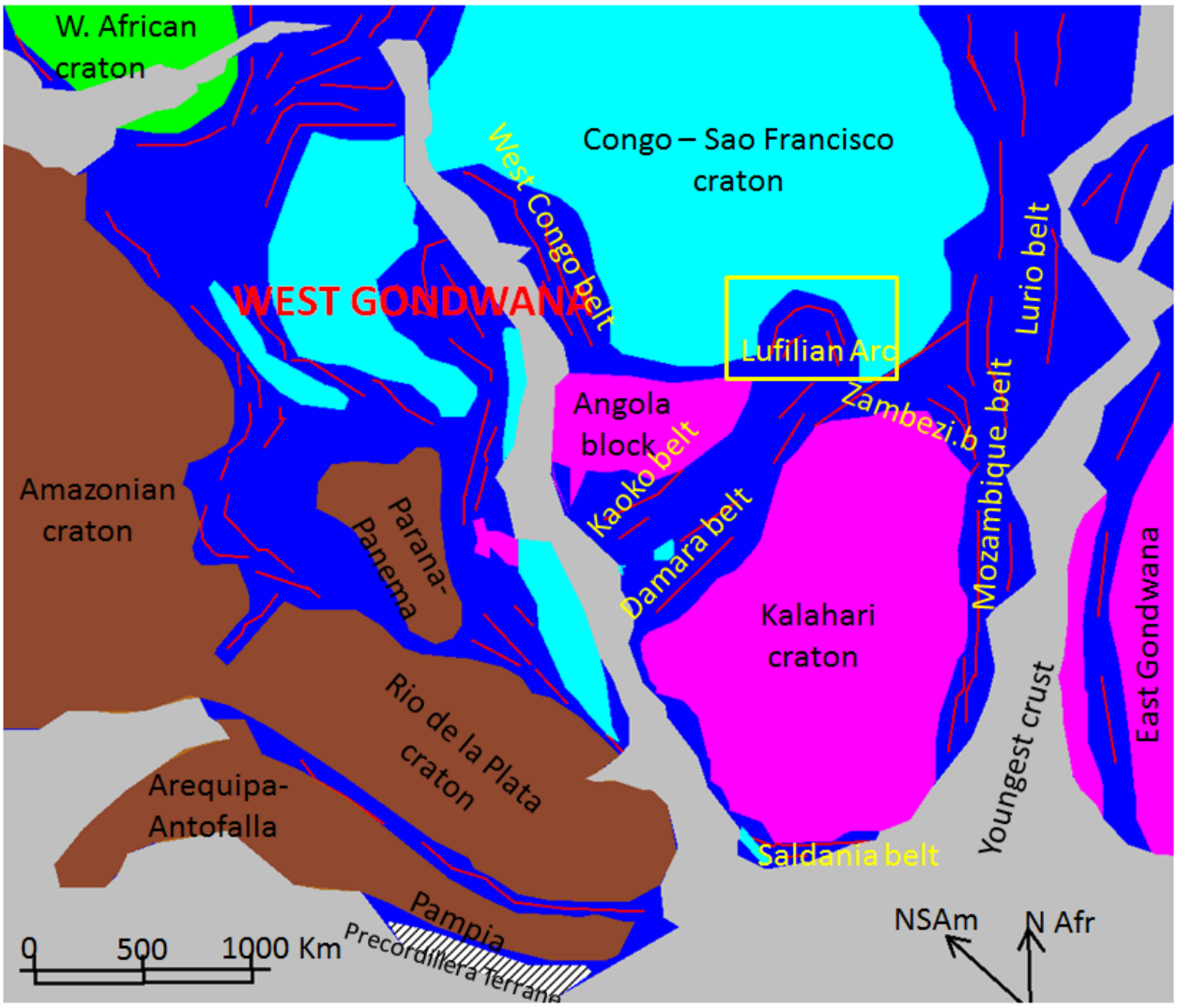

Figure 2: The Neoproterozoic Lufilian Arc and various cratons of south west Gondwana Modified after Frimmel et al., (2001); Kroner et al., (2004) and Kipata, (2013).

The Lufilian Arc has been subdivided into three structural domains (Figure 3): The outer Lufilian fold-and-thrust belt, the middle Lufilian Domes region and the inner Lufilian synclinorial belt (Daly et al., 1984). The inner Lufilian is exposed exclusively within Zambia, while the middle Lufilian is located in the D.R.C. along the Congo-Zambia border, and the outer Lufilian is entirely developed in the D.R.C.

The external Lufilian consists dominantly of Katangan sedimentary rocks and presents a folded structure with complex macro-scale fragmentation and recurrent thrust sheets (Selley

et al., 2005). It is delimited to the south and south-east by old crystalline complexes of the Domes region in Zambia and Democratic Republic of Congo (D.R.C.).

The Lufilian foreland extends northeast of the Lufilian Arc, up to Lake Tanganyika. It is mainly represented by the broadly tabular Kundelungu plateau. The foreland has a triangular shape pointing towards the north-east and is delimited by the Mesoproterozoic Kibara Belt (1.3 – 1.0 Ga) on the north western side and the Archean to Paleoproterozoic Bangweulu Block (2.05 – 1.8 Ga) on the eastern side (Kampunzu and Cailteux, 1999). The Lufilian foreland is considered by Kampunzu and Cailteux (1999) to be a molassic continental depression that received dominantly clastic sediments during the formation of the Lufilian Arc (Figure 3).

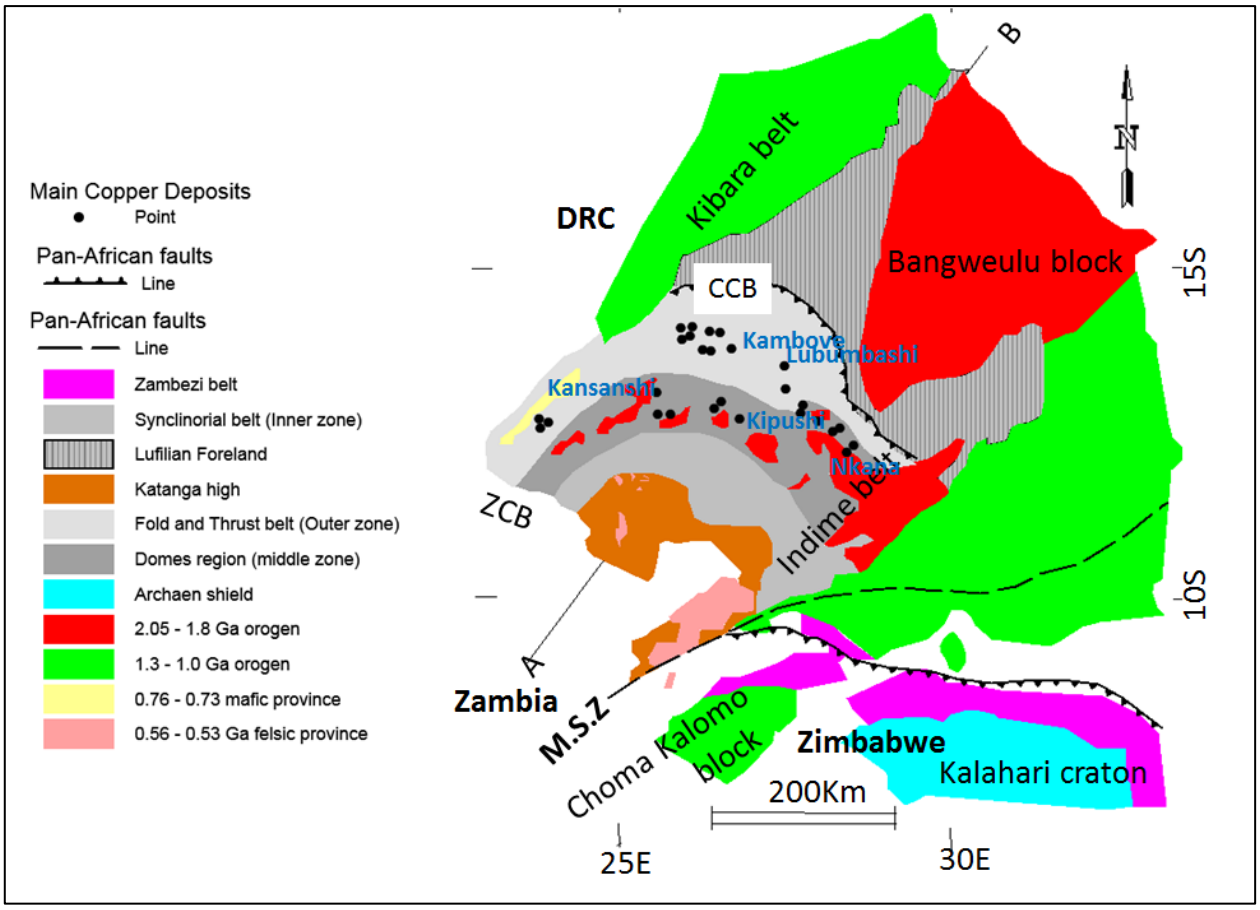

Figure 3: Figure: Map of the Pan-African Lufilian Arc showing the Archean, the Zambezi belt, pre- to syn-orogenic magmatic-volcanic rocks and the main deposits in the Zambian (**ZCB**) and Congolese Copper Belt (**CCB) in the** Katanga Copperbelt as well the pan-African faults. Modified after Kampunzu and Cailteux (1999), Selley et al. (2005), El Desouky (2009) and Kipata (2013).

The cross-section WSW (A) – ENE (B) through the Lufilian Arc (Figure 3) illustrates the different structural domains including the inner zone composed by the high Katanga to the

south and the synclinorium belt, the middle zone containing the domes region and the outer zone comprising the fold and thrust belt (Figure 4).

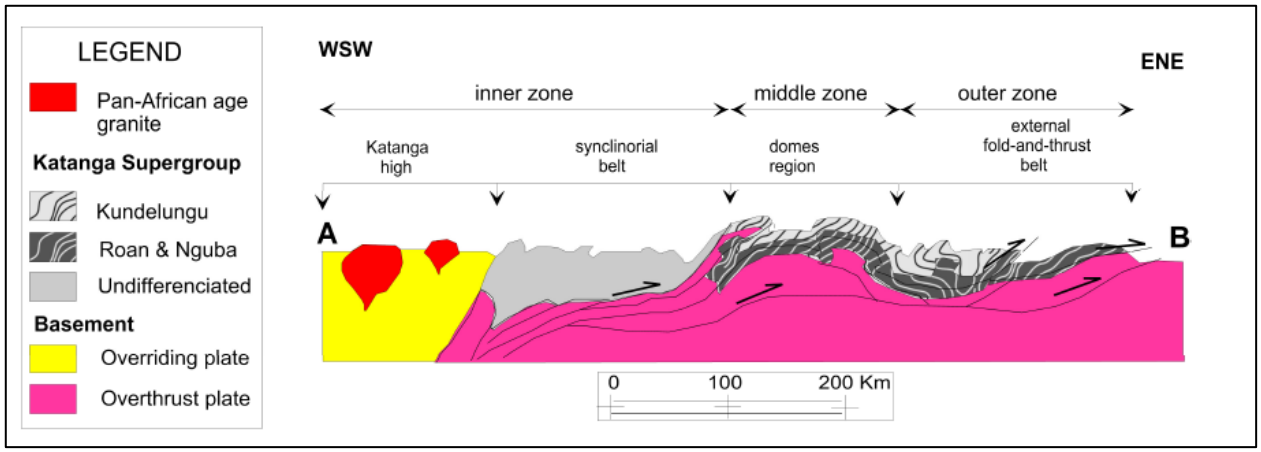

Figure 4: Schematic cross-section showing the different structural domain of the Lufilian Arc. Modified after Porada (1989) and Selley et al., (2005).

1.3 Location of area study

The Kinsevere and Nambulwa copper deposits are located in the Kipushi territory of the Haut Katanga Province within the southern part of the Democratic Republic of Congo (D.R.C.) at 11°20′ South latitude and 27°34′ East longitude. These deposits consist respectively of the exploitation permit PE528 allocated to Kinsevere and PE539 attributed to Nambulwa both held by MMG Kinsevere Company. The Kinsevere and Nambulwa deposits are situated respectively at 27 km and 55 km north of Lubumbashi town setting in 50 radius of the MMG Kinsevere exploration region which is set up from the central point of the Kinsevere open pit (Figure 5). The Kinsevere deposit can be reached from Lubumbashi town by the MMG private road extended to the north approximately 25 km with the mine property which developing the copper hosted in Mines Subgroup unit.

Geologically, the Kinsevere and Nambulwa copper deposits are set in the southeast part of the Lufilian Arc along the SE – NW trending structure lineament. This structure links the domes region of Zambia up to the Tenke Fungurume district through the Kimpe and Kambove southern lineament (Figure 1).

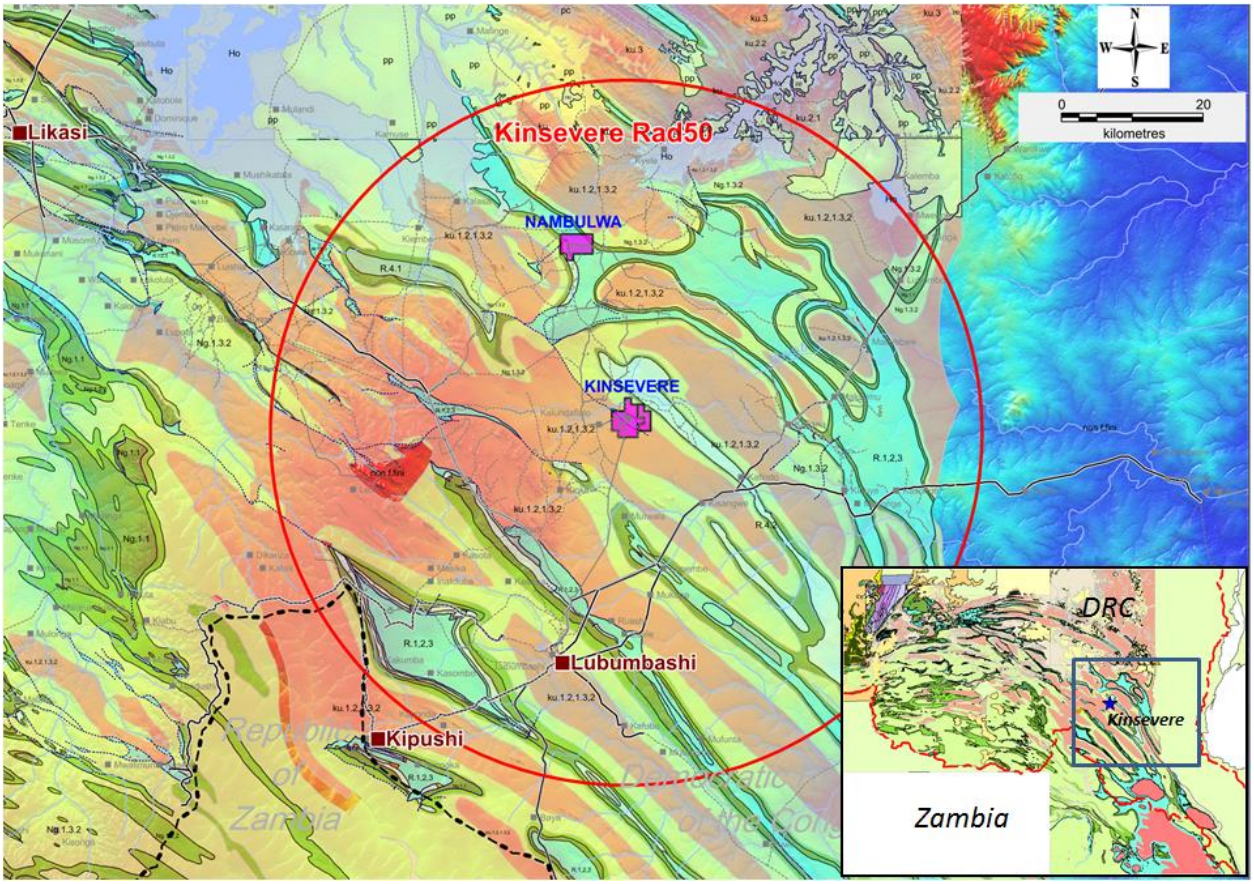

Figure 5: Map displaying the Kinsevere and Nambulwa within the southern side of the Lufilian Arc and the Kinsevere radius 50 setting on the regional geology over the topographic image in the exploration area (MMG Ltd map, 2017).

1.4 Aims

The aim of the research is to derive quantitative geochemical fingerprints for the R.A.T. and Dipeta Subgroup units using the petrographic features as a guide. As the lithologies of the R.A.T. and Dipeta are very similar and remain a subject of debate, the outcome of the geochemical characteristics from the petrographic study will contribute to refine the existing geological map of the area and will promote new thinking of the structural geology as well as the geological model of the deposit. Consequently, new guidance for the exploration of stratiform Cu-Co deposits may be led by the results.

The fold and thrust salt tectonics facilitated the decollement of R.A.T. Subgroup from its pre-Katangan basement by overprinting Mines Subgroup fragments associated with Dipeta blocks within the silty matrix which makes controversial the discrimination of stratigraphic units.

This study, conducted through evaluation of samples from the Kinsevere and Nambulwa copper deposits, has been designed to correlate the petrographic characteristics with geochemical signatures which may facilitate the distinction of the R.A.T. and the Dipeta stratigraphic units. Therefore, the results of the work will try to define a way of better understanding the local tectonic related to the area of study and elsewhere within the fold and thrust domain.

Chapter 2: Geological setting

2.1 General stratigraphy

Three main geological depositional basins are recognized in the Congolese Copper Belt (C.C.B.) by -Cahen *et al.,* (1954, 1967) from the bottom to top, as follows:

1. The Pre-Kibaran, called the Ubendian group (±2000 Ma), affected by the pre-Kibaran orogeny (1850±20Ma).
2. The Kibaran (> 1320 Ma), affected by the Kibaran orogeny (1320±40 Ma), and
3. The Katangan (>650 Ma to 600 Ma) which resulted from the Lufilian orogeny (600 ±20Ma).

2.2 Ubedian Supergroup

Studies done by Ngoie (1992) described the pre-Kibaran outcrops in Zambia and around the Luina and Mokambo domes, both located to the south of Katangan province within the Congolese Copper Belt. The author described the Ubendian Supergroup as a metamorphic gneissic granite complex.

2.3 Kibaran Supergroup

The Mesoproterozoic Kibaran belt is preserved as a northeast-trending zone of metamorphic and magmatic orogenic belt over 1300 km long extending across the Congo Craton. It outcrops from the Angola-Zambia-DRC border triple junction in the SW of Katanga, through Rwanda and Burundi, up to southwest Uganda and northwest Tanzania in the northeast (Tack et al., 2010). According Cahen et al., (1967), the Kibaran consists of a set of thick (10,000 m) metamorphosed quartzitic, siliclastic and pelitic sediments, intruded by granite and associated rocks with mineralised pegmatites hosting (Sn-Ta-W) ores.

2.4 Katanga Supergroup

The Neoproterozoic Katanga Supergroup forms a large part of the Lufilian Arc and its Kundelungu foreland. It stratigraphically overlies the Ubendian crystalline basement and Mesosoproterozoic Kibaran series (François, 1973; Cailteux et al., 2005; Cailteux and Misi,

2007). The Katanga Supergroup is limited by the Archaean to Paleoproterozoic Bangweulu block and the Paleoproterozoic Ubendian belt to the northeast and the Mesoproterozoic Irumide belt to the southeast and the Kibaran belt to the northwest (Figure 3). The Katanga Supergroup was deposited in an extensional (rift) context with a thickness of 7 to 10 km sedimentary succession (Kampunzu and Cailteux, 1999) and commonly sub-divided into three major lithostratigraphic units (François, 1995): The Roan, the Nguba Group, which incudes at its base a regional glaciogenic marker "Grand Conglomerat" and the Kundelungu Group which is also commences with a glaciogenic unit '' Petit Conglomerat'' (François, 1995; Cailteux et al., 2007, Hitzman, 2012) (Figure 6).

2.4.1 Roan Group

The Roan Group is formed of siliclastic sedimentary rocks and carbonates (mainly dolomites and dolomitic shales fluviatile and lacustrine sediments (Cailteux et al., 1994, 2005, Batumike et al., 2006), and volcanic and plutonic mafic rocks emplaced in a continental rift (Kampunzu et al., 2000). The Roan Group, including a basal conglomerate, rests unconformably on the pre-Katangan basement.

The stratigraphy column of the Roan Group is subdivided into 4 Subgroups from base to top: – the R.A.T. (Roches Argilo-Talqueuses), the Mines, the Dipeta and the Mwashya Subgroups (Cailteux, 1994). Two major transgressive regressive cycles are recognized in the sedimentary succession of the Roan Group (Cailteux, 1994). Each cycle started with continental to sub-continental depositional (R.A.T. and Dipeta Subgroups) and terminated by carbonated platform-type sediments (Mines and Mwashya Subgroups) (Cailteux, 1994).
The R.A.T. (Roches Argilo Talqueuses) Subgroup is made of sandy-argillaceous oxidized dolomitic rocks that are generally coarse to fine-grained at the bottom and consists of hematite-rich siliciclastic formations in the form of both authigenic plates and red pigment attesting to the primary oxidation conditions of the deposit. It grades to more dolomitic at the top and abundant talc (Cailteux, 1994; Cailteux et al., 2005b).
The base of the Mines Subgroup is made of alternating dolomite and dolomitic organic rich shales and/or siltstones. It represents a change from oxidizing to reducing conditions. This

stratigraphic unit is carrying the bulk of the stratiform copper-cobalt mineralisation. The dolomites of the Mines Subgroup are related to platform-type carbonate deposition in intertidal and lagoonal environments in reducing conditions (Cailteux et al., 2005). The Dipeta Subgroup is characterised by predominantly argillaceous and siliciclastic beds at the base and by mostly carbonate (François, 1987; Cailteux, 1994) and volcaniclastic beds at the top of the sequence (Cailteux et al., 2007). The Mwashya Subgroup consists of sedimentary sequences composed of an argillaceous-detrital succession of carbonaceous shales, siltstones and sandstones deposited over a basal conglomeratic unit (Cailteux et al., 2007). It is commonly divided into the predominantly dolomitic Lower Mwashya code (R-4.1) and the predominantly pelitic Upper Mwashya code (R-4.2) Formations, but there is no well-documented regional lithostratigraphic description of the transition and boundary between these two formations (François, 1974).

2.4.2 Nguba and Kundelungu Groups

The two diamictites that made a division of the Katanga Supergroup into three groups are called the ''Grand Conglomerat'' and the ''Petit Conglomerat'', which are located at the bases of the Nguba and Kundelungu Groups, respectively (Figure 6). These diamictites were correlated with the two worldwide Neoproterozoic glacial episodes, the Marinoan glaciation (660 Ma) and the Sturtian glaciation (715 Ma) respectively documented in detail by various workers (e.g., Young, 1995) and Cailteux (2018). The Nguba and Kundelungu Groups are mainly constituted of clastic sedimentary rocks with a main marker carbonate unit occurs in the Nguba Group called the Kakontwe Limestone (Figure 6). They consist of a thick carbonate and siliciclastic sedimentary band deposited in a broad basin, related to a major phase of extensional tectonics and normal faulting that mark the transition from rifting to a Red Sea type proto-ocean (Cailteux et al., 2007). Deposition of the Nguba Group ended with siliciclastic rocks and subordinate carbonates of the Bunkeya Subgroup code (Ng-2) (Batumike et al., 2007). The Kundelungu Group was deposited during the latest Neoproterozoic up to the early Paleozoic. It is commonly subdivided into the Gombela code (Ku-1), Ngule (Ku-2) and Biano code (Ku-3) Subgroups (Batumike et al., 2007).

Supergroup	Age	Group	Subgroup	Formation	Members and Lithologies
Katanga	±500 Ma	Kundelungu	Biano (Ku-3)		Arkose, conglomerates, argillaceous sandstones
			Ngule (Ku-2)	Sampwe Ku_2.3	Dolomitic pelite, argillaceous to sandy siltstone.
				Kiubo Ku-2.2	Dolomitic sandstones, siltstones and pelites
				Mongwe Ku-2.1	Dolomitic pelites, siltstones and sandstones
			Gombela (Ku-1)	Lubudi Ku-1.4	Alternanting pink oolitic limestone (calcaire de Lubudi) and sandy carbonate beds
	±620 Ma			Kanianga Ku-1.3	Carbonate siltstone and shales
				Lusele Ku-1.2	Pink to grey micritic dolomite (calcaire rose)
				Kyandamu Ku-1.1	Petit conglomerat tillite/diamictite
	750 Ma	Nguba	Bunkeya (Ng-2)	Monwezi Ng-2.1	Dolomitic sandstone, siltstone and pelites
				Katete Ng-2	Dolomitic sandstones or siltstone in the northern facies alternating shale and dolomite beds (series reccurente in the sourthern facies
			Muombe (Ng-1)	Kipushi Ng-1.4	Dolomite with dolomitic shales beds
				Kakontwe Ng-1.3	carbonate
				Kaponda Ng-1.2	Carbonate shale and siltstone, “dolomie tigré at the base
				Mwale Ng-1.1	Grand conglomerat tillite/diamictite
		Roan	Mwashya (R-4)	Kanzadi R-4.3	Sandstone alternating siltstone and shale
				Kafubu R-4.2	Black shale
				Kamoya R-4.2	Dolomitic shale, siltstone, sandstone conglomeratic beds and cherts in variable position
			Dipeta (R-3)	Kansunki R-3.4	Dolomite including vocaniclastics beds
				Mofya R-3.3	Dolomite, arenitic dolomites dolomitc siltstone
				R-3.2	Argillaceous to dolomitic siltstone with interbedded feldspathic sandstone or white dolomites, intrusive gabbro
				RGS R-3.1	Argillaceous dolomitic siltstone (‘’Roche greo-Schisteuses””)
			Mines (R-2)	Kambove R-2.3	Stromatolitic, laminated shaly or talcose or talcose dolomite, locally sandstones at base beds of siltstones at top.
				Shales Dolomitiques R-2.2	Dolomitique Shales including three carbonaceous horizons occasional dolomites
				Kamoto R-2.1	Stromatolitic dolomite (R.S.C.) silicified /arenitic dolomites (R.S.F./D.strat),grey argillaceous dolomitic siltstone
			Musonoi (R-1)	RAT R-1	Red argillaceous dolomitic siltstones and sandstones (“Roches Argillo-Talqueses”)
	Base of the R.A.T. sequence unknown				
	<900 Ma				Basal conglomerate

Figure 6 (previous page): The Katanga Supergroup Lithostratigraphy (modified after Cailteux et al 2007, Batumike 2007).

2.5 Tectonic setting

The Lufilian Arc comprises a succession of folded, faulted and thrusted belts. It is characterized by complex multiphase tectonics with superposed curved folds, thrusted terranes and shear zones, forming a northward convex structure (Kipata, 2013). The dominant structures observed are NE-verging folds, thrust sheets and left-lateral strike-slip faults. In a recent study based on a synthesis of observations and geological surveys carried out by several generations of geologists such as Kampunzu and Cailteux (1999) proposed the following revision of major events of the Lufilian orogeny and consist of the Kolwezian, Monwezian and Shilatembo events.

2.5.1 Kolwezian events (D1)

The Kolwezian event corresponds to a major deformation marked by folding and thrusting of Katangan terranes with a northwards transport direction. Folds associated with this deformation are inclined towards the north (Francois, 1993) (Figure 7). The axial cores planes of anticlines are generally faulted, and the anticlines are occupied by Roan megabreccia corresponding to fragments of Mines Subgroup named locally "ecailles" or Dipeta blocks which are located at several thousand meters beneath the Kundelungu and Nguba of the Katangan sediments sheets (Kipata, 2013). Evaporite-bearing beds facilitated the movement and piling of Katangan tectonic terranes with the formation of megabreccia composed of Roan fragments as large as 1 - 2 km (Cailteux and Kampunzu, 1999). The Kolwezian phase took place between 850 Ma and 690 Ma (François, 1973; Kampunzu and Cailteux, 1999).

2.5.2 Monwezian events (D2)

The second deformation called the Monwezian event corresponds to regional strike slip faulting which affected the folded and thrusted terranes by E-W sinistral faulting in the western part of the belt (Kipata, 2013) (Figure 7). Underlying fragments from the Lower Roan are injected through these faults and some deposits of uranium are associated with the fault, such as the Shinkolobwe ore deposit (Jackson, et al., 2003). The bending of the arc is

interpreted by Kampunzu and Cailteux (1999) as related to strike-slip tectonics of phase D2 due to the action of an indentor as in the India-Asia collision (Kipata, 2013). The event took place between 690 and 540 Ma (François, 1973; Kampunzu and Cailteux, 1999, Batumike et al., 2007).

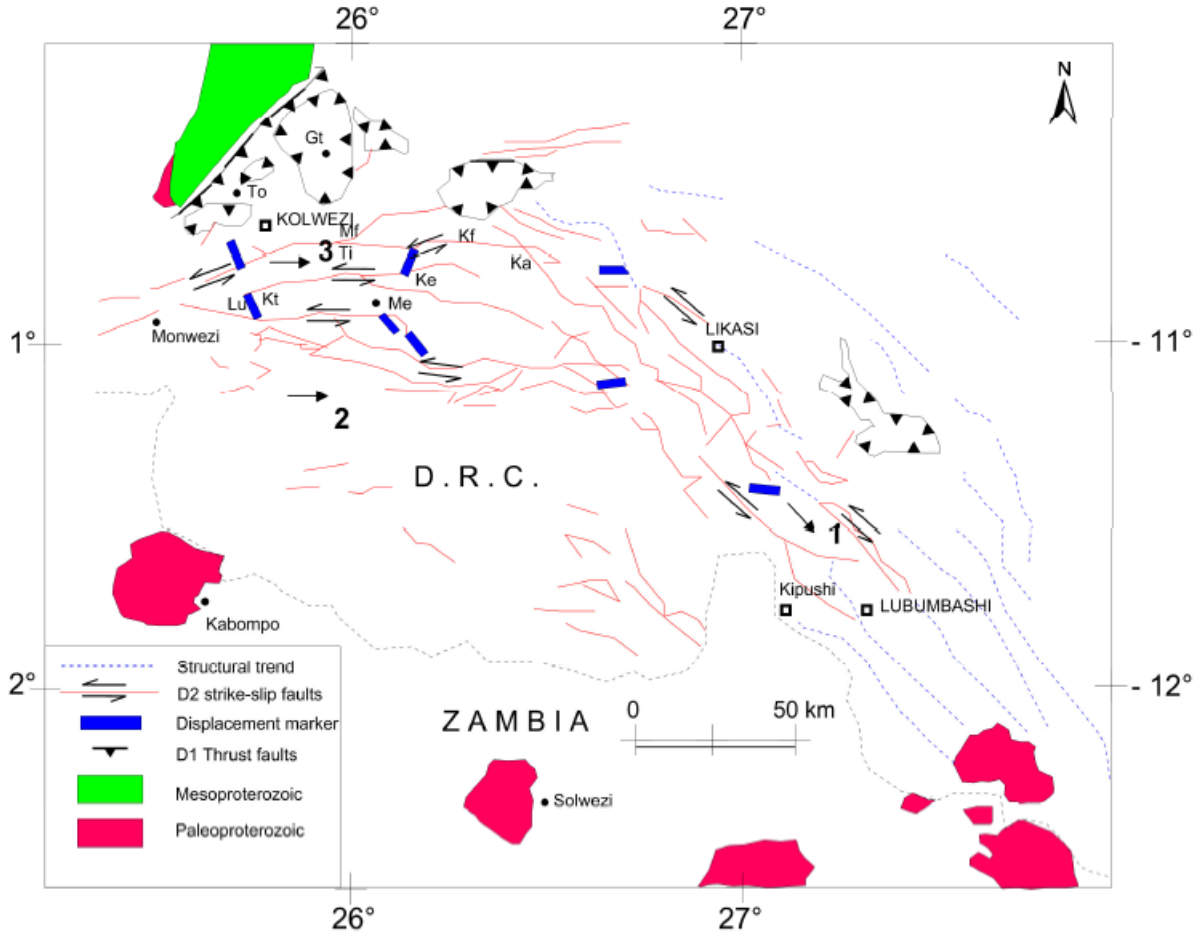

Figure 7: Map displaying the major deformational features that occurred during the Kolwezian (D1) and Monwezian events (D2) which affected the Katangan belt (Kipata, 2013).

2.5.3 Shilatembo event (D3)

The Chilatembo event is a late transverse fold event, younger than 540 Ma and probably dating from the early Palaeozoic. The phase is considered as responsible for transversal NE-SW trending open upright fold and conjugated N160 -170 and N70 – 80E trending folds in the eastern part of the Katangan belt, suggesting a NW – SE compression (Kampunzu and Cailteux, 1999). Similarly, several undulations of the D2 faults with horizontal throw were caused by D3 folding (Figure 8).

The Synclinorial Belt is characterised by late transverse folding, trending northeast-southwest and east-west as large open, upright folds (Kampunzu and Cailteux, 1999). D3 deformation (Shilatembo) is poorly documented but has been identified in the Etoile, Luiswishi and Luishia areas (Kampunzu and Cailteux, 1999). D3 deformation overprints the D2 deformation event with gentle undulating folds (Kampunzu and Cailteux, 1999). This late D3 deformation phase is known as the Shilatembo phase (Kipata et al., 2013).

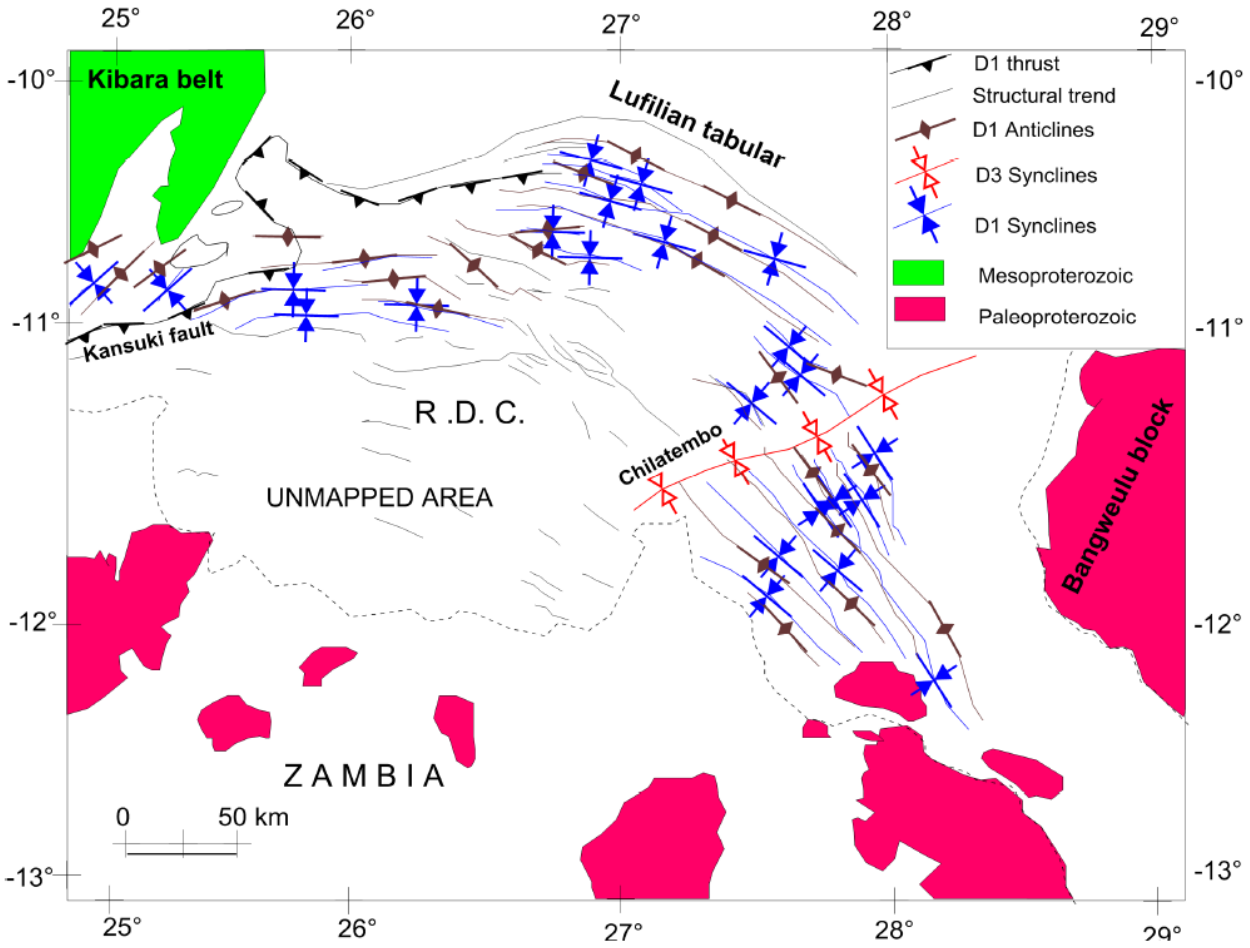

Figure 8: Map showing the major deformational features that occurred during Shilatembo events (D3) affecting the Lufilian arc belt (Kipata, 2013).

2.6 Katangan salt tectonic and Megabreccia structures

The rocks of the R.A.T., Mines and Dipeta Subgroups in the Katanga Supergroup are recognised as blocks (fragments) that occur as discordant and diapiritic megabreccia within a gravel to silty talcose, dolomitic, quartz and magnesian rich chloritic matrix (Hitzman, 2012, Cailteux, 2018). The size of fragment within megabreccia is very variable and can be measured from meters to several kilometres in length (Cailteux and Kampunzu, 1999). It appears that the large fragments commonly occur on the edges of megabreccia but may

also be present as float within it (Broughton, 2014) (Figure 9). An alternative hypothesis proposed that the megabreccias represent coarse clastic syn-orogenic sedimentary deposits supplied by north advancing nappes into a foreland basin (Wendorff, 2011). The megabreccia may also include blocks of the Nguba and Kundelungu Group rocks. According to Kampunzu and Cailteux (1999), the megabreccias are interpreted to derive from the mobilisation of the Roan Group evaporites, including gypsum, anhydrite and halite (Cailteux and Kampunzu 1999). The Sabkha facies, as well as the presence of gypsum and anhydrite crystals or pseudomorphs, overprinted the existence of the former Roan evaporates, associated with stratigraphic gaps underlying collapse breccia and chloride inclusions plus some saline springs (Jackson et al., 2003).

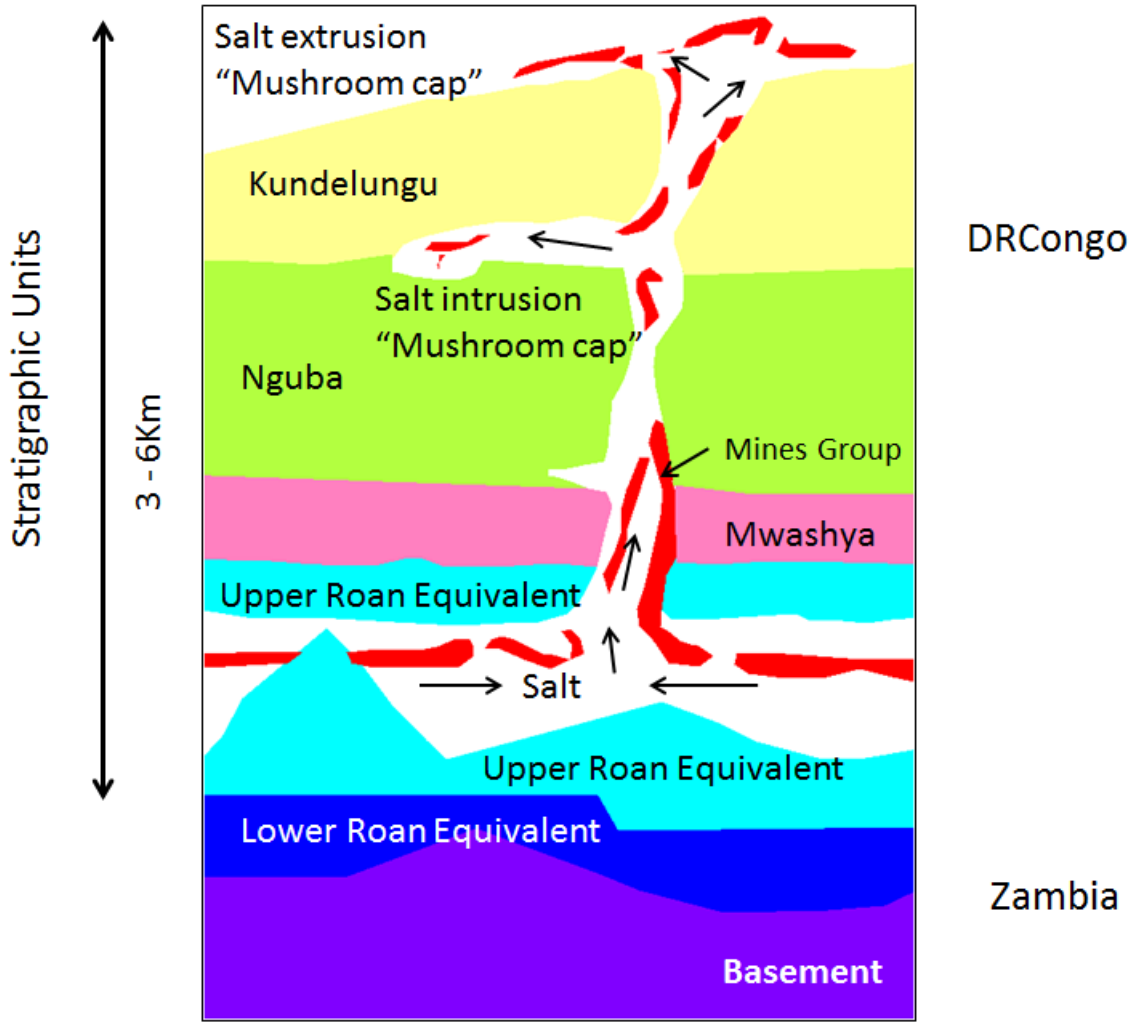

Figure 9: Model for the formation of the diapiric breccias and megabrecccias in the Central African Copperbelt (modified after Broughton, 2014).

In the main Katangan basin of the Congoleese Copperbelt, which hosts a thick evaporite level, blocks of R.A.T., Mines and Dipeta Subgroups were rafted upward with salt resulting in

the juxtaposition with younger stratigraphic units. In that context we observe that the Dipeta may appear to overlie the R.A.T. formation through the unconformity decollement surface of heterogeneous breccia.

Jackson et al. (2003) mentioned that the rapid deposition of the Grand Conglomerat (tillite) stratigraphy may have provided the necessary loading to initiate halokinesis. The megabreccia containing Mines and Dipeta Subgroup fragments was emplaced on a specific stratigraphic Kundelungu Group level. Therefore, salt movement occurred up during the deposition of the upper Kundelungu Group (Jackson et al., 2003).

2.7 Ore Mineralisation

The Central African Copper Belt (C.A.C.B.) is contained the largest sedimentary stratabound-hosted copper and cobalt deposits in the world (Kirkham, 1989). The Zambian deposits contain measured production and reserves in excess of 90 million tonnes copper (Kirkham, 1989), while combined production and reserve in the Democratic Republic of Congo (DRC) contains over 180 million tonnes of copper in three large deposits (Kolwezi, Tenke Fungurume and Kamoa) (Figure 1) and a number of smaller deposits (Broughton, 2014).

The various mineral occurrences in the Katanga Copperbelt can be classified into three distinct types: −the stratiform, the supergene enrichment and the vein-types. The stratiform ore mineralisation forms the largest group of deposits and are mainly found in Lower Roan (Mines Subgroup) rocks, which can be identified as ridges on satellite imagery (De Waele et al., 2006). These occur as Cu oxide and Cu-Fe sulphides in shales, siltstone, argillites or carbonate rocks (Kirkham, 1989) (Figure 10). The main phase of the stratiform mineralisation in the Katanga Copperbelt happened during diagenesis, preceding the Lufilian orogeny. After the formation of early diagenetic pyrite, the circulation of diagenetic Cu–Co-rich fluids resulted in the formation of the main mineralisation (De Waele et al., 2006). Essentially, syngenetic framboidal pyrite occurs in both in Zambia and Congolese deposits but is not associated with ore deposits (Hitzman, 2012). Sulfides in the Central African Copperbelt deposits have complex textural relationships that suggest various stage ore formation (Selley et al., 2005). Analysis of fluid inclusions indicates that H_2O–NaCl fluid with a minimum

temperature between 80° and 195°C and salinity between 8.4 and 18.4 eq. wt% NaCl circulated during the main phase of mineralisation (De Waele, 2006). The fluid constitutes a complex of high salinity and low H_2S with about 100 ppm content copper derived from volcanic rocks, such as mafic rocks leached during weathering or diagenesis (Brown, 1993).

In addition, deposits display different mineralisation styles and textures, such that the sulphides occur as veins or disseminations or both and as fine or coarse grains. Vertical and lateral zonation of copper minerals from chalcocite – bornite – chalcopyrite has also been noted (Hitzman et al., 2010).

Late diagenetic mineralisation is recorded by prefolding, bedding parallel sulfides-bearing veins, texturally and compositionally comparable disseminated Cu-Co sulfides, and evidence of sulfide precipitation due to interaction between the ore fluids and migrated hydrocarbons (Selley et al., 2005). Therefore, veins within the Katangan Supergroup could have been formed by fluid overpressure during the early diagenesis event (Hitzman et al., 2012). Supergene mineral occurrences are considered to be the result of late enrichment by mobilization of fluid along faults and fractures resulting in the formation of secondary Cu-oxides, carbonates and silicates, consisting of cuprite, malachite and chrysocolla respectively (De Waele, et al., 2006).

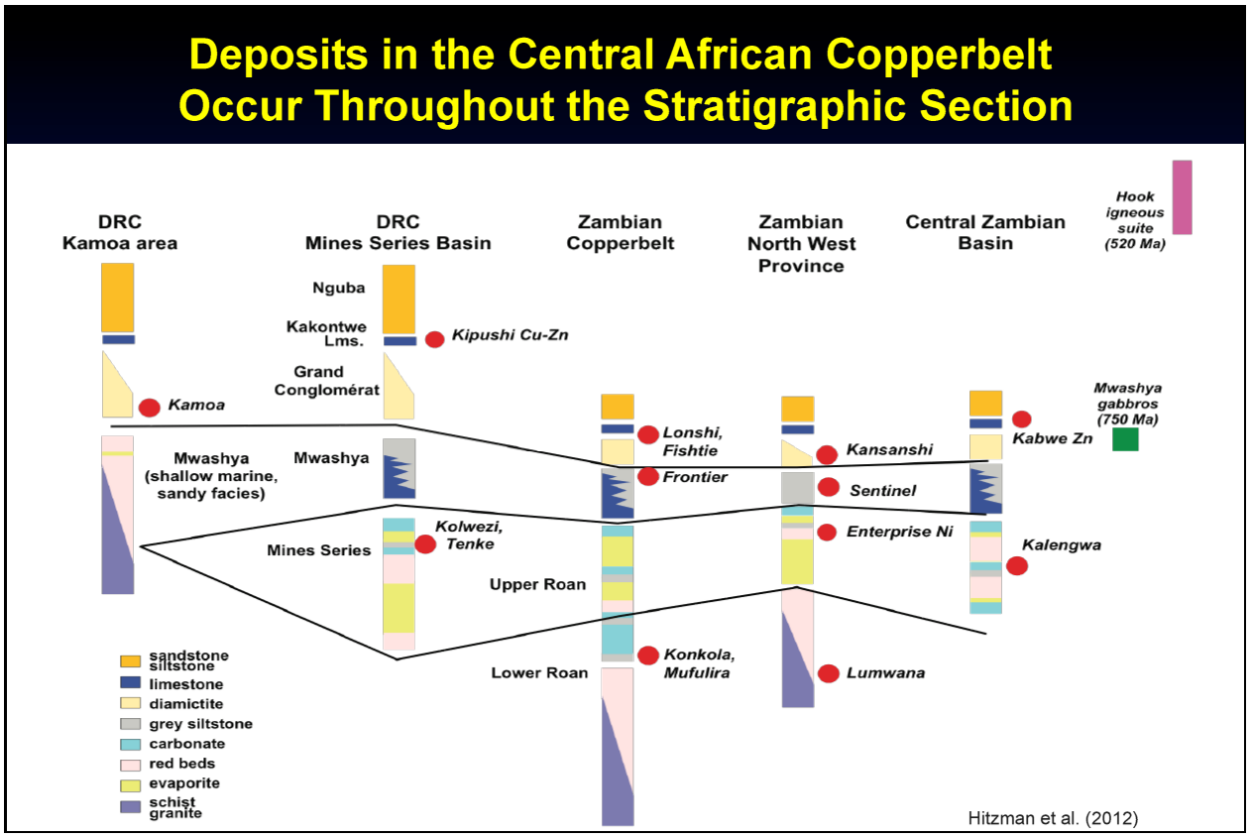

Figure 10: Stratigraphic section showing main type of deposits that occur in the Central African Copperbelt (Hitzman et al., 2012).

2.8 Local geology

The Kinsevere and Nambulwa deposits are set within the same structural salt tectonic domain characterised by an injection of the Roan Group, which consists of fragments of Mines and Dipeta Subgroups floating in the very fine-grained siltstone matrix. The Kinsevere deposit comprises the southern extension fault NW-SE strike derived from the main Nambulwa Roan diapir. The geology of the two deposits presents the same lithostratigraphic sequence, characterised by a similar sedimentary succession of siltstone, shale and dolomite, with the exception of the presence of the stromatolitic dolomite named R.S.C. (Roche Siliceuse Cellulaire) in Nambulwa. Hence, the focus here will be on the Kinsevere deposit, to be used as the representative geological setting for the area.

The Kinsevere deposit is subdivided into the Kinsevere Central, the Mashi, located to the north west of the Central deposit, and the Kinsevere hill, situated to the south east. The outcrops in the vicinity of the Kinsevere deposit are limited as the topography is almost flat, being covered by the thicker red soil and only evident as Mines Group outcrops showing at the Kinsevere pit. Therefore, the detailed geological map is based mainly on rocks observed in the open pit and from the different drill holes. The map for the area is characterised by dolomite, siltstone and intercalated breccia of Mines Subgroup affected by N-E trending faults associated by an intrusion of dolerite (Figure 11). An E-W- striking cross-section exhibits a block of Mines Subgroup separated by a decollement surface of a heterogeneous breccia (Figure 12).

Two main stratigraphic groups as well as breccia layers are recognised in the Kinsevere area:

1. The Kundelungu Neoproterozoic Group, consists of dolomites, sandstones, siltstones and shales, including the "Petit Conglomerat", and forms the Kalule Subgroup, currently re-named the Gombela Subgroup (Batumike et al., 2007). Those rocks surround the Kinsevere deposit and can be observed to the east, south-east, south and west of the Kinsevere mine. They are characterised as the Kundelungu 1.2

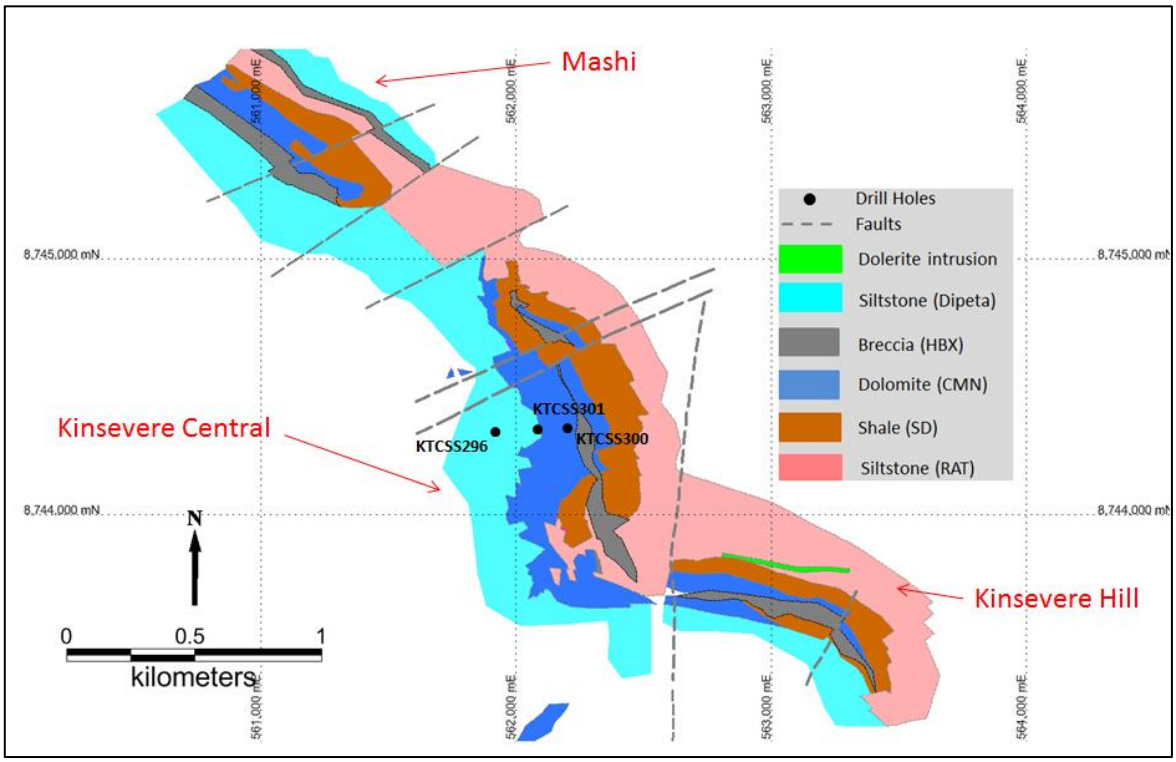

Figure 11: Detailed Kinsevere geologic map, displaying the different locations of the Kinsevere Central, Mashi and Kinsevere hill regions (MMG Ltd map, 2017).

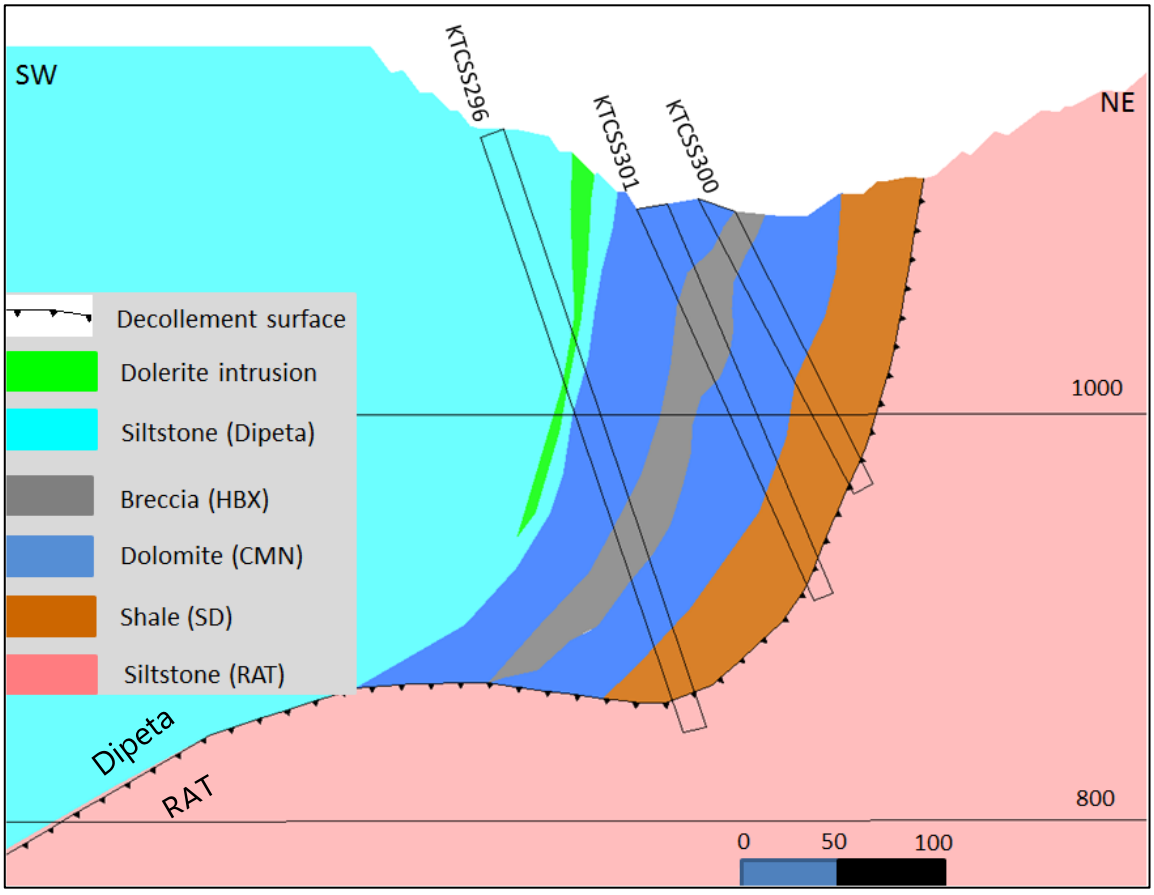

Figure 12: Cross section through diamond drill holes in Kinsevere Central reveals the decollement surface separating the overlying Dipeta from the underlying R.A.T. Subgroup (MMG Ltd map, 2017).

(stratigraphy name code Ku-1.2) rocks, which consist of alternating purplish and grey fine-grained sandstone and dolomite.

2. The Neoproterozoic Lower Roan Group formations in Kinsevere, consisting of the siliciclastic and dolomite/shale of Mines Group fragment rocks. They host Cu-Co mineralisation. Its relevant footwall is made by R.A.T. Subgroup which will be examined in more detail below.
3. Breccias: The heterogeneous decollement breccia often occurs between the Mines Group fragment and the R.A.T. or the Dipeta stratigraphic units. It was developed during the salt tectonics. Various lithologically nature of clasts have been recognised, comprising, centimetre-scale rounded and sub-rounded clasts in the silty carbonate matrix.

The detailed local stratigraphy recognised within the Roan Group in the Kinsevere deposit from the bottom to top observed in the pits and intersected in the drill holes are described in detail below:

2.8.1 RAT Subgroup

The R.A.T. (''Roches Argilo-Talqueuses'') Subgroup is a sedimentary sequence composed of red to pinkish, massive to irregularly bedded, terrigenous-dolomitic rocks, occurring at the base of the Katangan succession. In the Kinsevere deposit, the R.A.T. Subgroup can be subdivided into two units: – the pinkish lilac R.A.T. and the undifferentiated R.A.T. The pinkish lilac R.A.T.coded R.1.3 consists of 15-20m thick layer of massive, hematitic, chloritic–dolomitic siltstones, with infill intervals of sandstone with pervasive talc impregnation and manganese oxide along fractures, becoming slightly laminated towards the top (Kazadi, 2012). This layer is overlain by 15-18m of a pinkish-red bedded to massive siltstone with hematite staining along bedding planes and manganese oxides in fractures. Traces of sub-economic veinlets of copper mineralisation have been observed in the R.A.T. Both layers types contain coarsely crystalline specularite, quartz carbonate and spotted evaporite (Figure 13).

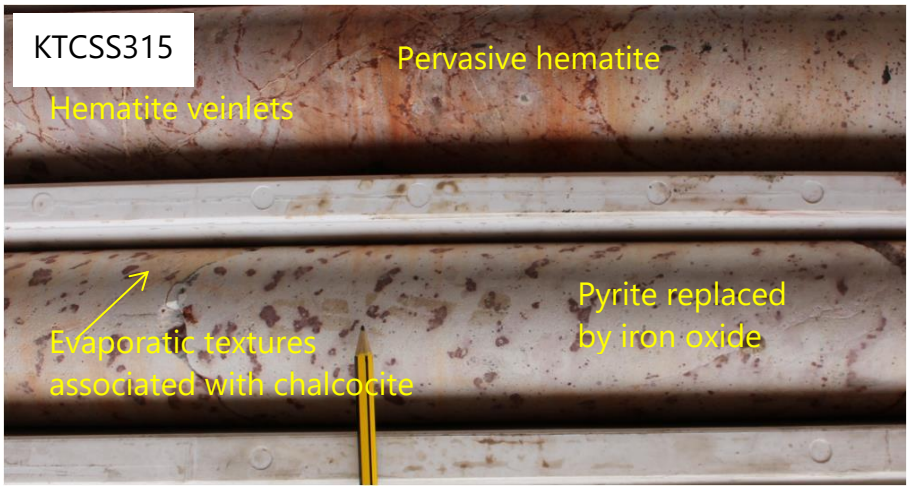

Figure 13: Pinkish very fine grained massive siltstone of R.A.T. with pervasive hematite enrichment and pyrite replaced by iron oxide. Spotted evaporitic texture is also evident.

2.8.2 Mines Subgroup

The Mines Subgroup, formerly called the Mines Series (François, 1973; 1974), constitutes the most significant set of host rocks of the Kinsevere copper deposit. The Mines Subgroup is the most explored unit and well-known stratigraphic part of the Neoproterozoic Roan Group due to the quality and the significant quantity of Cu-Co mineralisation hosted. The Kinsevere deposit is characterised by the absence of the stromatolitic silicified dolomite (Roche Siliceuse Cellulaire R.S.C.). From the bottom to top the Kinsevere deposit consists of the following: The Kamoto dolomite (R-2.1), the Shale Dolomitique or SD (R-2.2), the Kambove dolomite (code CMN: Calcaire a Minéraux Noirs; R-2.3) Formations (Figure 14).

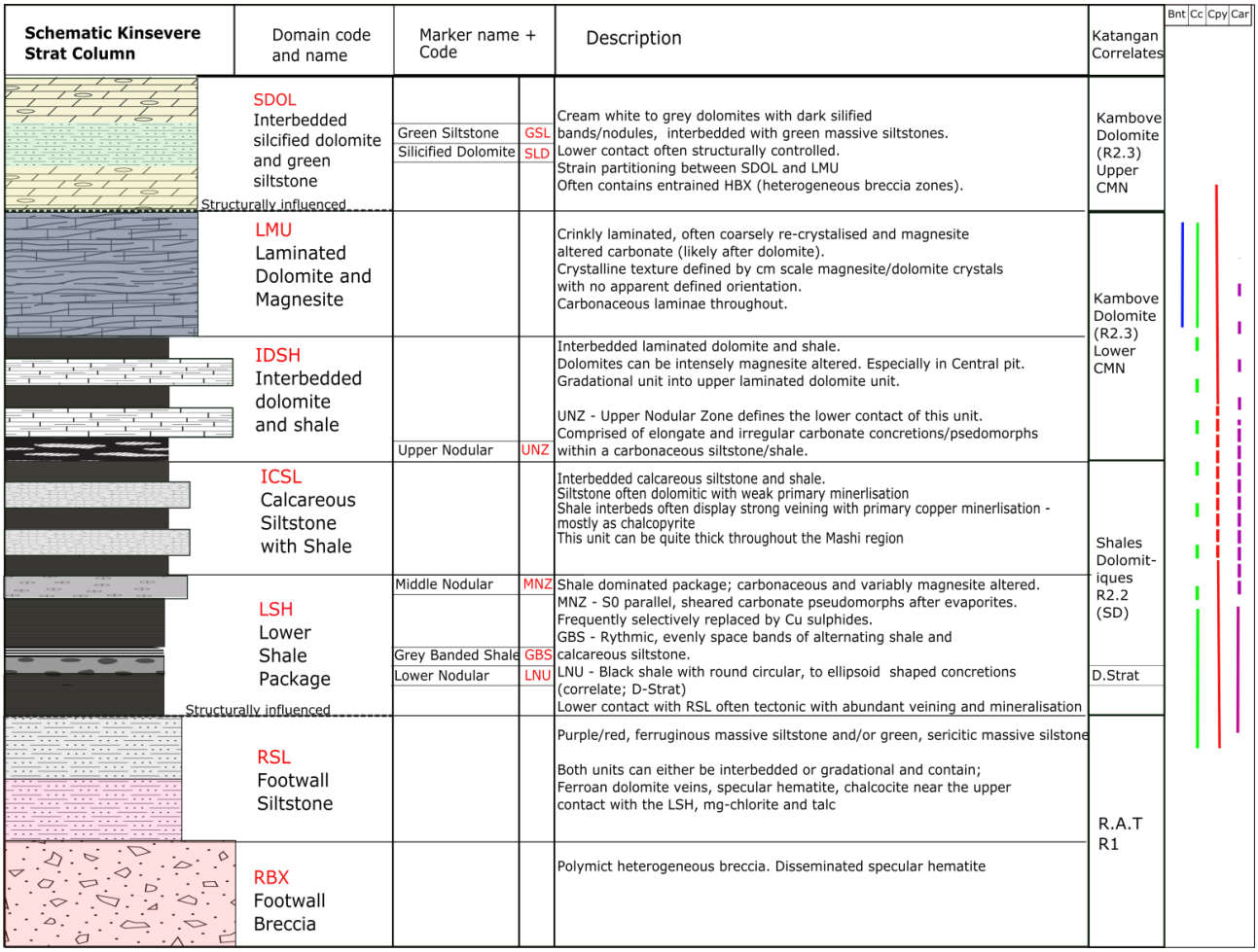

Figure 14: The recent detailed stratigraphic column of the Kinsevere deposit, and the Katangan stratigraphic equivalent shown on the right (MMG Ltd map, 2017).

2.8.2.1 Kamoto Dolomite Formation (R-2.1)

The thickness of this Formation ranges from 5 to 6 metres. The dolomite formation includes the Lower Nodular Zone (LNZ), which consists of the black banded dolomitic shale with round circular to ellipsoid shaped nodular concretions (Figure 15). The unit is a coarse carbonate, in filled with silty muddy rock, often displaying pressure shadows with carbonate rims replaced by copper sulphides. It is characterised by high degrees of silica alteration. The bottom contact with the footwall siltstone (R.A.T.) is often tectonised and contains abundant veining, hosting copper and cobalt mineralisation.

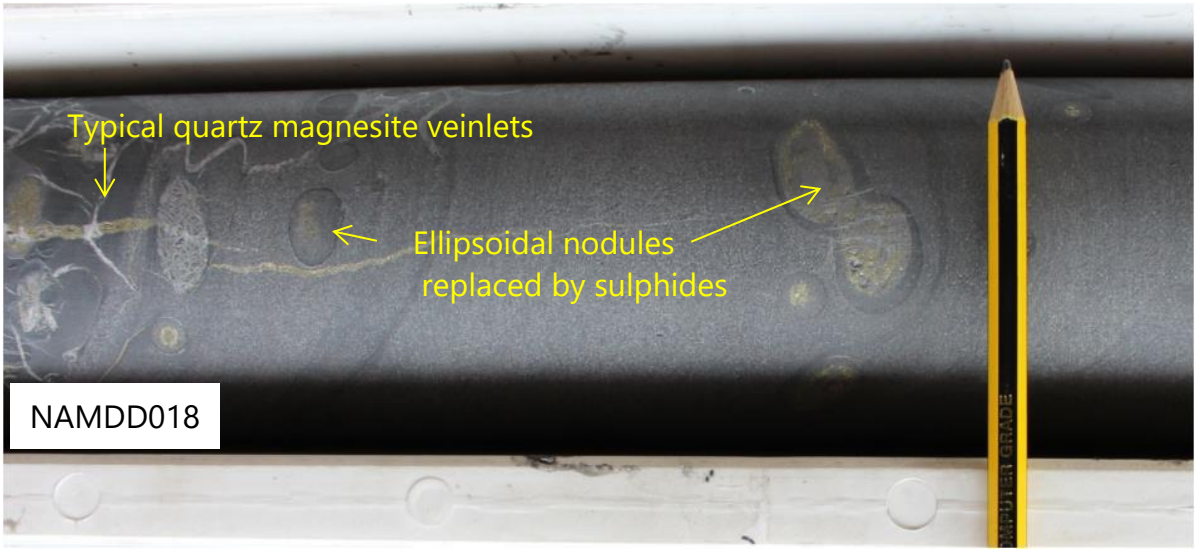

Figure 15: The banded dolomitic shale with ellipsoidal nodules with sulphide replacement, and quartz magnesite veins hosting sulphides mineralisation.

2.8.2.2 SD Formation (R-2.2)

The SD thickness ranges between 75 and 110 metres (Kazadi, 2012) and consists of very fine-grained to fine gained siliclastic rocks. In Kinsevere, the SD forms a succession of slightly greenish to grey dolomitic shale, which is finely-banded and weakly carbonaceous, alternating with dark, mostly carbonaceous shale/siltstone, progressing upward into largely pyritic carbonaceous siltstone and shales. Two distinct shaly nodular levels, named the Lower Middle Nodular Zone (MNZ) and the Upper Nodular Zone (UNZ), are used to determine a stratigraphic cut-off within the large normal succession of the Shale Dolomitique (SD) as follows:

1. The Middle Nodular Zone (MND): consists of a shale-dominated package alternating with carbonaceous shale. It is variably altered to magnesite and displays bedding parallel carbonate veins which are frequently selectively replaced by copper sulphide. The unit is intercalated with a calcareous siltstone (Figure 16).
2. The Upper Nodular Zone (UNZ): consists of interbedded calcareous siltstone and shale. The siltstone is often dolomitic with a weak primary copper mineralisation, while the shale interbeds often display strong veining with copper mineralisation mostly as chalcopyrite. The Upper Nodular Zone defines the upper contact of the unit with the CMN and overprints elongated and irregular carbonate concretions within the carbonaceous siltstone/shale.

Figure 16: NAMDD022: Carbonaceous shale with lenticular nodules parallel to stratification. Copper sulphide mineralisation occurs as replacement textures.

2.8.2.3 CMN Formation (R-2.3)

The CMN unit, known as the Kambove dolomite (R23), is the uppermost unit of the Mines Subgroup. Oosterbosch (1962) subdivided the CMN into two main units: A lower unit made by dark-coloured organic-rich dolostones, and an upper unit of clean dolomites interbedded with chloritic siltstones. The CMN unit is poorly studied but more detailed work was done by Cailteux (1978), overprinting a stratigraphic subdivision based on mapping surveys and cores drilled in the Kambove area. Cailteux recognised two main units with each unit comprising a number (three) of sub-units. The Lower CMN has been divided into three sub-units comprising mixtures of stromatolitic and laminated dolomite and talcose dolomite while the Upper CMN, consists of a mixture of massive dolomite, laminated slightly talcose dolomite and talcose graphitic dolomite (Cailteux, 1978).

Recent detailed work done in the Kinsevere area by MMG geologists divided the CMN into two stratigraphic units, with a thickness exceeding 150 metres:

1. A Lower CMN comprising the section between 40m to 80m thick.

   The bottom part consists of an interbedded laminated dolomite and dark carbonaceous finely laminated shaly dolomite, which can be intensely altered to magnesite. A gradational transition into the upper laminated dolomite is observed.

The bottom contact is marked by a presence of the Upper Nodular Zone, (UNZ) while the top contact is sharp (Figure 17). The top of the CMN is characterised by a crinkly-laminated, often coarsely recrystallised and magnesite-altered dolomite, with a crystalline texture defined by centimetre scale magnesite with no apparent defined orientation.

2. The Upper CMN is between 25 to 35m thick and consists of cream white to grey dolomite, with dark silicified bands of nodules interbedded with green massive silicified siltstone. The lower contact is often structurally controlled. The CMN consists of a clear distinction unit between the silicified dolomite and the laminated dolomite magnesite unit, which frequently occurs within a heterogeneous breccia zone.

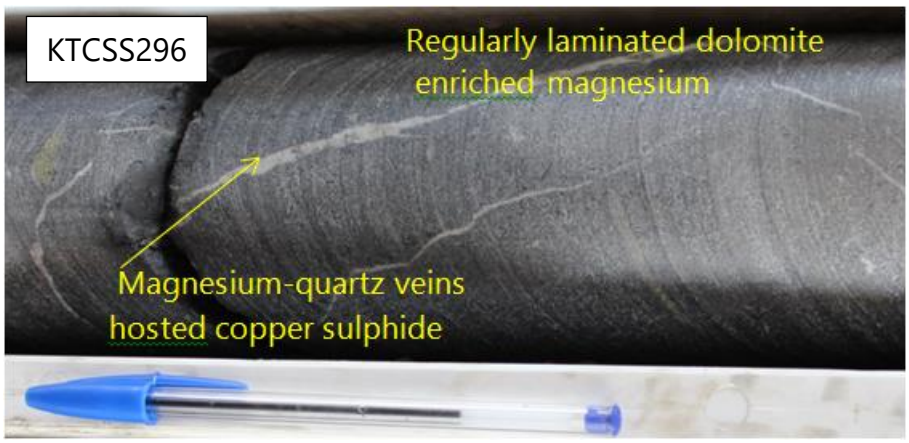

Figure 17: KTCSS296: Dark, coarse grained fresh rock regularly laminated dolomite enriched magnesium alteration, orthogonal magnesite quartz veins unfilled copper sulphide mineralisation.

2.8.3 Dipeta Subgroup

In Kinsevere, the base of the overlying Dipeta Subgroup comprises hematitic argillaceous dolomitic siltstones, sandstones, and locally conglomerates of the R.G.S. (Roches Gréso-Schisteuses) unit. The upper portions of the Dipeta Subgroup comprise an evaporatic lagoonal deposits, stromatolitic carbonate units, and deeper water dolomitic shales and siltstones. These are believed to have formed through similar processes of regressive and transgressive sedimentary cycles to the sediments of the Mines Subgroup (Broughton, 2014). However, some drill holes such as KHLSS274 carried out in the Kinsevere Hill intersected the

dolerite at the top of the sequence layer which contrasts with the Mines Subgroup sequence which does not feature magmatic layers.

The Dipeta Subgroup is overlain by the Mwashya Subgroup which is composed of a heterogeneous sequence of dolomitic shales and siltstones, carbonaceous siltstones, and minor sandstones.

Chapter 3: Methodology of work

3.1 Field work

Based on the lithostratigraphy, a total of four diamond drill holes were selected on which to conduct the study, comprising respectively the KHLSS274 hole for Kinsevere Hill deposit, the KTCSS315, KTCSS326 for Kinsevere deposit and the SM59016 from Safety Mineral. Detailed core logging was completed involving the lithology, the texture, the structure, the mode and intensity of alteration, the mineralisation type, the magnetic susceptibility and the stratigraphy of the rocks described. Details of geological logging are find in appendix 1.

The field work was mainly focused on describing the R.A.T. and Dipeta lithological formations in details, and better identifying the heterogeneous breccia which defines the unconformity decollement plane located between the studied footwall and the hangingwall units. The work was undertaken using, geological hand lens, a magnetic pen, dilute (10%) hydro-chloric acid (HCl), as well a geological hammer.

Representative half core samples were collected from appropriate drill holes for petrographic studies based on the nature of the lithology, the alteration, the texture/structure and the stratigraphic position. Samples of half HQ core of 10cm minimum of length were carefully collected, cleaned, labelled, marked and photographed, before subsequent thin section preparation.

.

3.2 Sampling and samples preparation

Drill-core sampling and sample preparation followed strict procedures. Core samples were collected at each meter according to the geologist's sample list instruction. The sample cutting line depended on the nature of the lithology or stratigraphy as well as the diameter of the drill hole. Systematic sampling was done across the mineralized zone, and composite samples collected at 1m or 2m intervals depending on whether the sampled zone was mineralised or barren, respectively. All samples are from fresh and altered borehole cores and are intended to be representative of the main lithological facies of both R.A.T. and Dipeta Subgroup units. 57 samples comprise the R.A.T. unit, 69 samples have been collected

from the Dipeta stratigraphic unit, and 24 samples related to the intercalated heterogeneous breccia were deemed useful for the geochemical studies.

The samples, of approximately 1kg, were packed in labelled plastic bags into which sample number tickets were inserted to avoid any mix up or swapping during the preparation. Precautions were taken during sampling to avoid wearing of metals or any design (rings and/or bracelets) that may have resulted in sample contamination.

The sample preparation process was designed to produce a representative homogeneous sub sample. A Boyd crusher was utilised to reduce the core sample to an expected particle size of 2mm followed by pulverisation to a particle size of 75 microns using LM2 mills. The generated pulps were split into two 100g samples for storage and analysis purposes respectively. The crusher and the mills were systematically cleaned by compressed air and quartz flush in between samples to reduce contamination effect.

3.3 Laboratory analysis for samples

The samples were dispatched to ALS Minerals laboratory in Johannesburg for whole-rock geochemical analysis. The major elements were determined using a Lithium borate flux. A prepared sample (0.100 g), mixed well and fused in a furnace at 1000°C. The resulting melt is then cooled and dissolved in 100 mL of 4% nitric acid/2% hydrochloric acid. This solution is then analysed by Inductively Coupled Plasma - Atomic Emission Spectroscopy (ICP-AES) and the results are corrected for spectral inter-element interferences. Oxide concentration is calculated from the determined elemental concentration. The total oxide content is determined from the ICP analyte concentrations and loss on Ignition (L.O.I.) values. The LOI is resulted from a prepared sample (1.0 g) placed in an oven at 1000°C for one hour, cooled and then weighed. The percent loss on ignition is calculated from the difference in weight.

Results of Rare Earth Elements (REE'S) were obtained by using a prepared sample (0.100 g) added to lithium metaborate/lithium tetraborate flux, mixed well and fused in a furnace at 1025°C. The resulting melt is then cooled and dissolved in an acid mixture containing nitric, hydrochloric and hydrofluoric acids. This solution is then analysed by inductively coupled plasma - Mass Spectrometry (IPC-MS).

Results of some volatile chalcophiles elements such as As, Bi, Hg, Sb, Te, Tl were obtained from a sample digested with *Aqua Regia* in a graphite heating block. After cooling, the resulting solution was diluted to 12.5 mL with deionized water, mixed and analysed by inductively coupled plasma – mass spectrometer. The analytical results were corrected for inter-element spectral interferences.

Preparation for analysis of base metals and additional elements (Cu, Co, Ni, Mo, Pb, Ag, As, Cd) more appropriately analysed by acid digestion were conducted using *Aqua Regia* or four acid digestion. The four-acid digestion is preferred when the targets include more resistive mineralization such as that associated with nickel and cobalt.

3.4 Quality Assurance/Quality Control (QA/QC)

QA/QC samples were inserted in all sample batches as part of the routine quality control procedure. Duplicates, standards and blanks samples were inserted amongst all the drill samples. The recommended procedure is to insert 5% standards, 5% duplicates and 2-3% blanks in a batch of less than 150 samples. This is done using sample numbers unknown to the lab. Two or three different standards were used to represent the range of data variability. The purpose of the insertion of standards is to evaluate the accuracy and the precision of the analyses, while the purpose of insertion of blanks is to check for contamination, both at the lab during the sample preparation stage, as well as to monitor the detection limit of the methods, and detect accidental samples switching or swapping. The purpose of insertion of field duplicates is to determine the analytical reproducibility.

The representative graphs below depict the QA/QC assessment made for the samples submitted for wet chemical analysis. It appears that the quality of the analytical data received from the ALS was found to be good and therefore acceptable (Figures 18 and 19).

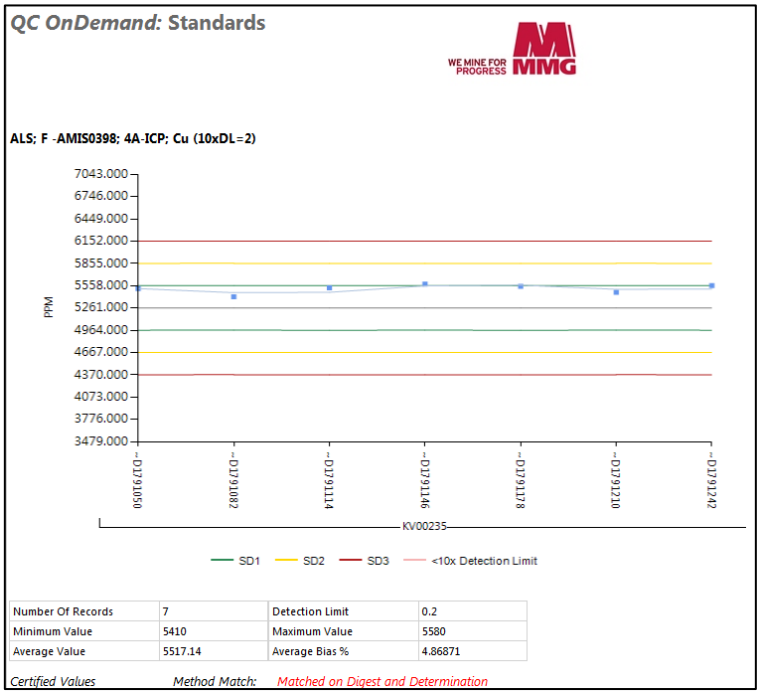

Figure 18: Good distribution related to the standard deviation of the Standard (AMIS0398), used to control and evaluate the analytical accuracy and precision of wet chemical analysis.

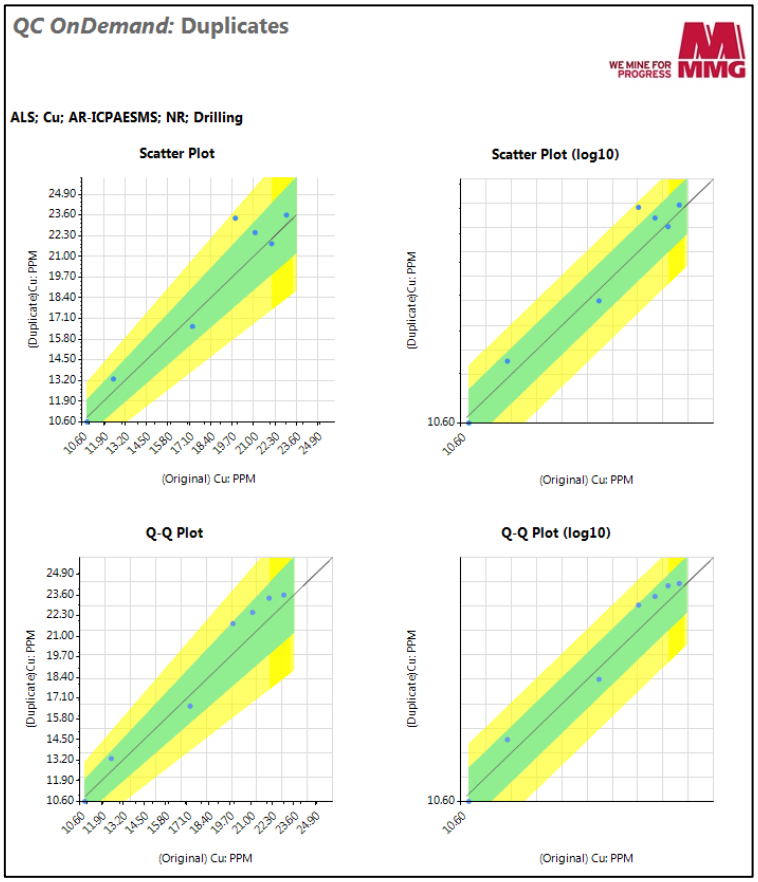

Figure 19: Good distribution related to the standard deviation of inserted field duplicates, used to determine the analytical reproducibility.

3.5 Reflected and Transmitted Light Microscopy

To better guide this study, a number of representative samples of the R.A.T. and Dipeta stratigraphic units collected from Nambulwa drill holes were polished. Eight thin sections were systematically examined using conventional reflected and polarised light microscopy, with the individual minerals being identified on the basis of their optical properties. Observations were completed using the Plane Polarised Light (PPL), Cross Polarised Light (XPL), as well Reflected Polarised Light (RPL). A series of photomicrographs were also prepared to illustrate important mineralogical and textural features. It appears that most of described samples were very fine-grained siltstone and dolomitic siltstone/shale, so mineral identification and textural features characterisations were not easy. Because of this, XRD, SEM and geochemistry were also employed to constrain the mineralogical and compositional variation respectively.

3.6 X-Ray Diffraction

X-Ray Diffraction (XRD) analyses were performed on samples to determine their bulk mineralogical composition where deemed appropriate. Suitably prepared samples were sent and analysed at Cardiff University laboratory using a Panalytical PW1840 diffractometer operating with Cu k-α radiation and using appropriate instrumental settings to ensure optimum resolution of the reflections. The individual minerals were identified by computer-matching their diffraction patterns against a standard database. The samples selected from Nambulwa drill holes were prepared as polished thin sections to enable diagnosis of the mineral contents of each sample. Details of the X-Ray Diffraction (XRD) results are find on appendix 2.

3.7 Scanning Electron Microscopy (SEM)

SEM studies were conducted at the Rhodes Electron Microscope unit. An Oxford instruments/INCA energy 350 microanalysis system Si-Li detector attached to a TESCAN Vega TS 5136LM SEM was used for spot analyses performed at 20kV. Each spot analysis was analysed with a time constant of 30 seconds per spot. A cobalt standard was used for a peak

calibration. Therefore, five polished thin section were examined, and individual minerals being identified on the basis of their mineral chemistry as determined by qualitative energy dispersive Microbeam analyses. A series of backscattered electron images were prepared to illustrate important mineralogical and textural features. The method is very useful in determining the detailed mineral composition of the samples, associated with their geochemical fingerprint.

Chapter 4 : Petrography

4.1 R.A.T. Subgroup

Two samples (R216805, R216808) belong to the R.A.T. Subgroup of the Roan Group were individually collected from Nambulwa drill holes. Petrographic discussion of the R.A.T. samples is mentioned below as follows.

4.1.1 Macroscopic Description

Macroscopic R.A.T. samples observation exhibits a greenish massive to diffusely laminated very fine grained argillaceous and magnesite chloritic siltstone. The host rocks exhibit a very fine disseminated of mica which is probably a sericite and show a light band representing a dolomitic bed with intercalated brecciated layers. Locally, talcose and small metallic lustre spots correspond to a specular hematite or possibly oxidised pyrite. The unit is cross cut by fractures or veinlets in filled by carbonate or abundance of hematite associated with limonite alteration. Very fine disseminated shining specularite is observed. R.A.T. samples exhibit a spotty texture possibly representing evaporitic pseudomorphs within a dolomitic matrix. The dolomitic siltstone overprints patchy or dendrite of manganese which appears concentrate in the fractures or in the brecciated rock (Figure 20).

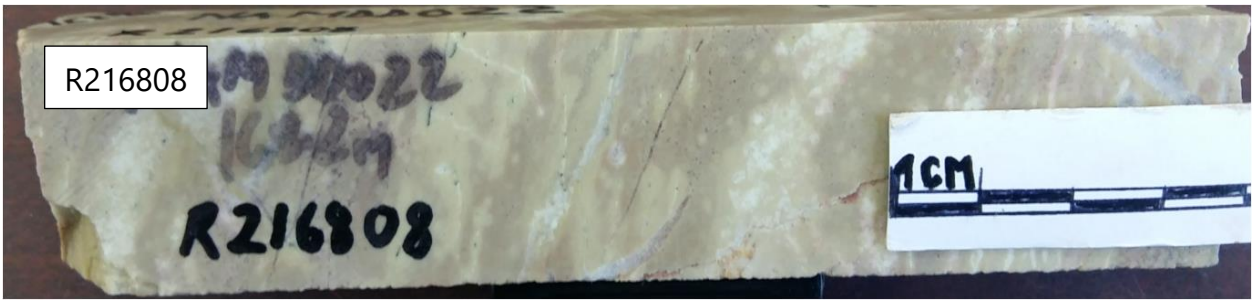

Figure 20 : R216808, consists of greenish magnesite chlorite and talcose very fine grained clayey massive to diffusely laminated siltstone. Lighter dolomitic layers and brownish banded layer is an oxidised hematitic level. Locally, immediate layer contains some interval of brecciated and evaporite veins and significant patchy of manganese.

4.1.2 XRD

X-Ray Diffraction (XRD) analysis conducted on four samples of R.A.T. confirms the presence of quartz, calcite, dolomite, smectite and kaolinite group clays, muscovite/illite and apatite. The quartz and magnesite are dominant minerals in the host rock while the dolomite, muscovite/illite are less abundant minerals. A representative graphic of XRD analysis conducted at R.A.T. samples is shown on the figure as per the illustration below (Figure 21).

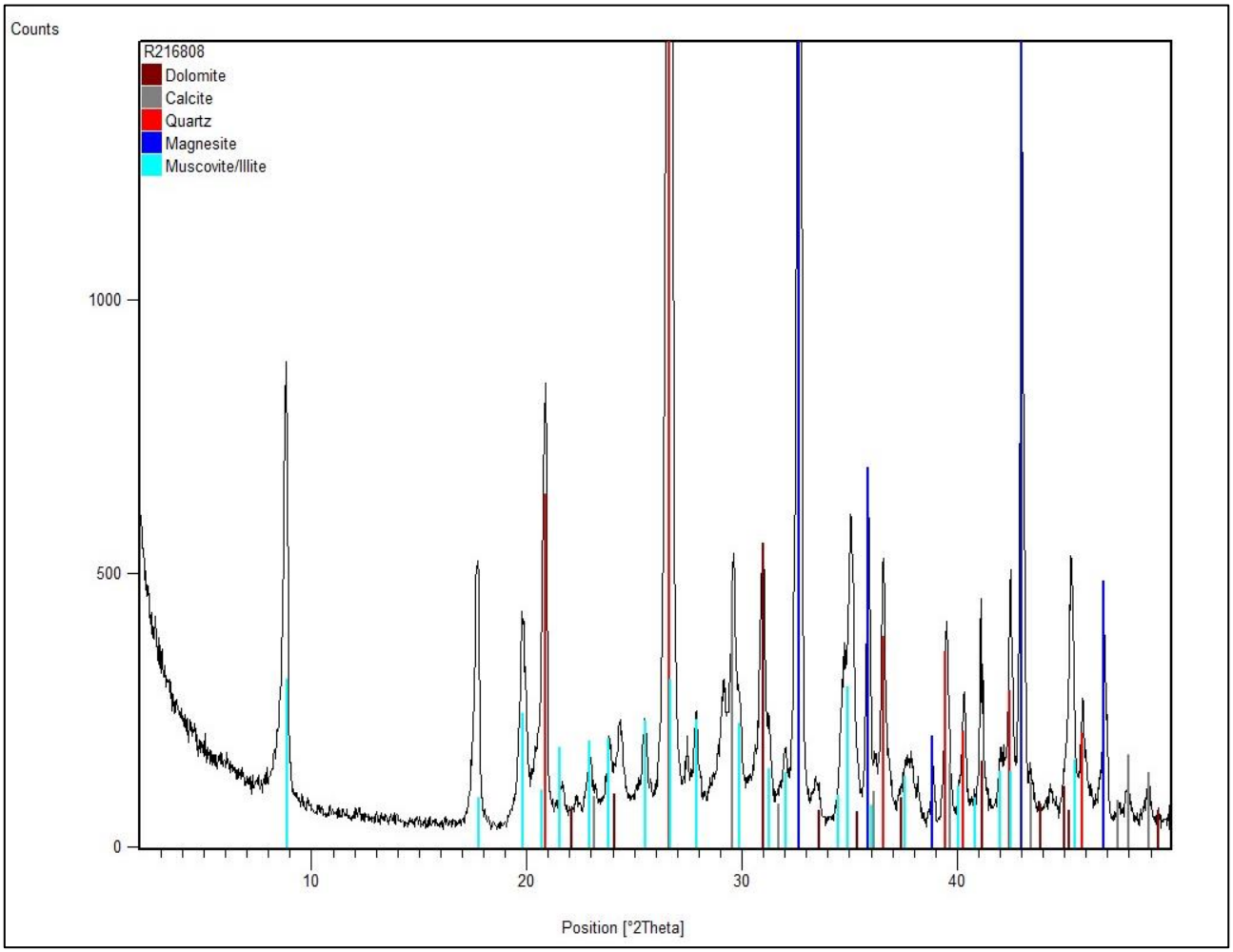

Figure 21: An X-ray diffractogram illustrating the dominant crystalline minerals identified in the sample.

4.1.3 Mineralogy

The microscopic observation of R.A.T. sample was designed to emphasise the alteration assemblages found. The geological processes relating to alteration involve diffuse ion exchange, chemical weathering, alteration, leaching, pseudomorphism, metasomatism, diagenesis and metamorphism, which are linked by common features in which one mineral or mineral assemblage is replaced by a more stable assemblage.

Aspects relating to crystal growth will also explain. The expected mineral assemblage consists of carbonates, composed essentially of magnesite and dolomite, oxides (hematite, ilmenite, and rutile), sulphates (evaporitic) and bulk of rocks consisting of silicates, comprising feldspar, muscovite, sericite, chlorite, kaolinite and others accessory minerals.

4.1.3.1 Carbonates

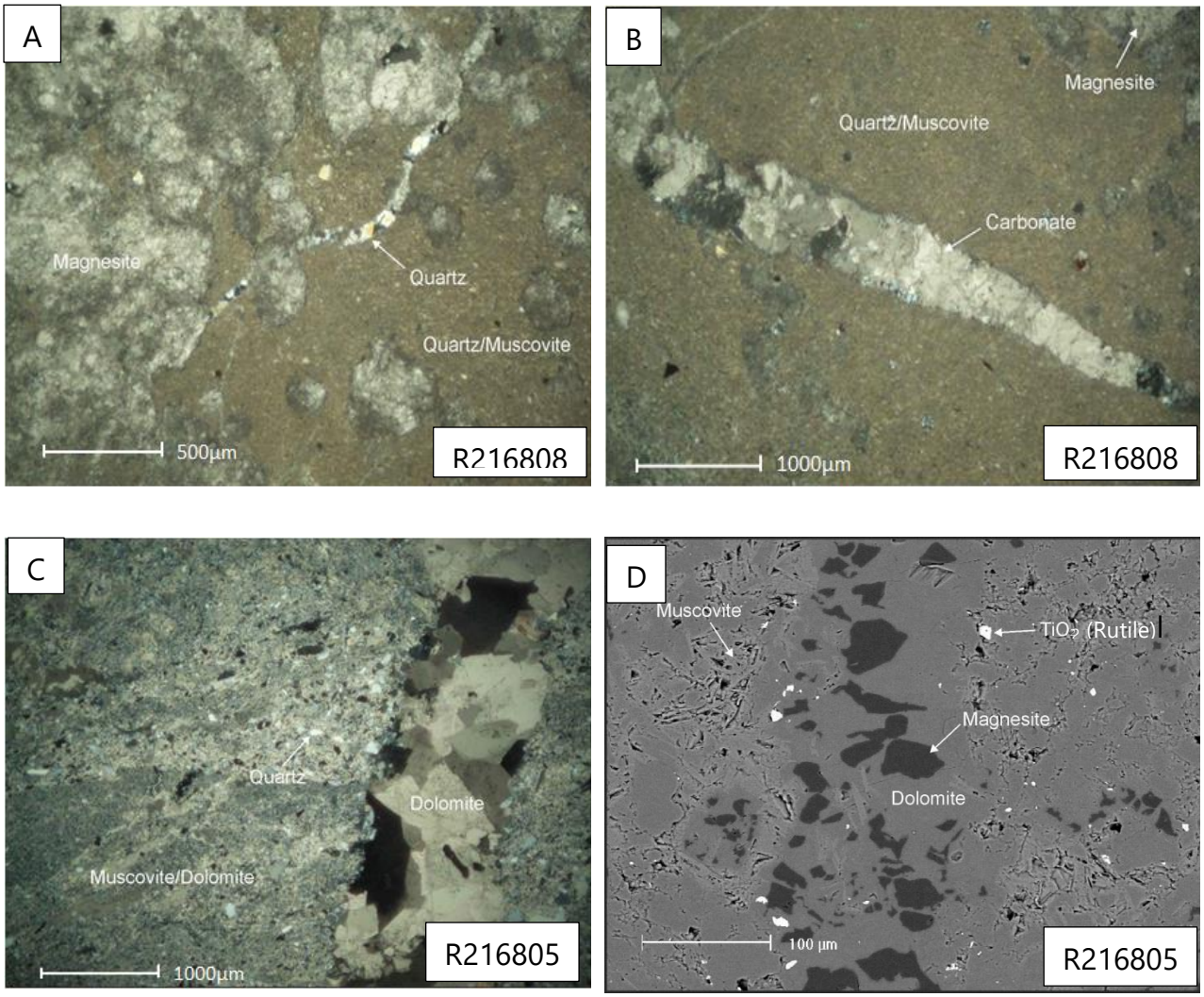

Figure 22: A) = A transmitted light photomicrograph under crossed polars illustrates the typical nature and appearance of the sample which consists of very fine-grained quartz and muscovite, partially replaced by magnesite. A narrow quartz veinlet is also present and appears to pre-date the magnesite. B) = This image illustrates a carbonate (probably dolomite or magnesite) filled fracture parting in the fine-grained quartz muscovite host rock. C) = A transmitted light photomicrograph under crossed polars illustrating coarse-grained dolomite veinlets with a euhedral texture that traverses the host rock. D) = A backscattered electron image illustrating dolomite that has extensively replaced a former magnesite vein. The matrix of the host rock consists largely of muscovite and dolomite (undifferentiated). Minor apatite is also present.

The R.A.T. samples show very fine grained detrital muscovite and quartz grains which are partial replaced by relatively coarsely crystalline magnesite. There are subordinate amounts of magnesite throughout the matrix of the host rock, typically exhibiting extensive replacement by dolomite (Figure 22 A). Coarser grained muscovite is also commonly associated with the dolomite replacement of the magnesite, and is presumably associated with recrystallization of the host rock muscovite. Carbonate−rich veins are also prominent (Figure 22B).

The in-filled carbonate veins probably contain magnesite and recrystallised euhedral dolomite associated with quartz (Figure 22 C). On other hand, the dolomite has, however, extensively replaced earlier-formed magnesite, with abundant relict magnesite being commonly observed in the veins. In addition, there is late stage of dolomite and minor calcite showing partial replacement of magnesite. This indicates that the calcite appears to be a mineral reaction product, replacing the magnesite along grain boundaries where the magnesite is in close contact with the later dolomite (Figure 22D).

4.1.3.2 Oxides

R.A.T. samples exhibit euhedral quartz with its characteristic absence of cleavage, appearing as a common mineral in the gangue. In addition, discrete layers of coarser-grained detrital quartz are also evident in the host rock (Figure 23A). Trace amounts of iron oxide occur within the dolomite (confirmed by qualitative SEM analysis). Accessory phases observed include minor to trace of rutile exhibiting a subrounded texture which suggests that the mineral was involved in detrital depositional processes, with grains located mostly between quartz grains (Figure 23B). Rounded and subangular rutile is disseminated throughout the sample and associated with accessory apatite, which is being replaced by dolomite in the matrix of the host rock. Minor relict magnesite is also associated with dolomite (Figure 23C).

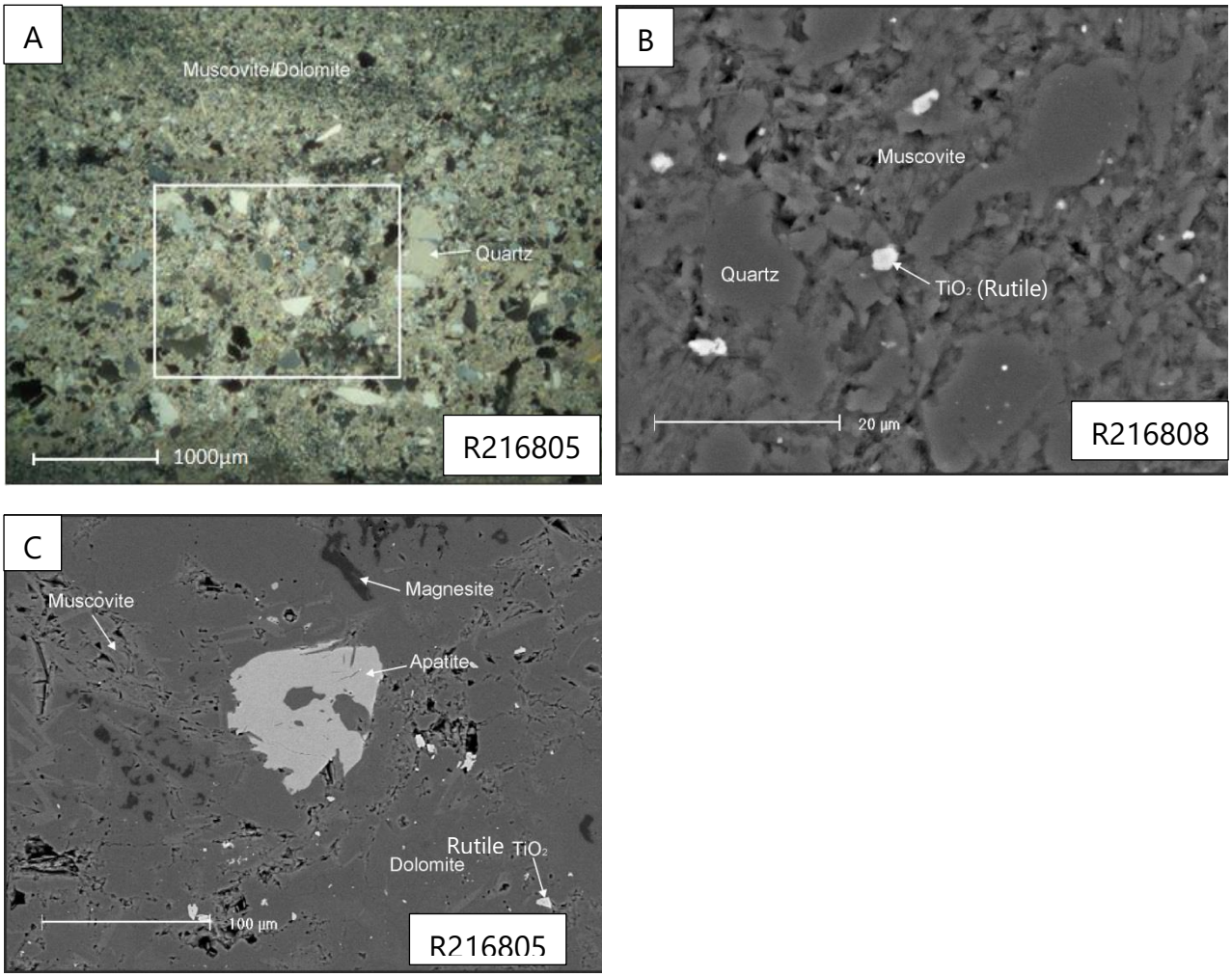

Figure 23: A) = A transmitted light image under crossed polars illustrating the typical appearance of R.A.T. samples, which consist of a relatively fine-grained muscovite and quartz-rich siltstone. Coarser layers of detrital quartz are evident locally. B) = A backscattered electron image illustrates the presence of accessory apatite in the matrix of the host rock. Finely disseminated rutile is present throughout the host rock. C) = A backscattered electron image illustrating the presence of accessory apatite in the matrix of the host rock. Minor amounts of relict magnesite are also present associated with finely angular rutile within the host rock.

4.1.3.3 Silicates

The R.A.T. samples consist of very fine grained detrital muscovite and sericite. Analysis of the samples shows a dolomitic siltstone like rock that consists largely of fine grained elongated muscovite (Figure 24 A). Accessory phases include zircon associated with xenotime, which may represent a non-detrial mineral and occurs not-so-resistant diagenetic mineral within the dolomitic matrix. Rounded zircon may suggest detrital deposition of otherwise immobile elements. Image illustrates a xenotime nucleated on the zircon and grown during the diagenesis (Figure 24 B).

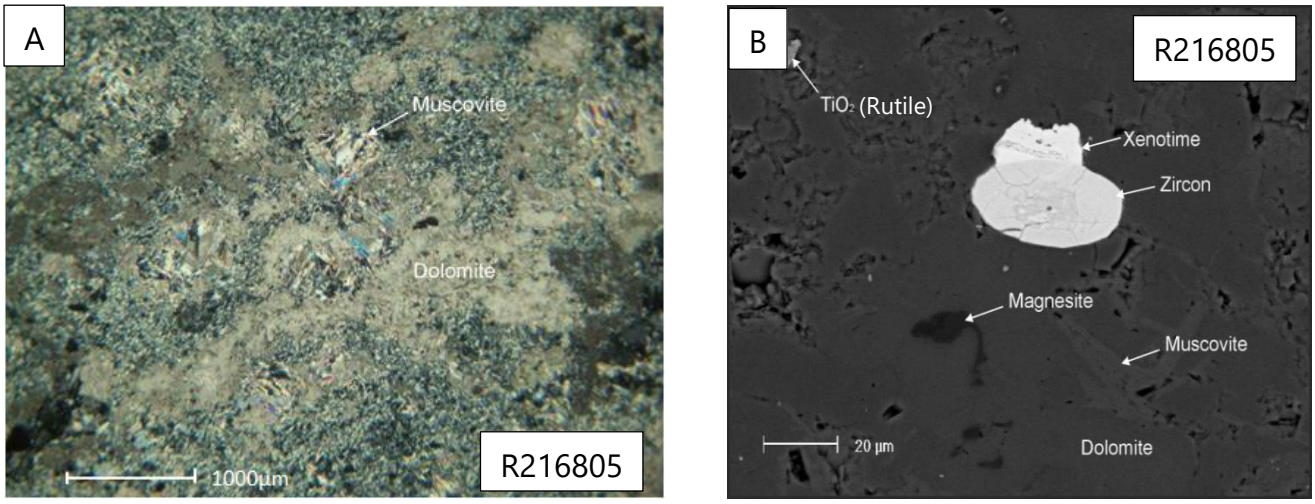

Figure 24: A) = A transmitted light under crossed polars image illustrating the extensive replacement of the fine-grained muscovite matrix (various bright blues, reds and pale yellows) by dolomite (light grey-brown). Spectacular elongated muscovite is recognised. B) = A Scanning Electron Microscopic image illustrating the presence of minor accessory rounded zircon associated with xenotime.

4.1.3.4 Sulphides

The R.A.T. samples show minor poikiloblastic pyrite that may be associated with coarser layers in the host rock, or with porosity resulting from evaporite dissolution or replacement, which has thus controlled sulphide mineralisation (Figure 25 A) but no copper sulfide has been observed. Accessory pyrite can occur as well-developed anhedral cubic crystalline masses within the dolomite matrix of the host rock. Quartz veins containing of magnesite (shown within the white-bounded square in Fig.25B) and associated with apatite occurs together with massive pyrite (Figure 25 B).

4.1.3.5 Sulphates

In addition, the accessory minerals observed include apatite and a Ca-sulphate phase, which is probably gypsum. The dispersed Ca-sulphate is intimately associated with the magnesite which it looks like an inclusion mineral (Figure 26).

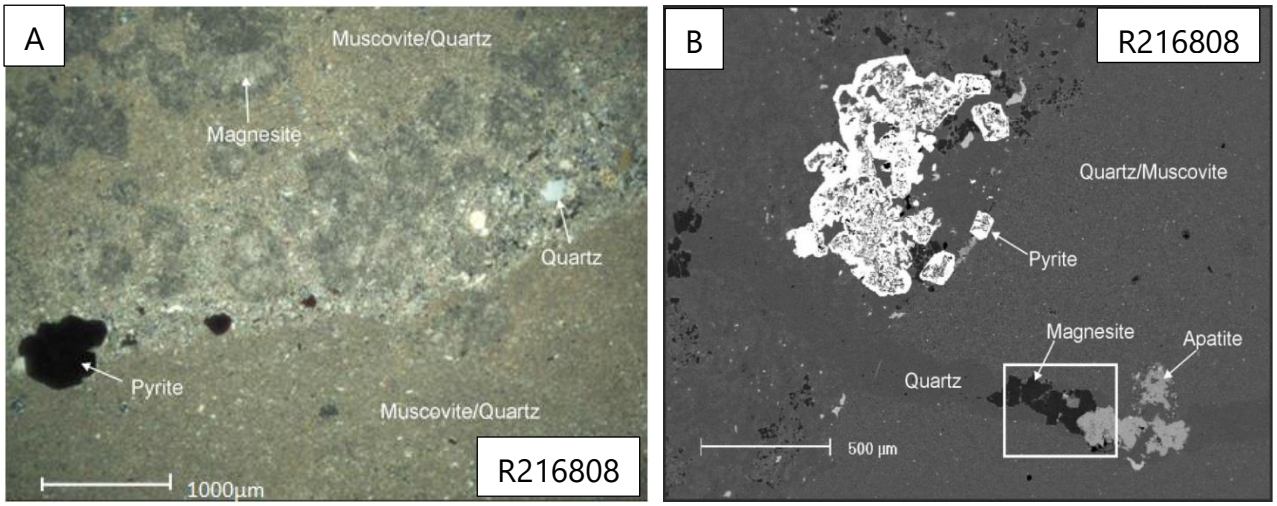

Figure 25: A)= A transmitted light under crossed polars image illustrating the presence of euhedral poikiloblastic pyrite (black) in a coarser layer containing detrital quartz. B) = A SEM image illustrating well-developed poikiloblastic pyrite as an anhedral cubic crystalline masse within the dolomite matrix.

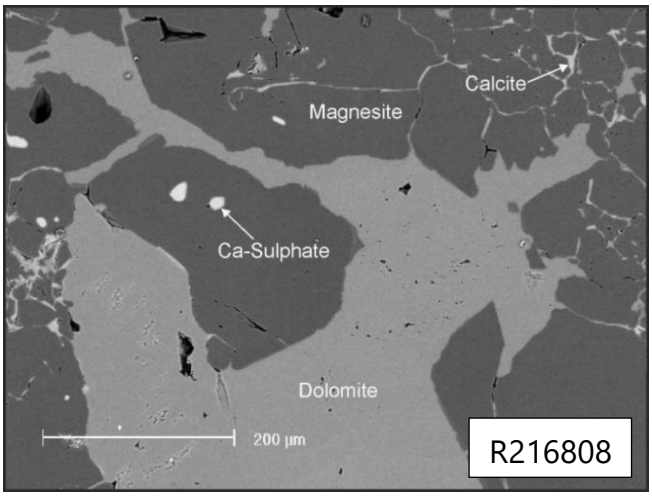

Figure 26: SEM backscatter image showing partial replacement of magnesite by dolomite and calcite. Ca-sulphate (probably gypsum) is a common accessory phase associated with the magnesite.

4.1.3.6 Other Minerals

The samples containing coarse grained carbonate veins feature intergrowths of euhedral calcite and apatite partially replacing the original euhedral magnesite in the veins. Quartz occurs as relict mineral which has evolved a sharp contact with the magnesite replacement texture. Cross cutting quartz veinlets indicate another minor late event (Figure 27).

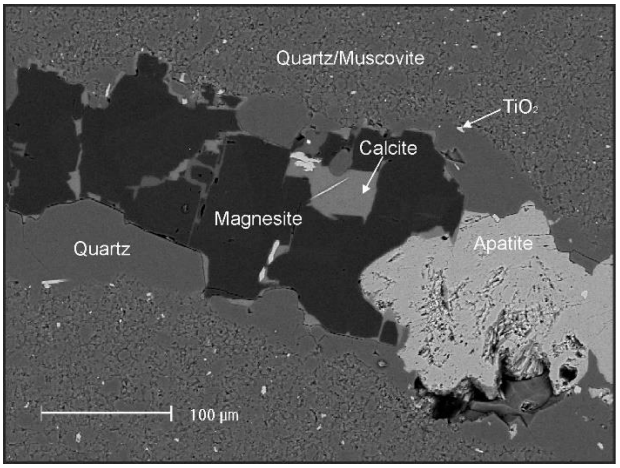

Figure 27: A magnesite and apatite infill associated with a quartz veinlet which traverses the fine-grained quartz/muscovite host rock. Calcite appears to partially replace the magnesite.

4.2 Dipeta Subgroup

Tree samples (R216801, R216802 and R216814) belonging to the Dipeta Subgroup were individually collected on the Kinsevere and Nambulwa diamond drill holes. The petrographic discussion of these samples is described below.

4.2.1 Macroscopic description

The Dipeta samples consist of pale cream-coloured, clay-carbonate in a reddish, brownish and greenish coloured matrix. Macroscopic observation reveals a laminated to banded siltstone with pervasive hematite alteration associated with vuggy texture, locally alternating with dolomitic pelitic layers. In either case, the bands may represent detrital heavy mineral banding, with ilmenite as a significant component. The coarse-grained iron- rich dolomite matrix contains interstitial pervasive manganese oxide, which appears as a common mineral, especially in brecciated zones. Slumping and relict evaporitic textures are recognised in other samples. Intrusion of dolerite has characterised the Dipeta unit locally. In addition, rock observation indicates that the hydrothermal carbonate stockworks veins are associated with rare vuggy texture featuring in-filled recrystallised quartz. In addition, grey minerals colour occurs in the stockworks of host rock which probably include ilmenite (Figure 28).

Figure 28: Photo shows a grey, very fine grained, hand sample, composed of a clasts-supported breccia. There is a reddish brown dolomite-rich matrix, with grey bands that may represent detrital heavy mineral banding with ilmenite. The unit illustrates a pervasive hematitic-matrix alteration, and a banded dolomite vuggy texture infilled with recrystallised quartz, alternating with dolomitic siltstone layers.

4.2.2 XRD

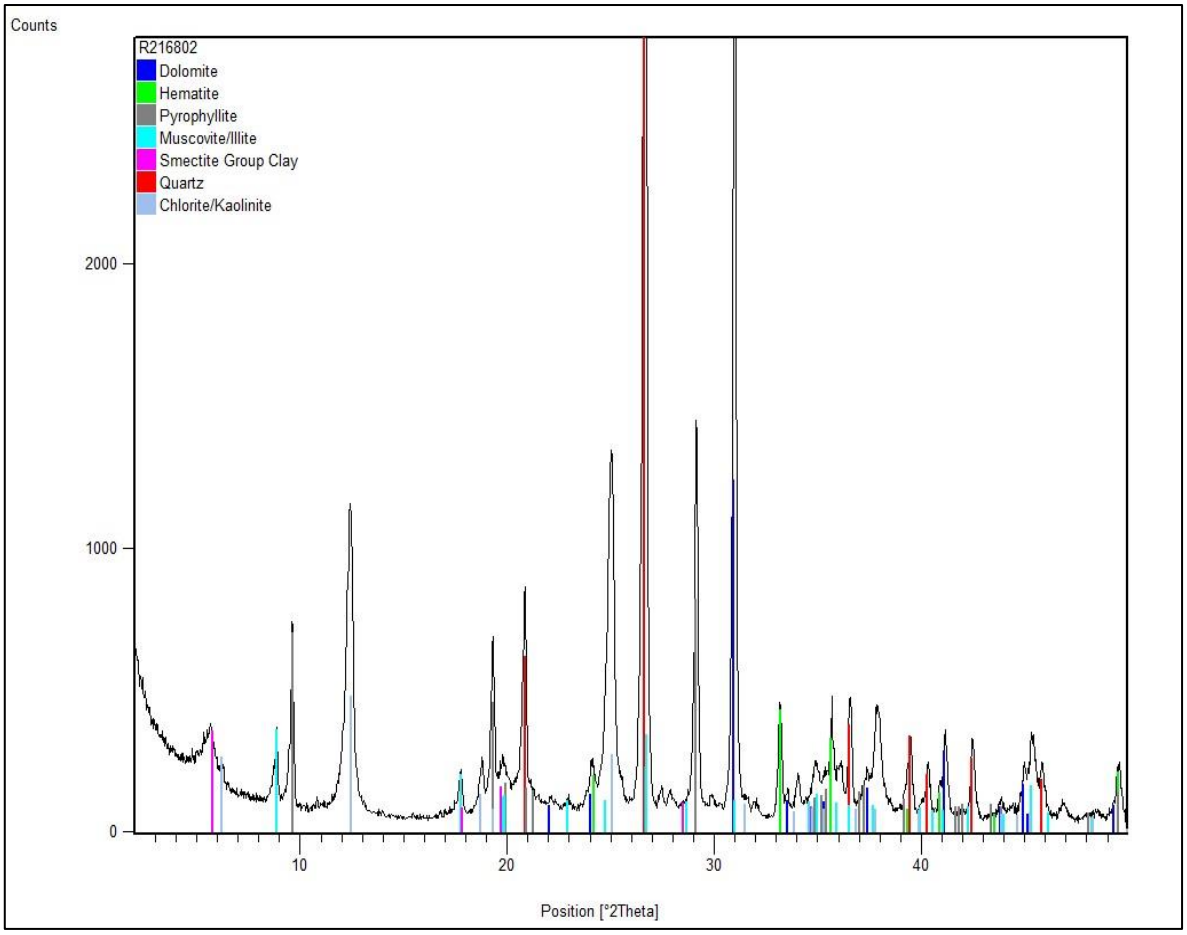

Figure 29: An X-ray diffractogram illustrating the dominant crystalline minerals identified in this sample composed by quartz, dolomite, muscovite/illite, kaolinite and pyrophyllite.

X-Ray Diffraction (XRD) analysis applied to four Dipeta samples displays the presence of quartz, calcite, dolomite, smectite and kaolinite group clays, muscovite/illite, pyrophyllite and apatite. The quartz and dolomite are dominant minerals in the host rock while, the

muscovite/illite, hematite, chlorite are less abundant minerals. A representative graphic of the XRD analysis of the Dipeta samples is shown above (Figure 29).

4.2.3 Mineralogy

The purpose of microscopic examination of Dipeta samples was to determine the mineralogy and the textures related to the described host rock. The mineral assemblage is described here in terms of mineral class, composed of carbonates (magnesite and dolomite), oxides (hematite, ilmenite, and rutile), sulphate (evaporites) and the silicates (feldspar, muscovite, sericite, kaolinite and chlorite).

4.2.3.1 Carbonates

The host rock samples consist of fine grained clay-rich clasts in a reddish-brown dolomite rich matrix. The reddish brown coloured matrix is dominated by the presence of dolomite together with subordinate amounts of mono−crystalline quartz grains (Figure 30 A). Detailed examination of the dolomite using Scanning Electron Microscopy (SEM) confirms the presence of minor but variable amounts of manganese oxide and illustrating fine-grained secondary apatite infill in the dolomite and clay matrix. The textures in the dolomite are complex, variously reflecting, zoning, recrystallisation, dissolution, replacement and cavity filling by dolomite. In addition, the dolomite shows a complex spheroidal texture (Figure 30 B and C), and commonly exhibits euhedral morphologies in the matrix. A backscattered electron image illustrates fine-grained secondary apatite infill replacing dolomite and clay matrix along fractures (Figure 30 D).

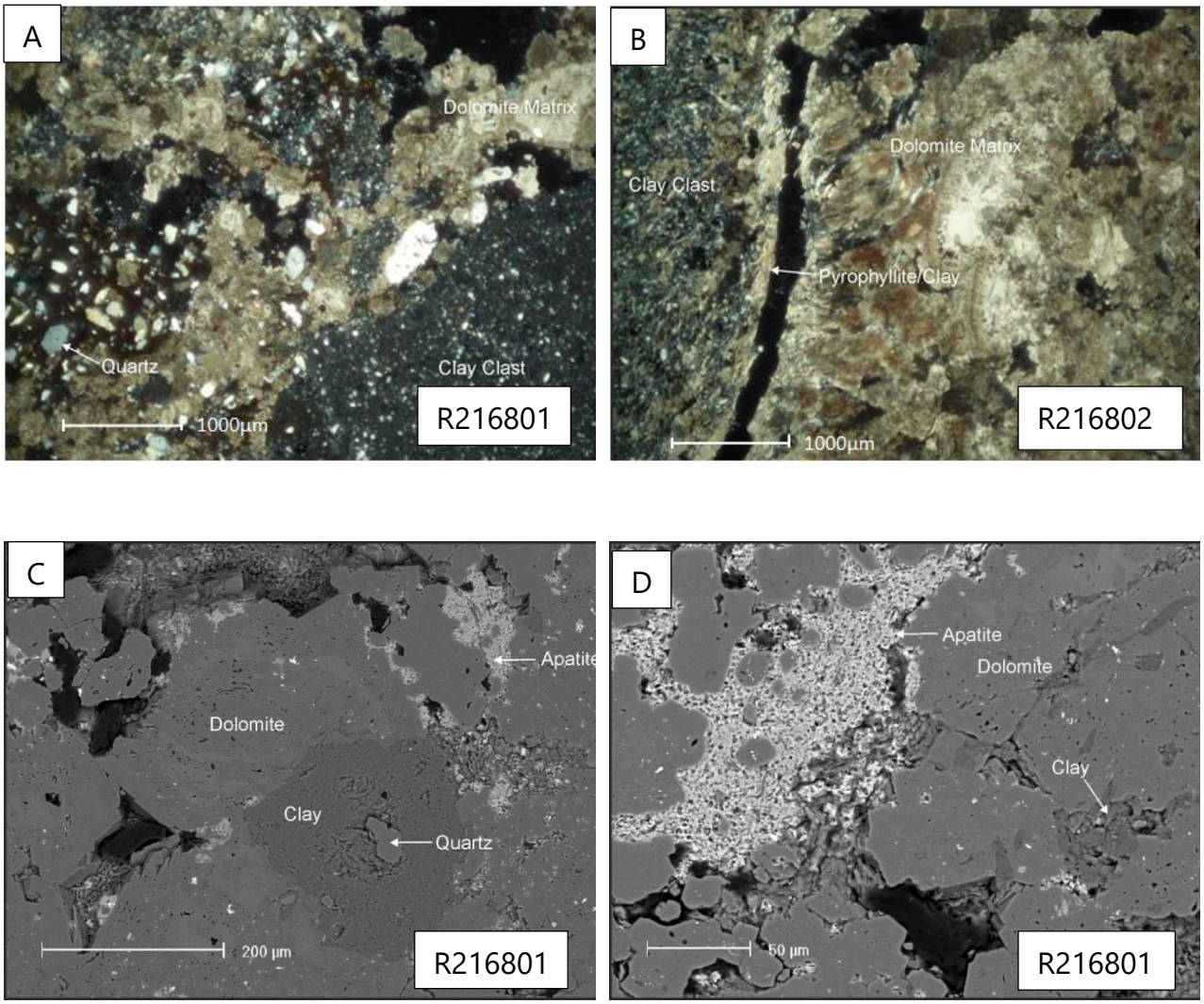

Figure 30: A) = A transmitted light image under crossed polars illustrating the typical appearance of this sample, comprising clay-rich clasts (lower right) and a zoned dolomite matrix (pale grey/brown shades). Quartz crystals (white to pale yellow/grey) are abundant in the matrix. B) = A transmitted light picture with crossed polarisers illustrating complex spheroidal textures in the dolomite matrix. C) = A backscattered electron (SEM) image display an area with zoned dolomite (Mn-rich areas are lighter grey), fine-grained clay (formerly a small clast), quartz and a fine-grained secondary apatite infill. D) = A backscattered electron image (SEM) illustrating fine-grained secondary apatite infill in the dolomite and clay matrix.

4.2.3.2 Oxides

Microscopic observation demonstrates that the quartz is a common accessory phase within the clasts occurring as fine-grained disseminations throughout the sample, while the hematite has replaced earlier FeTi-oxides ilmenite in a number of the clasts (Figure 31 A). Observations show that the hematite is also present within the matrix in minor to moderate amounts and occurs predominantly as a pseudomorphous replacement of earlier tabular ilmenite crystals (Figure 31 B). In addition, the samples indicate that the hematite often forms

complex intergrowths with rutile, reflecting relicts of the crystal structure of the replaced FeTi-oxides (e.g. ilmenite and magnetite). The bulk of the rutile in this sample appears to be either detrital or secondary in nature.

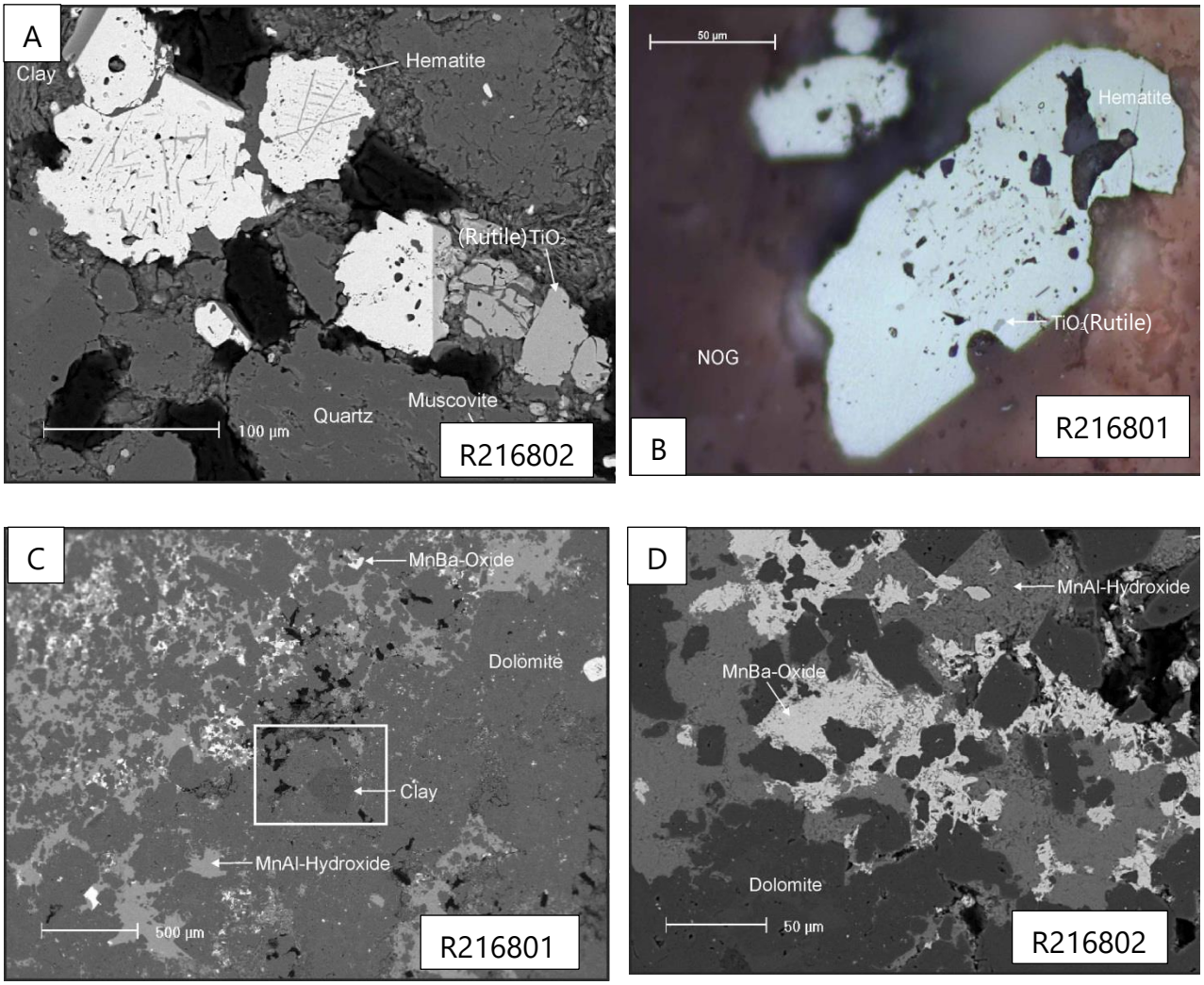

Figure 31: A) = A backscattered electron image illustrating complex textures between hematite and TiO_2, reflecting alteration and replacement of earlier FeTi-oxides. The altered FeTi-oxides are present in a heavy mineral layer associated with coarse quartz. Fine muscovite is also present along with the detrital quartz. B) = A reflected light photomicrograph illustrating a relict ilmenite grain that has been extensively replaced by hematite and minor rutile. Secondary hematite has also overgrown the ilmenite. NOG is Non-Opaque Gangue. C) = A backscattered electron image illustrating the typical appearance of this sample. The matrix is dominated by dolomite (lower right portion of image). The upper left portion of the image is dominated by relict clasts that have been extensively replaced by Mn-rich oxides/hydroxides. D= A backscattered electron image illustrating replacement of the host rock by MnAl-hydroxide and a Mn Ba-oxide, ideally $Ba(Mn_4+,Mn^{2+})_8O_{16}$.

The Dipeta host rock also exhibits some degree of replacement by secondary Mn-oxides/hydroxides that display a distinctive black appearance in hand specimen (Figures 31 C and D). These secondary Mn-rich phases may partially replace the matrix, infill cavities and

also the clay-rich clasts. Two distinct manganese phases were observed including an unidentified MnAl-oxide/hydroxide.

4.2.3.4 Silicates

Microscopic observation shows very fine-grained clasts consisting largely of clays smectite and kaolinite groups, although very fine chlorite may also be present. The chlorite undifferentiated from kaolinite on the SEM and is also associated with subordinate amounts of muscovite and fine-grained quartz (Figures 32 A). SEM examination of the clay clasts confirms that they consist predominantly of a MgAlSi-rich clay that probably represents a mixture of smectite and kaolinite/serpentine group clay. The muscovite is typically very fine-grained and may exhibit a preferred orientation. The clasts often illustrate a delicate layering that may, in part, reflect primary detrital depositional textures. The SEM analysis also identified sericite, with morphology indicative of replacement of detrital feldspar (Figure 32 B). Pyrophyllite exhibits a pale cream colour in the hand specimen and is a common accessory phase in these samples, occurring predominantly along the contact between the clasts and dolomite matrix. The pyrophyllite is often intimately associated with the smectite group clay, and appears to be partially replaced by the smectite.

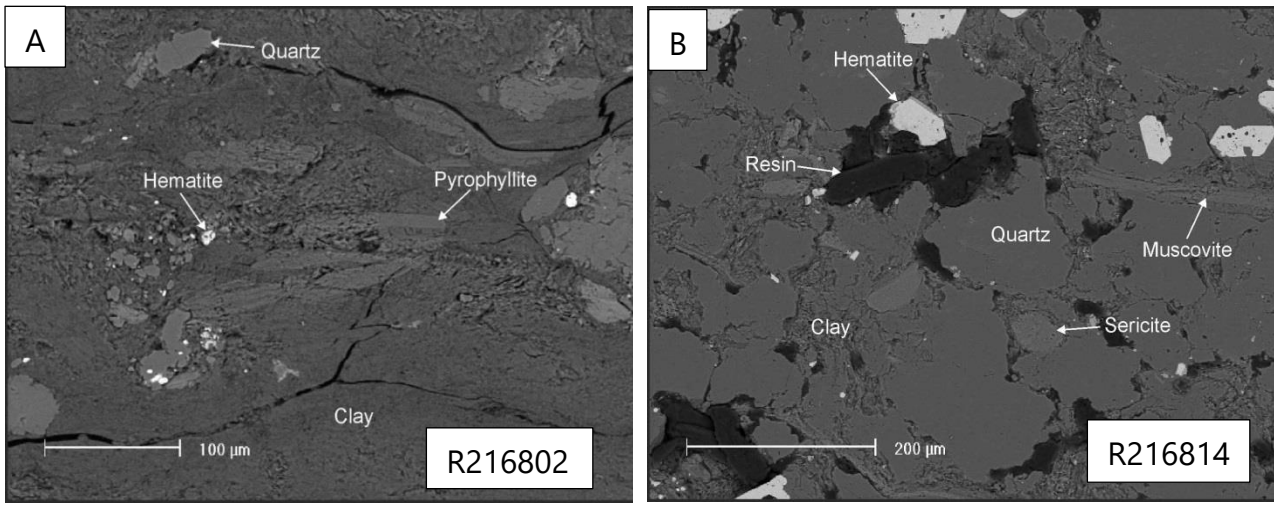

Figure 32: A) = A backscattered electron image illustrating pyrophyllite laths in the fine-grained clay. The pyrophyllite appears to be partially replaced by the clay. B) = The area shown illustrating sericite (fine-grained muscovite) in the heavy mineral layer. The sericite might indicate originally detrital feldspar replaced by sericite/muscovite.

Accessory minerals observed include zircon and xenotime (Figures 33 A). The zircon and xenotime are most abundant in the heavy mineral layers and are often intergrown with the altered FeTi-oxides. The zircon and xenotime probably represent relict resistant detrital phases. Euhedral zircons may be overgrown with hematite, such that. Trellis-like textures in the hematite consisting of fine lamellae of rutile suggest that aggregate was formerly Ti-magnetite that has been replaced and overgrown by hematite (Figure 33 B).

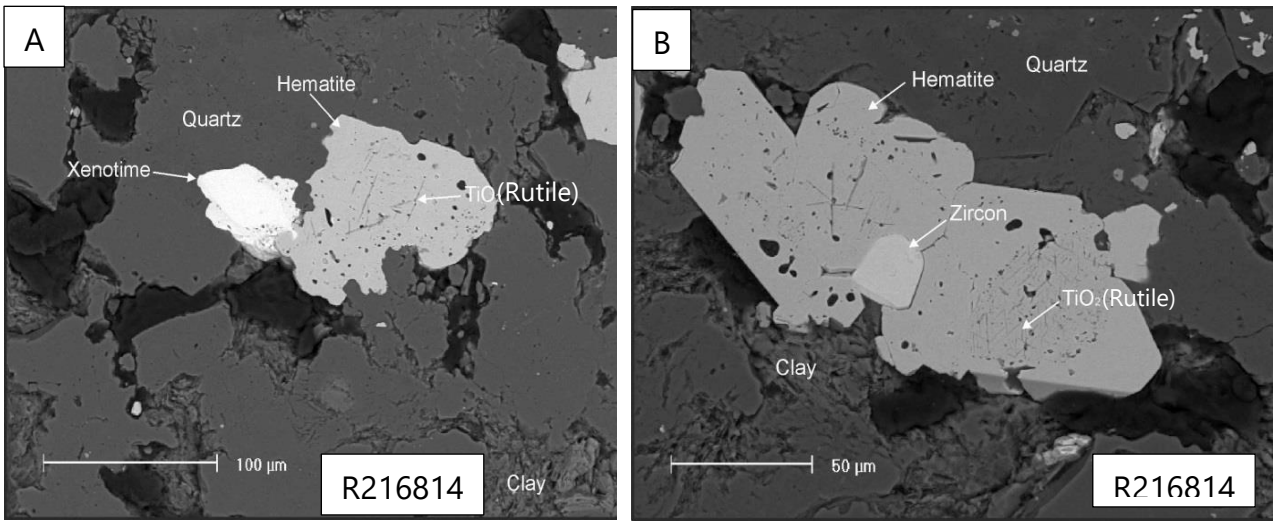

Figure 33: A) = the image illustrating hematite (after FeTi-oxide), coarse detrital quartz and xenotime in the heavy mineral layer. The xenotime probably represents a relict resistate phase that is also detrital in nature. B) = The presence of a zircon overgrowth with hematite. Trellis-like textures in the hematite consist of fine lamellae of TiO_2 and suggest this aggregate was formerly Ti-magnetite that has been replaced and overgrown by hematite.

4.2.3.5 Sulphate

The XPL microscopic observation exhibits a perfect association between the euhedral quartz and the accessory anhydrite, observed as inclusions. The quartz might demonstrate a progressive replacement by clay minerals. The spheroidal textural of the dolomite is common and reflects compositional zoning (Figure 34).

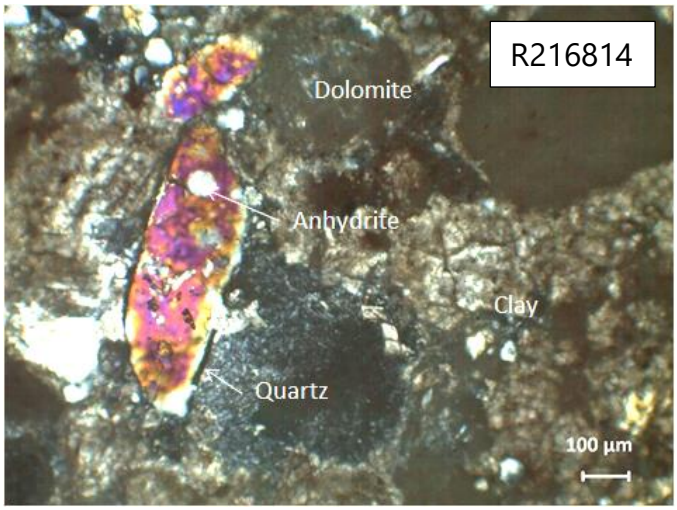

Figure 34: XPL observation indicates an anhydrite inclusion with partial replacement of quartz by clay minerals. Anhydrite is present as an accessory phase. Spheroidal dolomite may reflect zoning.

Chapter 5: Geochemistry

The geochemical work is intended to facilitate the application of known mineralogical influences on the geochemistry analysis diagrams in order to distinguish between the R.A.T. and Dipeta units. The geochemical analysis of the carbonates will focus on the potential influence of the dolomite or magnesite minerals, while for silicates, mineral control by micas, albite, feldspars, and clays will be highlighted.

5.1 Major elements

A summary of compositional ranges for R.A.T. and Dipeta siltstones is shown in the Table 1 while, a detail of the major element data is given in Table 2 below. The raw geochemical data are provided as Appendix 5. The major element compositions for siltstones of R.A.T. and Dipeta are summarised as follows: - The R.A.T. contains 12–13 wt.% Al_2O_3, 48–49 wt.% SiO_2, 11–15 wt.% MgO and total alkali (Na_2O+K_2O) values of >1 wt.%, a Fe_2O_3 concentrations comprise between 2–5 wt.% and CaO content is <5 wt.% in the R.A.T. By contrast, the Dipeta samples are characterised by high MgO contents ranged between16 -21 wt.% versus low total alkali (Na_2O+K_2O) <0.5 wt. % with large variation of Al_2O_3 and high CaO concentrations (2–12 wt. % and 3 – 21 wt. % respectively), and 18 – 45 wt. % SiO_2.

Major element oxides	**R.A.T.** (wt. %)	**Dipeta** (wt. %)
SiO_2	48 - 49	18 - 45
Al_2O_3	12 - 13	2 -12
MgO	11-15	16 - 21
CaO	<5	3 - 21
Fe_2O_3*	2 - 5	2 - 3
$K_2O + Na_2O$	>1	<0.5

Table 1: Summary of compositional ranges for the R.A.T. and the Dipeta siltstones for major element oxide. * = total iron as Fe_2O_3.

The high silica content in the R.A.T stratigraphic unit can partly be ascribed as an intense silicification alteration of hangingwall expressed by a presence of Mines Subgroup units. The average loss on ignition (LOI) is 12 wt.% for the R.A.T and 22 wt.% for the Dipeta and

show more potential for sulphides and carbonate compounds in Dipeta unit. Therefore, the existing carbon is assumed to belong to the carbonate minerals. Correlation coefficients between the major elements are illustrated in the Table 3. Many elements have clear positive linear correlation coefficients with potassium and aluminium, suggesting that the abundances of these elements are primarily controlled by alumina−silicate minerals such as clays and feldspars.

5.2 Trace elements

Trace element concentrations are presented in Table 2. Among elements analysed, three (SiO_2, TiO_2, and Sc) show relatively good correlation with Al_2O_3 both in the R.A.T and in the Dipeta units. The TiO_2 component is common in sedimentary suites, due to primary control of detrital depositional. The CaO, C, and LOI (Loss of Ignition) are negative correlated with Al_2O_3 and poorly correlated with MgO elements and might express a low carbonate component in the R.A.T samples, while in contrast, the Dipeta samples appears dolomitic with relatively high value of CaO<20wt.% and MgO<20wt.%, respectively (Table 2 and 3).

Incompatible trace elements (Ga, Gd, Hf, Li, Nb, Nd, Pr, Sm, Ta and Th) indicate a significant correlation with Al_2O_3 in Dipeta, suggesting that their abundances might be controlled by stratigraphic domain, conversely the same elements are poorly correlated within the R.A.T. unit. (Table 3). Transition elements typically occur in trace amounts in sedimentary rocks. Here, Cu and Co are found in relatively significant concentrations in the R.A.T., ranged with an average of 0.43_ppm while in opposite, the copper is less than 15_ppm in the Dipeta unit (Table 2). Cobalt and nickel concentrations display the same chemical trends, with the highest average values of cobalt (<70_ppm) recorded in R.A.T. while in contrast the highest average values of nickel (<60_ppm) is noted in Dipeta (Table 2).

Table 2: Average major and trace element concentrations for different regions of R.A.T. and Dipeta stratigraphic units.

Strat. Code	RATKHL	RAT KNS	RAT SM	Av. RAT	DIP KHL	DIP KNS	DIP SM	Av. DIP	HBX KHL	HBX KNS	HBX SM	Av. HBX
n	28	16	13	57	55	3	11	69	8	1	15	24
SiO_2_wt.%	48.189	49.144	48.569	48.634	45.789	37.767	18.449	34.002	43	40.5	36.367	39.956
TiO_2_wt.%	0.699	0.691	0.698	0.696	0.53	0.44	0.135	0.368	0.661	0.54	0.701	0.634
Al_2O_3_wt.%	12.8	12.643	12.416	12.62	12.563	11.003	2.218	8.595	12.221	11.6	9.533	11.118
Fe_2O_3_wt.%	5.653	1.959	4.878	4.163	3.079	6.29	1.948	3.772	6.42	4.87	8.299	6.53
MgO_wt.%	11.993	15.756	14.569	14.106	16.965	21.833	19.059	19.286	11.646	17.95	16.497	15.365
CaO_wt.%	4.845	4.731	4.816	4.797	5.317	3.897	21.29	10.168	6.935	7.13	8.995	7.687
Na_2O_wt.%	0.052	0.036	0.048	0.045	0.027	0.023	0.048	0.033	0.071	0.04	0.043	0.052
K_2O_wt.%	3.716	0.763	1.507	1.995	0.137	0.025	0.417	0.193	3.262	0.005	0.322	1.196
P_2O_5_wt.%	0.161	0.157	0.147	0.155	0.136	0.12	0.052	0.103	0.134	0.13	0.149	0.137
LOI_wt.%	11.566	13.019	12.192	12.259	14.982	18.45	35.328	22.92	14.499	16.85	18.763	16.704
Cu_ppm	10.286	36.188	83.846	43.44	11.727	6	23.364	13.697	55	40	19	38
Ni_ppm	29.464	59.688	36.846	41.999	32.418	148	8.682	63.033	30.875	114	48.6	64.492
Cr_ppm	58.571	65	71.538	65.037	56.182	56.667	47.273	53.374	51.25	60	67.333	59.528
Co_ppm	15.893	133.938	62.538	70.79	8.255	16.667	7.5	10.807	15.875	37	25.933	26.269
V_ppm	92.571	92.25	95.231	93.351	49.382	61	20.591	43.658	85.75	85	144	104.917
Rb_ppm	116.482	25.663	62.915	68.353	5.087	0.667	14.218	6.657	84.775	0.4	11.44	32.205
Ba_ppm	279.089	227.313	139.154	215.185	27.8	56.033	80.555	54.796	101.15	24.3	30.48	51.977
Zr_ppm	238	267.625	270.846	258.824	132.018	120.667	56.182	102.956	259.25	156	122	179.083
Ag_ppm	0.293	0.25	0.25	0.264	0.25	0.25	0.473	0.324	0.25	0.25	0.25	0.25
As_ppm	4.064	5.5	7.262	5.609	3.198	4.133	4.191	3.841	2.888	4.4	15.553	7.614
BaO_wt.%	0.03	0.024	0.014	0.023	0.006	0.007	0.01	0.008	0.012	0.005	0.006	0.008
Bi_ppm	0.156	0.064	0.139	0.12	0.012	0.013	0.116	0.047	0.315	0.02	0.009	0.115
C_wt.%	1.951	2.104	1.932	1.995	2.217	3.533	9.207	4.986	2.891	2.94	3.722	3.184
Cd_ppm	0.25	0.25	0.365	0.288	0.25	0.25	0.25	0.25	0.281	0.25	0.627	0.386
Ce_ppm	92.832	28.225	71.523	64.193	80.316	102.533	14.5	65.783	84.4	45.8	32.88	54.36
Cr_2O_3_ppm	76.786	88.75	93.846	86.461	74.545	83.333	76.364	78.081	71.25	90	88.667	83.306
Cs_ppm	2.676	0.595	1.426	1.566	0.592	0.037	1.031	0.553	1.568	0.07	0.685	0.774
Dy_ppm	6.426	6.538	6.35	6.438	3.865	14.883	1.016	6.588	5.773	37.2	3.605	15.526

Strat. Code	RATKHL	RAT KNS	RAT SM	Av. RAT	DIP KHL	DIP KNS	DIP SM	Av. DIP	HBX KHL	HBX KNS	HBX SM	Av. HBX
n	28	16	13	57	55	3	11	69	8	1	15	24
Er_ppm	3.634	3.693	3.99	3.772	2.305	8.533	0.59	3.809	3.274	23.6	2.437	9.77
Eu_ppm	1.619	0.973	1.552	1.381	1.147	2.387	0.242	1.259	1.491	3.99	0.761	2.081
Ga_ppm	19.182	22.013	20.777	20.657	7.751	17.633	3.364	9.583	17.925	24.9	10.82	17.882
Gd_ppm	6.777	5.893	7.37	6.68	4.668	11.403	1.107	5.726	6.349	21.6	3.181	10.377
Ge_ppm	2.5	2.5	2.5	2.5	2.5	2.5	2.5	2.5	2.5	2.5	2.667	2.556
Hf_ppm	6.389	6.963	7.3	6.884	3.558	3.267	1.045	2.623	4.963	4.2	3.12	4.094
Hg_ppm	0.007	0.019	0.009	0.011	0.003	0.007	0.01	0.006	0.003	0.015	0.007	0.008
Ho_ppm	1.236	1.311	1.307	1.285	0.766	3.22	0.213	1.4	1.13	8.58	0.809	3.506
In_ppm	0.022	0.011	0.01	0.014	0.048	0.021	0.029	0.033	0.172	0.033	0.019	0.075
La_ppm	45.882	15.731	34.046	31.887	47.675	152.2	6.527	68.801	45.275	32.2	21.94	33.138
Li_ppm	152.857	213.75	303.077	223.228	95.818	176.667	50.909	107.798	93.75	210	162.667	155.472
Lu_ppm	0.482	0.508	0.538	0.509	0.337	1.01	0.08	0.476	0.409	2.93	0.355	1.231
MnO_ppm	735.714	331.25	469.231	512.065	1143.636	1866.667	636.364	1215.556	1875	2600	806.667	1760.556
Mo_ppm	1.589	2.156	3.308	2.351	0.873	1	0.955	0.942	0.938	1	0.7	0.879
Nb_ppm	28.325	30.644	31.277	30.082	13.442	11.533	3.191	9.389	18.35	15.5	12.2	15.35
Nd_ppm	41.493	13.15	32.715	29.119	33.86	76.167	6.791	38.939	38.238	37.6	15.46	30.433
Pb_ppm	4.036	4.063	7.231	5.11	1	1.333	3	1.778	1.375	1	4.267	2.214
Pr_ppm	10.79	3.443	8.628	7.62	9.177	23.713	1.711	11.534	9.953	8.99	4.222	7.722
Re_ppm	0.001	0.002	0.007	0.003	0.001	0.001	0.001	0.001	0.001	0.001	0.001	0.001
S_wt.%	0.019	0.141	0.063	0.074	0.01	0.013	0.014	0.012	0.021	0.02	0.014	0.019
Sb_ppm	0.186	0.095	0.103	0.128	0.025	0.053	0.522	0.2	0.034	0.05	0.171	0.085
Sc_ppm	12.036	12.938	11.769	12.247	9.145	16	2.545	9.23	11.625	25	13.2	16.608
Se_ppm	0.139	1.006	2.038	1.061	0.115	0.1	0.118	0.111	0.138	0.1	0.593	0.277
Sm_ppm	7.926	3.77	7.234	6.31	6.177	9.103	1.425	5.569	7.648	10.05	3.184	6.961
Sn_ppm	3.5	5	4.923	4.474	1.364	4	1.045	2.136	2.5	3	2.367	2.622
Sr_ppm	57.85	120.681	38.415	72.316	109.685	124.033	204.709	146.143	94.388	75.4	242.007	137.265
SrO_ppm	0.009	0.013	0.005	0.009	0.014	0.008	0.019	0.014	0.013	0.005	0.026	0.015
Ta_ppm	1.982	1.963	2.031	1.992	1.007	0.8	0.241	0.683	1.375	1.1	0.823	1.099
Tb_ppm	1.049	1.089	1.174	1.104	0.648	2.19	0.162	1	1.016	4.95	0.571	2.179
Te_ppm	0.023	0.064	0.017	0.035	0.009	0.005	0.008	0.007	0.02	0.01	0.014	0.015
Th_ppm	14.37	14.159	16.385	14.971	12.849	11.983	2.075	8.969	15.794	14.6	9.146	13.18

Strat. Code	RATKHL	RAT KNS	RAT SM	Av. RAT	DIP KHL	DIP KNS	DIP SM	Av. DIP	HBX KHL	HBX KNS	HBX SM	Av. HBX
n	28	16	13	57	55	3	11	69	8	1	15	24
Tl_ppm	0.052	0.036	0.028	0.039	0.011	0.01	0.038	0.02	0.029	0.01	0.012	0.017
Tm_ppm	0.511	0.529	0.561	0.534	0.339	1.143	0.083	0.522	0.46	3.25	0.361	1.357
U_ppm	5.108	4.912	8.942	6.32	2.826	1.043	13.478	5.783	3.625	1.29	3.654	2.856
W_ppm	2.179	2.75	2.385	2.438	2.091	2	1.818	1.97	2	2	2.533	2.178
Y_ppm	32.586	32.625	35.569	33.593	23.405	79.9	5.345	36.217	30.75	211	23.367	88.372
Yb_ppm	3.341	3.351	3.599	3.43	2.245	7.077	0.53	3.284	2.911	19.9	2.318	8.376
Zn_ppm	27.464	7.063	23.615	19.381	6.127	10.333	74.364	30.275	203	14	37.2	84.733
SiO_2/Al_2O_3	3.776	3.894	3.924	3.865	3.644	3.438	30.876	12.652	3.514	3.491	4.588	3.864
K_2O/Na_2O	71.473	20.911	30.896	41.094	4.307	1.222	6.572	4.034	42.385	0.125	6.292	16.267
K_2O/Al_2O_3	0.294	0.061	0.12	0.159	0.01	0.002	0.406	0.14	0.258	0	0.049	0.102
Na_2O/K_2O	0.015	0.203	0.038	0.086	1.562	2.389	0.286	1.412	0.519	8	1.858	3.459
TiO_2/Zr	0.003	0.003	0.003	0.003	0.004	0.004	0.001	0.003	0.003	0.003	0.005	0.004
La/Sc	3.84	1.161	2.941	2.647	5.37	9.259	2.04	5.556	4.034	1.288	1.811	2.377
Th/SC	1.198	1.095	1.408	1.234	1.511	0.77	0.568	0.95	1.369	0.584	0.774	0.909
Cr/Ni	2.657	1.549	2.662	2.289	2.383	0.56	40.468	14.471	2.357	0.789	2.612	1.92

*Note that the iron is presented as total Fe (ΣFe) given as Fe_2O_3.

Table 3: Correlation matrix of selected major and trace elements.

[Visible] RAT KHL RAT KNS RAT SM

Correlation - 57 r...	Al2O3_pct	MgO_pct	CaO_pct	C_pct	Ga_ppm	Gd_ppm	Hf_ppm	In_ppm	Li_ppm	LOI_pct	Nb_ppm	Nd_ppm	Sc_ppm	Se_ppm	SiO2_pct	Sm_ppm	Ta_ppm	Th_ppm	TiO2_pct
Al2O3_pct	1	-0.02	-0.89	-0.9	0.57	0.0018	-0.051	-0.46	0.1	-0.9	0.057	0.11	0.61	-0.28	0.83	0.069	0.15	0.41	0.7
MgO_pct	-0.02	1	-0.21	-0.13	0.42	0.085	0.24	-0.46	0.62	0.17	0.22	-0.37	0.029	0.058	-0.058	-0.34	0.12	-0.017	-0.28
CaO_pct	-0.89	-0.21	1	0.98	-0.61	-0.19	-0.1	0.57	-0.31	0.92	-0.21	-0.11	-0.56	0.16	-0.84	-0.13	-0.26	-0.48	-0.61
C_pct	-0.9	-0.13	0.98	1	-0.55	-0.21	-0.11	0.52	-0.3	0.95	-0.21	-0.21	-0.53	0.17	-0.85	-0.22	-0.28	-0.52	-0.61
Ga_ppm	0.57	0.42	-0.61	-0.55	1	0.05	0.35	-0.62	0.54	-0.44	0.41	-0.39	0.35	0.0021	0.69	-0.36	0.36	0.38	0.42
Gd_ppm	0.0018	0.085	-0.19	-0.21	0.05	1	0.74	-0.11	0.26	-0.19	0.75	0.45	-0.13	-0.24	0.13	0.63	0.78	0.57	-0.087
Hf_ppm	-0.051	0.24	-0.1	-0.11	0.35	0.74	1	-0.17	0.35	-0.032	0.97	0.048	-0.12	-0.12	0.23	0.2	0.94	0.36	-0.11
In_ppm	-0.46	-0.46	0.57	0.52	-0.62	-0.11	-0.17	1	-0.58	0.4	-0.21	0.17	-0.34	-0.055	-0.49	0.13	-0.16	-0.41	-0.32
Li_ppm	0.1	0.62	-0.31	-0.3	0.54	0.26	0.35	-0.58	1	-0.12	0.34	-0.13	0.0069	0.27	0.23	-0.044	0.24	0.4	0.048
LOI_pct	-0.9	0.17	0.92	0.95	-0.44	-0.19	-0.032	0.4	-0.12	1	-0.14	-0.3	-0.53	0.19	-0.87	-0.31	-0.25	-0.53	-0.71
Nb_ppm	0.057	0.22	-0.21	-0.21	0.41	0.75	0.97	-0.21	0.34	-0.14	1	0.083	-0.043	-0.16	0.33	0.23	0.97	0.43	-0.041
Nd_ppm	0.11	-0.37	-0.11	-0.21	-0.39	0.45	0.048	0.17	-0.13	-0.3	0.083	1	-0.069	-0.32	-0.019	0.96	0.22	0.32	0.026
Sc_ppm	0.61	0.029	-0.56	-0.53	0.35	-0.13	-0.12	-0.34	0.0069	-0.53	-0.043	-0.069	1	-0.13	0.54	-0.086	-0.026	0.25	0.59
Se_ppm	-0.28	0.058	0.16	0.17	0.0021	-0.24	-0.12	-0.055	0.27	0.19	-0.16	-0.32	-0.13	1	-0.18	-0.27	-0.28	-0.16	-0.065
SiO2_pct	0.83	-0.058	-0.84	-0.85	0.69	0.13	0.23	-0.49	0.23	-0.87	0.33	-0.019	0.54	-0.18	1	0.0064	0.37	0.53	0.66
Sm_ppm	0.069	-0.34	-0.13	-0.22	-0.36	0.63	0.2	0.13	-0.044	-0.31	0.23	0.96	-0.086	-0.27	0.0064	1	0.34	0.45	0.025
Ta_ppm	0.15	0.12	-0.26	-0.28	0.36	0.78	0.94	-0.16	0.24	-0.25	0.97	0.22	-0.026	-0.28	0.37	0.34	1	0.46	0.031
Th_ppm	0.41	-0.017	-0.48	-0.52	0.38	0.57	0.36	-0.41	0.4	-0.53	0.43	0.32	0.25	-0.16	0.53	0.45	0.46	1	0.39
TiO2_pct	0.7	-0.28	-0.61	-0.61	0.42	-0.087	-0.11	-0.32	0.048	-0.71	-0.041	0.026	0.59	-0.065	0.66	0.025	0.031	0.39	1

[Visible] DIP KHL DIP KNS DIP SM

Correlation - 69 r...	Al2O3_pct	MgO_pct	CaO_pct	C_pct	Ga_ppm	Gd_ppm	Hf_ppm	In_ppm	Li_ppm	LOI_pct	Nb_ppm	Nd_ppm	Sc_ppm	Se_ppm	SiO2_pct	Sm_ppm	Ta_ppm	Th_ppm	TiO2_pct
Al2O3_pct	1	-0.65	-0.96	-0.97	0.51	0.55	0.93	0.37	0.56	-0.96	0.85	0.55	0.66	-0.095	0.94	0.64	0.84	0.92	0.84
MgO_pct	-0.65	1	0.59	0.67	-0.22	-0.17	-0.73	-0.38	-0.074	0.67	-0.62	-0.22	-0.25	0.079	-0.7	-0.42	-0.59	-0.58	-0.66
CaO_pct	-0.96	0.59	1	0.99	-0.59	-0.61	-0.92	-0.35	-0.56	0.99	-0.82	-0.59	-0.7	0.094	-0.97	-0.64	-0.8	-0.86	-0.83
C_pct	-0.97	0.67	0.99	1	-0.57	-0.53	-0.93	-0.37	-0.51	1	-0.82	-0.52	-0.65	0.078	-0.99	-0.61	-0.81	-0.86	-0.84
Ga_ppm	0.51	-0.22	-0.59	-0.57	1	0.51	0.54	0.12	0.45	-0.57	0.46	0.42	0.77	0.0064	0.52	0.42	0.49	0.32	0.63
Gd_ppm	0.55	-0.17	-0.61	-0.53	0.51	1	0.51	0.31	0.55	-0.54	0.46	0.91	0.73	-0.15	0.5	0.88	0.42	0.43	0.7
Hf_ppm	0.93	-0.73	-0.92	-0.93	0.54	0.51	1	0.4	0.45	-0.92	0.89	0.51	0.65	-0.099	0.91	0.59	0.86	0.88	0.81
In_ppm	0.37	-0.38	-0.35	-0.37	0.12	0.31	0.4	1	0.013	-0.37	0.5	0.27	0.35	-0.15	0.35	0.37	0.51	0.39	0.36
Li_ppm	0.56	-0.074	-0.56	-0.51	0.45	0.55	0.45	0.013	1	-0.51	0.44	0.51	0.54	-0.087	0.46	0.45	0.41	0.55	0.4
LOI_pct	-0.96	0.67	0.99	1	-0.57	-0.54	-0.92	-0.37	-0.51	1	-0.81	-0.52	-0.65	0.079	-0.99	-0.62	-0.8	-0.85	-0.84
Nb_ppm	0.85	-0.62	-0.82	-0.82	0.46	0.46	0.89	0.5	0.44	-0.81	1	0.49	0.59	-0.12	0.8	0.55	0.97	0.88	0.72
Nd_ppm	0.55	-0.22	-0.59	-0.52	0.42	0.91	0.51	0.27	0.51	-0.52	0.49	1	0.69	-0.21	0.51	0.95	0.42	0.46	0.74
Sc_ppm	0.66	-0.25	-0.7	-0.65	0.77	0.73	0.65	0.35	0.54	-0.65	0.59	0.69	1	-0.088	0.59	0.66	0.58	0.53	0.73
Se_ppm	-0.095	0.079	0.094	0.078	0.0064	-0.15	-0.099	-0.15	-0.087	0.079	-0.12	-0.21	-0.088	1	-0.091	-0.18	-0.14	-0.14	-0.083
SiO2_pct	0.94	-0.7	-0.97	-0.99	0.52	0.5	0.91	0.35	0.46	-0.99	0.8	0.51	0.59	-0.091	1	0.62	0.77	0.83	0.83
Sm_ppm	0.64	-0.42	-0.64	-0.61	0.42	0.88	0.59	0.37	0.45	-0.62	0.55	0.95	0.66	-0.18	0.62	1	0.48	0.51	0.85
Ta_ppm	0.84	-0.59	-0.8	-0.81	0.49	0.42	0.86	0.51	0.41	-0.8	0.97	0.42	0.58	-0.14	0.77	0.48	1	0.85	0.7
Th_ppm	0.92	-0.58	-0.86	-0.86	0.32	0.43	0.88	0.39	0.55	-0.85	0.88	0.46	0.53	-0.14	0.83	0.51	0.85	1	0.64
TiO2_pct	0.84	-0.66	-0.83	-0.84	0.63	0.7	0.81	0.36	0.4	-0.84	0.72	0.74	0.73	-0.083	0.83	0.85	0.7	0.64	1

The values indicate correlation coefficients (R). A negative value indicates inverse correlation, while a positive value indicates a direct correlation. Values in each case greater or less than -0.9 or 0.9, respectively value, may be regarded as significant.

5.3 R.A.T. Subgroup

150 samples extracted from 4 diamond holes were analysed for major and trace elements. Geochemical characterisation of the R.A.T. Subgroup is presented below from the Kinsevere, Kinsevere Hill and Safety Mineral regions, for comparison with the Dipeta.

5.3.1 Carbonates

The major cations and anions of common carbonate minerals include C, Ca, Mg, and CO_3. The dolomite has a chemistry composition of Ca Mg $(CO_3)_2$. This means, the ratio of Ca/Mg in the dolomite mineral is 1:1 with each cation equal to 0.5, with both axes normalised to C. Similarly, the formula of magnesite is $MgCO_3$, so the ratio of Mg/C is 1. The molar ratio plot such as Ca-mol/kg/C-mol/kg : Mg-mol/kg/C-mol/kg is used to obtain a linear distribution from the composition and proportion of dolomite and magnesite minerals in the host rock.

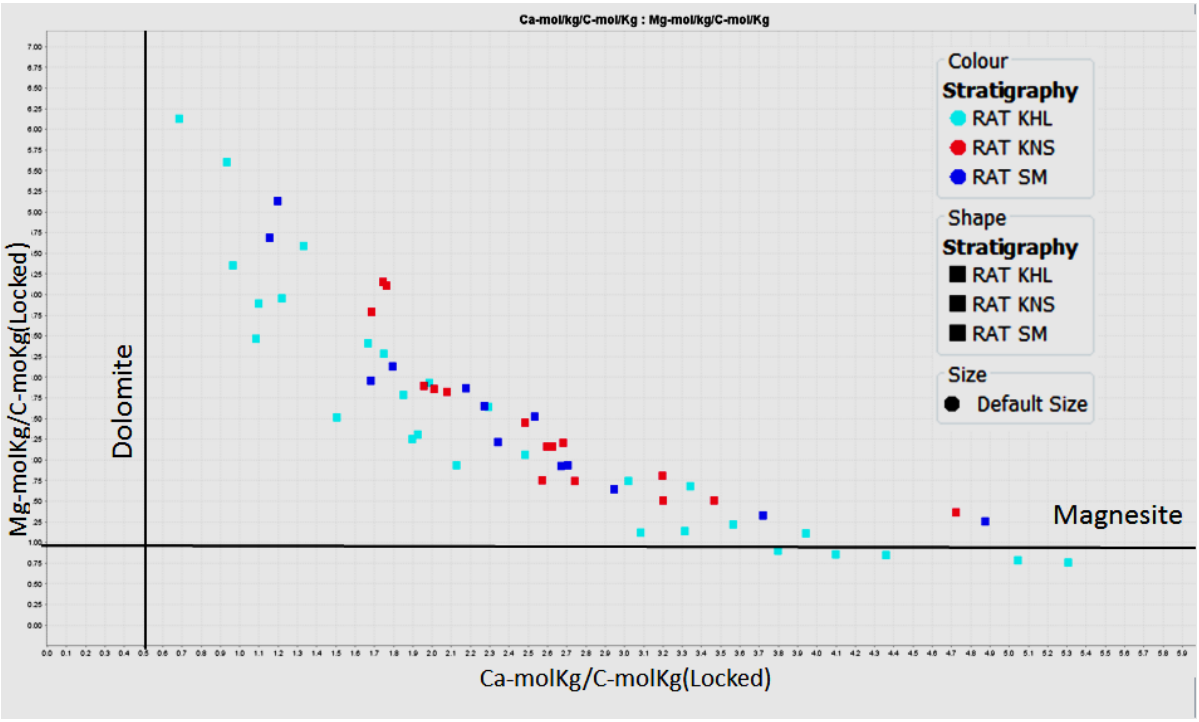

Figure 35: The plot illustrates a distribution correlated to the magnesite and dolomite alteration. A negative trend demonstrates a systematic a depletion of dolomite while the magnesite is enriched in the R.A.T. samples. The R.A.T at Kinsevere Hill appears more dolomitic and magnesitic compare to the remains of samples.

Therefore, the carbonate can be tracked by monitoring with these element ratios as demonstrated in Figure 35. A negative trend demonstrates a systematic depletion of dolomite while the magnesite is enriched in the R.A.T. samples.

5.3.2 Plot of MgO versus CaO

Two carbonate−rich groups are observed from the Kinsevere Hill R.A.T. samples. The first group exhibits a positive trend of correlated MgO and CaO in rocks, passing from low to highly dolomitic clay siltstone (Figure 36 A). The second grouping involving both the Kinsevere Hill, Kinsevere and Safety Mineral R.A.T. which illustrate samples enriched in magnesium mineral while the calcium proportion is decreasing during an alteration phase. Locally, the geochemical plot suggests one or multiple magnesian alteration phases resulted in the formation of fine grained chlorite/ talc/ or montmorillonite minerals (Figure 36 A, 36B and 37 A). The data illustrates that the R.A.T. unit in the studied area is characterised by a major alteration phase resulted on an assembly mineral formed by:-dolomie-magnesite-chlorite minerals (Figure 37B).

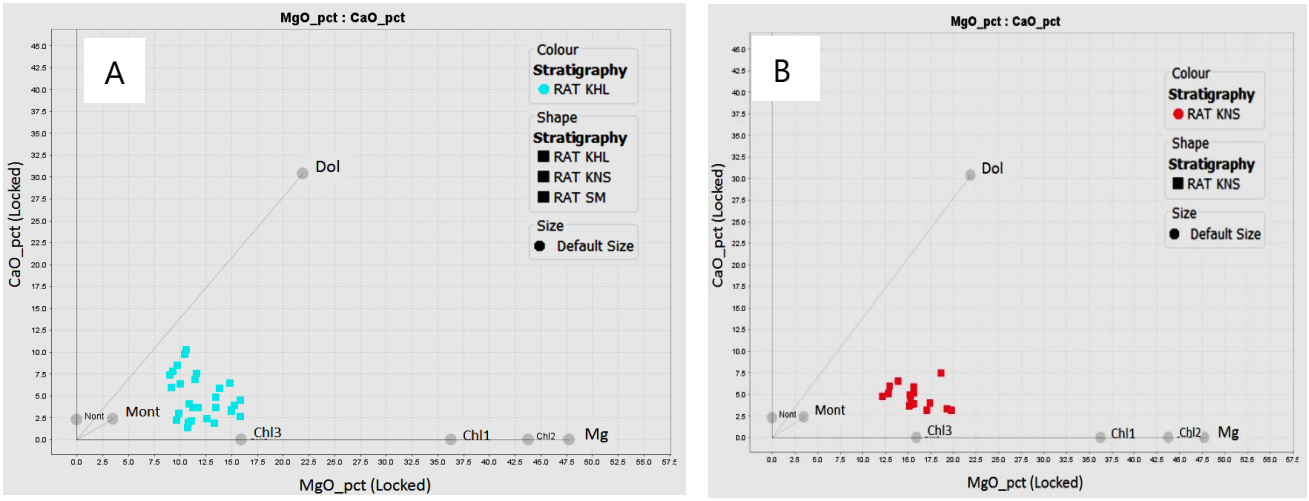

Figure 36: Plots of MgO vs CaO for R.A.T. samples. Compositions of dolomite (Dol), magnesite (Mg), montmorillonite clay (Mont) and Chlorite (Chl) are provided for reference. A) = R.A.T. samples from Kinsevere Hill (KHL) and B) = R.A.T. samples from Kinsevere (KNS).

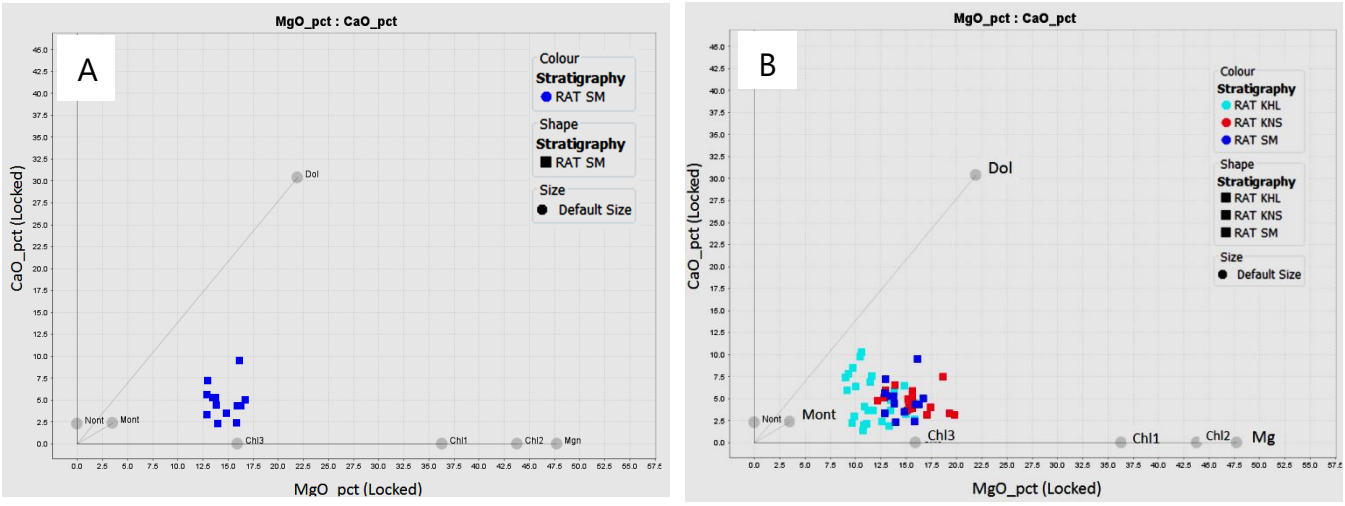

Figure 37: A=Plots MgO vs CaO for R.A.T. samples. Compositions of dolomite (Dol), magnesite (Mg) and montmorillonite clay (Mont) and Chlorite (Chl) are provided for the reference. A) = R.A.T. samples Safety Mineral (SM) and B) = A combined plot for all R.A.T. data from Figure 36 and Figure 37 A.

5.3.4 Silicates

The alteration of original felsic rock on K-feldspars, muscovite and kaolinite (clay) is investigated using molar ratio plots (Davies and Whitehead, 2006). The argillite/arenite proportion in the sample is reflected in the proportions of the molar ratios of K_2O/Al_2O_3 and Na_2O/Al_2O_3. Molar ratio plots such as K_2O/Al_2O_3 and Na_2O/Al_2O_3 can generate a linear distribution from which the composition and proportions of the minerals comprising the arenite and argillite components of these mixed sedimentary rocks can be determined. Various mineralogical assemblages can also be observed. These ratios, along with SiO_2/Al_2O_3, are sufficient to identify the plagioclase compositions and the proportions of K- feldspars, plagioclase, illite and quartz within the sedimentary mixtures (Davies and Whitehead, 1994). Although Davies & Whitehead's plot is designed to visualise alteration trends in K and Na correlated to Al in igneous rocks, the method is used to identify metasomatic patterns in other rocks as well, such as in sedimentary sequences.

Analysis of the molar ratio diagram shows a trend of alteration composes of higher muscovite correlated to Kinsevere Hill samples and clays (kaolinite) associated with the entire R.A.T. unit (Figure 38). The trend indicates a progressive decrease in K during a fluid

alteration at low temperature, with a corresponding enrichment in clay minerals according to the chemical reactions provided by Davies and Whitehead (2006), reproduced here.

The alteration of K-feldspar to muscovite by addition of H^+ and loss of K^+ occurs according to the following reaction:

- $3KAlSiO_8 + 12\ H_2O + 2H^+ = KAl_3Si_3O_{10}(OH)_2 + 2K^+ + 6H_4SiO_4$

Alteration of muscovite to chlorite occurs by addition of Mg^{2+}, Fe^{2+}, OH^- and H_4SiO_4 and loss of K^+:

- $KAl_3Si_3O_{10}(0H)_2 + 15\ (Mg, Fe)OH^+ + 3H_4Si0_4 + 3H_20 = 3(Mg,Fe)_5Al_2SiO_3O_{10}(OH)_8 + 2K^+ + 13H^+$

Alteration of chlorite to clay mineral (kaolinite) occurs as follows:

- $(Mg,Fe)_5Al_2SiO_3O_{10}(OH)_8 + 5CO_2 = 5MgCO_3 + Al_2SiO_5(OH)_4 + 2H_2O$

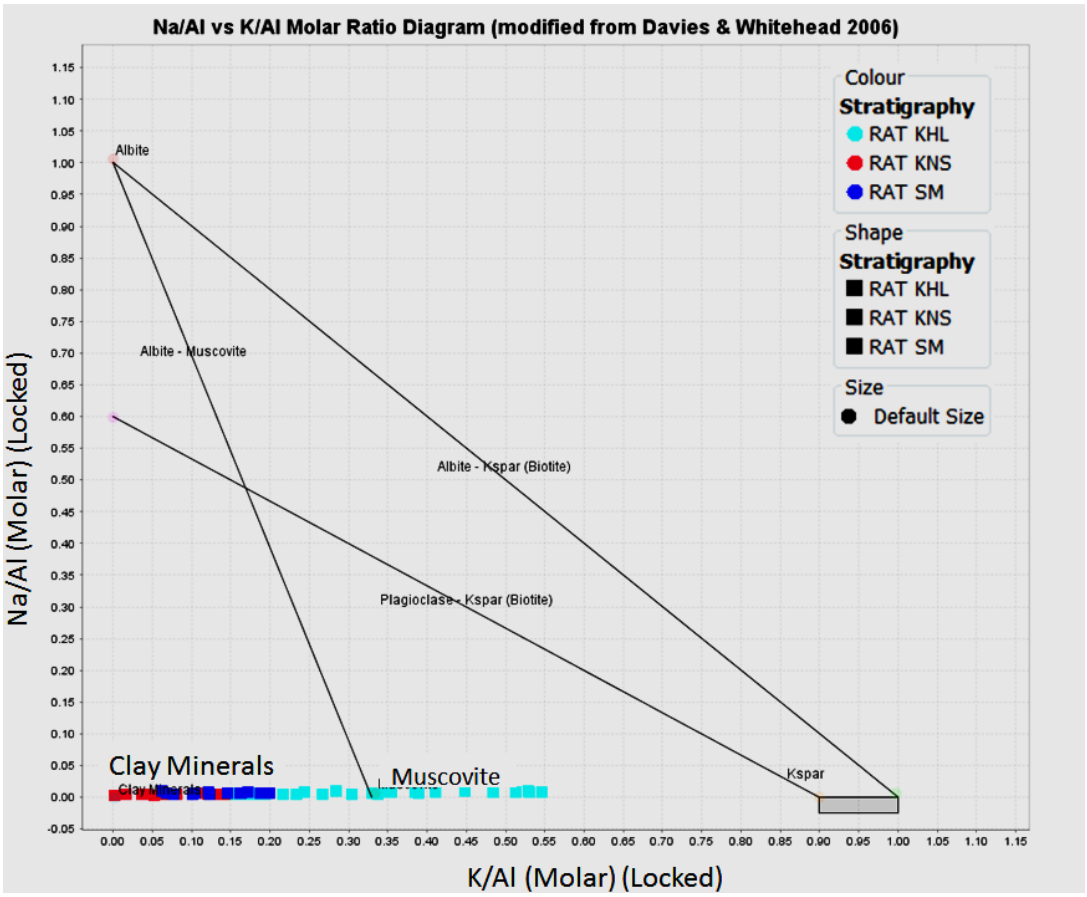

Figure 38: Diagram of Na/Al vs K/Al molar ratio diagram for R.A.T. samples, displaying a depletion of K during the low temperature reactions involving the muscovite and clay minerals.

Chlorite, which is a common phase in highly altered felsic rock, is more usefully displayed on a K_2O/Al_2O_3 vs MgO/Al_2O3 molar ratio plot (e.g. Figure 39), which shows the relationship between muscovite and chlorite. This plot, the alkali–alumina diagram (Figure 39) shows two major alteration trends: - those of muscovite–chlorite and chlorite–K-Feldspars. The first tend indicates the significant chlorite alteration linked to the Kinsevere, Kinsevere Hill and Safety Mineral samples. The Kinsevere Hill presents also a trend evolving from K-Feldspar, muscovite to chlorite alteration. The relative absence of biotite in the R.A.T. is consistent with the diagram and with the petrography description (Chapter 4).

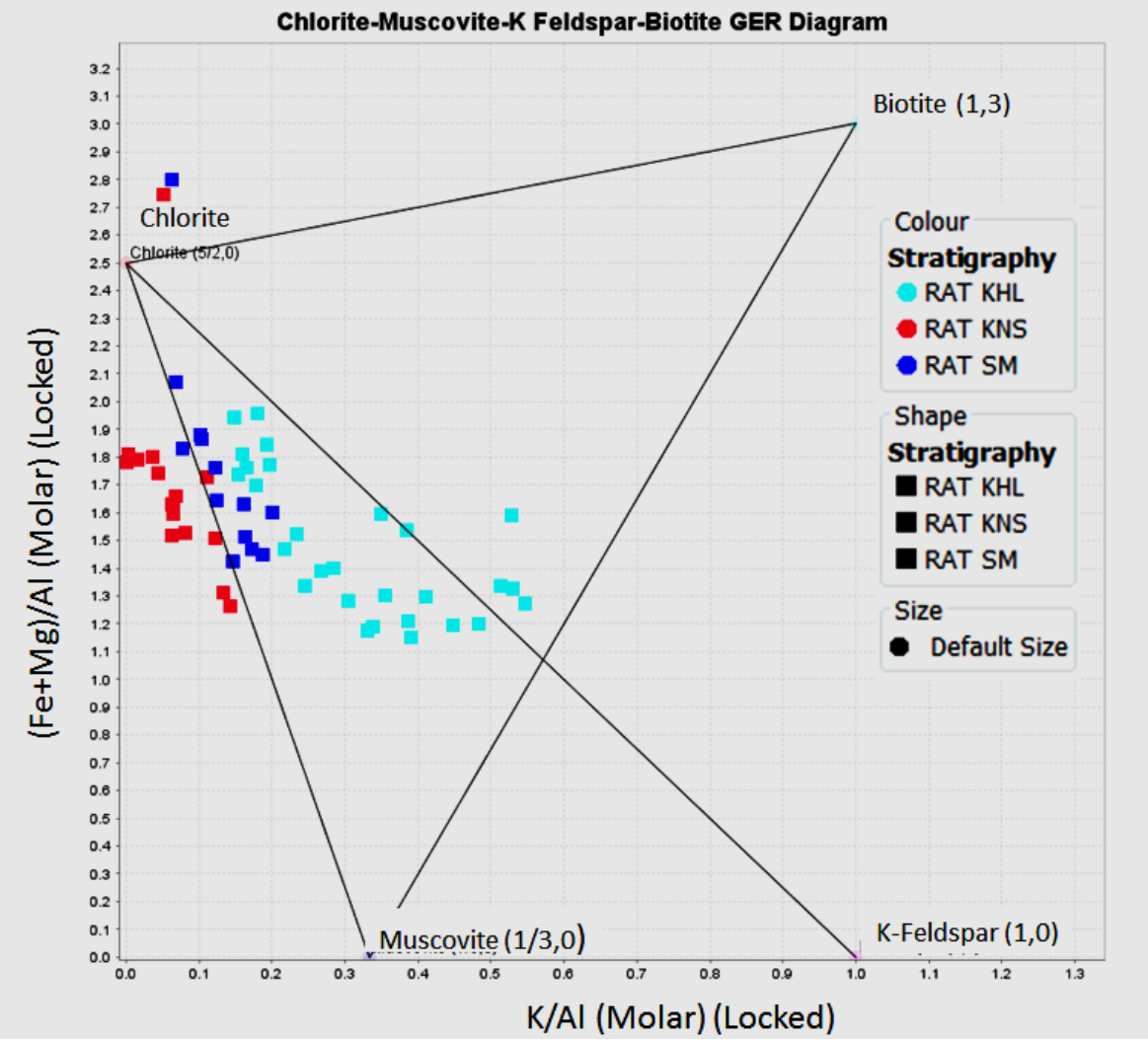

Figure 39: The alkali-alumina diagram for R.A.T. samples, with reference compositions for chlorite-muscovite, K-feldspars and biotite. The sample distribution shows different types of alteration involving mostly the muscovite and chlorite minerals, while the biotite is effectively absent.

5.4 Dipeta Subgroup

The same geochemical approach has been applied for the Dipeta sample set, below.

5.4.1 Carbonates

The same ratios applied to the R.A.T. stratigraphic unit for geochemical studies will be implemented to the Dipeta samples.

5.4.1.1 Plot MgO vs CaO

Two carbonate groups are observed in the Dipeta samples from Safety Mineral. The first group displays a positive trend of correlated MgO and CaO in rocks, passing from low to highly dolomitic rock (Figure 40 A). The second grouping involving the Kinsevere Hill and Safety Mineral Dipeta units illustrates samples enriched in magnesium while the calcium proportion is depleted during an alteration phase. Locally, the geochemical plot suggests one or multiple alteration phases resulted in the formation of clay group minerals of chlorite/ talc or montmorillonite (Figure 40 B, 41A).

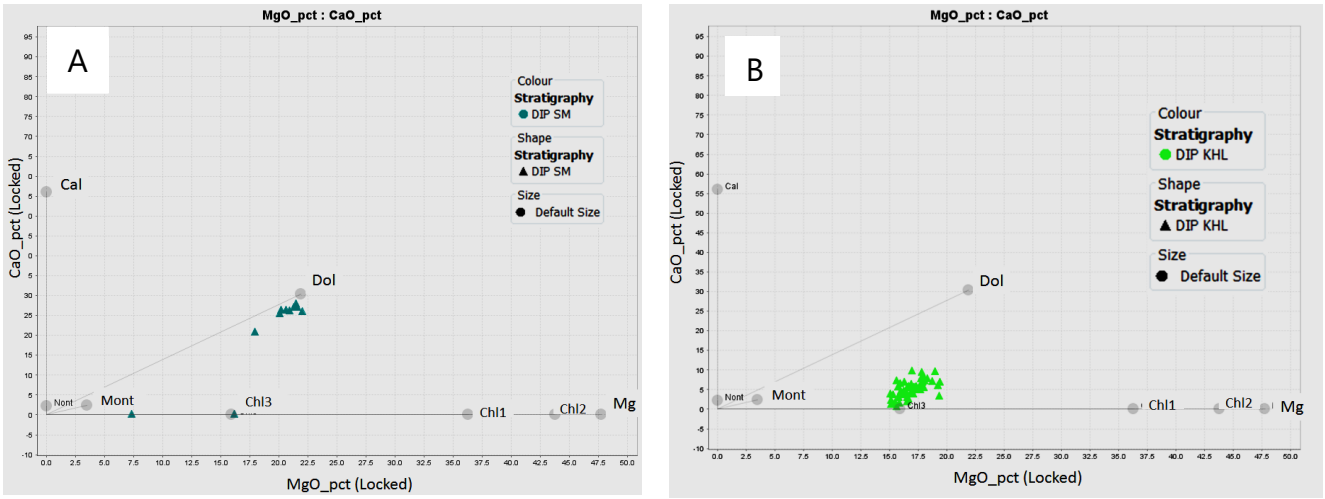

Figure 40 : Plots of MgO vs CaO for Dipeta samples. Composition of dolomite (Dol), magnesite (Mg) chlorite (Chl) and montmorillonite clay (Mont) are provided for reference. A) = Dipeta samples from Safety Mineral (SM). B) = Dipeta samples from Kinsevere Hill.

The data illustrates that the Dipeta unit in the studied area is characterised by two major alteration phases resulted on an assembly mineral formed by magnesite - chlorite minerals and a dolomite alteration phase (Figure 41B).

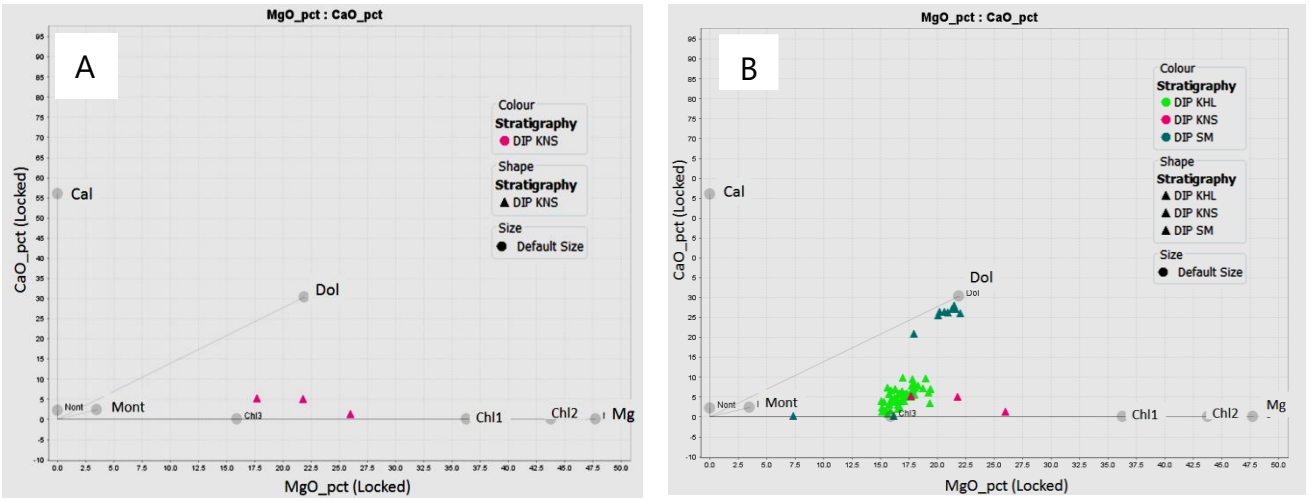

Figure 41: A=Plots MgO vs CaO for Dipeta samples. Composition of dolomite (Dol), magnesite (Mg) chlorite (Chl) and montmorillonite clay (Mont) are provided for reference. A) = Dipeta samples from Kinsevere (KNS), B) = A combined plot of all Dipeta data from Figure 41 and Figure 42 A. This demonstrates the extensive magnesite alteration at Kinsevere and Kinsevere Hill, while the Safety Mineral location remains dolomitic.

5.4.1.2 Mg vs Sr and Ca vs Sr ratios

The calcium and magnesium have a certain chemical coherency and affinity in carbonates and sulphates. The Sr can replace calcium in the carbonate and anhydrite minerals. The distribution by stratigraphic unit illustrates that magnesium and calcium show the largest differences in groups from the studied areas, as observed in the images. The distribution indicates a distinctive stratigraphic marker on the plots of MgO versus SrO and CaO versus SrO.

Three distinctive carbonate groups are observed in the region from the MgO:SrO and CaO:SrO ratios. The figures 42 A and B exhibit samples from Safety Mineral which are characterised by the higher magnesian alteration and high calcium contents in Dipeta stratigraphic unit, which presumes that the unit is more dolomitic (Figure 42 B). In contrast, the Kinsevere Hill samples are moderately enriched in strontium and calcium and appears to correlate chemically with the Kinsevere Dipeta samples (Figure 42B).

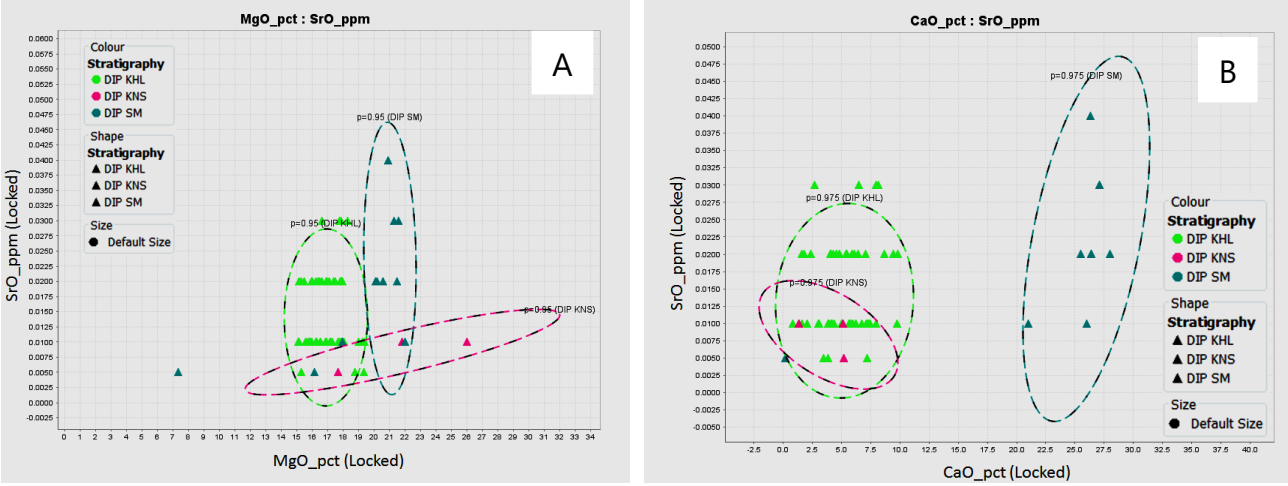

Figure 42: Plots of Sr vs. MgO (A) and CaO (B) for Dipeta samples, illustrating three subgroups according to geographical location.

5.4.2 Silicates

The diagram of silicates alteration is applied to the Dipeta geochemistry data in order to have a reading of minerals association resulted to the alteration process minerals of the molar plot ratio K_2O/Al_2O_3 vs Na_2O/AlO_3 as well as the K_2O/Al_2O_3 vs MgO/Al_2O_3 ratio. The diagrams below exhibit two trends of alteration: - muscovite - clay minerals and K-feldspar-albite-muscovite. The Dipeta samples indicate a trend evolving from K- feldspar- muscovite and clay minerals such as talc, chlorite, smectite and montmorillonite alteration. K-feldspar-albite trend is locally related to the Safety Mineral samples with plagioclase/biotite as formed minerals (Figure 43). The depletion of K in the system of low temperature resulted to a formation of clay minerals as shown by the trend (Figure 43). The same result is observed in the ternary diagram (Al-K-Mg) applied to the Dipeta samples, where the chlorite-rich samples are connected to Kinsevere Hill and Kinsevere region, in contrast, the Dipeta at Safety Mineral is increased in magnesium, which presumes a dolomitic nature (Figure 44).

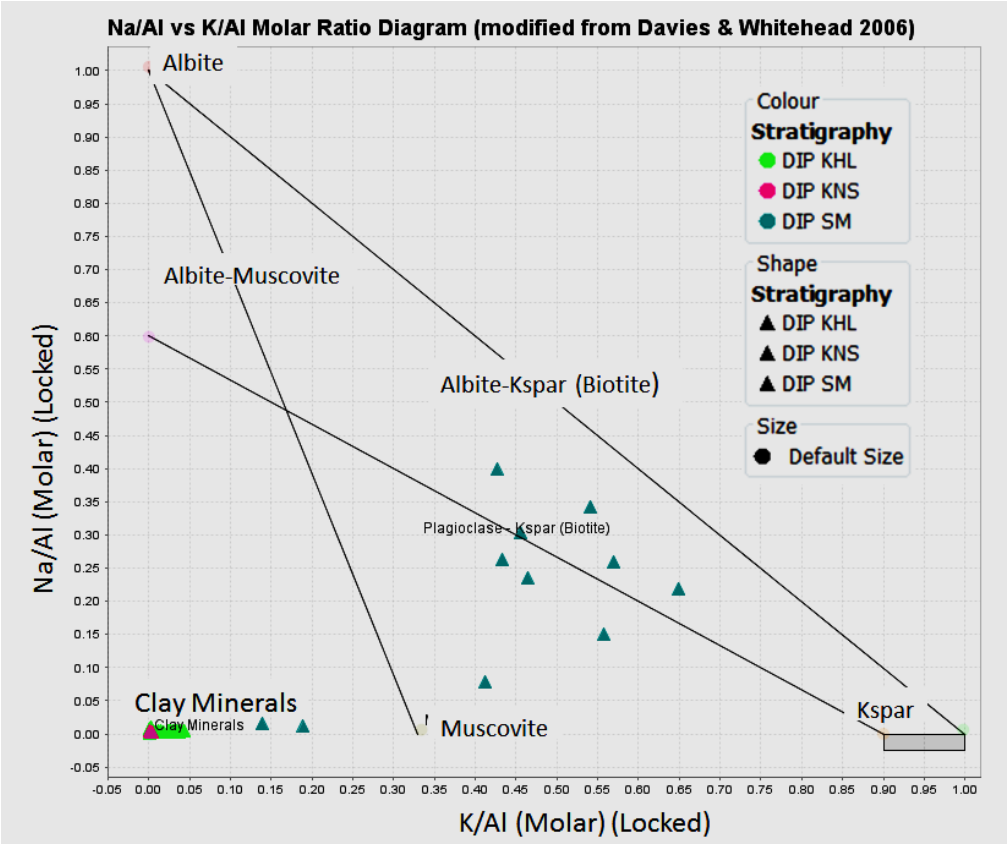

Figure 43: Molar ratio plots alkali-alumina ratios for the Dipeta samples. Compositions K-feldspar, muscovite, chlorite and biotite are provided for reference.

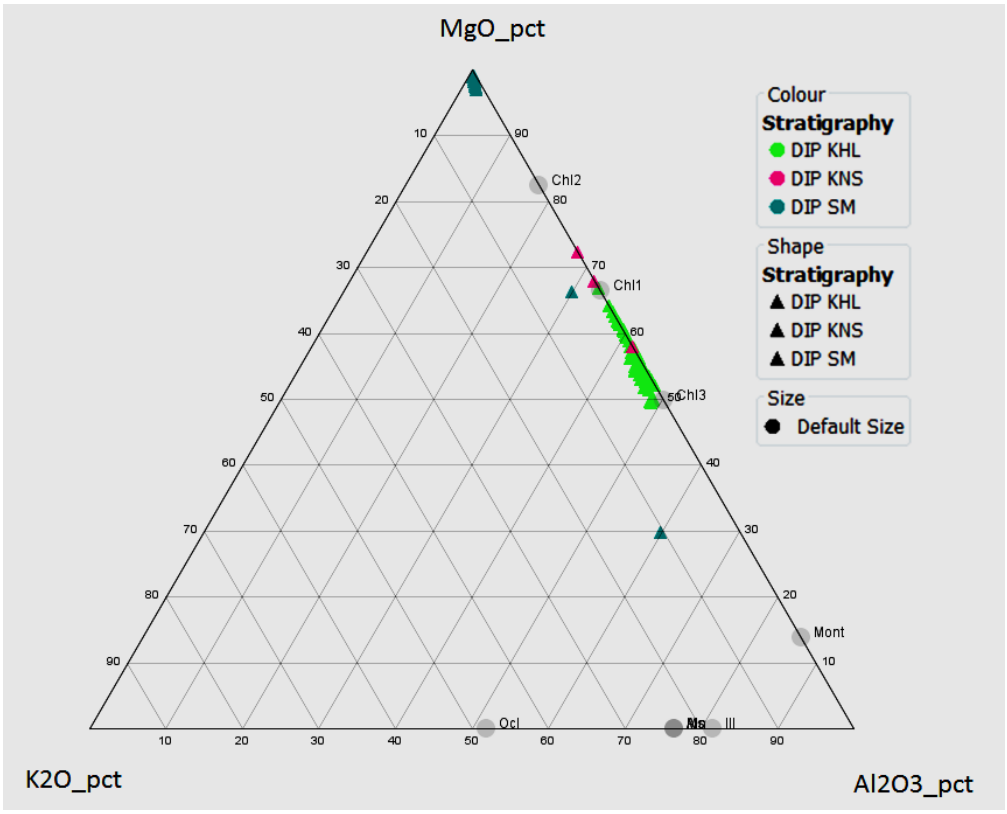

Figure 44: Dipeta samples plotted in the ternary diagram (Al, K, and Mg). Kinsevere Hill samples are highly chloritic with the Safety Mineral samples being highly magnesian or otherwise variable, but not especially chloritic.

5.5 Immobile elements

The most immobile elements analysed are Ti, Zr, Hf, Nb, Ta, Cr, Th, Sc, V, Al, Ce and La. These elements are primarily hosted in resistant heavy minerals such as ilmenite, rutile, zircon, apatite, and spinels. These are minerals that generally survive even intense weathering and alteration, and the elements themselves are not typically soluble in aqueous fluids (which is why the elements are called immobile). Therefore, ratios of these elements represent an important tracer of their protolith rock for distinguishing the depositional environment of the units.

5.5.1 Al_2O_3 to TiO_2 ratio

The Al_2O_3 versus TiO_2 ratio of most clastic rocks can be used to determine the source rock compositions. For example, the Al_2O_3/TiO_2 ratio increases from 3 to 8 for mafic igneous rocks, from 8 to 21 for intermediate rocks, and from 21 to 70 for felsic igneous rocks (Nagarajan et al., 2007). The Dipeta unit shows an Al_2O_3 versusTiO_2 ratio ranges from 16 to 25 with an average value of 23 while the R.A.T increases from 17 to 18 with an average value of 17 (Table 2).

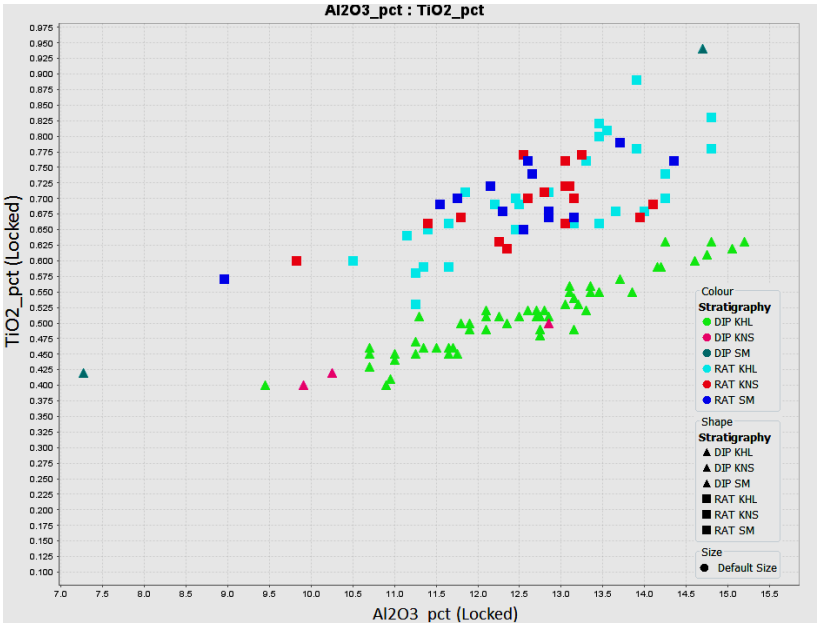

Figure 45: Al_2O_3 vs TiO_2 for R.A.T. and Dipeta samples from this study. The higher elevated TiO_2 values observed in the R.A.T can be attributed to a detrital depositional of the rutile over the basement.

The Al_2O_3/TiO_2 ratio of these suites suggests that intermediate to felsic granitoid rocks are the probable source rocks for R.A.T and Dipeta siltstone formation (Figure 45). The higher

elevated TiO_2 value observed to the R.A.T. can be associated to a detrital depositional of the rutile in the transgressive sequence of R.A.T. setting over the pre- Katangan basement.

5.5.2 TiO_2 vs Cr and Cr vs V

Titanium and vanadium are immobile elements that almost have a linear correlation with Cr. The plot of TiO_2 vs Cr (Figure. 46A) exhibits two distinctive linear trends. One trend, associated with the Safety Minerals samples from Dipeta, shows strong enrichment in chrome, while the second trend illustrates enrichment in TiO_2 associated with the Dipeta and R.A.T. samples. The trend displays a systematic increase in chrome and titanium might correspond to a volcaniclastic or mafic rock source.

Similarly, the plot of Cr vs V (Fig. 46B) also exhibits two distinctive linear trends. The first trend corresponds to the Dipeta samples, which exhibit a significant enrichment in the chromite for a given V content. Vanadium is expected to be strongly adsorbed onto iron oxides where the pH of the equilibrating fluids remains relatively low (Maja A., 2014). The V-enrichment trend might therefore correspond to ilmenite, hematite, magnetite, or sulphides, with iron oxidation associated with alteration.

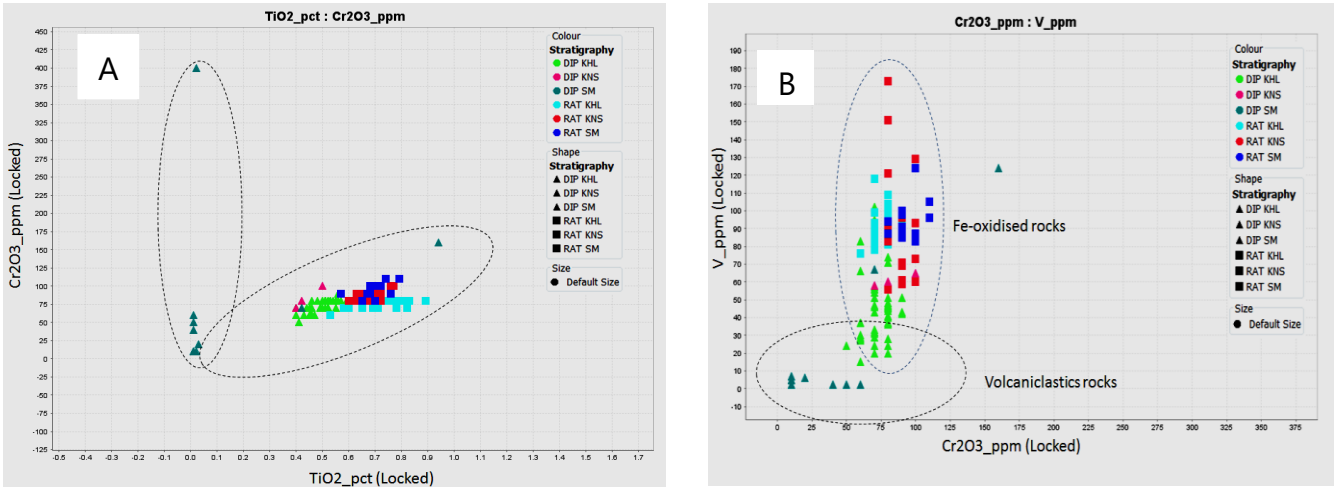

Figure 46: A= Ti vs. Cr. B= Ti vs. V. R.A.T. and Dipeta samples show two distinct trends, corresponding to variations in source and in alteration fluid environments.

Chapter 6: Discussion

The R.A.T is made of syn-diagenetic sediments deposited underneath the Dipeta unit. The contact between the R.A.T. and the Dipeta Subgroups occurred as unconformable tectonic boundary through a heterogeneous breccia made by an argillo-ferroan dolomitic matrix.
The stratigraphic observation between the R.A.T. and Dipeta Subgroups presents almost identical facies as each depositional sequence unit is being characterised predominantly by argillaceous and siliclastic beds (Cailteux, 1994). The R.A.T. Subgroup is made of sandy-argillaceous oxidized dolomitic rocks that are generally fine grained and consists of hematite-rich siliciclastic formations with a dolomitic bed at the top (Cailteux, 1994). Conversely, the Dipeta Subgroup is characterised by predominantly argillaceous and siliciclastic beds at the base and by mostly carbonate beds at the top (François, 1987; Cailteux, 1994).

6.1 Sedimentary provenance: tectonic setting

The most relevant tectonic settings for the sources of Copper Belt sediments include oceanic island arcs, continental island arcs, active continental margins, and passive margins. Of these, the oceanic island arc and continental arc settings represent convergent plate margins. They correspond to some of the tectonic settings of orogenic volcanic rocks, while, active continental margin settings are characterised by plate convergence and orogenic volcanic rocks, and strike-slip continental margins. Sedimentary basins associated with active continental margins may present various characteristic geomorphic settings. However, all these basins are typically associated with thick and elevated continental crust, resulting in strong similarities in derived sediments. The passive margin tectonic setting comprises rifted continental margins of the Atlantic-type developed along the edges of continents; sedimentary basins on trailing continental margins are supplied from orogenic collision.

Immobile trace elements, such as La, Ce, Nd, Th, Zr, Nb, Y, Sc and Cr, may be used to discriminate between tectonic settings. According to Bathia (1986), there is a systematic

increase in light rare earth elements (La, Ce, Nd), Th, Nb and the Ba/Sr, Rb/Sr, La/Y and Ni/Co ratios and a decrease in V, Sc and the Ba/Rb, K/Th and K/U ratios from oceanic island arc to continental island arc to active continental margin to passive margin settings.

The discrimination of the tectonic settings of sedimentary basins can be completed by one of the various combinations including the ternary La-Th-Sc, the ratio Ti/Zr-La/Sc, and La/Y-Sc/Cr (Barthia and Crook 1986). Here the ternary La–Th–Sc diagram has been used to constrain the provenance and tectonic settings for the deposition of the R.A.T. and Dipeta Formations (Figure 47). Sediments from both R.A.T. and Dipeta boreholes plot within the continental island arc as well active and passive continental margins (Figure 48). Results from the ternary diagram indicate that no samples are characterised by the oceanic island arc setting (Figure 47). It's observed that the continental margin samples plot near the La pole with a high La/Sc ratio about 2.6 for the R.A.T. and 5.5 for the Dipeta (Table 2). The continental island arc for the R.A.T. and Dipeta samples plot in between the two fields and have an intermediate La/Sc ratio.

According to Bathia and Crook (1986), Ti/Zr and La/Sc ratios provide an excellent discrimination of the various graywacke types and tectonic settings. Therefore, the oceanic island arc samples are characterised by Ti/Zr ratios generally more than 40 and La/Sc ratios less than 1. As displayed in the Table 2, the Ti/Zr ratio is relatively less than 0.005 for both the R.A.T. and the Dipeta. Thus, no samples are related to the oceanic island arc, as mentioned above. Continental island arc samples are in general characterised by Ti/Zr ratios between 10 and 35, and La/Sc ratios between 1 and 3. La/Sc ratios about 2.6 can be attributed to the R.A.T. and 5.5 to the Dipeta unit. Active continental margins can be discriminated from the continental island arc type by their higher La/Sc ratio, which ranges from 3 to 6. Conversely, the passive margin shows larger variation in the La/Sc ratio and can be distinguished from graywackes (sandstone/siltstone) of other tectonic settings by their Ti/Zr ratio of, generally less than 10, and a higher La/Sc ratio, generally between 3 and 9. The La/Sc ratio reported in Table 2 displays a range between 2.6 and 5.5 attributed to the R.A.T

and Dipeta samples respectively, and therefore is consistent with both the active continental and passive margins tectonic settings (Figure 47).

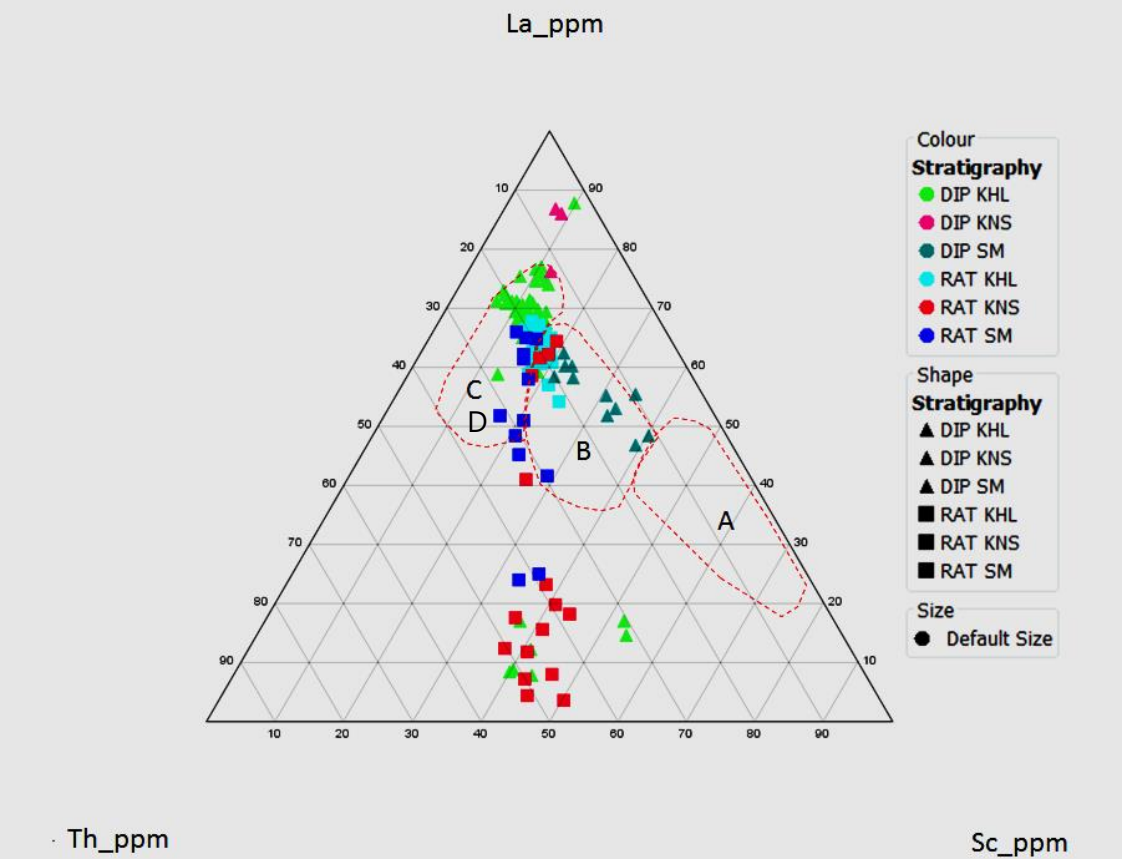

Figure 47: Tectonic setting ternary diagram (La-Th-Sc) for RAT and Dipeta showing tectonic settings delineated as: A: oceanic island arc; B: continental island arc, C: active continental margin and D: passive margins.

6.2 Rock source

The trace element signature (Th, Sc) can also be used to discern the mafic–felsic source component for the sediments formation (Mclennan et al., 1993). The authors show that a low Th/Sc ratio (<1) indicates a mafic source which is usually enriched in Sc compatible elements, while the incompatibility of Th results in higher concentrations at differentiated felsic rocks (Th/Sc >1). In our case study, the Th/Sc ratio is 1.2 for the R.A.T. and around 0.95 in the Dipeta unit (Table 2). However, apart from the Kinsevere, Safety Minerals samples, the values Th/Sc of the Dipeta are 0.77 and 0.56, respectively, suggesting that, the Dipeta formation are derived from dominantly mafic source rock. However, the low Cr/Ni ratios of between 2.2 and 14.4 for each formation (Table 2), are high than the Upper Continental Crust

(1.75) and distinct from the signature of mafic source which requires a Cr/Ni ratio around 8.25 (Taylor and McLennan, 1985). This apparent inconsistency may indicate that not all of these elements have remained immobile in the system.

6.3 Depositional environment

The Roan in Lufilian Belt is characterised by cyclical sedimentations. Lefebre (1978) defined a typical sequence of different depositional litho-facies including: - the alluvial fan, Sabkha, supra to intertidal, lagoonal reef and marine settings. The R.A.T. stratigraphic unit is the first known transgressive sequence deposited over the pre-Katangan basement. The R.A.T. is coarse grained in the lower part and becomes more dolomitic in the upper zone, interpreted as supratidal deposition (Katekesha, 1975). A change from the oxidised to reduced environment defines the beginning of Mines Subgroup, marked mainly by intertidal, reef and lagoonal carbonate sedimentation, which indicate transgressive and regressive cycles (Cailteux, 1994). The Sabkha type sequences are characterised by oxidised sandy argillaceous facies at the bottom, and the lagoonal type carbonate facies is related to the Dipeta Subgroup (Francois, 1987).

The R.A.T., Mines Subgroup as well Dipeta sediments were deposited in a confined evaporitic environment (Katekesha, 1975; Cailteux, 1978, Cailteux et al., 1994). According to Kampunzu et al., 2005, the following features indicate that RAT and Dipeta rocks were deposited in an evaporitic setting:

- Mineral compositions including the association Mg-chlorite, talc, dolomite, magnesite, anhydrite, Mg-tourmaline, scapolite, phlogopite and rare albite.
- The presence of high Li-Mg-chlorites.

6.4 Analysis of primary sedimentary characteristics

On a regional scale, the R.A.T. and Dipeta rocks show substantial increase of SiO_2 and Al_2O_3 from west to east in the study area. This supports the evolutionary trend to more clastic

deposition in south-eastern lithologies, as documented by Cailteux (1994), where clastic sedimentary processes favour Si and Al in residual aluminosilicates as compared to more Ca, Mg and Fe rich chemical sedimentation. The K_2O/Al_2O_3 ratio of sediments can also be used as an indicator of the original composition of ancient sediments. According to Cox et al., (1995), the K_2O/Al_2O_3 ratios for clay minerals and feldspars are indicated by ranges of 0.0 to 0.3 and 0.3 to 0.9 respectively. Therefore, since the R.A.T. exhibits average K_2O/Al_2O_3 ratios of 0.15, while the Dipeta express average K_2O/Al_2O_3 ratios around 0.14, this suggests that while both Dipeta and R.A.T. samples are based on clayey minerals, the Dipeta is more clay-rich than the R.A.T. unit. The relatively high value of MgO and CaO content in both R.A.T. and Dipeta is consistent with the magnesite and dolomitic alteration described earlier, which can define a typical sequence of different depositional litho facies units or a syn-diagenetic depositional environment. The Dipeta contains the largest proportion of depositional carbonate beds at its top (François, 1987; Cailteux, 1994).

A presence of carbonate-quartz pseudomorphs after anhydrite and gypsum indicate an evaporitic environment during the deposition of the uppermost R.A.T. and Mines Subgroups (Katekesha, 1975; Cailteux, 1978, 1994). During Lufilian deformation, the evaporites were variably remobilised and resulted locally in the growth of up to several cubic meter- sized of magnesite aggregate in the R.A.T. and Mines Subgroup (Ngongo, 1975; Cailteux, 1978). The SEM analysis applied to R.A.T. and Dipeta samples exhibits a presence of Ca−sulphate gypsum which is intimately associated with a magnesite in a common phase confirming an evaporitic environment domain.

Oosterboch (1962), recognised 5–6 vol. % of albite in R.A.T. from Fungurume region located to North West of the studied areas, but it is not yet known if it is diagenetic, metamorphic or detrital. However, detrital feldspar represents an important rock component (>5 vol. %) at same area (Oosterbosch, 1962). Conversely, observations made on the petrographic of R.A.T. and Dipeta samples indicate a presence of detrital feldspar grains supposed sodium-plagioclase that has been altered and replaced by the sericite/muscovite minerals. It's known that titanium is mainly concentrated in phyllosilicates (Condie et al., 1992) and is relatively

immobile compared to other elements during various sedimentary processes. It is therefore a potentially useful discriminant of source rocks (McLennan et al., 1993). The Ti_2O value of R.A.T. and Dipeta samples is relatively low, ranging between 0.69 and 0.36. This suggests the presence of highly evolved (felsic) material in the source rocks.

Detrital quartz, feldspar minerals associated with micas, tourmaline, ilmenite; zircon and illite are recognised at 85 vol.%. in the R.A.T. (Oosterbosch, 1962; Katekesha, 1975; Cailteux, 1983). The amounts of these minerals made by previous authors was not consistent with the findings of the current petrographic and XRD studies conducted on the R.A.T. and Dipeta samples, in which the samples are dominated by dolomite, calcite, silica, magnesite and group clay minerals. Therefore, it's important to emphasise that the absence of tourmaline and biotite minerals identified in this study through SEM may be attributed to a low metamorphic grade which does not exceed a stage of anchizone (Oosterbosch, 1962). Conversely, it was observed that the zircon and xenotime are most abundant heavy minerals, often intergrown with the altered FeTi-oxides replaced by a hematite in the Dipeta and R.A.T Subgroups.

The phosphate value is significant in both R.A.T. and Dipeta, with a value of 1550_ppm and 1030_ppm respectively, can be attributed to the presence of moderate amounts of accessory phases, such as apatite and monazite described. The copper content in the R.A.T. samples ranges between 10_ppm to 83_ppm, with an average around 43_ppm. In contrast, Cu content in the Dipeta is lower ranging between 6–23_ppm. The difference may be attributed to leaching processes which has variable effects on the different stratigraphic units. For example, the high copper values in the R.A.T. could be attributed to a process affecting the mineralised immediate hangingwall contact with the Mines Subgroup or by a secondary enrichment from meteoric circulation fluid.

6.5 Diagenetic transformations

The detrital quartz grains are the main constituent mineral in these sediments, rimmed by diagenetic quartz growths with dolomite and diagenetic magnesite-chlorite (Oosterbosch, 1950; Katekesha, 1975). It has been observed that the chlorite in R.A.T. is associated with the matrix, and might result from a diagenetic alteration of the illite mineral (Katekesha, 1975). This argument is consistent with the diagram results of Davies and Whitehead (2006) and supported by the geochemical distribution evident in this study as displayed in alteration diagrams showing chlorite derived from alteration of detrital alumino-silicate minerals in both R.A.T and Dipeta samples (Figures 39 and 43). Pyrophyllite has been described in the Dipeta samples occurring predominantly along the contact between the clasts and dolomite matrix. According to Hemley (1958), the pyrophyllite is made from the reaction between the kaolinite and the quartz at low temperatures and pressures (about 300^{o} and 1000_bars partial pressure of water) by the reaction:

- $Al_2Si_2O_5(OH)_4 + 2SiO_2 = Al_2Si_4O_{10}(OH)_2 + H_2O$

  Kaolinite + Quartz = Pyrophyllite

Also, low grade metamorphism (greenschist facies) can yield the pyrophyllite minerals from alumino-silicates with or without the presence of water (Meyer, 1948), according to the reaction:

$$4K_2Al_4(AlSi_3O_{10})_2(OH)_4 + 8H^+ = 3Al_4(Si_4O_{10})_2(OH)_4 + 6Al_2O_3.H_2O + 8K^+$$

Muscovite = pyrophyllite + boehmite

6.6 Alteration trends

Many authors have recognised the process of hydrothermal alteration in the sedimentary system affecting rocks or minerals through the interactions with hydrothermal fluids in the Roan Subgroup. It is understood that hydrothermal alteration can be isochemical, as in traditional metamorphism, dominated by mineralogical changes, or it can be metasomatic

and result in significant addition or removal of elements. Where alteration is intense, it can also result in significant volume changes such that mass balance approaches using immobile elements are required to fully understand the alteration process (Gresens, 1967). Here, however, the use of Isocon diagrams to analyse the gain or loss of material during the alteration process is beyond the scope of this study, and has not been undertaken.

Alteration minerals in low metamorphosed lithologies may consist of quartz and other forms of silica, phylosilicates including illite, sericite, smectite, chlorite, talc, kaolinite pyrophyllite, pyrite, carbonates, sulphates (anhydrite), and oxides (magnetite, hematite, ilmenite) within the system in equilibrium with low temperature fluids. The studies of alteration assemblages in these hydrothermal settings have led to a series of commonly recognized alteration events: potassic, argillic, sericitic, chloritic and carbonate, each with distinct characteristic mineral assemblages (Bonnet et al., 2007).

Given the presence of the carbonates and alumina silicate in the system defined by the R.A.T. and Dipeta Subgroups, a ternary plot composed of Mg-K-Al has been constructed displaying four distinct alteration trends (Figure 48) consisting of:

- Potassic alteration, with corresponding minerals K-feldspar, muscovite and kaolinite. The potassic alteration resulted in the formation of fine-grained potassium feldspar and micas such as muscovite and phlogopite (Hitzman, 2010). As noted by Hitzman, (2010), it is evident that the potassic alteration is restricted to the argillaceous units of the R.A.T. and the Dipeta siltstones and derived breccia units. Copper mineralisation that occurred during potassic alteration is more evident in the Zambian Copperbelt than in the Congolese Copperbelt (Selly *et al.,* 2005). Evidence for an association between copper-cobalt mineralisation and potassic alteration is present at the base of the "SD" stratigraphic Mines Subgroup formation in the where weak but pervasive potassic alteration occurs in conjunction with disseminated sulphides (Hitzman, 2010).
- Magnesium/carbonate alteration: dolomite, chlorite and smectite. The magnesian alteration is the main alteration type seen in the Roan Group including the R.A.T. and

Dipeta units and is not obviously constrained to any particular lithological sequence but is rather distributed throughout the stratigraphy to varying degrees (Hitzman, 2010). Copper mineralisation that occurred during magnesite alteration is more evident in the Congolese Copperbelt. The quartz crystallisation that resulted from early silicification is commonly replaced by and associated with dolomite, as seen in this study (e.g., Figure 30, 31) consistent with the observation of Hitzman, (2010). Silicification therefore occurred prior to potassic alteration and magnesian alteration due to the silicified units being commonly over-printed and replaced by the magnesian alteration minerals, magnesian chlorite and talc (Selley et al., 2005; Selley et al., 2010).

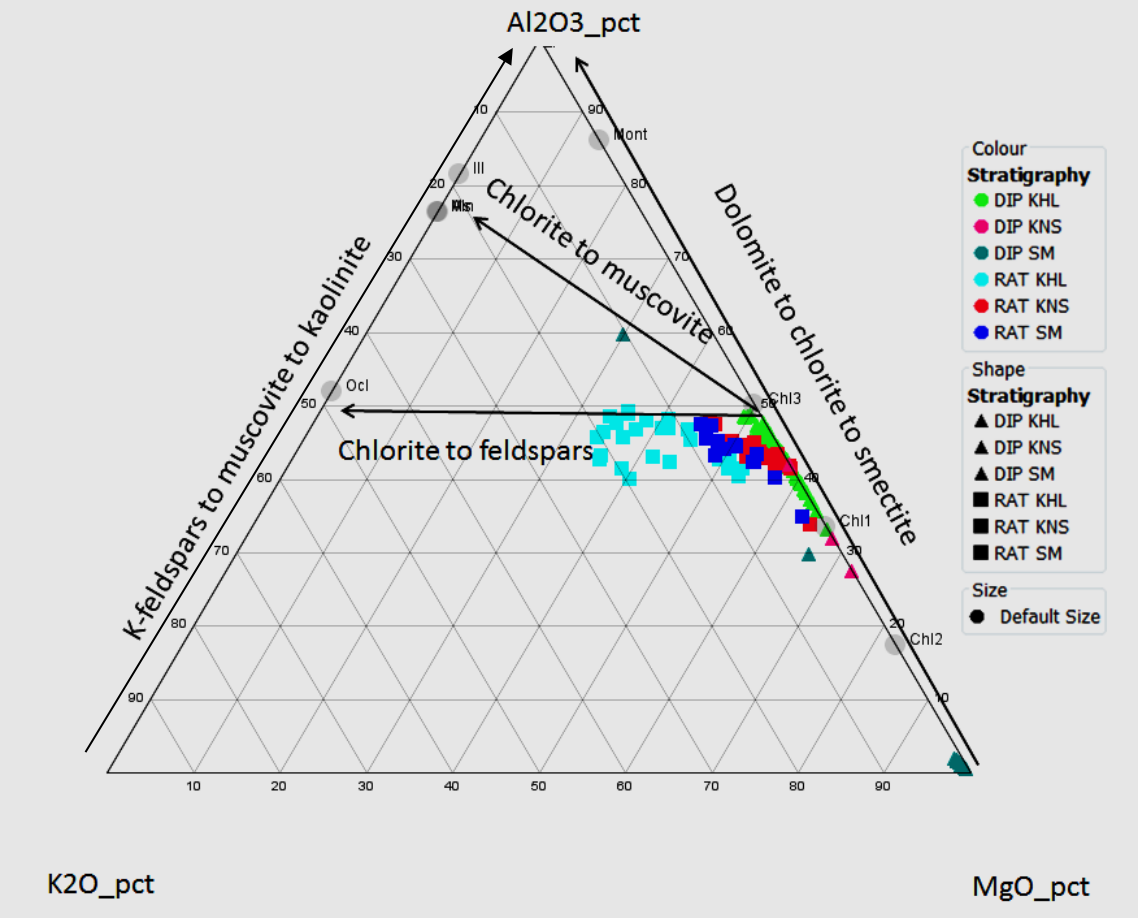

Figure 48: A ternary plot composed of Mg-K-Al has been constructed displaying four distinct mineral alteration trends from the R.A.T. and Dipeta results, composed of: K-feldspar-muscovite-kaolinite, dolomite-chlorite-smectite, Chlorite-muscovite and chlorite-K-feldspars.

- Chloritic alteration, composed of chlorite, muscovite and chlorite, and K-feldspar. The most common magnesian alteration assemblage seen is chlorite-talc dolomite-quartz, which crosscuts and replaces the potassic alteration mineral assemblages (Hitzman, 2010).

6.7 Carbonate alteration phases

The R.A.T. and Dipeta sediments are composed mainly of diagenetic carbonate, detrital quartz, muscovite and silicate minerals. Early after sedimentation, framboidal and euhedral pyrite are formed (Dewaele et al., 2006), who noted that the pyrite is partially replaced by chalcopyrite in the reduced environment of the upper R.A.T. unit. Anhydrite and gypsum, formed in the evaporitic environment, were replaced by early diagenetic dolomitisation (Katekesha et al., 1975). This early diagenetic dolomite also partly replaced the evaporite nodules or precipitated in dissolution cavities (Dewaele et al., 2006).

According to Dewaele et al., (2006), the main mineralization phase is followed by a second dolomite generation associated with digenite and corroded chalcocite grains. They observed growth zoning texture in the dolomite, which corroborate to a result of the petrographic description of the Dipeta and R.A.T. samples showing a dolomite with a complex texture reflecting one or more of growth zoning with a recrystallisation, dissolution and cavity filling by dolomite, as seen in Fig.30A. The dolomite may also show a complex spheroidal texture. A third, coarse-crystalline dolomite generation, occurs together with chalcocite, digenite and hematite, concentrated in spots or irregularly (Dewaele et al., 2006). The qualitative Scanning Electron Microscopic (SEM) analysis of the R.A.T and Dipeta samples indicates that the dolomite contains trace amounts of iron oxide (hematite) but without associated copper sulphide.

6.8 Metamorphic grade

It's known that the level of regional metamorphism that affected the Lufilian Fold and Thrust Belt is relatively low-grade. The metamorphism does not exceed the stage of anchizone

(Oosterbosch, 1962). Only sericite, chlorite and occasionally biotite are developed in the south-eastern part of the Lufilian Arc (Cailteux, 1973). The degree of metamorphism increases from the Katangan foreland to Fold Thrust and Belt into the Domes region. Conversely, Oosterbosch (1962), observed that the low-grade metamorphism that affected all Katangan sediments is even more attenuated from the base (Roan Group) to the top (Nguba and Kundelungu Groups). According to Lefebvre and Patterson (1982), the metamorphic grade ranges from amphibolite and locally eclogite facies in the south part of the belt through greenschist facies to virtually low-grade metamorphism in the outermost zone (Fold and Thrust Belt) in the north. However, in the Lufilian fold-and-thrust belt, the metamorphism can be locally distributed owing to hydrothermal activity (unpublished Kazadi, 2012).

In the project areas, the metamorphic assemblage mineral recorded is composed of chlorite, muscovite associated with apatite, quartz and carbonate. According Selley (2006), phlogopite is an abundant constituent metamorphosed argillite characterised by the assemblage K-feldapar-dolomite-chlorite. No phlogopite or biotite has been described in R.A.T. and Dipeta samples, demonstrating the relatively low metamorphosed nature of these samples. The assemblage Mg-chlorite-muscovite-quartz-talc observed in the R.A.T. and Dipeta units may be explained by the hydration of the pre-existing metasomatic feldspar (Selley., 2006).

6.9 Comparison of RAT and Dipeta units

	R.A.T. Unit	**Dipeta Unit**
Alteration	• Very fine-grained muscovite sericite and quartz grains are partially replaced by magnesite. • The dolomite includes trace amounts of iron oxide (hematite). • Accessory phases observe a detrital zircon associated with a xenotime. • Euhedral pyrite is well developed, and accessory minerals observed in	• Dolomite is replaced a former magnesite and present a spheroidal texture. • Hematite is present in the matrix as pseudomorphous replacement of former tabular ilmenite crystals. • Zircon and xenotime are most abundant detrital heavy mineral

	minor amounts include apatite and Ca-sulphate phase probably gypsum. • An amount of apatite in filled progressively the vein associated with quartz minerals.	intergrowth with altered Fe-Ti-oxide. • Apatite occurs as an infill in very fine dolomite. • The pyrophyllite is present and often intimately associated with smectite group clay.
Geochemistry	• The average of SiO_2 content is about 48% and of calcite less than 5wt.%. • MgO is ranged between 11-15wt.% • Al, Fe, Cr, Th, Ga, Ti are elements depleted in the breccia hangingwall zone • The alteration trend indicates a progressive increasing of Al_2O_3 element during alteration process result on enrichment of the clays minerals. • The alteration trend suggests the Mg-chlorite rich whereas. • RAT is less dolomitic and moderate magnesian content.	• The proportion of SiO_2 content is variable between 18% to 45%, and avarage calcite is cmprise between 3-21wt.% • MgO is comprised between 16-21wt.% • Al, Fe, Cr, Th, Ga, Ti are elements increased in the breccia footwall zone. • The alteration trend indicates a progressive decreasing of Al_2O_3 element during alteration process result on enrichment of dolomite. • The alteration trend suggests the Mg-chlorite-dolomite rich whereas • The Dipeta unit is more dolomitic and magnesian content.
Mineral assemblage	• The R.A.T. is composed by: – muscovite-chlorite-quartz associated with accessory minerals including the apatite-rutile-zircon-xenotime.	• The Dipeta is composed by: –muscovite pyrophyllite-chlorite-quartz associated with accessory minerals composed by apatite-rutile-zircon-xenotime.

6.10 Fingerprinting the R.A.T. and Dipeta

The geochemical fingerprints of R.A.T. and Dipeta stratigraphic units derive from the study of selected four/depth strip logs composed of the drill holes: _ SM59016, KHLSS274, KTCSS315 and KTCSS326 belonging to Safety Mineral, Kinsevere Hill and Kinsevere

respectively, to examine the geochemical variations. Details concerning the strip logs can be found in Appendix 4, and in Figure 49.

Overall observations made from the R.A.T. and Dipeta strip logs illustrate that certain elements are depleted in the footwall of the intercalated heterogeneous breccia (HBX) corresponding to the top of the R.A.T. unit and are correspondingly enriched in the hanging wall of the breccia forming the base of the Dipeta. A summary of the enrichment or the depletion of elements versus the thickness of R.A.T. and Dipeta units are detailed in Appendix 6. The strip logs of selected drill holes display major (Mg, Ca, Al, and Fe) elements as well as immobiles trace (Th, Cr) elements exhibit profile distributions across the stratigraphy, including both Dipeta and R.A.T. The down−hole profiles show a distinct stratigraphic discrimination between the two Subgroups and the intercalated heterogeneous breccia in between them. An example from drill hole SM59016 is shown in the Figure 49.

Ideally, element abundances or ratios may be used to distinguish a lithostratigraphic sequence based on geochemical characteristics of each unit. It can be observed that the Dipeta exhibits noticeably higher average abundances of CaO, MgO and U, elements which are lower, on average, in the R.A.T. which is broadly consistent with the Dipeta being more dolomitic than the R.A.T. On the other hand, Ga, Cr, Ti, and Th are lower in the Dipeta and, higher in the R.A.T. The breccia profiles show a distinct correlation both in Dipeta and R.A.T. (Figure 49).

Analysis of data indicates that the R.A.T. and Dipeta Subgroups of the Nambulwa region present almost the same abundance geochemical characteristics of most elements, consistent with their broadly similar provenance, depositional and diagenetic history. Major elements including Al_2O_3, Fe_2O_3, MgO, MnO and Na_2O display similarly scattered distributions both in the R.A.T. and Dipeta units such that it becomes more complex to dissociate them as stratigraphic discriminant using elemental ratios.

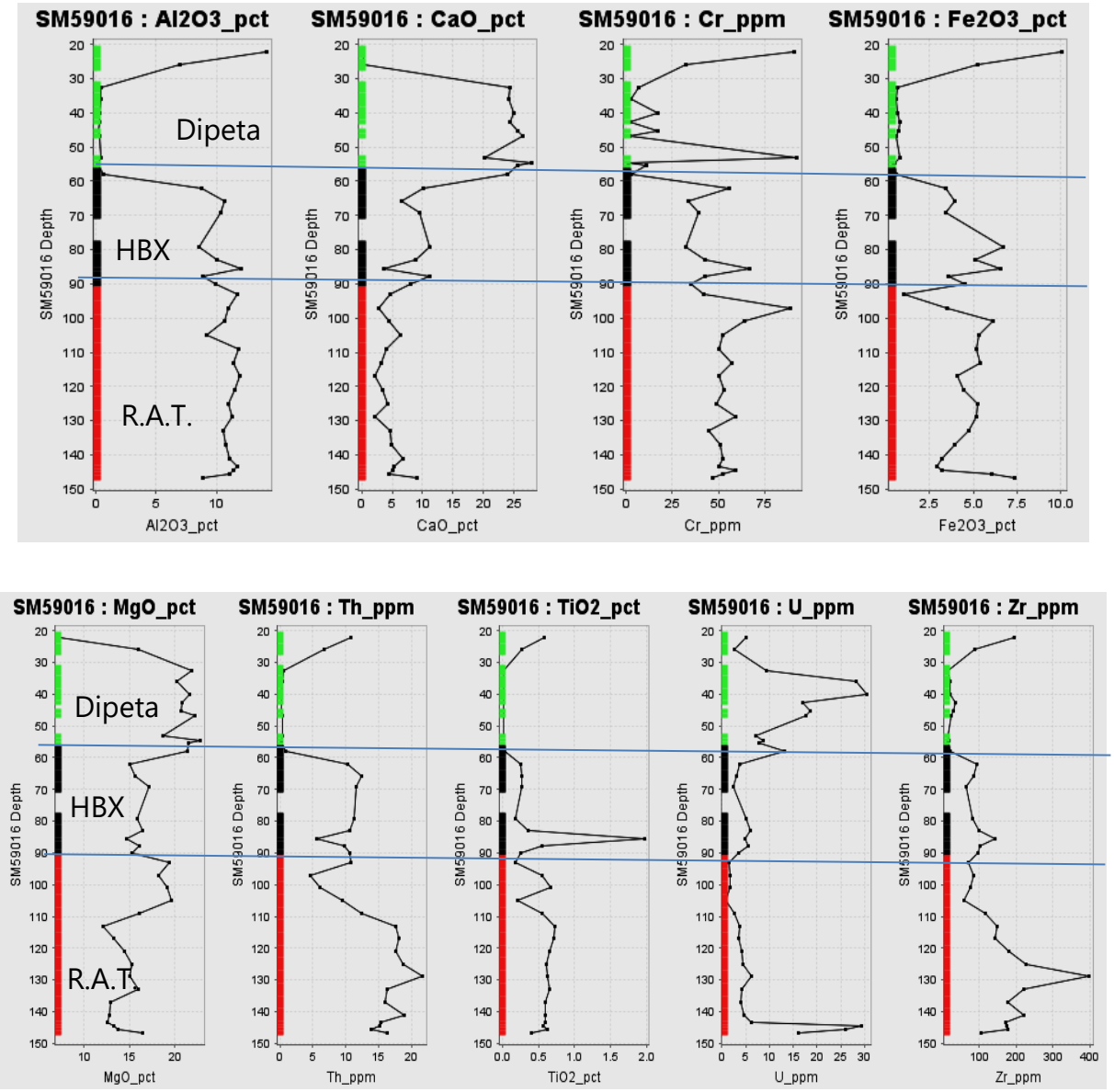

Figure 49: SM59016 Strip log showing geochemical element profiles according to stratigraphic bounderies of the R.A.T. and Dipeta units as well as the un-mineralised breccia in between them.

The fingerprints of R.A.T. and Dipeta units result from the geochemical down-hole stratigraphic logs show a better indication of vertical compositional variations between the R.A.T. and the Dipeta particularly in proximity to the decollement (Mines Subgroup) zone, with characteristics summarised in Table 4 below.

The particular scenario involving contamination might involve upwards migration of low temperature hydrothermal fluids containing mobile elements such as Ca, Mg, Fe^{3+} and others (U) which are subsequently precipitated out in the hangingwall (Dipeta) through the breccia units as phase of the magnesian metasomatic activity involving movement of warm, mildly acidic fluids. This has the effect of enriching the immobile elements in the residue of

the leached footwall, and correspondingly diluting their concentrations in the hangingwall where re-precipitation of the mobile components has occurred.

Unit	**Elements depleted in contact zone**	**Elements enriched in contact zone**
Dipeta Subgroup within ~20 m above Mines Subgroup (ore zone)	Al, Fe, Cr, Th, Ga, Ti	Ca *(± U, Mg)*
R.A.T. Subgroup within ~5 m below Mines Subgroup (ore zone)	U, Ca	Al, Fe, Cr, Th, Ga, Ti

Table 4: Showing the vertical composition variation between the R.A.T. and the Dipeta Subgroups.

It is presumed that TiO_2 enrichment in the R.A.T. and depletion Dipeta may be due also to the predominantly pseudomorphous replacement of former tabular ilmenite crystals by hematite present in the matrix in minor to moderate amounts, as noted in this study (e.g. Fig. 31). Conversely, the depletion of the Al_2O_3 in the R.A.T. can be explained by the geochemical process of leaching and feldspar breakdown and subsequent clay mineral mobility due to hydrothermal fluid movement. Selley (2006) observed that the alteration appears more intense in brecciated units that may control and/or record lateral or upwards fluid migration through zones controlled by porosity and permeability during early stages of tectonic brecciation. In contrast, geochemical elements are leached, mixed up along the immediate contact zone controlled by the intercalated heterogeneous breccia. Therefore, the R.A.T. and the Dipeta units are enriched on TiO_2 and Al_2O_3, respectively (Figure 50).

Based on the preceding data analysis, the ratio Al_2O_3/ TiO_2 appears to be the most diagnostic and can be considered as a fingerprint for stratigraphic discrimination between the R.A.T. and Dipeta Subgroups. The Al_2O_3/ TiO_2 might therefore be useful as a litho-geochemical marker for the geological mapping, stratigraphic interpretation, as well a geological model on the exploration area (Figure 50). Attempts to use elements such as Ca, U and Th as discriminants were less successful. This may be attributed to a combination of the relative mobility of Ca and U in aqueous fluids inducing extra scatter, and to the immobility of the high field strength elements (e.g., Th, Zr) in diagenetic fluids causing them to retain

provenance signatures rather than reflecting influence from diagenetic fluid metasomatic processes effectively.

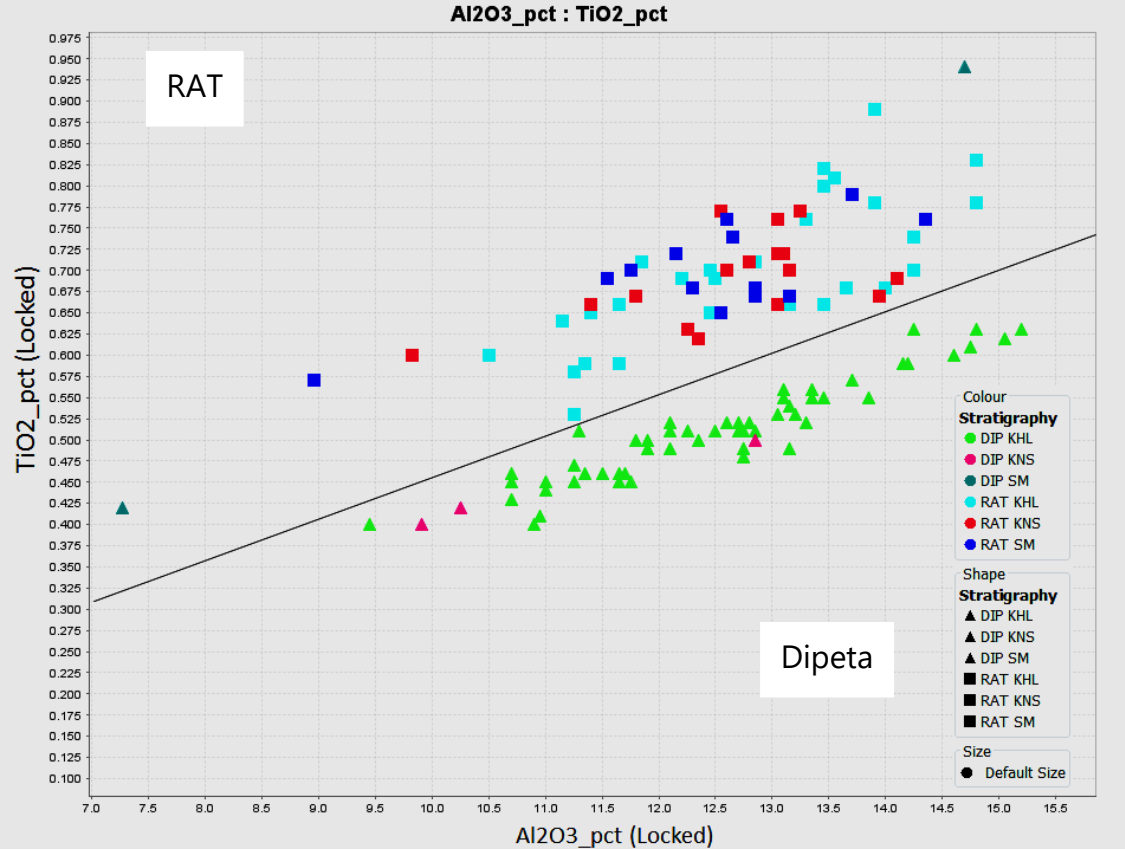

Figure 50: Plot of Ti-Al variation showing a significantly improved stratigraphic discrimination between R.A.T. (plotting mostly above the reference line) and Dipeta (plotting below).

Chapter 7: Summary and Conclusion

The petrographic and geochemical characterisation of the hangingwall Dipeta and the footwall R.A.T. units of the Kinsevere and Nambulwa deposits belonging to the Lufilian Arc, southern Democratic Republic of Congo (DRC) present the same lithostratigraphic oxic depositional environment, represented by siltstone, shale and overlying by dolomite sequences. The R.A.T. and Dipeta facies are very similar as both lithologies are reddish to purple, greenish, very fine grained, and massive to banded, argillaceous magnesite dolomitic-siltstone enriched hematite, with minor disseminated pyrite more abundant in the R.A.T. The unconformity decollement surface composed of a heterogeneous breccia appears macroscopically as an important structural marker from which we can discriminate based on the stratigraphy, the footwall and hangingwall lithostratigraphic units. The dolerite intrusion typical of the Dipeta unit reinforces the criteria of the stratigraphy discrimination, as volcanic activities have been recognised during the Dipeta deposition.

Mineralogical characterisation (by petrography, SEM and XRD) of the R.A.T. and Dipeta samples demonstrates the presence of silicate minerals including muscovite; chlorite, and smectite resulted from the hydrothermal alteration of the K-feldspar. The distinct pyrophyllite observed in the Dipeta may represent local low-grade metamorphism affecting the aluminosilicate phases (such as muscovite) during magmatic/volcanic events. Both the R.A.T. and the Dipeta include oxide mineral phases including rutile, hematite, ilmenite and other accessory minerals, such as xenotime, apatite and detrital zircon in various amounts corresponding to the protolith lithology.

Geochemically, the significant carbonate content in both R.A.T. and Dipeta indicates that the magnesian alteration is higher both in the Dipeta and R.A.T units, while high dolomite (carbonate) component is also found in the Dipeta unit. The copper content in the different R.A.T. samples has an average of 43_ppm, in contrast to the lower concentrations between 6-23 ppm in the Dipeta. The high copper values in the R.A.T. could be attributed to a process affecting the mineralised immediate hangingwall contact with the Mines Subgroup or a

secondary enrichment from meteoric circulation fluid. It's observed that the compositional characteristics of the immediate footwall and hangingwall to the ore zone are consistent with upwards migration of fluids transporting mobile elements such as $Ca^{2+,}$ $Mg^{2+,}$ $Fe^{3+,}$ and U precipitating in the Dipeta becomes more dolomitic, while the immobiles $TiO_{2,}$ Zr are enriched in the R.A.T. with Al_2O_3 remobilised from the R.A.T. by geochemical process of leaching.

The ratio TiO_2/Al_2O_3 appears here as fingerprint characteristics that can make a lithostratigraphic discrimination between R.A.T. and Dipeta. Intense brecciation tectonic affecting the Kinsevere R.A.T. might favorise lateral or upwards fluid migration with a leaching and mixed up of Al_2O_3 element on unconformity contact of the heterogeneous breccia.

References

Batumike, M.J, Kampunzu, A.B, Cailteux, JH., 2006. Petrology and geochemistry of the Neoproterozoic Nguba and Kundelungu Groups, Katangan Supergroup, southeast Congo: Implications for provenance, paleoweathering and geotectonic setting. Journal of African Earth Sciences 44, pp. 97–115.

Batumike, M.J., Caillteux, J.L.H. and Kampunzu, A.B., 2007. Lithostratigraphy, basin development, base metal deposits and regional correlations of the Neoproterozoic Nguba and Kundelungu rock succession; Central African Copper Belt: Gondwana Research 11, pp. 432-447.

Bhatia, M.R., Crook, K.A.W., 1986. Trace-element characteristics of graywackes and tectonic setting discrimination of sedimentary basins. Contributions to Mineralogy and Petrology 92 (2), pp. 181–193.

Boniface, N., Schenk, V., Appel, P., 2012. paleoproterozoic eclogites of MORB-type chemistry and three Proterozoic orogenic cycles in the ubendian belt (Tanzania) : evidence from monazite and zircon geochronology and geochemistry. Precambrian Research, 192: pp. 16-33.

Bonnet, A.-L., and Corriveau, L., 2007, Alteration vectors to metamorphosed hydrothermal systems in gneissic terranes, in Goodfellow, W.D., ed., Mineral deposits of Canada—A synthesis of major deposit-types, district metallogeny, the evolution of geological provinces, and exploration methods: Geological Association of Canada, Mineral Deposits Division, Special Publication No. 5, p. 1035–1049.

Brems, D., Muchez, P., Sikazwe, O., and Mukumba, W., 2009. Metallogenesis of the kana Copper –Cobalt Southern Orebody, Zambia, Journal of African Earth Science 55(3-4): pp. 185-196.

Brock, B.B., 1961. The structural setting of the Copperbelt. In: Mendelsohn (Ed.), The Geology of the Northern Rhodesian Copperbelt. MacDonald, London, pp. 81–89.

Broughton, D.W., 2014. Geology and ore deposits of the Central African Copper ; Phd, thesis Colorado School of Mines, USA 174 p.

Brown, A.C., 1993. Sediment-hosted stratiform copper deposits. In: Sheahan, P.A., Cherry, M.E. (Eds.), Ore Deposit Models, volume II. Geological Association Canada Geoscience Canada Reprint Series 6, pp. 99-116.

Cahen, L, DELHAL, J. and Deutsch., 1967. Rubidium-strontium geochronology of some granitic rocks from the Kibaran belt (Central Katanga, Rep. of the Congo). Annales des Sciences Géologiques, Musée Royal de l'Afrique Centrale, Tervuren, Belgium. Série in 8°, pp. 59-65.

Cahen, L., 1954. Geologie du Congo Belge. Vaillant Carmanne, Liege, 577 p.

Cailteux, 1978. La succession stratigraphique du CMN (ou R.2.3) au centre de la sous province cuprifère Shabienne. Annale de la société Géologique de Belgique, T100, 1977, pp.73-85.

Cailteux, 1994. Lithostratigraphy of the Neoproterozoic Shaba type (Zaire) Roan Supergroup and metallogenis of associated stratiform mineralization. Journal of African Earth Science, vol 19, N°4 pp. 279-301.

Cailteux, J.L.H., Kampunzu, A.B.H. and Batumike, M.J., 2005b. Lithostratigraphic position and petrographic characteristics of R.A.T. ("Roches Argilo-Talqueuses") Subgroup, Neoproterozoic Katangan Belt (Congo), Journal of African Earth Sciences vol. 42 pp 82-94.

Cailteux, J.L.H., Kampunzu, A.B. and Lerouge, C., 2007. The Neoproterozoic Mwashya-Kansuki sedimentary rock succession in the central African Copperbelt, its Cu - Co mineralisation, and regional correlations. Gondwana Research 11(3): pp. 414-431.

Cailteux, J.L.H. and Misi, A., 2007. Neoproterozoic sediment-hosted base metal deposits of Western Gondwana. Gondwana Research 11 (3): 344-345.

Cailteux, J.L.H. Deputer, T., 2018. The Neoproterozoic Katanga Supergroup (D.R.Congo): state of the art and revisions of the lithostraigraphy, sedimentary basin and geodynamic evolution. Journal of African Earth Sciences vol. 150 pp 522-531.

Condie, K.C., Boryta, M.D., Liu, J., Quian, X., 1992. The origin of khondalites: geochemical evidence from the Archean to Early Proterozoic granulitic belt in the North China Craton: Precambrian Research, 59(3-4), pp. 207-223.

Cox, R., Lowe, D.R., Cullers, R.L., 1995. The influence of sediment recycling and basement composition on evolution of mudrock chemistry in the southwestern United States: Geochimica et Cosmochimica Acta, 59(14), pp. 2919-2940.

Daly, M.C., Chakraborty, S.K., Kasolo, P., Musiwa, M., Mumba, P., Naidu, B.,Namateba, C., Ngambi, O. and Coward, M.P., 1984. The Lufilian arc and Irumide belt of Zambia: results of a traverse across their intersection. Journal of African Earth Science 4: pp. 311-318.

Davies, J.F., and Whitehead, R.E., 1994. Molar ratios in the study of unaltered and hydrothermally altered greywackes and shales: Chemical Geology, v. 111, 85–100p.

Davies J.F., Whitehead R.E., 2006. Alkali-alumina and MgO-alumina molar ratios of analtered and altered rhyolites. Exploration and Mining Geology, vol 15, 1-2, 75–88p.

Dejonghe, L., and Noyi, K., 1995. Le gisement de Kinsenda (Sud-est du Zaire): une concentration cuprifère stratoide dans les formations détritiques du Roan (Protérozoïque Supérieur). Chronique de la recherche minière, 521 : 19-37p.

DePutter, Th., Mees, F., Decrée, S., Dewaele, S., 2010. Malachite, an indicator of major Pliocene Cu emobilization in a karstic environment (Katanga, DR Congo). Ore Geology Review 38: pp. 90-100.

Dewaele .S Muchez. Ph . Vets a.J, Fernandez-Alonzo b M, L. Tack, 2006. Multiphase origin of the Cu–Co ore deposits in the western part of the Lufilian fold-and-thrust belt, Katanga (Democratic Republic of Congo) Journal of African Earth Sciences, 46, pp 455-469.

Floyd, P.A., Winchester, J.A., Park, R.G., 1989, Geochemistry and tectonic setting of Lewisian clastic metasediments from the Early Proterozoic Loch Maree Group of Gairloch, N.W. Scotland: Precambrian Research, 45(1-3), pp. 203-214.

Francois, A., 1973. L'extremite occidentale de l'Arc Cuprifere Shabien, etude geologique: Mémoire edite par la Department Geologique de la Gecamines, Likasi, Democrati Republic of the Congo. Brussels, Belgium, 81p.

François, A., 1974. Stratigraphie, tectonique et minéralisations dans l'arc cuprifère du Shaba (Rép. du Zaïre). In: Bartholomé (Ed.), Gisements Stratiformes et Provinces Cuprifères. Centenaire de la Société Belge de Géologie, Liège, 79-101p.

François, A., 1987. Synthèse géologique sur l'arc cuprifère du Shaba (Rép. du Zaïre). Centenaire de la Société Belge de Géologie, 15–65 p.

François, A., 1993. La structure tectonique du Katanguien dans la région de Kolwezi (Shaba, Rep. Du Zaire). Annales de la société géologique de Belgique, T.116-1193 pp 87-104.

François, A., 1995. Problèmes rélatifs au Katanguien du Shaba. Musée Royal de l'Afrique centrale, Tervuren (Belgium) Annales des Sciences Géologiques 101: pp. 1- 20.

Frimmel, H., Tack, L., Basei, M., Nutman, A. and Boven, A., 2006. Provenance and chemostratigraphy of the Neoproterozoic West Congolian Group in the Democratic Republic of Congo. Journal of African Earth Sciences 46: pp. 221-239.

Frimmel, H. E., Basei, M. S. & Gaucher, C., 2011. Neoproterozoic geodynamic evolution of SW Gondwana: a southern African perspective. International Journal of Earth Sciences, 100 (2-3), pp. 323-354.

Haest, M., P. Muchez, and Vanhaecke, F., 2009b. The influence of supergene processes on variations in the Cu isotopic composition in the Dikulushi Cu-Ag deposit (DRC).

Proceedings of the 10th Biennial SGA Meeting, 17-20 August 2009, Townsville, North Queensland, Australia: pp. 322-324.

Haest, M. and Muchez, P., 2011. Stratiform and vein-type deposits in the Pan-African Orogen in Central and Southern Africa: evidence for multiphase mineralisation. Geologica Belgica 14(1-2), pp. 23-44.

Hemley, J. J., 1958 Some mineralogical equilibria in the system K_2O-Al_2O_3-SiO_2-H_20 : Am jour.sc. univ. of California, Berkeley V..257. 241-270p.

Hitzman, M.W., Selley, D., and Bull, S., 2010. Formation of sediment-hosted stratiform copper deposits through Earth history: Economic Geology, 105, pp. 627–640

Jackson M. P. A., Warin O. N., Woad G. M., Hudec M. R., 2003. Neoproterozoic allochthonous salt tectonics during the Lufilian orogeny in the Katangan Copperbelt, Central Africa. Geological Society of American Bulletin, 115, pp. 314–330.

Kampuzu A.B and Cailteux, J., 1999. Tectonic Evolution of the Lufilian Arc (Central Africa Copper Belt) During Neoproterozoic Pan African Orogenesis, Gondwana research , V2 N0.3, pp. 401-421.

Kampunzu, A.B., Tembo, F., Matheis, G., Kapenda, D. and Huntsman-Mapila, P., 2000. Geochemistry and tectonic setting of mafic igneous units in the Neoproterozoic Katangan Basin, Central Africa: Implication for Rodinia break up. Gondwana Research, 3: pp. 125–153.

Katekesha, W.M., 1975. Conditions de formation du gisement cuprocobaltifere de Kamoto Principal (Shaba-Zaïre). Thèse de Doctorat en Sciences, University of Liège (Belgium), 237p.

Kazadi, B., S-B., 2012. Structural geology of the Kinsevere Copper Deposit, DRC: Unpub. M.S. thesis, Department of Geology, Faculty of Natural and Agricultural Sciences, University of Pretoria, South Africa, 223 p.

Kipata, M.L., 2007. Inventaire et analyse au moyen d'un SIG de la tectonique active dans le SE de l'Afrique : Sud-est de la RDC et Nord de la Zambie. MSc. Thesis, Geodynamics and Geofluids Research Group, KU.Leuven, Belgium, 106 p.

Kipata, M.L., 2013. Brittle tectonics in the Lufilian fold and-thrust belt and its foreland. An insight into the stress field record in relation to moving plates (Katanga, DRC). Phd, Thesis, Katholieke Universiteit Leuven, Belgium, 160 p.

Kirkham, R.V., 1989. Distribution, settings, and genesis of sediment-hosted stratiform copper deposits: Geological Association of Canada: Special Paper 36, p. 3–38.

Lefebre, J.J., 1978. Le groupe de Mwashya, megacyclotheme terminal du Roan (Shaba, Zaïre Sud-oriental). I – Approche lithostratigraphique et étude de l'environnement sédimentaire. Annales Société Géologique Belgique 101, pp. 209-225.

Maja, A., 2014. Vanadium in soils chemistry and exotoxicity. Phd, thesis Swedish University of Agricultural Sciences, Department of Soil and Environment, Uppsala, 58p.

McLennan, S.M., Hemming, S., McDaniel, D.K., Hanson, G.N., 1993. Geochemical approaches to sedimentation, provenance, and tectonics, *in* Johnson, M.J., Basu, A. (eds.), Processes Controlling the Composition of Clastic Sediments: Geological Society of America, Special Paper, 284, pp. 21-40.

Nagaraja, R., Madhavaraju, J., Nagendra, R., Selvamony, J., Moutte, J., 2207. Geochemistry of Neoproterozoic shales of the Rabanpalli Formation, Bhima Basin, Northern Karnataka, southern India: implications for provenance and paleoredox conditions: Revista Mexicana de Ciencias Geológicas, V. 24, núm. 2, p. 150-160.

Ngoy, L., 1992. Les minéralisations cuprifères du Katanguien associées aux dômes granitiques Ubendiens (Province métallogenique Zaïro-Zambienne). L'exemple du gisement de Kinsenda-Luina (Zaïre), Thèse de doctorat ; Université Libre de Bruxelles, 253 p.

Oosterbosch, R., 1962. Les minéralisations dans le système de Roan au Katanga. In Lombard J,Nicolini P (Eds.) Gisements stratiformes de cuivre en Afrique. Association des Services Géologiques Africains, 71-136.

Porada, H. and Berhorst, V., 2000. Towards a new understanding of the Neoproterozoic-Early Palaeozoic Lufilian and northern Zambezi Belts in Zambia and the Democratic Republic of Congo. Journal of African Earth Sciences 30(3): pp. 727-771.

Selley, D. Broughton, D., Scott, R., Hitzman, M., Bull, S., Large, R., McGoldrick, P., Croaker, M., Pollington, N., Barra, F., 2005. A new look at the geology of the Zambian Copperbelt, in Hedequist, J.W., Thompson,J.F.H., Goldfarb, R.J., and Richards, J.P.,eds. Economic Geology, 100th Anniversary: 965-1000.

Steven, N.M., 2000. A Shaba-type Cu–Co (–Ni) deposit at Luamata, West of the Kabompo Dome, northwestern Zambia. Exploration Mining Geology 9, pp. 277-287.

Tack, L., Wingate, M.T.D., De Waele, B., Belousova, E., Griffin, B., Tahon, A. and Fernandez-Alonso, M., 2010. The 1375 Ma "Kibaran Event" in Central Africa: prominent emplacement of bimodal magmatism under extensional regime. Gondwana Research, doi: 10.1016/j.precamres. 264 p.

Wendorff, M., 2011. Tectonosedimentary expressions of the evolution of the Fungurume foreland basin in the Lufillian arc, neoproterozoic-lower Palaeozoic, central Africa. In: Van Hinsbergen, D.J.J., Buiter, S.J.H., Torsvik, T.H., Gaina, C., Webb, S.J. (Eds.), The Formation and Evolution of Africa: a Synopsis of 3.8 Ga of Earth History, vol. 357. Geological Society of London, Special Publications, pp. 69–83.

Young, G.M., 1995. Are Neoproterozoic glacial deposits preserved on the margins of Laurentia related to the fragmentation of two supercontinents? Geology 23, pp. 153-156.

1 Appendix 1: Drill Holes Geological logging

Prospect	Hole_ID	from	to	Strat.	Lith	Metcode	Colour	Comments	Min1	Alt_Min1	Alt_Min2
NAMBULWA	NAMDD009	1.5	36.8	RAT	SDO	OX	BRN	Brownish massive and bedded dolomite with manganese alteration mainly in fractures.		mn	hd
NAMBULWA	NAMDD009	36.8	80	RAT	SSH	OX	GRY	Whitish grey brecciated clay dolomitic shale (RAT)		cy	
NAMBULWA	NAMDD009	80	81.6	HBX	BHB	OX		Ferroan dolomite matrix supported siltstone breccia. Clasts incorporate local hanging wall and footwall (illmenite/hematite bearing siltstone) to breccia. Protolith appears same on both sides of breccia. Breccia is interpreted as a syn-depositional or compaction and dissolution related breccia rather than tectonic origin.		hd	
NAMBULWA	NAMDD009	81.6	116.4	DIP	SSL	OX	GRY	Whitish grey laminated and brecciated dolomitic siltstone		cy	tc
NAMBULWA	NAMDD009	116.4	140.3	DIP	SSL	OX	WHT	whitish massive to laminated slightly talcose siltstone intercalated with monolithic breccia of R.A.T.		cy	tc
NAMBULWA	NAMDD022	30.8	41.3	RAT	SSL	OX	PNK	pinkish to dark brown strongly weathered monolithic breccia		tc	mn
NAMBULWA	NAMDD022	41.3	42.8	NR	CVT			cavity		tc	mn
NAMBULWA	NAMDD022	42.8	51.8	RAT	SSL	OX	PNK	pinkish to dark talcose monolithic breccia		tc	mn
NAMBULWA	NAMDD022	51.8	53.3	NR	CVT			cavity		tc	mn
NAMBULWA	NAMDD022	53.3	56.7	RAT	SSL	OX	BRN	dark brown strongly weathered polymictic breccia of dolomite and siltstone clasts		tc	mn
NAMBULWA	NAMDD022	56.7	57.8	HBX	SSL	OX	BRN	dark brown polymictic breccia		mn	hl
NAMBULWA	NAMDD022	57.8	63.8	NR	CVT			cavity		mn	hl

Prospect	Hole_ID	from	to	Strat.	Lith	Metcode	Colour	Comments	Min1	Alt_Min1	Alt_Min2
NAMBULWA	NAMDD022	63.8	64.7	HBX	SSL	OX	BRN	dark brown strongly weathered polymictic breccia of dolomite and siltstone clasts		mn	hl
NAMBULWA	NAMDD022	64.7	66.8	NR	CVT			cavity		mn	hl
NAMBULWA	NAMDD022	66.8	68.3	HBX	SSL	OX	BRN	dark brown strongly weathered polymictic breccia of dolomite and siltstone clasts		mn	hl
NAMBULWA	NAMDD022	68.3	69.8	NR	CVT			cavity		mn	hl
NAMBULWA	NAMDD022	145.2	150.77	RAT	STD	OX	BRN	Mg chlorite/talcose fine grained siltstone. Lighter bands may represent dolomitic horizons? Small metallic lustre spots are likely specular hematite. Thin cross cutting quartz vein orthogonal to bedding. This is immediate footwall to our Lower Ore body unit and is considered true RAT.	ma	si	mn
NAMBULWA	NAMDD022	150.77	168.9	RAT	STD	POX	GRY	light grey massive dolomitic siltstone with chlorite and talc alteration		tc	
SAFETY MINERALS	SM59016	0	1	OVB	LOS		BRN	Dark brown humus top soil			
SAFETY MINERALS	SM59016	1	9	OVB	LOS		BRN	Lateritic transported material			
SAFETY MINERALS	SM59016	9	20.4	OVB	LOS			Lateritic transported materials with some rounded and sub-angular clasts			
SAFETY MINERALS	SM59016	20.4	27	DIP	SDO		YEL	Yellow-brown extremely weathered soft formation. Could be weathered dolomite			
SAFETY MINERALS	SM59016	30.9	47.7	DIP	SDO		WHT	White massive to medium grained dolomite			
SAFETY MINERALS	SM59016	52.4	56	DIP	SDO		WHT	White massive to medium grained dolomite with some spot of malachite and chalcopyrite	ma	cb	
SAFETY MINERALS	SM59016	56	67.6	DIP	BHB			Polymictic breccia; clasts supported made of shale; siltstone and sandstone clasts cemented by fine grained carbonate-hematite matrix.		hm	cb

Prospect	Hole_ID	from	to	Strat.	Lith	Metcode	Colour	Comments	Min1	Alt_Min1	Alt_Min2
SAFETY MINERALS	SM59016	67.6	70	HBX	SSL		WHT	Whitish medium grained dolomitic siltstone			
SAFETY MINERALS	SM59016	70	71	HBX	SSL		PPL	Purple brecciated dolomitic siltstone			
SAFETY MINERALS	SM59016	71	72.05	HBX	SST		RED	Light reddish Sandstone			
SAFETY MINERALS	SM59016	72.05	77.4	HBX	SSL			Pinkish to purple massive to diffusely laminated siltstone of breccia iron oxide alteration intercalated some interval of brecciated, evaporite veins and manganese patchy.			
SAFETY MINERALS	SM59016	77.4	85.1	HBX	BHB	OX	RED	Polymictic breccia; clasts supported made of shale; siltstone and sandstone clasts cemented by medium grained sandy carbonate-hematite matrix. Presence of fragment of medium grained Siltstone with pervasive chlorite alteration and with some disseminated leucoxine minerals		hm	cy
SAFETY MINERALS	SM59016	85.1	86.8	HBX	BHB		GRE	Greenish medium grained chloritic and dolomitic Siltstone or dolomite with some disseminated leucoxine mineralization and crosscut by carbonate hematite veins		ch	lx
SAFETY MINERALS	SM59016	86.8	90.8	HBX	BHB		RED	Polymictic breccia; clasts supported made of Shale and Siltstone clasts cemented by carbonate-hematite matrix. Presence of specularite hematite in matrix.		hm	
SAFETY MINERALS	SM59016	90.8	95.3	HBX	SSL		GRN	Bleached or light green grey coarse grained chloritic dolomite		ch	cl
SAFETY MINERALS	SM59016	95.3	107	RAT	SSL		GRN	Greenish brown crackle breccia of chloritic medium grained dolomitic Siltstone cemented by carbonate-hematite-clay matrix		ch	cl

Prospect	Hole_ID	from	to	Strat.	Lith	Metcode	Colour	Comments	Min1	Alt_Min1	Alt_Min2
SAFETY MINERALS	SM59016	107	108.6	RAT	SSL		BRN	Bleached or light brown laminated dolomitic Siltstone (medium grained with some disseminated specularite hematite		hm	
SAFETY MINERALS	SM59016	108.6	147.3	RAT	SSL		PPL	Brecciated purple massive Siltstone and some greenish Shale crosscut by carbonate-hematite veins. Presence of Chalcocite at the bottom contact in a brecciated and silicified zone.	py	hm	cl
KINSEVERE	KHLSS274	0	4.5	DIP	LAT		KHA	laterite pisolitic, massive strongly weathered, khaki to purple, fine grained having manganese, limonite in pervasive mode		mn	lm
KINSEVERE	KHLSS274	4.5	32.7	DIP	SSL		GRY	siltstone unit massive grey strongly weathered fine grained having manganese limonite in pervasive mode		mn	lm
KINSEVERE	KHLSS274	32.7	49	DIP	IGB		YEL	intrusive gabbroic rock massive moderate weathered fine-grained yellow having manganese, limonite in pervasive mode		mn	lm
KINSEVERE	KHLSS274	49	86.1	DIP	SSL		GRY	siltstone unit, massive grey to white moderate weathered fine grained having hematite and clay in pervasive mode		hm	cy
KINSEVERE	KHLSS274	86.1	128.5	DIP	SSL		GRY	siltstone unit having nodular; moderate weathered; fine grained; grey to yellow; contains hematite, manganese and clay in pervasive mode		hm	mn
KINSEVERE	KHLSS274	128.5	134	HBX	SSL		GRY	Slightly weathered siltstone breccia unit; grey to purple; having clast of dolomitic shale and rat cemented by clay and contains oxide of iron probably hematite and limonite.		cy	fe
KINSEVERE	KHLSS274	134	161.8	RAT	SSL		GRY	slightly weathered siltstone unit massive fine-grained grey to pink having hematite quartz and clay in the veins and pervasive mode	cp	hm	qt

2 Appendix 2: XRD analysis results

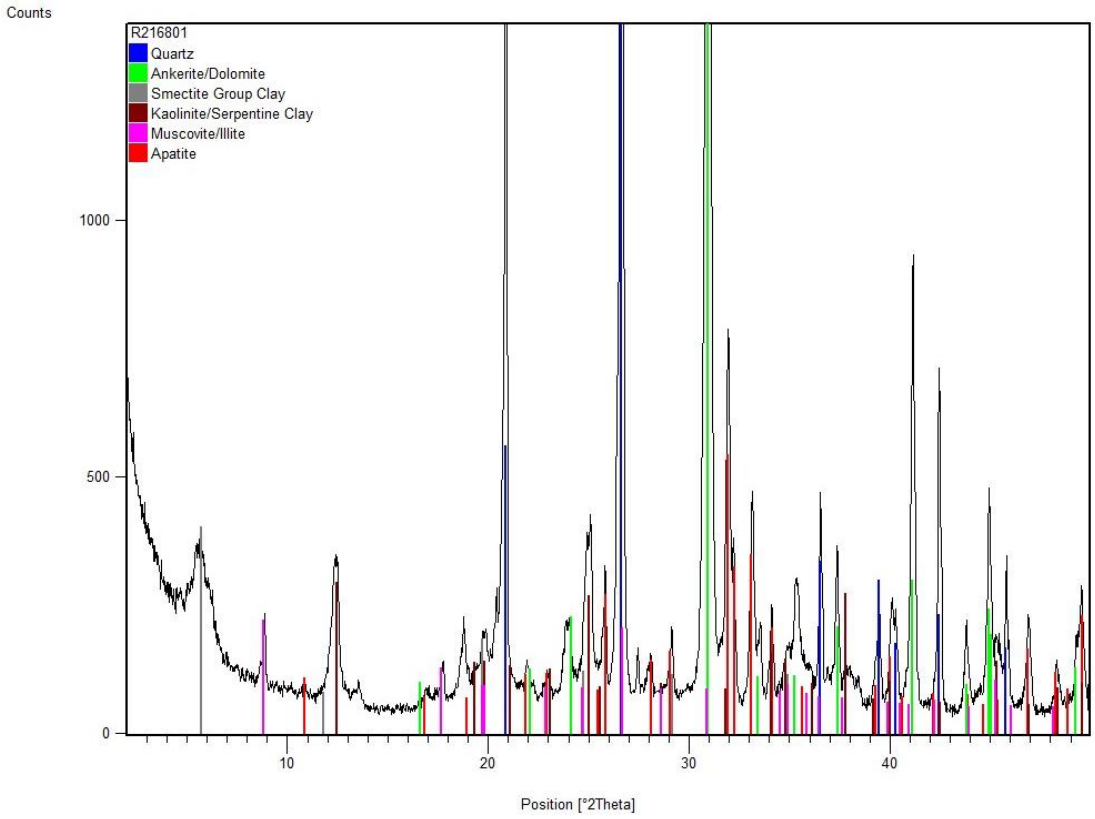

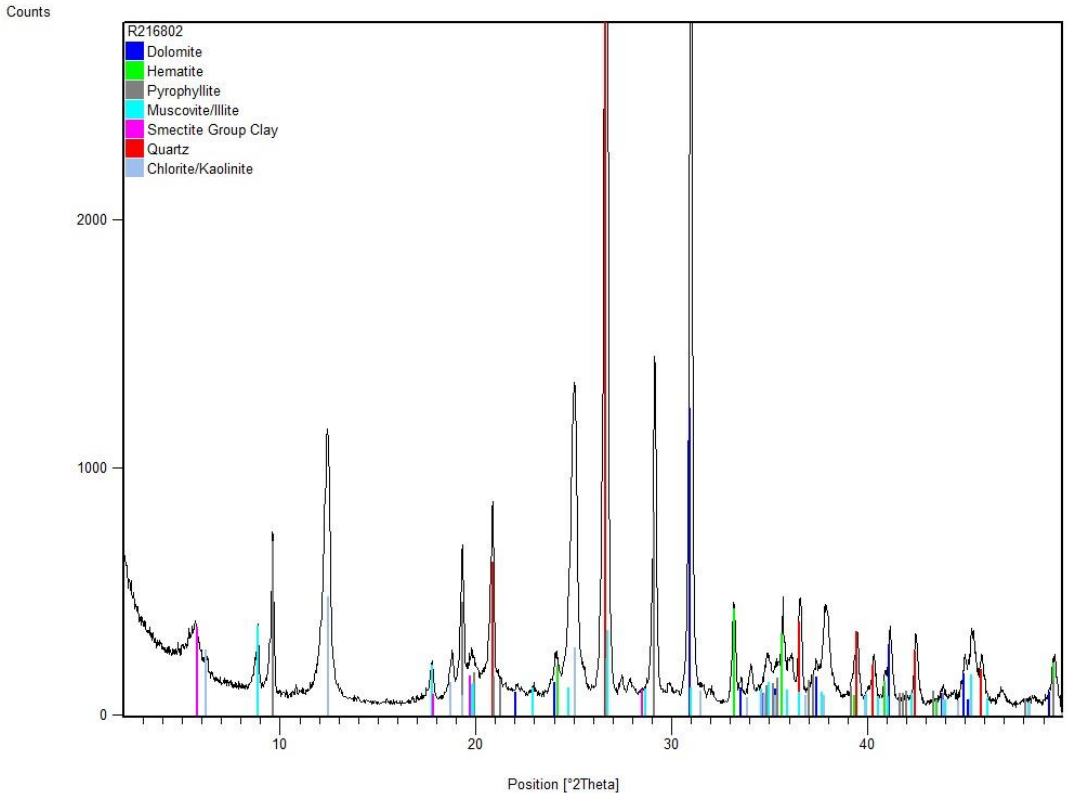

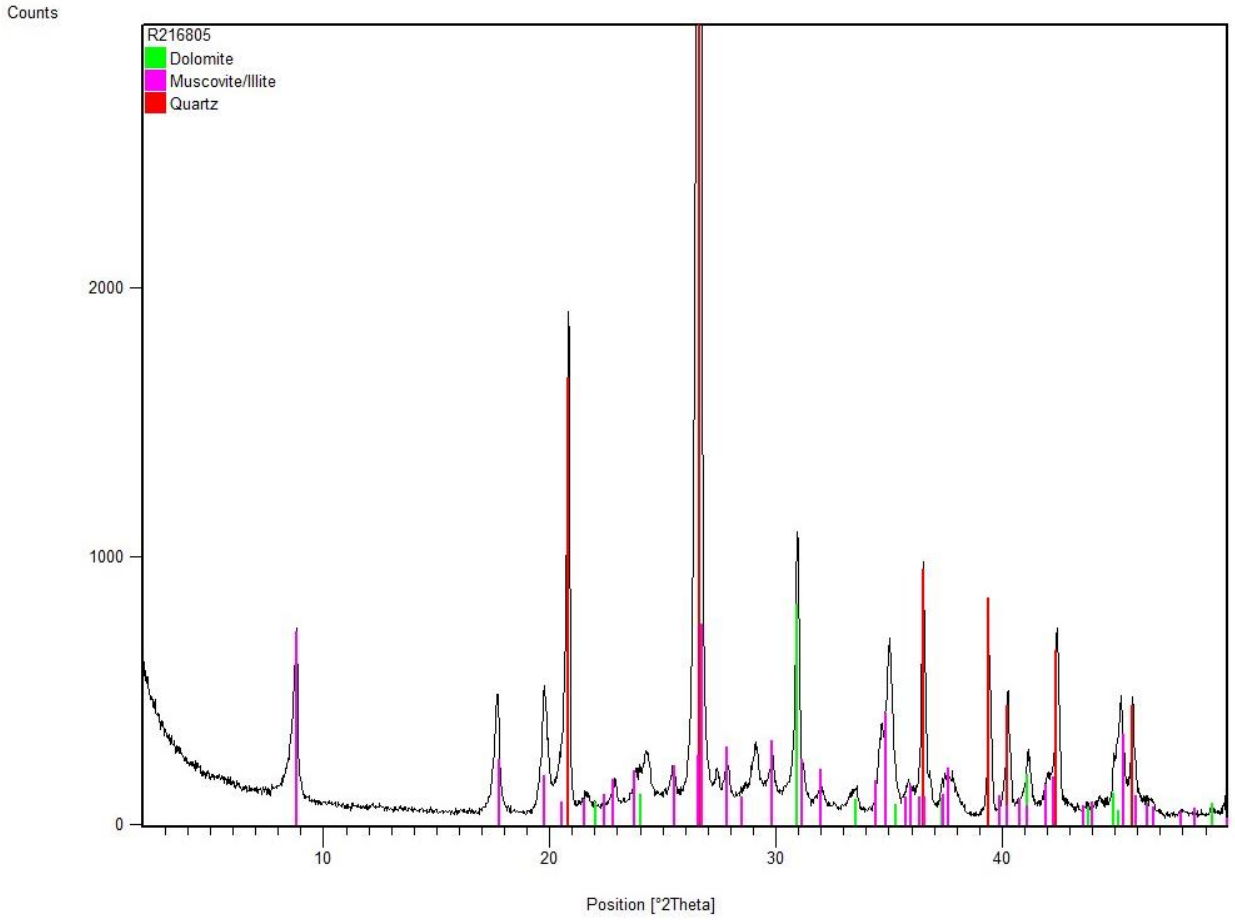
Counts
R216805
Dolomite
Muscovite/Illite
Quartz
2000
1000
0
10
20
30
40
Position [°2Theta]

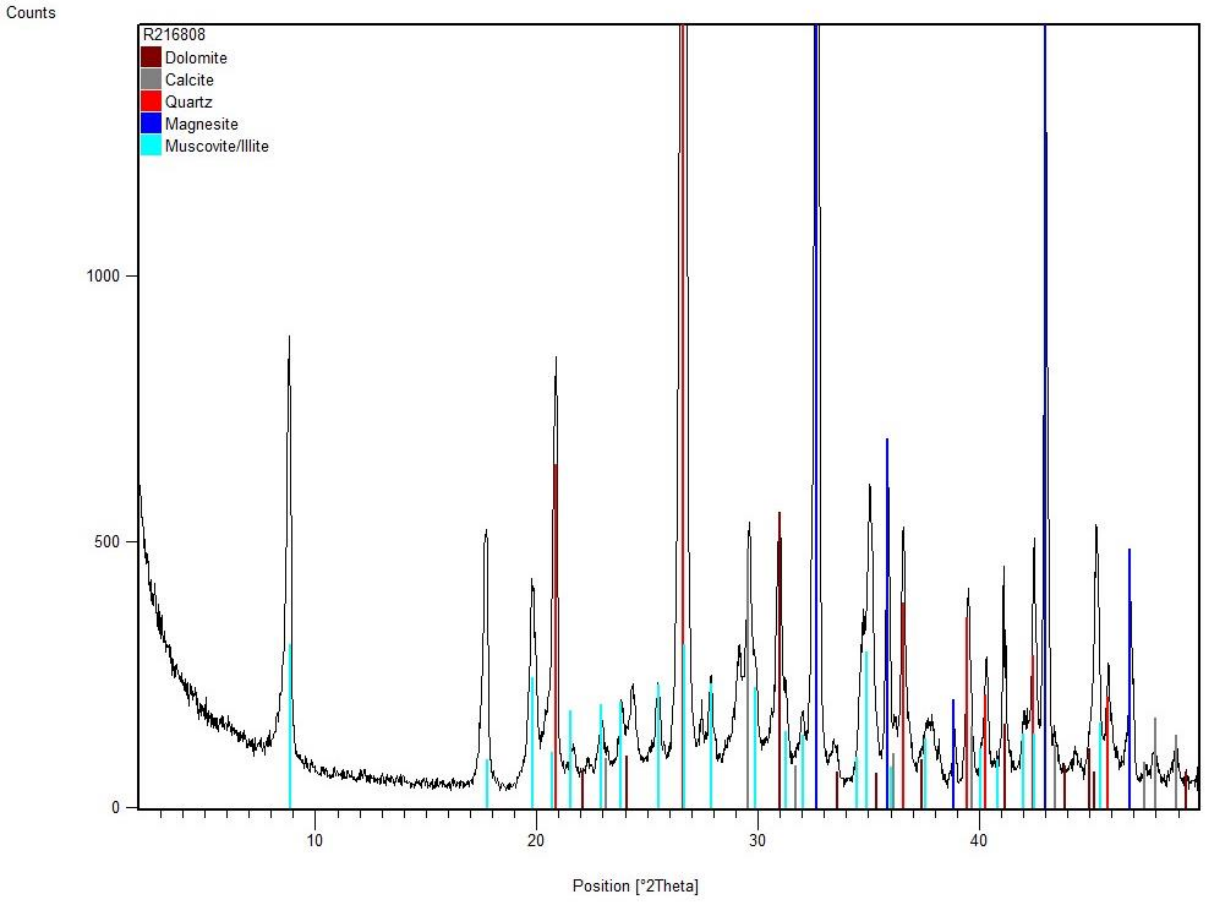
Counts
R216808
Dolomite
Calcite
Quartz
Magnesite
Muscovite/Illite
1000
500
0
10
20
30
40
Position [°2Theta]

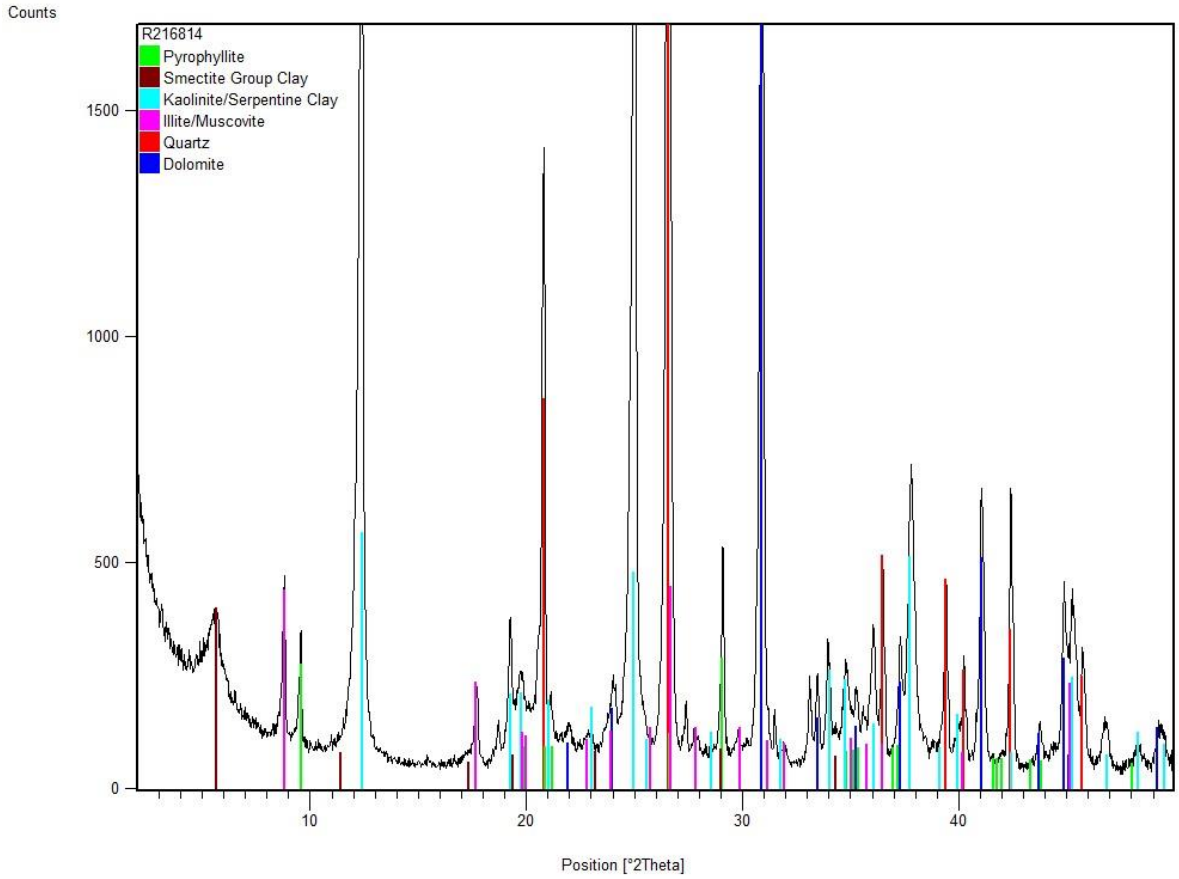

3 Appendix 3: Mineral formulae

Apatite	$Ca_{10}(PO_4)_6(OH)_2$
Calcite	$CaCO_3$
chlorite	$(Mg,Fe^{2+})_5Al(Si_3Al)O_{10}(OH)_8$
Dolomite	$CaMg(CO_3)_2$
Gypsum	$CaSO_4.2H_2O$
Hematite	Fe_2O_3
Hollandite	$Ba(Mn^{4+},Mn^{2+})_8O_{16}$
Kaolinite	$Al_2Si_2O_5(OH)_4$
Magnesite	$MgCO_3$
Muscovite	$KAl_2(Si_3Al)O_{10}(OH,F)_2$
Pyrite	FeS_2
Pyrophyllite	$Al_2Si_4O_{10}(OH)_2$
Quartz	SiO_2
Rutile	TiO_2
Xenotime	YPO_4
Zircon	$ZrSiO_4$
illite	$K,\mathbf{H_3O})(Al,Mg,Fe)_2(Si,Al)_4O_{10}[(OH)_2,(\mathbf{H_2O})]$
Smectite	$(Na,Ca)0,3(Al,Mg)_2Si4O10(OH)_2•n(H2O)$

4 Appendix 4: strip logs

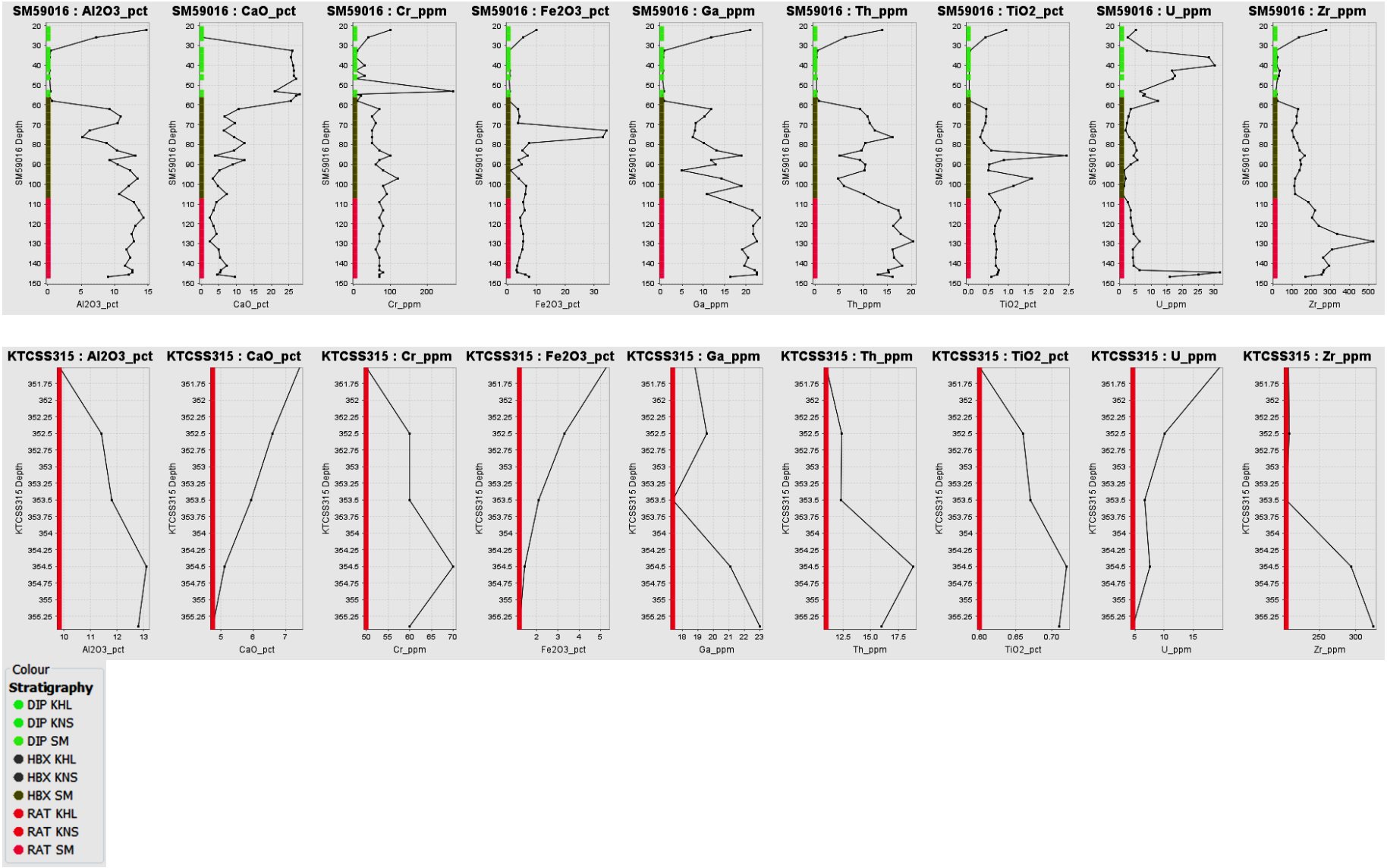

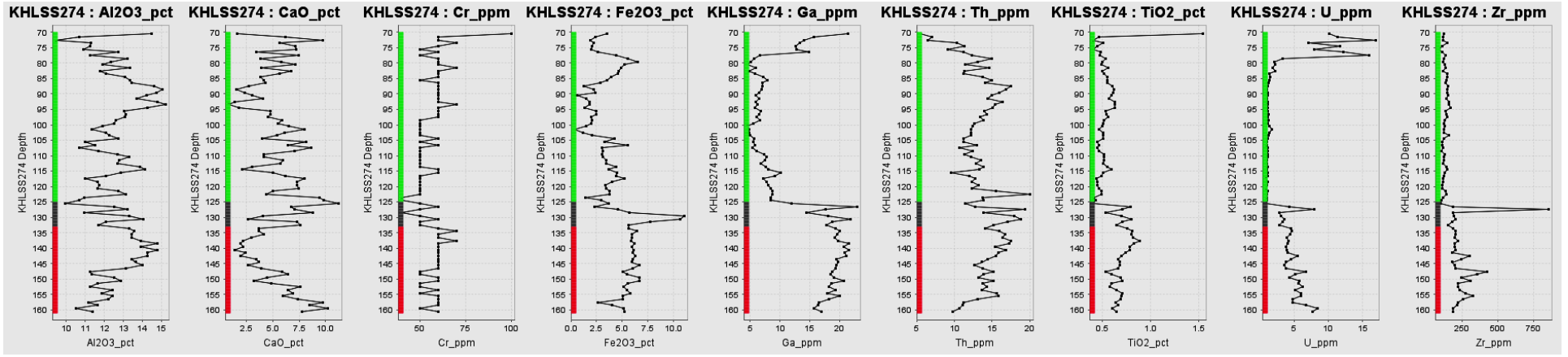
KHLSS274 : Al2O3_pct
KHLSS274 : CaO_pct
KHLSS274 : Cr_ppm
KHLSS274 : Fe2O3_pct
KHLSS274 : Ga_ppm
KHLSS274 : Th_ppm
KHLSS274 : TiO2_pct
KHLSS274 : U_ppm
KHLSS274 : Zr_ppm
KHLSS274 Depth
Al2O3_pct
CaO_pct
Cr_ppm
Fe2O3_pct
Ga_ppm
Th_ppm
TiO2_pct
U_ppm
Zr_ppm

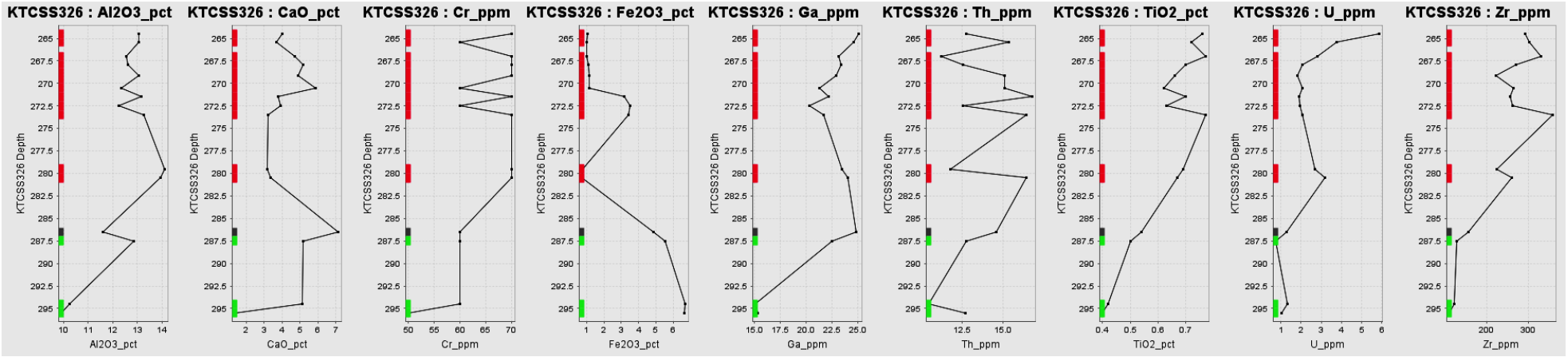
KTCSS326 : Al2O3_pct
KTCSS326 : CaO_pct
KTCSS326 : Cr_ppm
KTCSS326 : Fe2O3_pct
KTCSS326 : Ga_ppm
KTCSS326 : Th_ppm
KTCSS326 : TiO2_pct
KTCSS326 : U_ppm
KTCSS326 : Zr_ppm
KTCSS326 Depth
Al2O3_pct
CaO_pct
Cr_ppm
Fe2O3_pct
Ga_ppm
Th_ppm
TiO2_pct
U_ppm
Zr_ppm

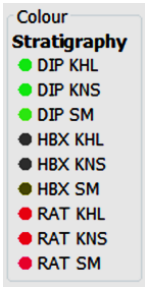
Colour
Stratigraphy
DIP KHL
DIP KNS
DIP SM
HBX KHL
HBX KNS
HBX SM
RAT KHL
RAT KNS
RAT SM

5 Appendix 5: Geochemistry wet results

Hole_ID	Depth_From	Depth_To	Strat. Code	Ag_ppm	Al2O3 %	As_ppm	Ba_ppm
KHLSS274	70	71	DIP KHL	0.25	14.5	1.9	16.2
KHLSS274	71	72	DIP KHL	0.25	10.7	1.6	22.8
KHLSS274	72	73	DIP KHL	0.25	9.45	2.1	19.3
KHLSS274	73	74	DIP KHL	0.25	11.3	1.7	15.4
KHLSS274	74	75	DIP KHL	0.25	11.25	2.4	15
KHLSS274	75	76	DIP KHL	0.25	10.9	2.2	13.8
KHLSS274	76	77	DIP KHL	0.25	12.75	2.4	14.7
KHLSS274	77	78	DIP KHL	0.25	11.25	6.4	20.9
KHLSS274	78	79	DIP KHL	0.25	13.2	3.8	10.6
KHLSS274	79	80	DIP KHL	0.25	12.35	3.6	10.7
KHLSS274	80	81	DIP KHL	0.25	11.9	2.9	8.8
KHLSS274	81	82	DIP KHL	0.25	13.35	2.8	7.3
KHLSS274	82	83	DIP KHL	0.25	11.8	2.5	8.9
KHLSS274	83	84	DIP KHL	0.25	12.1	2.7	7.7
KHLSS274	84	85	DIP KHL	0.25	13.1	3	13.3
KHLSS274	85	86	DIP KHL	0.25	13.35	3.6	68.4
KHLSS274	86	87	DIP KHL	0.25	13.45	3.7	54.2
KHLSS274	87	88	DIP KHL	0.25	14.6	4.7	51.3
KHLSS274	88	89	DIP KHL	0.25	15.05	6.8	100.5
KHLSS274	89	90	DIP KHL	0.25	14.75	6.8	97.8
KHLSS274	90	91	DIP KHL	0.25	14.2	6.5	81.8
KHLSS274	91	92	DIP KHL	0.25	13.7	4.8	73.2
KHLSS274	92	93	DIP KHL	0.25	14.8	3.4	79.5
KHLSS274	93	94	DIP KHL	0.25	15.2	3.9	71.5
KHLSS274	94	95	DIP KHL	0.25	14.25	3.9	73.7
KHLSS274	95	96	DIP KHL	0.25	13.05	4	74.3
KHLSS274	96	97	DIP KHL	0.25	13.15	3.6	79.5
KHLSS274	97	98	DIP KHL	0.25	13.1	3.1	59.8
KHLSS274	98	99	DIP KHL	0.25	12.6	3.9	53.6
KHLSS274	99	100	DIP KHL	0.25	12.5	3.5	16.1
KHLSS274	100	101	DIP KHL	0.25	11.9	2.8	7
KHLSS274	101	102	DIP KHL	0.25	11.35	2.4	7.3
KHLSS274	102	103	DIP KHL	0.25	12.1	2.4	6.5
KHLSS274	103	104	DIP KHL	0.25	12.25	2.2	6.1
KHLSS274	104	105	DIP KHL	0.25	12.75	2.3	5.4
KHLSS274	105	106	DIP KHL	0.25	11	2.2	7.3
KHLSS274	106	107	DIP KHL	0.25	11.5	2.8	6.7
KHLSS274	107	108	DIP KHL	0.25	10.7	2.5	6.8
KHLSS274	108	109	DIP KHL	0.25	11.7	2.8	7.4
KHLSS274	109	110	DIP KHL	0.25	12.7	2.8	19.7
KHLSS274	110	111	DIP KHL	0.25	13.3	3	28.7
KHLSS274	111	112	DIP KHL	0.25	12.8	3	22.5
KHLSS274	112	113	DIP KHL	0.25	12.7	2.8	19.8
KHLSS274	113	114	DIP KHL	0.25	13.85	3	30.5
KHLSS274	114	115	DIP KHL	0.25	14.15	2.9	26
KHLSS274	115	116	DIP KHL	0.25	12.85	3	8.5

Hole_ID	Depth_From	Depth_To	Strat. Code	Ag_ppm	Al2O3 %	As_ppm	Ba_ppm
KHLSS274	116	117	DIP KHL	0.25	12.1	3.1	8.3
KHLSS274	117	118	DIP KHL	0.25	11	2.9	8.4
KHLSS274	118	119	DIP KHL	0.25	11.65	2.9	7.4
KHLSS274	119	120	DIP KHL	0.25	11.75	2.7	7.6
KHLSS274	120	121	DIP KHL	0.25	11.65	2.6	7.8
KHLSS274	121	122	DIP KHL	0.25	12.75	2.6	8.5
KHLSS274	122	123	DIP KHL	0.25	13.15	2.8	8.4
KHLSS274	123	124	DIP KHL	0.25	10.95	2.6	7.4
KHLSS274	124	125	DIP KHL	0.25	10.7	2.6	8.4
KHLSS274	125	126	HBX KHL	0.25	9.97	3.2	6.7
KHLSS274	126	127	HBX KHL	0.25	12.5	2.6	58.9
KHLSS274	127	128	HBX KHL	0.25	13.2	3.5	249
KHLSS274	128	129	HBX KHL	0.25	10.95	2.2	78.4
KHLSS274	129	130	HBX KHL	0.25	13.3	1.7	85
KHLSS274	130	131	HBX KHL	0.25	14.05	1.7	97.2
KHLSS274	131	132	HBX KHL	0.25	12.1	3.7	120.5
KHLSS274	132	133	HBX KHL	0.25	11.7	4.5	113.5
KHLSS274	133	134	RAT KHL	0.25	13.3	2.9	122.5
KHLSS274	134	135	RAT KHL	0.25	13.55	2.6	207
KHLSS274	135	136	RAT KHL	0.25	13.45	3.1	249
KHLSS274	136	137	RAT KHL	0.25	13.45	3	293
KHLSS274	137	138	RAT KHL	0.25	13.9	2.3	334
KHLSS274	138	139	RAT KHL	0.25	14.8	3.1	313
KHLSS274	139	140	RAT KHL	0.25	13.9	3.2	289
KHLSS274	140	141	RAT KHL	0.25	14.8	1.2	323
KHLSS274	141	142	RAT KHL	0.25	14.25	2.7	262
KHLSS274	142	143	RAT KHL	0.25	14.25	1.6	233
KHLSS274	143	144	RAT KHL	0.25	13.45	2.9	201
KHLSS274	144	145	RAT KHL	0.25	13.65	3.5	240
KHLSS274	145	146	RAT KHL	0.25	14	0.9	176.5
KHLSS274	146	147	RAT KHL	0.25	13.15	2.3	178
KHLSS274	147	148	RAT KHL	0.25	11.25	6	174
KHLSS274	148	149	RAT KHL	0.25	11.35	5	167
KHLSS274	149	150	RAT KHL	0.25	12.5	2.4	163.5
KHLSS274	150	151	RAT KHL	0.25	12.85	2.1	195
KHLSS274	151	152	RAT KHL	0.25	11.65	1.8	178
KHLSS274	152	153	RAT KHL	0.25	11.25	3.4	255
KHLSS274	153	154	RAT KHL	0.25	12.45	2.3	301
KHLSS274	154	155	RAT KHL	0.25	11.85	3	274
KHLSS274	155	156	RAT KHL	0.25	12.45	1.4	337
KHLSS274	156	157	RAT KHL	0.25	12.2	2.8	347
KHLSS274	157	158	RAT KHL	0.25	11.15	4.6	384
KHLSS274	158	159	RAT KHL	1.2	11.65	11.4	511
KHLSS274	159	160	RAT KHL	0.5	10.5	19.4	518
KHLSS274	160	161	RAT KHL	0.25	11.4	12.9	589
KTCSS315	351	352	RAT KNS	0.25	9.83	22.6	124.5
KTCSS315	352	353	RAT KNS	0.25	11.4	5.6	221
KTCSS315	353	354	RAT KNS	0.25	11.8	11.9	99.1
KTCSS315	354	355	RAT KNS	0.25	13.1	7	286

Hole_ID	Depth_From	Depth_To	Strat. Code	Ag_ppm	Al2O3 %	As_ppm	Ba_ppm
KTCSS315	355	355.8	RAT KNS	0.25	12.8	3.5	283
KTCSS326	264	265	RAT KNS	0.25	13.05	5	84.4
KTCSS326	265	265.9	RAT KNS	0.25	13.05	2.4	98.4
KTCSS326	266.5	267.5	RAT KNS	0.25	12.55	2.2	107
KTCSS326	267.5	268.3	RAT KNS	0.25	12.6	2.3	148
KTCSS326	268.3	270	RAT KNS	0.25	13.05	3.6	207
KTCSS326	270	271	RAT KNS	0.25	12.35	4	109.5
KTCSS326	271	272	RAT KNS	0.25	13.15	4.4	125.5
KTCSS326	272	273	RAT KNS	0.25	12.25	4.1	108.5
KTCSS326	273	274	RAT KNS	0.25	13.25	4.5	1535
KTCSS326	279	280	RAT KNS	0.25	14.1	2.2	42
KTCSS326	280	281	RAT KNS	0.25	13.95	2.7	58.1
KTCSS326	286	287	HBX KNS	0.25	11.6	4.4	24.3
KTCSS326	287	288	DIP KNS	0.25	12.85	3.6	12.7
KTCSS326	294	295	DIP KNS	0.25	10.25	4.9	19.4
KTCSS326	295	296	DIP KNS	0.25	9.91	3.9	136
SM59016	20.4	24	DIP SM	0.25	14.7	17.8	194
SM59016	24	27.9	DIP SM	2.7	7.27	10	277
SM59016	30.9	34	DIP SM	0.25	0.42	1.7	22.9
SM59016	34	38	DIP SM	0.25	0.33	4.3	66.8
SM59016	38	42	DIP SM	0.25	0.24	2.7	40.6
SM59016	42	43.4	DIP SM	0.25	0.25	2.7	47.5
SM59016	44.4	46	DIP SM	0.25	0.19	2.3	21.4
SM59016	46	47.4	DIP SM	0.25	0.33	0.9	10.1
SM59016	52.4	54	DIP SM	0.25	0.38	1.1	33.5
SM59016	54	55	DIP SM	0.25	0.14	1.2	16.8
SM59016	55	56	DIP SM	0.25	0.15	1.4	155.5
SM59016	56	60	HBX SM	0.25	0.65	2.9	91.5
SM59016	60	64	HBX SM	0.25	9.24	1.8	95.8
SM59016	64	67.6	HBX SM	0.25	10.85	62.4	42.9
SM59016	67.6	71	HBX SM	0.25	10.4	96.6	17.9
SM59016	71	75	HBX SM	0.25	6.21	11.5	13.4
SM59016	75	77.4	HBX SM	0.25	5.17	22.8	8.7
SM59016	77.4	81	HBX SM	0.25	8.82	15.7	23.3
SM59016	81	85	HBX SM	0.25	10.35	1.9	39.7
SM59016	85	86.4	HBX SM	0.25	13.15	2	16.7
SM59016	86.4	89	HBX SM	0.25	9.21	2.7	43.7
SM59016	89	90.8	HBX SM	0.25	10.5	5.7	44.1
SM59016	90.8	95	HBX SM	0.25	12.3	2.1	3.4
SM59016	95	99	HBX SM	0.25	13.4	1.9	4.4
SM59016	99	103	HBX SM	0.25	12.1	1.9	5
SM59016	103	107	HBX SM	0.25	10.65	1.4	6.7
SM59016	107	111	RAT SM	0.25	12.85	1.2	89.7
SM59016	111	115	RAT SM	0.25	13.7	1.2	238
SM59016	115	119	RAT SM	0.25	14.35	1.5	199
SM59016	119	123	RAT SM	0.25	13.15	1.4	220
SM59016	123	127	RAT SM	0.25	12.55	1.5	139
SM59016	127	131	RAT SM	0.25	12.85	1.6	118
SM59016	131	135	RAT SM	0.25	11.75	1.9	154

Hole_ID	Depth_From	Depth_To	Strat. Code	Ag_ppm	Al2O3 %	As_ppm	Ba_ppm
SM59016	135	139	RAT SM	0.25	12.3	1.8	113.5
SM59016	139	143	RAT SM	0.25	11.55	4.3	104.5
SM59016	143	144	RAT SM	0.25	12.6	1.6	128
SM59016	144	145	RAT SM	0.25	12.65	3.8	119
SM59016	145	146	RAT SM	0.25	12.15	17.7	113
SM59016	146	147.3	RAT SM	0.25	8.96	54.9	73.3

Hole_ID	Depth_From	Depth_To	Strat. Code	BaO_%	Bi_ppm	C_%	CaO_%
KHLSS274	70	71	DIP KHL	0.005	0.02	0.29	1.62
KHLSS274	71	72	DIP KHL	0.005	0.005	2.37	6.21
KHLSS274	72	73	DIP KHL	0.005	0.005	3.8	9.76
KHLSS274	73	74	DIP KHL	0.005	0.005	2.22	5.63
KHLSS274	74	75	DIP KHL	0.005	0.005	2.78	7.11
KHLSS274	75	76	DIP KHL	0.005	0.005	2.83	7.22
KHLSS274	76	77	DIP KHL	0.005	0.005	1.34	3.46
KHLSS274	77	78	DIP KHL	0.005	0.005	2.89	7.44
KHLSS274	78	79	DIP KHL	0.005	0.01	1.55	3.84
KHLSS274	79	80	DIP KHL	0.005	0.005	2.39	5.83
KHLSS274	80	81	DIP KHL	0.005	0.005	2.94	7.11
KHLSS274	81	82	DIP KHL	0.005	0.005	1.62	3.93
KHLSS274	82	83	DIP KHL	0.005	0.005	2.77	6.73
KHLSS274	83	84	DIP KHL	0.005	0.01	2.46	5.67
KHLSS274	84	85	DIP KHL	0.005	0.005	1.63	3.87
KHLSS274	85	86	DIP KHL	0.01	0.005	1.78	4.12
KHLSS274	86	87	DIP KHL	0.01	0.005	1.79	4.33
KHLSS274	87	88	DIP KHL	0.01	0.005	1.07	2.7
KHLSS274	88	89	DIP KHL	0.01	0.005	0.62	1.58
KHLSS274	89	90	DIP KHL	0.01	0.005	0.92	2.34
KHLSS274	90	91	DIP KHL	0.01	0.005	1.22	3.02
KHLSS274	91	92	DIP KHL	0.01	0.005	1.69	4.09
KHLSS274	92	93	DIP KHL	0.01	0.005	0.52	1.37
KHLSS274	93	94	DIP KHL	0.01	0.005	0.29	0.81
KHLSS274	94	95	DIP KHL	0.01	0.005	0.73	1.82
KHLSS274	95	96	DIP KHL	0.01	0.005	2.01	4.78
KHLSS274	96	97	DIP KHL	0.01	0.005	2	4.79
KHLSS274	97	98	DIP KHL	0.01	0.005	1.92	4.56
KHLSS274	98	99	DIP KHL	0.01	0.005	2.54	5.91
KHLSS274	99	100	DIP KHL	0.005	0.005	2.35	5.48
KHLSS274	100	101	DIP KHL	0.005	0.005	2.78	6.48
KHLSS274	101	102	DIP KHL	0.005	0.005	3.51	7.97
KHLSS274	102	103	DIP KHL	0.005	0.005	2.67	6.11
KHLSS274	103	104	DIP KHL	0.005	0.005	2.35	5.42
KHLSS274	104	105	DIP KHL	0.005	0.005	1.73	4.03
KHLSS274	105	106	DIP KHL	0.005	0.005	3.57	8.15
KHLSS274	106	107	DIP KHL	0.005	0.005	2.75	6.43
KHLSS274	107	108	DIP KHL	0.005	0.01	3.81	8.67
KHLSS274	108	109	DIP KHL	0.005	0.005	3.03	7.05
KHLSS274	109	110	DIP KHL	0.005	0.005	1.8	4.18
KHLSS274	110	111	DIP KHL	0.005	0.005	1.77	4.19

Hole_ID	Depth_From	Depth_To	Strat. Code	BaO_%	Bi_ppm	C_%	CaO_%
KHLSS274	111	112	DIP KHL	0.005	0.005	2.39	5.94
KHLSS274	112	113	DIP KHL	0.005	0.005	2.41	5.73
KHLSS274	113	114	DIP KHL	0.005	0.005	1.3	3.06
KHLSS274	114	115	DIP KHL	0.005	0.01	0.88	2.07
KHLSS274	115	116	DIP KHL	0.005	0.01	2.19	5.04
KHLSS274	116	117	DIP KHL	0.005	0.01	2.63	6.21
KHLSS274	117	118	DIP KHL	0.005	0.02	3.43	7.97
KHLSS274	118	119	DIP KHL	0.005	0.02	3.11	7.28
KHLSS274	119	120	DIP KHL	0.005	0.04	3.08	7.3
KHLSS274	120	121	DIP KHL	0.005	0.05	3.18	7.43
KHLSS274	121	122	DIP KHL	0.005	0.08	2.12	5
KHLSS274	122	123	DIP KHL	0.005	0.08	1.85	4.37
KHLSS274	123	124	DIP KHL	0.005	0.05	4.07	9.46
KHLSS274	124	125	DIP KHL	0.005	0.02	4.19	9.79
KHLSS274	125	126	HBX KHL	0.005	0.23	4.8	11.2
KHLSS274	126	127	HBX KHL	0.01	0.3	2.88	6.72
KHLSS274	127	128	HBX KHL	0.03	0.39	2.94	7.08
KHLSS274	128	129	HBX KHL	0.01	0.82	3.77	8.83
KHLSS274	129	130	HBX KHL	0.01	0.31	1.73	4.08
KHLSS274	130	131	HBX KHL	0.01	0.19	1.08	2.68
KHLSS274	131	132	HBX KHL	0.01	0.15	2.91	7.27
KHLSS274	132	133	HBX KHL	0.01	0.13	3.02	7.62
KHLSS274	133	134	RAT KHL	0.01	0.03	1.49	3.68
KHLSS274	134	135	RAT KHL	0.02	0.03	1.52	3.7
KHLSS274	135	136	RAT KHL	0.03	0.02	1.67	4.12
KHLSS274	136	137	RAT KHL	0.03	0.02	1.17	2.97
KHLSS274	137	138	RAT KHL	0.04	0.07	0.83	2.2
KHLSS274	138	139	RAT KHL	0.04	0.02	0.74	1.96
KHLSS274	139	140	RAT KHL	0.03	0.02	0.85	2.19
KHLSS274	140	141	RAT KHL	0.04	0.02	0.52	1.42
KHLSS274	141	142	RAT KHL	0.03	0.02	0.95	2.39
KHLSS274	142	143	RAT KHL	0.02	0.01	0.71	1.91
KHLSS274	143	144	RAT KHL	0.02	0.02	1.36	3.45
KHLSS274	144	145	RAT KHL	0.02	0.02	1.44	3.66
KHLSS274	145	146	RAT KHL	0.02	0.02	1.03	2.66
KHLSS274	146	147	RAT KHL	0.02	0.02	1.55	3.9
KHLSS274	147	148	RAT KHL	0.02	0.03	2.37	5.88
KHLSS274	148	149	RAT KHL	0.02	0.1	2.63	6.47
KHLSS274	149	150	RAT KHL	0.02	0.02	1.79	4.5
KHLSS274	150	151	RAT KHL	0.02	0.01	1.31	3.24
KHLSS274	151	152	RAT KHL	0.02	0.01	1.95	4.83
KHLSS274	152	153	RAT KHL	0.03	0.01	3.11	7.59
KHLSS274	153	154	RAT KHL	0.03	0.01	2.61	6.4
KHLSS274	154	155	RAT KHL	0.03	0.02	2.8	6.91
KHLSS274	155	156	RAT KHL	0.03	0.01	2.43	5.95
KHLSS274	156	157	RAT KHL	0.04	0.02	2.98	7.38
KHLSS274	157	158	RAT KHL	0.04	0.01	3.97	9.76
KHLSS274	158	159	RAT KHL	0.06	0.58	3.42	8.47
KHLSS274	159	160	RAT KHL	0.06	1.85	4.18	10.25

Hole_ID	Depth_From	Depth_To	Strat. Code	BaO_%	Bi_ppm	C_%	CaO_%
KHLSS274	160	161	RAT KHL	0.06	1.35	3.25	7.81
KTCSS315	351	352	RAT KNS	0.01	0.47	4.08	7.44
KTCSS315	352	353	RAT KNS	0.02	0.2	2.75	6.59
KTCSS315	353	354	RAT KNS	0.01	0.11	2.57	5.94
KTCSS315	354	355	RAT KNS	0.03	0.02	2.2	5.11
KTCSS315	355	355.8	RAT KNS	0.03	0.01	2.07	4.75
KTCSS326	264	265	RAT KNS	0.01	0.02	2.12	4.02
KTCSS326	265	265.9	RAT KNS	0.01	0.02	1.56	3.7
KTCSS326	266.5	267.5	RAT KNS	0.01	0.06	2.11	4.7
KTCSS326	267.5	268.3	RAT KNS	0.02	0.02	2.11	5.19
KTCSS326	268.3	270	RAT KNS	0.02	0.01	2.1	4.91
KTCSS326	270	271	RAT KNS	0.01	0.01	2.58	5.89
KTCSS326	271	272	RAT KNS	0.01	0.03	1.6	3.8
KTCSS326	272	273	RAT KNS	0.01	0.02	1.65	3.94
KTCSS326	273	274	RAT KNS	0.17	0.01	1.34	3.2
KTCSS326	279	280	RAT KNS	0.005	0.005	1.42	3.16
KTCSS326	280	281	RAT KNS	0.01	0.01	1.4	3.35
KTCSS326	286	287	HBX KNS	0.005	0.02	2.94	7.13
KTCSS326	287	288	DIP KNS	0.005	0.02	2.3	5.2
KTCSS326	294	295	DIP KNS	0.005	0.01	3.89	5.12
KTCSS326	295	296	DIP KNS	0.01	0.01	4.41	1.37
SM59016	20.4	24	DIP SM	0.02	0.5	0.06	0.19
SM59016	24	27.9	DIP SM	0.03	0.47	0.09	0.2
SM59016	30.9	34	DIP SM	0.005	0.09	11.2	26
SM59016	34	38	DIP SM	0.01	0.05	11	25.5
SM59016	38	42	DIP SM	0.005	0.02	11.35	26.3
SM59016	42	43.4	DIP SM	0.005	0.01	11.35	26.4
SM59016	44.4	46	DIP SM	0.005	0.01	11.45	26.4
SM59016	46	47.4	DIP SM	0.005	0.03	11.65	27.1
SM59016	52.4	54	DIP SM	0.005	0.06	9.13	21
SM59016	54	55	DIP SM	0.005	0.02	12.25	28
SM59016	55	56	DIP SM	0.02	0.02	11.75	27.1
SM59016	56	60	HBX SM	0.01	0.01	10.95	25.5
SM59016	60	64	HBX SM	0.01	0.02	4.59	10.65
SM59016	64	67.6	HBX SM	0.005	0.01	2.86	6.56
SM59016	67.6	71	HBX SM	0.005	0.01	4.15	9.52
SM59016	71	75	HBX SM	0.005	0.01	2.61	6.37
SM59016	75	77.4	HBX SM	0.005	0.005	3.85	9.44
SM59016	77.4	81	HBX SM	0.005	0.005	4.84	12.3
SM59016	81	85	HBX SM	0.005	0.01	3.72	9.4
SM59016	85	86.4	HBX SM	0.005	0.02	1.52	3.96
SM59016	86.4	89	HBX SM	0.005	0.01	4.86	12.2
SM59016	89	90.8	HBX SM	0.005	0.005	3.53	8.89
SM59016	90.8	95	HBX SM	0.005	0.005	2.12	5.09
SM59016	95	99	HBX SM	0.005	0.005	1.28	3.15
SM59016	99	103	HBX SM	0.005	0.005	1.97	4.65
SM59016	103	107	HBX SM	0.005	0.005	2.98	7.25
SM59016	107	111	RAT SM	0.01	0.005	1.69	4.32
SM59016	111	115	RAT SM	0.03	0.01	1.3	3.36

Hole_ID	Depth_From	Depth_To	Strat. Code	BaO_%	Bi_ppm	C_%	CaO_%
SM59016	115	119	RAT SM	0.02	0.01	0.89	2.33
SM59016	119	123	RAT SM	0.02	0.01	1.41	3.48
SM59016	123	127	RAT SM	0.01	0.01	1.79	4.39
SM59016	127	131	RAT SM	0.01	0.01	0.92	2.41
SM59016	131	135	RAT SM	0.02	0.01	1.97	5.01
SM59016	135	139	RAT SM	0.01	0.01	2.12	5.28
SM59016	139	143	RAT SM	0.01	0.01	2.92	7.23
SM59016	143	144	RAT SM	0.01	0.01	2.34	5.59
SM59016	144	145	RAT SM	0.01	0.01	2.08	5.26
SM59016	145	146	RAT SM	0.01	0.69	1.86	4.44
SM59016	146	147.3	RAT SM	0.01	1.01	3.82	9.51

Hole_ID	Depth_From	Depth_To	Strat. Code	Cd_ppm	Ce_ppm	Co_ppm	Cr_ppm
KHLSS274	70	71	DIP KHL	0.25	324	42	100
KHLSS274	71	72	DIP KHL	0.25	6.9	35	60
KHLSS274	72	73	DIP KHL	0.25	6.4	35	60
KHLSS274	73	74	DIP KHL	0.25	3.4	25	70
KHLSS274	74	75	DIP KHL	0.25	4	21	60
KHLSS274	75	76	DIP KHL	0.25	6.2	16	50
KHLSS274	76	77	DIP KHL	0.25	3.6	21	60
KHLSS274	77	78	DIP KHL	0.25	8.3	9	50
KHLSS274	78	79	DIP KHL	0.25	61.8	6	60
KHLSS274	79	80	DIP KHL	0.25	81.1	4	60
KHLSS274	80	81	DIP KHL	0.25	61	4	60
KHLSS274	81	82	DIP KHL	0.25	95.8	4	70
KHLSS274	82	83	DIP KHL	0.25	60.4	4	60
KHLSS274	83	84	DIP KHL	0.25	88.3	4	60
KHLSS274	84	85	DIP KHL	0.25	92.7	4	60
KHLSS274	85	86	DIP KHL	0.25	89.3	5	50
KHLSS274	86	87	DIP KHL	0.25	97	4	60
KHLSS274	87	88	DIP KHL	0.25	118.5	4	60
KHLSS274	88	89	DIP KHL	0.25	112	4	60
KHLSS274	89	90	DIP KHL	0.25	110	4	60
KHLSS274	90	91	DIP KHL	0.25	104	5	60
KHLSS274	91	92	DIP KHL	0.25	97.7	4	60
KHLSS274	92	93	DIP KHL	0.25	102	3	60
KHLSS274	93	94	DIP KHL	0.25	99.6	4	70
KHLSS274	94	95	DIP KHL	0.25	106.5	4	60
KHLSS274	95	96	DIP KHL	0.25	85.3	5	60
KHLSS274	96	97	DIP KHL	0.25	82.7	5	60
KHLSS274	97	98	DIP KHL	0.25	87.6	4	60
KHLSS274	98	99	DIP KHL	0.25	79.4	5	50
KHLSS274	99	100	DIP KHL	0.25	93	5	50
KHLSS274	100	101	DIP KHL	0.25	102	4	50
KHLSS274	101	102	DIP KHL	0.25	104.5	5	50
KHLSS274	102	103	DIP KHL	0.25	110	5	50
KHLSS274	103	104	DIP KHL	0.25	101.5	6	50
KHLSS274	104	105	DIP KHL	0.25	91.8	6	60
KHLSS274	105	106	DIP KHL	0.25	93.1	5	50

Hole_ID	Depth_From	Depth_To	Strat. Code	Cd_ppm	Ce_ppm	Co_ppm	Cr_ppm
KHLSS274	106	107	DIP KHL	0.25	84.8	5	60
KHLSS274	107	108	DIP KHL	0.25	73.4	5	50
KHLSS274	108	109	DIP KHL	0.25	81.6	7	50
KHLSS274	109	110	DIP KHL	0.25	70.6	6	50
KHLSS274	110	111	DIP KHL	0.25	75.7	6	50
KHLSS274	111	112	DIP KHL	0.25	72.9	4	50
KHLSS274	112	113	DIP KHL	0.25	70.7	6	50
KHLSS274	113	114	DIP KHL	0.25	83.1	6	50
KHLSS274	114	115	DIP KHL	0.25	82.4	7	60
KHLSS274	115	116	DIP KHL	0.25	41.3	5	60
KHLSS274	116	117	DIP KHL	0.25	75.4	7	50
KHLSS274	117	118	DIP KHL	0.25	72.5	6	50
KHLSS274	118	119	DIP KHL	0.25	70.3	7	50
KHLSS274	119	120	DIP KHL	0.25	77.2	8	50
KHLSS274	120	121	DIP KHL	0.25	70.6	7	50
KHLSS274	121	122	DIP KHL	0.25	87.9	8	50
KHLSS274	122	123	DIP KHL	0.25	104	7	50
KHLSS274	123	124	DIP KHL	0.25	78.8	8	40
KHLSS274	124	125	DIP KHL	0.25	72.8	9	40
KHLSS274	125	126	HBX KHL	0.25	89.8	12	50
KHLSS274	126	127	HBX KHL	0.25	69.9	21	60
KHLSS274	127	128	HBX KHL	0.25	98.3	20	50
KHLSS274	128	129	HBX KHL	0.25	65.3	13	40
KHLSS274	129	130	HBX KHL	0.25	88.8	12	50
KHLSS274	130	131	HBX KHL	0.25	93.4	14	60
KHLSS274	131	132	HBX KHL	0.5	89.1	16	50
KHLSS274	132	133	HBX KHL	0.25	80.6	19	50
KHLSS274	133	134	RAT KHL	0.25	76.7	21	60
KHLSS274	134	135	RAT KHL	0.25	94.9	16	70
KHLSS274	135	136	RAT KHL	0.25	91.8	13	60
KHLSS274	136	137	RAT KHL	0.25	98.5	12	60
KHLSS274	137	138	RAT KHL	0.25	90.2	12	70
KHLSS274	138	139	RAT KHL	0.25	107	12	60
KHLSS274	139	140	RAT KHL	0.25	98.2	11	60
KHLSS274	140	141	RAT KHL	0.25	102.5	11	60
KHLSS274	141	142	RAT KHL	0.25	93.6	12	60
KHLSS274	142	143	RAT KHL	0.25	111	12	60
KHLSS274	143	144	RAT KHL	0.25	103.5	11	60
KHLSS274	144	145	RAT KHL	0.25	91.7	11	60
KHLSS274	145	146	RAT KHL	0.25	95.5	12	60
KHLSS274	146	147	RAT KHL	0.25	94.1	11	60
KHLSS274	147	148	RAT KHL	0.25	101	9	50
KHLSS274	148	149	RAT KHL	0.25	103.5	9	50
KHLSS274	149	150	RAT KHL	0.25	99	11	60
KHLSS274	150	151	RAT KHL	0.25	112	11	60
KHLSS274	151	152	RAT KHL	0.25	79.9	10	50
KHLSS274	152	153	RAT KHL	0.25	93.7	7	50
KHLSS274	153	154	RAT KHL	0.25	102	7	60
KHLSS274	154	155	RAT KHL	0.25	86.5	6	50

Hole_ID	Depth_From	Depth_To	Strat. Code	Cd_ppm	Ce_ppm	Co_ppm	Cr_ppm
KHLSS274	155	156	RAT KHL	0.25	107	7	60
KHLSS274	156	157	RAT KHL	0.25	98.6	7	60
KHLSS274	157	158	RAT KHL	0.25	74.4	9	60
KHLSS274	158	159	RAT KHL	0.25	73.9	23	60
KHLSS274	159	160	RAT KHL	0.25	67.5	83	50
KHLSS274	160	161	RAT KHL	0.25	51.1	69	60
KTCSS315	351	352	RAT KNS	0.25	2.2	1090	50
KTCSS315	352	353	RAT KNS	0.25	11.3	164	60
KTCSS315	353	354	RAT KNS	0.25	13.2	129	60
KTCSS315	354	355	RAT KNS	0.25	8.9	82	70
KTCSS315	355	355.8	RAT KNS	0.25	3.8	100	60
KTCSS326	264	265	RAT KNS	0.25	6.8	112	70
KTCSS326	265	265.9	RAT KNS	0.25	12.8	68	60
KTCSS326	266.5	267.5	RAT KNS	0.25	11.3	48	70
KTCSS326	267.5	268.3	RAT KNS	0.25	9.3	36	70
KTCSS326	268.3	270	RAT KNS	0.25	32.2	40	70
KTCSS326	270	271	RAT KNS	0.25	75.7	46	60
KTCSS326	271	272	RAT KNS	0.25	71.9	53	70
KTCSS326	272	273	RAT KNS	0.25	91.1	55	60
KTCSS326	273	274	RAT KNS	0.25	92.6	54	70
KTCSS326	279	280	RAT KNS	0.25	4	31	70
KTCSS326	280	281	RAT KNS	0.25	4.5	35	70
KTCSS326	286	287	HBX KNS	0.25	45.8	37	60
KTCSS326	287	288	DIP KNS	0.25	54.1	28	60
KTCSS326	294	295	DIP KNS	0.25	118	10	60
KTCSS326	295	296	DIP KNS	0.25	135.5	12	50
SM59016	20.4	24	DIP SM	0.25	95.2	42	100
SM59016	24	27.9	DIP SM	0.25	44.5	27	40
SM59016	30.9	34	DIP SM	0.25	3.7	3	10
SM59016	34	38	DIP SM	0.25	3.1	1	5
SM59016	38	42	DIP SM	0.25	1.7	1	30
SM59016	42	43.4	DIP SM	0.25	1.7	3	5
SM59016	44.4	46	DIP SM	0.25	1.3	2	30
SM59016	46	47.4	DIP SM	0.25	2.5	0.5	5
SM59016	52.4	54	DIP SM	0.25	2.5	2	270
SM59016	54	55	DIP SM	0.25	1.5	0.5	5
SM59016	55	56	DIP SM	0.25	1.8	0.5	20
SM59016	56	60	HBX SM	0.8	4	1	10
SM59016	60	64	HBX SM	0.25	48.4	13	70
SM59016	64	67.6	HBX SM	0.25	39.6	11	50
SM59016	67.6	71	HBX SM	0.25	69	8	60
SM59016	71	75	HBX SM	2	5.7	5	50
SM59016	75	77.4	HBX SM	2.1	8.4	4	50
SM59016	77.4	81	HBX SM	0.8	28.1	7	50
SM59016	81	85	HBX SM	0.6	7.6	56	70
SM59016	85	86.4	HBX SM	0.25	134	158	100
SM59016	86.4	89	HBX SM	0.25	56.5	35	70
SM59016	89	90.8	HBX SM	0.25	71.3	10	60
SM59016	90.8	95	HBX SM	0.25	3.7	6	80

Hole_ID	Depth_From	Depth_To	Strat. Code	Cd_ppm	Ce_ppm	Co_ppm	Cr_ppm
SM59016	95	99	HBX SM	0.25	5.9	30	120
SM59016	99	103	HBX SM	0.5	7.3	34	80
SM59016	103	107	HBX SM	0.6	3.7	11	90
SM59016	107	111	RAT SM	0.25	36.9	17	70
SM59016	111	115	RAT SM	0.25	122	31	80
SM59016	115	119	RAT SM	0.25	68.2	32	70
SM59016	119	123	RAT SM	0.25	55.6	32	80
SM59016	123	127	RAT SM	0.25	99.7	30	70
SM59016	127	131	RAT SM	0.25	75.2	32	70
SM59016	131	135	RAT SM	0.25	84.1	28	60
SM59016	135	139	RAT SM	0.25	107	21	70
SM59016	139	143	RAT SM	0.25	99.9	17	70
SM59016	143	144	RAT SM	0.25	20.2	30	70
SM59016	144	145	RAT SM	0.25	45.5	66	80
SM59016	145	146	RAT SM	0.6	17.6	96	70
SM59016	146	147.3	RAT SM	1.4	97.9	381	70

Hole_ID	Depth_From	Depth_To	Strat. Code	Cr2O3_ppm	Cs_ppm	Cu_ppm	Dy_ppm
KHLSS274	70	71	DIP KHL	130	0.68	20	10.25
KHLSS274	71	72	DIP KHL	70	0.3	42	0.98
KHLSS274	72	73	DIP KHL	70	0.2	93	1.37
KHLSS274	73	74	DIP KHL	80	0.25	19	1.03
KHLSS274	74	75	DIP KHL	70	0.21	50	1.3
KHLSS274	75	76	DIP KHL	60	0.16	12	1.8
KHLSS274	76	77	DIP KHL	80	0.17	7	1.6
KHLSS274	77	78	DIP KHL	60	0.8	13	2.86
KHLSS274	78	79	DIP KHL	80	0.68	2	6.23
KHLSS274	79	80	DIP KHL	80	0.61	4	3.9
KHLSS274	80	81	DIP KHL	70	0.47	5	2.11
KHLSS274	81	82	DIP KHL	90	0.57	7	2.53
KHLSS274	82	83	DIP KHL	80	0.5	4	1.85
KHLSS274	83	84	DIP KHL	80	0.61	5	2.04
KHLSS274	84	85	DIP KHL	80	0.59	5	3.86
KHLSS274	85	86	DIP KHL	80	0.98	8	2.8
KHLSS274	86	87	DIP KHL	80	0.86	7	1.95
KHLSS274	87	88	DIP KHL	80	0.87	7	2.16
KHLSS274	88	89	DIP KHL	80	1.1	7	1.8
KHLSS274	89	90	DIP KHL	80	1.31	6	3.66
KHLSS274	90	91	DIP KHL	80	1	6	1.77
KHLSS274	91	92	DIP KHL	80	0.86	7	1.56
KHLSS274	92	93	DIP KHL	90	0.93	7	2.02
KHLSS274	93	94	DIP KHL	90	0.75	8	1.96
KHLSS274	94	95	DIP KHL	80	0.83	6	3.41
KHLSS274	95	96	DIP KHL	80	0.94	5	4.56
KHLSS274	96	97	DIP KHL	80	0.96	5	5.13
KHLSS274	97	98	DIP KHL	80	0.91	6	8.04
KHLSS274	98	99	DIP KHL	70	0.9	5	3.27
KHLSS274	99	100	DIP KHL	70	0.56	5	2.86
KHLSS274	100	101	DIP KHL	70	0.42	13	2.56

Hole_ID	Depth_From	Depth_To	Strat. Code	Cr2O3_ppm	Cs_ppm	Cu_ppm	Dy_ppm
KHLSS274	101	102	DIP KHL	60	0.5	12	3.26
KHLSS274	102	103	DIP KHL	80	0.4	7	3.1
KHLSS274	103	104	DIP KHL	80	0.48	10	2.82
KHLSS274	104	105	DIP KHL	80	0.45	9	4.85
KHLSS274	105	106	DIP KHL	60	0.37	7	3.23
KHLSS274	106	107	DIP KHL	80	0.37	7	6.43
KHLSS274	107	108	DIP KHL	70	0.35	7	3.66
KHLSS274	108	109	DIP KHL	60	0.38	7	8.93
KHLSS274	109	110	DIP KHL	70	0.52	8	8.29
KHLSS274	110	111	DIP KHL	70	0.59	10	6.95
KHLSS274	111	112	DIP KHL	80	0.51	29	5.73
KHLSS274	112	113	DIP KHL	70	0.53	9	5.43
KHLSS274	113	114	DIP KHL	70	0.61	11	10.1
KHLSS274	114	115	DIP KHL	70	0.64	11	6.76
KHLSS274	115	116	DIP KHL	80	0.5	6	9.92
KHLSS274	116	117	DIP KHL	70	0.49	8	6.49
KHLSS274	117	118	DIP KHL	70	0.5	9	4.31
KHLSS274	118	119	DIP KHL	60	0.46	9	2.83
KHLSS274	119	120	DIP KHL	60	0.46	10	2.46
KHLSS274	120	121	DIP KHL	60	0.46	9	2.42
KHLSS274	121	122	DIP KHL	70	0.46	12	2.74
KHLSS274	122	123	DIP KHL	70	0.48	15	3.67
KHLSS274	123	124	DIP KHL	50	0.49	15	2.23
KHLSS274	124	125	DIP KHL	60	0.58	12	2.74
KHLSS274	125	126	HBX KHL	60	0.59	9	8.69
KHLSS274	126	127	HBX KHL	80	1.03	56	5.17
KHLSS274	127	128	HBX KHL	70	2.65	154	6.29
KHLSS274	128	129	HBX KHL	60	1.16	75	4.8
KHLSS274	129	130	HBX KHL	70	1.42	23	4.91
KHLSS274	130	131	HBX KHL	70	1.81	24	5.74
KHLSS274	131	132	HBX KHL	80	1.73	49	5.19
KHLSS274	132	133	HBX KHL	80	2.15	50	5.39
KHLSS274	133	134	RAT KHL	80	2.97	39	5.71
KHLSS274	134	135	RAT KHL	80	2.58	15	6.33
KHLSS274	135	136	RAT KHL	80	2.86	8	6.31
KHLSS274	136	137	RAT KHL	70	2.94	4	5.72
KHLSS274	137	138	RAT KHL	80	3	3	5.93
KHLSS274	138	139	RAT KHL	80	3.94	3	6.1
KHLSS274	139	140	RAT KHL	70	3.94	3	5.57
KHLSS274	140	141	RAT KHL	80	4.56	3	6.12
KHLSS274	141	142	RAT KHL	80	3.82	2	5.42
KHLSS274	142	143	RAT KHL	80	3.3	2	7.78
KHLSS274	143	144	RAT KHL	80	2.89	2	6.81
KHLSS274	144	145	RAT KHL	80	3.2	2	6.06
KHLSS274	145	146	RAT KHL	90	2.41	2	6.01
KHLSS274	146	147	RAT KHL	80	2.22	2	6.1
KHLSS274	147	148	RAT KHL	60	1.97	2	9.94
KHLSS274	148	149	RAT KHL	70	1.7	2	8.14
KHLSS274	149	150	RAT KHL	80	1.82	2	6.65

Hole_ID	Depth_From	Depth_To	Strat. Code	Cr2O3_ppm	Cs_ppm	Cu_ppm	Dy_ppm
KHLSS274	150	151	RAT KHL	90	2.01	2	8.21
KHLSS274	151	152	RAT KHL	70	1.83	2	6.37
KHLSS274	152	153	RAT KHL	70	2	1	6.27
KHLSS274	153	154	RAT KHL	70	2.43	1	6.25
KHLSS274	154	155	RAT KHL	70	2.05	2	7.03
KHLSS274	155	156	RAT KHL	80	2.46	3	7.51
KHLSS274	156	157	RAT KHL	70	2.71	4	6.23
KHLSS274	157	158	RAT KHL	80	2.11	6	5.42
KHLSS274	158	159	RAT KHL	80	2.15	34	5.53
KHLSS274	159	160	RAT KHL	70	2.07	91	5.74
KHLSS274	160	161	RAT KHL	80	2.98	46	4.67
KTCSS315	351	352	RAT KNS	80	0.38	132	5.51
KTCSS315	352	353	RAT KNS	80	0.76	43	4.97
KTCSS315	353	354	RAT KNS	80	0.74	60	4.26
KTCSS315	354	355	RAT KNS	80	0.9	9	7.03
KTCSS315	355	355.8	RAT KNS	80	1.01	6	7.57
KTCSS326	264	265	RAT KNS	100	0.57	13	6.53
KTCSS326	265	265.9	RAT KNS	90	0.69	8	6.74
KTCSS326	266.5	267.5	RAT KNS	100	0.74	31	7.64
KTCSS326	267.5	268.3	RAT KNS	90	0.66	23	7.25
KTCSS326	268.3	270	RAT KNS	90	0.81	46	6.22
KTCSS326	270	271	RAT KNS	80	0.64	35	6.34
KTCSS326	271	272	RAT KNS	90	0.72	52	6.5
KTCSS326	272	273	RAT KNS	90	0.47	44	5.42
KTCSS326	273	274	RAT KNS	100	0.27	51	8.46
KTCSS326	279	280	RAT KNS	100	0.1	14	6.63
KTCSS326	280	281	RAT KNS	90	0.06	12	7.53
KTCSS326	286	287	HBX KNS	90	0.07	40	37.2
KTCSS326	287	288	DIP KNS	100	0.03	10	9.15
KTCSS326	294	295	DIP KNS	80	0.05	4	14.9
KTCSS326	295	296	DIP KNS	70	0.03	4	20.6
SM59016	20.4	24	DIP SM	160	2.19	75	6.21
SM59016	24	27.9	DIP SM	70	4.2	54	3.64
SM59016	30.9	34	DIP SM	20	0.81	6	0.29
SM59016	34	38	DIP SM	10	0.78	10	0.15
SM59016	38	42	DIP SM	50	0.43	13	0.11
SM59016	42	43.4	DIP SM	10	0.49	11	0.15
SM59016	44.4	46	DIP SM	60	0.46	10	0.11
SM59016	46	47.4	DIP SM	10	0.53	8	0.15
SM59016	52.4	54	DIP SM	400	0.85	16	0.16
SM59016	54	55	DIP SM	10	0.31	5	0.11
SM59016	55	56	DIP SM	40	0.29	49	0.1
SM59016	56	60	HBX SM	20	0.33	65	0.32
SM59016	60	64	HBX SM	110	1.08	23	3.42
SM59016	64	67.6	HBX SM	70	0.54	3	3.04
SM59016	67.6	71	HBX SM	90	0.26	5	4.85
SM59016	71	75	HBX SM	70	0.12	3	3.71
SM59016	75	77.4	HBX SM	60	0.1	10	3.03
SM59016	77.4	81	HBX SM	60	0.32	9	3.29

Hole_ID	Depth_From	Depth_To	Strat. Code	Cr2O3_ppm	Cs_ppm	Cu_ppm	Dy_ppm
SM59016	81	85	HBX SM	90	0.56	55	2.28
SM59016	85	86.4	HBX SM	130	3.96	101	7.7
SM59016	86.4	89	HBX SM	90	1.71	4	3.9
SM59016	89	90.8	HBX SM	70	0.99	1	6.06
SM59016	90.8	95	HBX SM	100	0.05	2	1.37
SM59016	95	99	HBX SM	160	0.13	2	1.15
SM59016	99	103	HBX SM	100	0.1	1	1.39
SM59016	103	107	HBX SM	110	0.02	1	8.56
SM59016	107	111	RAT SM	90	1.05	0.5	6.63
SM59016	111	115	RAT SM	110	1.88	1	5.5
SM59016	115	119	RAT SM	90	1.88	0.5	4.94
SM59016	119	123	RAT SM	90	1.58	0.5	5.74
SM59016	123	127	RAT SM	80	1.33	0.5	7.37
SM59016	127	131	RAT SM	100	1.17	0.5	13.05
SM59016	131	135	RAT SM	80	0.94	0.5	7.36
SM59016	135	139	RAT SM	90	1.6	2	5.98
SM59016	139	143	RAT SM	100	1.55	0.5	6.61
SM59016	143	144	RAT SM	90	1.75	0.5	4.92
SM59016	144	145	RAT SM	110	1.57	4	5.01
SM59016	145	146	RAT SM	100	1.47	353	4.79
SM59016	146	147.3	RAT SM	90	0.77	726	4.65

Hole_ID	Depth_From	Depth_To	Strat. Code	Er_ppm	Eu_ppm	Fe2O3_%	Ga_ppm
KHLSS274	70	71	DIP KHL	3.68	5.84	3.53	21.4
KHLSS274	71	72	DIP KHL	0.61	0.28	2.42	15.7
KHLSS274	72	73	DIP KHL	0.95	0.17	1.87	14.1
KHLSS274	73	74	DIP KHL	0.76	0.08	2.26	13.3
KHLSS274	74	75	DIP KHL	0.86	0.14	2.07	12.7
KHLSS274	75	76	DIP KHL	1.02	0.16	2.02	12.8
KHLSS274	76	77	DIP KHL	1.44	0.23	2.6	14.9
KHLSS274	77	78	DIP KHL	1.64	0.61	4.42	6.6
KHLSS274	78	79	DIP KHL	2.89	1.4	5.56	5.7
KHLSS274	79	80	DIP KHL	1.82	1.3	6.5	5.1
KHLSS274	80	81	DIP KHL	1.12	1.09	5.25	4.5
KHLSS274	81	82	DIP KHL	1.22	1.11	4.87	5.9
KHLSS274	82	83	DIP KHL	1.05	1.1	4.65	4.8
KHLSS274	83	84	DIP KHL	1.07	1.1	4.55	5.8
KHLSS274	84	85	DIP KHL	2.32	1.09	3.96	7.2
KHLSS274	85	86	DIP KHL	1.7	1.1	3.54	7.9
KHLSS274	86	87	DIP KHL	1.11	1.35	2.89	7.1
KHLSS274	87	88	DIP KHL	1.21	1.61	1.23	7.1
KHLSS274	88	89	DIP KHL	1.02	1.23	2.2	7
KHLSS274	89	90	DIP KHL	2.05	1.26	2.39	6.5
KHLSS274	90	91	DIP KHL	1.17	1.34	0.63	6
KHLSS274	91	92	DIP KHL	1.17	1.16	1.5	6.5
KHLSS274	92	93	DIP KHL	1.27	1.16	1.81	5.9
KHLSS274	93	94	DIP KHL	1.21	1.22	1.83	6.3
KHLSS274	94	95	DIP KHL	2.21	1.76	1.35	5.8
KHLSS274	95	96	DIP KHL	3.27	1.28	2.43	6.8

Hole_ID	Depth_From	Depth_To	Strat. Code	Er_ppm	Eu_ppm	Fe2O3_%	Ga_ppm
KHLSS274	96	97	DIP KHL	3.62	1.43	2.51	6.5
KHLSS274	97	98	DIP KHL	5.95	1.3	2	6.1
KHLSS274	98	99	DIP KHL	2.28	1.15	2.06	6.6
KHLSS274	99	100	DIP KHL	1.68	1.17	2	5.5
KHLSS274	100	101	DIP KHL	1.75	0.99	1.5	4.6
KHLSS274	101	102	DIP KHL	1.8	1.14	0.32	4.8
KHLSS274	102	103	DIP KHL	1.62	1.28	1.15	4.9
KHLSS274	103	104	DIP KHL	1.8	1.1	2.08	5
KHLSS274	104	105	DIP KHL	2.73	0.94	4.28	5.7
KHLSS274	105	106	DIP KHL	1.8	1.01	3.32	5.5
KHLSS274	106	107	DIP KHL	3.52	1.27	5.58	5.8
KHLSS274	107	108	DIP KHL	2.17	1.07	3.02	5.4
KHLSS274	108	109	DIP KHL	5.13	1.29	3.08	6.1
KHLSS274	109	110	DIP KHL	5.03	1.34	3.07	7.4
KHLSS274	110	111	DIP KHL	4.21	1.31	3.16	7.8
KHLSS274	111	112	DIP KHL	3.56	1.26	3.47	7.5
KHLSS274	112	113	DIP KHL	3.65	1.29	3.43	6.8
KHLSS274	113	114	DIP KHL	6.47	1.5	4.41	7.6
KHLSS274	114	115	DIP KHL	4.33	1.34	3.69	8
KHLSS274	115	116	DIP KHL	6.73	1.2	4.47	10.2
KHLSS274	116	117	DIP KHL	3.86	1.01	4.41	9.2
KHLSS274	117	118	DIP KHL	2.35	1.09	5.22	7.2
KHLSS274	118	119	DIP KHL	1.47	0.88	3.98	7.8
KHLSS274	119	120	DIP KHL	1.14	0.92	3.38	8.1
KHLSS274	120	121	DIP KHL	1.34	0.94	3.48	8.4
KHLSS274	121	122	DIP KHL	1.49	1.02	3.77	8.7
KHLSS274	122	123	DIP KHL	2.3	1.03	3.79	8.8
KHLSS274	123	124	DIP KHL	1.59	0.79	1.43	8.5
KHLSS274	124	125	DIP KHL	1.57	0.88	2.97	8.4
KHLSS274	125	126	HBX KHL	5.32	1.18	3.67	11.9
KHLSS274	126	127	HBX KHL	2.92	1.32	2.32	22.9
KHLSS274	127	128	HBX KHL	3.06	1.95	4.59	17.7
KHLSS274	128	129	HBX KHL	2.99	1.06	5.71	14.4
KHLSS274	129	130	HBX KHL	2.96	1.4	11.05	18.1
KHLSS274	130	131	HBX KHL	3.23	1.83	10.65	21.8
KHLSS274	131	132	HBX KHL	2.78	1.81	7.76	18.8
KHLSS274	132	133	HBX KHL	2.93	1.38	5.61	17.8
KHLSS274	133	134	RAT KHL	3.3	1.39	5.6	19.4
KHLSS274	134	135	RAT KHL	3.26	1.66	6.42	20
KHLSS274	135	136	RAT KHL	3.51	1.54	5.98	19.6
KHLSS274	136	137	RAT KHL	3.14	1.6	5.93	19.2
KHLSS274	137	138	RAT KHL	3.56	1.54	5.88	19.8
KHLSS274	138	139	RAT KHL	3.5	1.67	6.19	21.6
KHLSS274	139	140	RAT KHL	3.07	1.52	5.94	20.7
KHLSS274	140	141	RAT KHL	3.27	1.5	6.09	21.6
KHLSS274	141	142	RAT KHL	3.03	1.59	6.02	20.9
KHLSS274	142	143	RAT KHL	4.4	1.88	6.3	21.1
KHLSS274	143	144	RAT KHL	3.81	1.69	6.03	19.5
KHLSS274	144	145	RAT KHL	3.14	1.39	5.93	19.7

Hole_ID	Depth_From	Depth_To	Strat. Code	Er_ppm	Eu_ppm	Fe2O3_%	Ga_ppm
KHLSS274	145	146	RAT KHL	3.49	1.51	6.68	19.5
KHLSS274	146	147	RAT KHL	3.36	1.6	6.08	19.3
KHLSS274	147	148	RAT KHL	6.03	1.81	5.1	18.8
KHLSS274	148	149	RAT KHL	4.76	1.62	5.5	18.5
KHLSS274	149	150	RAT KHL	3.8	1.59	6.67	19
KHLSS274	150	151	RAT KHL	4.61	1.95	6.69	20.8
KHLSS274	151	152	RAT KHL	3.56	1.49	5.56	18.6
KHLSS274	152	153	RAT KHL	3.31	1.76	5.15	18.2
KHLSS274	153	154	RAT KHL	3.58	1.88	5.51	19.4
KHLSS274	154	155	RAT KHL	4.01	1.64	5.81	18
KHLSS274	155	156	RAT KHL	4.44	1.92	5.11	20.1
KHLSS274	156	157	RAT KHL	3.59	1.98	5.04	18.2
KHLSS274	157	158	RAT KHL	3.13	1.56	2.6	16.5
KHLSS274	158	159	RAT KHL	3.17	1.43	4.05	16.4
KHLSS274	159	160	RAT KHL	3.06	1.43	5.16	15.7
KHLSS274	160	161	RAT KHL	2.86	1.19	5.26	17
KTCSS315	351	352	RAT KNS	2.78	0.65	5.29	18.8
KTCSS315	352	353	RAT KNS	2.97	0.8	3.32	19.6
KTCSS315	353	354	RAT KNS	2.47	0.76	2.1	17.4
KTCSS315	354	355	RAT KNS	4.04	1.32	1.43	21.1
KTCSS315	355	355.8	RAT KNS	4.16	1.14	1.19	23
KTCSS326	264	265	RAT KNS	3.77	0.69	1.04	25.1
KTCSS326	265	265.9	RAT KNS	3.87	0.77	1.01	24.6
KTCSS326	266.5	267.5	RAT KNS	4.39	0.89	1.02	23.2
KTCSS326	267.5	268.3	RAT KNS	4.04	0.81	1.08	23.4
KTCSS326	268.3	270	RAT KNS	3.43	0.89	1.15	22.9
KTCSS326	270	271	RAT KNS	3.75	1.23	1.14	21.3
KTCSS326	271	272	RAT KNS	3.74	1.15	3.15	22.2
KTCSS326	272	273	RAT KNS	3.23	1.17	3.53	20.3
KTCSS326	273	274	RAT KNS	4.7	1.82	3.42	21.7
KTCSS326	279	280	RAT KNS	3.73	0.69	0.74	23.5
KTCSS326	280	281	RAT KNS	4.01	0.79	0.73	24.1
KTCSS326	286	287	HBX KNS	23.6	3.99	4.87	24.9
KTCSS326	287	288	DIP KNS	5.79	1.82	5.53	22.5
KTCSS326	294	295	DIP KNS	8.46	2.39	6.68	15.1
KTCSS326	295	296	DIP KNS	11.35	2.95	6.66	15.3
SM59016	20.4	24	DIP SM	3.53	1.5	10.05	21
SM59016	24	27.9	DIP SM	2.08	0.89	5.43	11.8
SM59016	30.9	34	DIP SM	0.22	0.06	0.65	0.7
SM59016	34	38	DIP SM	0.13	0.04	0.63	0.5
SM59016	38	42	DIP SM	0.07	0.03	0.65	0.4
SM59016	42	43.4	DIP SM	0.09	0.015	0.84	0.5
SM59016	44.4	46	DIP SM	0.08	0.015	0.72	0.4
SM59016	46	47.4	DIP SM	0.08	0.03	0.61	0.4
SM59016	52.4	54	DIP SM	0.07	0.04	0.91	0.7
SM59016	54	55	DIP SM	0.06	0.03	0.51	0.3
SM59016	55	56	DIP SM	0.08	0.015	0.43	0.3
SM59016	56	60	HBX SM	0.16	0.07	0.6	0.8
SM59016	60	64	HBX SM	2.06	0.72	3.57	11.9

Hole_ID	Depth_From	Depth_To	Strat. Code	Er_ppm	Eu_ppm	Fe2O3_%	Ga_ppm
SM59016	64	67.6	HBX SM	1.76	0.54	4	10.3
SM59016	67.6	71	HBX SM	3.26	0.83	3.48	8.2
SM59016	71	75	HBX SM	2.58	0.68	34.1	8
SM59016	75	77.4	HBX SM	2.19	0.91	33	7.5
SM59016	77.4	81	HBX SM	2.2	0.65	7.51	10.1
SM59016	81	85	HBX SM	1.53	0.37	5.24	13.1
SM59016	85	86.4	HBX SM	3.59	3.06	6.96	19
SM59016	86.4	89	HBX SM	2.19	1.19	3.78	11.8
SM59016	89	90.8	HBX SM	3.79	1.17	4.92	12.8
SM59016	90.8	95	HBX SM	1.19	0.16	1.05	4.9
SM59016	95	99	HBX SM	1.31	0.22	3.78	14.2
SM59016	99	103	HBX SM	1.2	0.24	6.44	18.9
SM59016	103	107	HBX SM	7.55	0.61	6.05	10.8
SM59016	107	111	RAT SM	5.5	0.92	5.35	16.3
SM59016	111	115	RAT SM	3.32	2.07	5.91	21.6
SM59016	115	119	RAT SM	3.07	1.27	4.33	23.2
SM59016	119	123	RAT SM	3.67	1.25	4.57	21.8
SM59016	123	127	RAT SM	4.5	2.03	5.48	21.7
SM59016	127	131	RAT SM	7.34	2.57	5.4	22.5
SM59016	131	135	RAT SM	4.34	1.97	5.01	19.2
SM59016	135	139	RAT SM	3.64	2.17	4.17	20.5
SM59016	139	143	RAT SM	4.11	2.27	3.23	19.7
SM59016	143	144	RAT SM	3.25	0.83	3.03	22.1
SM59016	144	145	RAT SM	3.3	0.93	3.3	22.5
SM59016	145	146	RAT SM	3.33	0.71	6.22	22.6
SM59016	146	147.3	RAT SM	2.5	1.19	7.41	16.4

Hole_ID	Depth_From	Depth_To	Strat. Code	Gd_ppm	Ge_ppm	Hf_ppm	Hg_ppm
KHLSS274	70	71	DIP KHL	17.15	2.5	3.4	0.0025
KHLSS274	71	72	DIP KHL	0.95	2.5	3	0.0025
KHLSS274	72	73	DIP KHL	1.41	2.5	2.8	0.0025
KHLSS274	73	74	DIP KHL	0.73	2.5	3.9	0.0025
KHLSS274	74	75	DIP KHL	1.02	2.5	3	0.0025
KHLSS274	75	76	DIP KHL	1.54	2.5	2.3	0.0025
KHLSS274	76	77	DIP KHL	1.07	2.5	3.1	0.0025
KHLSS274	77	78	DIP KHL	2.99	2.5	3.5	0.0025
KHLSS274	78	79	DIP KHL	6.3	2.5	3.3	0.0025
KHLSS274	79	80	DIP KHL	4.75	2.5	3.5	0.0025
KHLSS274	80	81	DIP KHL	4.53	2.5	3.4	0.0025
KHLSS274	81	82	DIP KHL	4.57	2.5	3.8	0.0025
KHLSS274	82	83	DIP KHL	4.07	2.5	3.1	0.0025
KHLSS274	83	84	DIP KHL	4.28	2.5	3.8	0.0025
KHLSS274	84	85	DIP KHL	4.56	2.5	3.7	0.0025
KHLSS274	85	86	DIP KHL	3.98	2.5	4	0.0025
KHLSS274	86	87	DIP KHL	4.42	2.5	3.9	0.0025
KHLSS274	87	88	DIP KHL	6.07	2.5	4.3	0.0025
KHLSS274	88	89	DIP KHL	4.48	2.5	4	0.0025
KHLSS274	89	90	DIP KHL	4.47	2.5	4.1	0.0025
KHLSS274	90	91	DIP KHL	4.31	2.5	4.1	0.0025

Hole_ID	Depth_From	Depth_To	Strat. Code	Gd_ppm	Ge_ppm	Hf_ppm	Hg_ppm
KHLSS274	91	92	DIP KHL	4	2.5	4	0.0025
KHLSS274	92	93	DIP KHL	3.94	2.5	4.4	0.0025
KHLSS274	93	94	DIP KHL	3.85	2.5	4.5	0.0025
KHLSS274	94	95	DIP KHL	6.1	2.5	4.6	0.0025
KHLSS274	95	96	DIP KHL	4.93	2.5	3.7	0.0025
KHLSS274	96	97	DIP KHL	5.66	2.5	3.9	0.0025
KHLSS274	97	98	DIP KHL	6.25	2.5	4.3	0.0025
KHLSS274	98	99	DIP KHL	4.48	2.5	3.6	0.0025
KHLSS274	99	100	DIP KHL	4.72	2.5	3.4	0.0025
KHLSS274	100	101	DIP KHL	4.04	2.5	3.4	0.0025
KHLSS274	101	102	DIP KHL	5.03	2.5	3.2	0.0025
KHLSS274	102	103	DIP KHL	5.67	2.5	3.2	0.0025
KHLSS274	103	104	DIP KHL	4.57	2.5	4.3	0.0025
KHLSS274	104	105	DIP KHL	4.68	2.5	3.3	0.0025
KHLSS274	105	106	DIP KHL	4.99	2.5	2.9	0.0025
KHLSS274	106	107	DIP KHL	5.67	2.5	3.1	0.0025
KHLSS274	107	108	DIP KHL	4.81	2.5	3.2	0.0025
KHLSS274	108	109	DIP KHL	7.04	2.5	3	0.0025
KHLSS274	109	110	DIP KHL	7	2.5	3.3	0.0025
KHLSS274	110	111	DIP KHL	6.02	2.5	3.2	0.0025
KHLSS274	111	112	DIP KHL	5.79	2.5	3.3	0.0025
KHLSS274	112	113	DIP KHL	5.78	2.5	3.2	0.0025
KHLSS274	113	114	DIP KHL	7.38	2.5	4	0.0025
KHLSS274	114	115	DIP KHL	6.23	2.5	4	0.0025
KHLSS274	115	116	DIP KHL	6.05	2.5	3.7	0.0025
KHLSS274	116	117	DIP KHL	5.09	2.5	3.5	0.0025
KHLSS274	117	118	DIP KHL	4.83	2.5	3.4	0.0025
KHLSS274	118	119	DIP KHL	3.57	2.5	3.3	0.0025
KHLSS274	119	120	DIP KHL	3.57	2.5	3	0.0025
KHLSS274	120	121	DIP KHL	3.29	2.5	3	0.0025
KHLSS274	121	122	DIP KHL	3.95	2.5	4.4	0.0025
KHLSS274	122	123	DIP KHL	3.81	2.5	4.1	0.0025
KHLSS274	123	124	DIP KHL	3.16	2.5	3.4	0.0025
KHLSS274	124	125	DIP KHL	3.16	2.5	2.9	0.0025
KHLSS274	125	126	HBX KHL	6.29	2.5	2.9	0.0025
KHLSS274	126	127	HBX KHL	5.67	2.5	4.1	0.0025
KHLSS274	127	128	HBX KHL	8.61	2.5	8.7	0.0025
KHLSS274	128	129	HBX KHL	4.53	2.5	4.4	0.0025
KHLSS274	129	130	HBX KHL	5.57	2.5	5.1	0.0025
KHLSS274	130	131	HBX KHL	6.72	2.5	5.6	0.0025
KHLSS274	131	132	HBX KHL	7.14	2.5	4.8	0.0025
KHLSS274	132	133	HBX KHL	6.26	2.5	4.1	0.0025
KHLSS274	133	134	RAT KHL	5.95	2.5	5.3	0.0025
KHLSS274	134	135	RAT KHL	6.41	2.5	5.5	0.0025
KHLSS274	135	136	RAT KHL	6.64	2.5	5.5	0.0025
KHLSS274	136	137	RAT KHL	6.99	2.5	5.4	0.0025
KHLSS274	137	138	RAT KHL	6.54	2.5	6.1	0.0025
KHLSS274	138	139	RAT KHL	6.89	2.5	5.4	0.0025
KHLSS274	139	140	RAT KHL	6.67	2.5	5.6	0.0025

Hole_ID	Depth_From	Depth_To	Strat. Code	Gd_ppm	Ge_ppm	Hf_ppm	Hg_ppm
KHLSS274	140	141	RAT KHL	6.56	2.5	5.5	0.0025
KHLSS274	141	142	RAT KHL	6.29	2.5	5.2	0.0025
KHLSS274	142	143	RAT KHL	8.04	2.5	8.1	0.0025
KHLSS274	143	144	RAT KHL	7.35	2.5	6.7	0.0025
KHLSS274	144	145	RAT KHL	6.35	2.5	5.3	0.0025
KHLSS274	145	146	RAT KHL	6.61	2.5	5.2	0.009
KHLSS274	146	147	RAT KHL	6.64	2.5	5.5	0.007
KHLSS274	147	148	RAT KHL	10.5	2.5	11.1	0.008
KHLSS274	148	149	RAT KHL	8.19	2.5	9.3	0.005
KHLSS274	149	150	RAT KHL	6.64	2.5	6.8	0.007
KHLSS274	150	151	RAT KHL	8.6	2.5	8.2	0.005
KHLSS274	151	152	RAT KHL	6.59	2.5	5.7	0.006
KHLSS274	152	153	RAT KHL	6.7	2.5	6	0.0025
KHLSS274	153	154	RAT KHL	6.47	2.5	6.5	0.0025
KHLSS274	154	155	RAT KHL	6.75	2.5	7.6	0.0025
KHLSS274	155	156	RAT KHL	7.63	2.5	8.6	0.0025
KHLSS274	156	157	RAT KHL	6.69	2.5	6.7	0.0025
KHLSS274	157	158	RAT KHL	5.49	2.5	5.7	0.009
KHLSS274	158	159	RAT KHL	5.91	2.5	6.1	0.034
KHLSS274	159	160	RAT KHL	5.41	2.5	5.1	0.038
KHLSS274	160	161	RAT KHL	4.26	2.5	5.2	0.012
KTCSS315	351	352	RAT KNS	6.6	2.5	5.3	0.07
KTCSS315	352	353	RAT KNS	5.39	2.5	5.6	0.018
KTCSS315	353	354	RAT KNS	4.41	2.5	5.1	0.038
KTCSS315	354	355	RAT KNS	7.35	2.5	7.2	0.058
KTCSS315	355	355.8	RAT KNS	6.88	2.5	8.3	0.0025
KTCSS326	264	265	RAT KNS	5.06	2.5	7.8	0.019
KTCSS326	265	265.9	RAT KNS	5.72	2.5	7.8	0.02
KTCSS326	266.5	267.5	RAT KNS	6.1	2.5	8.7	0.014
KTCSS326	267.5	268.3	RAT KNS	5.97	2.5	7.5	0.015
KTCSS326	268.3	270	RAT KNS	5.51	2.5	5.9	0.005
KTCSS326	270	271	RAT KNS	5.8	2.5	6.6	0.0025
KTCSS326	271	272	RAT KNS	5.36	2.5	6.6	0.0025
KTCSS326	272	273	RAT KNS	5.32	2.5	6.7	0.012
KTCSS326	273	274	RAT KNS	7.53	2.5	9.3	0.01
KTCSS326	279	280	RAT KNS	5.37	2.5	6.1	0.01
KTCSS326	280	281	RAT KNS	5.91	2.5	6.9	0.014
KTCSS326	286	287	HBX KNS	21.6	2.5	4.2	0.015
KTCSS326	287	288	DIP KNS	7.41	2.5	3.4	0.013
KTCSS326	294	295	DIP KNS	11.25	2.5	3.3	0.0025
KTCSS326	295	296	DIP KNS	15.55	2.5	3.1	0.005
SM59016	20.4	24	DIP SM	6.73	2.5	7.1	0.014
SM59016	24	27.9	DIP SM	3.99	2.5	3.3	0.017
SM59016	30.9	34	DIP SM	0.21	2.5	0.2	0.0025
SM59016	34	38	DIP SM	0.23	2.5	0.2	0.007
SM59016	38	42	DIP SM	0.13	2.5	0.1	0.006
SM59016	42	43.4	DIP SM	0.16	2.5	0.1	0.006
SM59016	44.4	46	DIP SM	0.17	2.5	0.1	0.0025
SM59016	46	47.4	DIP SM	0.15	2.5	0.1	0.018

Hole_ID	Depth_From	Depth_To	Strat. Code	Gd_ppm	Ge_ppm	Hf_ppm	Hg_ppm
SM59016	52.4	54	DIP SM	0.19	2.5	0.1	0.013
SM59016	54	55	DIP SM	0.1	2.5	0.1	0.005
SM59016	55	56	DIP SM	0.12	2.5	0.1	0.02
SM59016	56	60	HBX SM	0.33	2.5	0.3	0.05
SM59016	60	64	HBX SM	3.39	2.5	3.4	0.011
SM59016	64	67.6	HBX SM	2.55	5	3.2	0.0025
SM59016	67.6	71	HBX SM	3.17	2.5	3.1	0.0025
SM59016	71	75	HBX SM	2.39	2.5	2.7	0.007
SM59016	75	77.4	HBX SM	2.78	2.5	2.6	0.005
SM59016	77.4	81	HBX SM	3	2.5	3	0.0025
SM59016	81	85	HBX SM	2.3	2.5	3.5	0.008
SM59016	85	86.4	HBX SM	10.95	2.5	4.3	0.0025
SM59016	86.4	89	HBX SM	4.88	2.5	3.6	0.0025
SM59016	89	90.8	HBX SM	5.24	2.5	3.9	0.0025
SM59016	90.8	95	HBX SM	0.91	2.5	3.9	0.0025
SM59016	95	99	HBX SM	1.06	2.5	3.1	0.0025
SM59016	99	103	HBX SM	1.1	2.5	3	0.0025
SM59016	103	107	HBX SM	3.67	2.5	3.2	0.0025
SM59016	107	111	RAT SM	4.89	2.5	5.2	0.0025
SM59016	111	115	RAT SM	8.1	2.5	6	0.0025
SM59016	115	119	RAT SM	5.75	2.5	5.9	0.0025
SM59016	119	123	RAT SM	6.12	2.5	6.5	0.0025
SM59016	123	127	RAT SM	9.05	2.5	8.9	0.0025
SM59016	127	131	RAT SM	14.6	2.5	13.6	0.0025
SM59016	131	135	RAT SM	8.85	2.5	8.1	0.0025
SM59016	135	139	RAT SM	7.5	2.5	6.9	0.008
SM59016	139	143	RAT SM	7.75	2.5	8	0.007
SM59016	143	144	RAT SM	5.65	2.5	7.1	0.011
SM59016	144	145	RAT SM	5.87	2.5	7.1	0.024
SM59016	145	146	RAT SM	4.76	2.5	6.8	0.032
SM59016	146	147.3	RAT SM	6.92	2.5	4.8	0.011

Hole_ID	Depth_From	Depth_To	Strat. Code	Ho_ppm	In_ppm	K2O_%	La_ppm
KHLSS274	70	71	DIP KHL	1.41	0.068	0.04	190
KHLSS274	71	72	DIP KHL	0.19	0.008	0.01	3.9
KHLSS274	72	73	DIP KHL	0.3	0.0025	0.005	3
KHLSS274	73	74	DIP KHL	0.21	0.0025	0.01	1.7
KHLSS274	74	75	DIP KHL	0.28	0.0025	0.005	2
KHLSS274	75	76	DIP KHL	0.34	0.0025	0.005	2.4
KHLSS274	76	77	DIP KHL	0.44	0.0025	0.005	1.8
KHLSS274	77	78	DIP KHL	0.52	0.014	0.03	4.6
KHLSS274	78	79	DIP KHL	1.04	0.015	0.03	31.5
KHLSS274	79	80	DIP KHL	0.69	0.021	0.02	45.8
KHLSS274	80	81	DIP KHL	0.37	0.034	0.02	34.6
KHLSS274	81	82	DIP KHL	0.39	0.023	0.03	66.1
KHLSS274	82	83	DIP KHL	0.35	0.043	0.01	32.4
KHLSS274	83	84	DIP KHL	0.3	0.052	0.02	46.2
KHLSS274	84	85	DIP KHL	0.76	0.049	0.05	52.4
KHLSS274	85	86	DIP KHL	0.59	0.049	0.36	48.4

Hole_ID	Depth_From	Depth_To	Strat. Code	Ho_ppm	In_ppm	K2O_%	La_ppm
KHLSS274	86	87	DIP KHL	0.37	0.045	0.32	52.3
KHLSS274	87	88	DIP KHL	0.42	0.042	0.32	63.5
KHLSS274	88	89	DIP KHL	0.33	0.03	0.6	59.3
KHLSS274	89	90	DIP KHL	0.72	0.039	0.58	58.8
KHLSS274	90	91	DIP KHL	0.34	0.042	0.49	54.5
KHLSS274	91	92	DIP KHL	0.35	0.049	0.44	50
KHLSS274	92	93	DIP KHL	0.4	0.023	0.45	53
KHLSS274	93	94	DIP KHL	0.35	0.029	0.38	52.1
KHLSS274	94	95	DIP KHL	0.67	0.045	0.35	55.2
KHLSS274	95	96	DIP KHL	1.03	0.048	0.47	45.6
KHLSS274	96	97	DIP KHL	1.18	0.043	0.45	43.4
KHLSS274	97	98	DIP KHL	1.95	0.039	0.36	46.7
KHLSS274	98	99	DIP KHL	0.68	0.047	0.37	42.6
KHLSS274	99	100	DIP KHL	0.53	0.052	0.08	52.6
KHLSS274	100	101	DIP KHL	0.5	0.04	0.02	63.1
KHLSS274	101	102	DIP KHL	0.59	0.052	0.01	69.2
KHLSS274	102	103	DIP KHL	0.58	0.044	0.01	74.1
KHLSS274	103	104	DIP KHL	0.53	0.054	0.02	68.7
KHLSS274	104	105	DIP KHL	1.01	0.055	0.02	62.9
KHLSS274	105	106	DIP KHL	0.63	0.064	0.01	62.3
KHLSS274	106	107	DIP KHL	1.24	0.044	0.01	53.8
KHLSS274	107	108	DIP KHL	0.66	0.066	0.01	46.7
KHLSS274	108	109	DIP KHL	1.78	0.069	0.02	51.9
KHLSS274	109	110	DIP KHL	1.77	0.052	0.12	42.7
KHLSS274	110	111	DIP KHL	1.59	0.055	0.22	44.6
KHLSS274	111	112	DIP KHL	1.21	0.076	0.17	43.9
KHLSS274	112	113	DIP KHL	1.16	0.072	0.14	46.1
KHLSS274	113	114	DIP KHL	2.19	0.052	0.23	47.5
KHLSS274	114	115	DIP KHL	1.36	0.049	0.15	47.4
KHLSS274	115	116	DIP KHL	2.14	0.069	0.01	25.4
KHLSS274	116	117	DIP KHL	1.26	0.075	0.005	50.2
KHLSS274	117	118	DIP KHL	0.8	0.097	0.01	45.5
KHLSS274	118	119	DIP KHL	0.55	0.097	0.005	46
KHLSS274	119	120	DIP KHL	0.41	0.095	0.005	48.5
KHLSS274	120	121	DIP KHL	0.47	0.098	0.005	45.1
KHLSS274	121	122	DIP KHL	0.52	0.08	0.005	58.7
KHLSS274	122	123	DIP KHL	0.7	0.077	0.01	72.1
KHLSS274	123	124	DIP KHL	0.49	0.086	0.005	55.6
KHLSS274	124	125	DIP KHL	0.51	0.069	0.005	53.7
KHLSS274	125	126	HBX KHL	1.75	0.097	0.005	68
KHLSS274	126	127	HBX KHL	1.03	0.094	1.87	38
KHLSS274	127	128	HBX KHL	1.15	0.139	7.67	48.3
KHLSS274	128	129	HBX KHL	0.96	0.475	3.63	33
KHLSS274	129	130	HBX KHL	1.03	0.14	3.29	46.2
KHLSS274	130	131	HBX KHL	1.06	0.162	4.05	44.5
KHLSS274	131	132	HBX KHL	0.98	0.121	3.25	41.6
KHLSS274	132	133	HBX KHL	1.08	0.15	2.33	42.6
KHLSS274	133	134	RAT KHL	1.11	0.058	3	37.5
KHLSS274	134	135	RAT KHL	1.13	0.015	3.55	46.1

Hole_ID	Depth_From	Depth_To	Strat. Code	Ho_ppm	In_ppm	K2O_%	La_ppm
KHLSS274	135	136	RAT KHL	1.23	0.013	4.41	44.8
KHLSS274	136	137	RAT KHL	1.15	0.013	4.81	48.2
KHLSS274	137	138	RAT KHL	1.16	0.01	5	43.8
KHLSS274	138	139	RAT KHL	1.16	0.009	4.62	51.8
KHLSS274	139	140	RAT KHL	1.09	0.009	3.91	48.1
KHLSS274	140	141	RAT KHL	1.14	0.009	4.52	51
KHLSS274	141	142	RAT KHL	1.01	0.01	3.52	46.5
KHLSS274	142	143	RAT KHL	1.54	0.009	2.85	54.7
KHLSS274	143	144	RAT KHL	1.3	0.016	2.22	51.8
KHLSS274	144	145	RAT KHL	1.11	0.013	2.95	46.3
KHLSS274	145	146	RAT KHL	1.12	0.012	2	47.7
KHLSS274	146	147	RAT KHL	1.23	0.015	2	47.1
KHLSS274	147	148	RAT KHL	1.99	0.023	2.01	50
KHLSS274	148	149	RAT KHL	1.56	0.023	1.89	50.8
KHLSS274	149	150	RAT KHL	1.32	0.019	1.72	49.1
KHLSS274	150	151	RAT KHL	1.59	0.014	1.89	55.2
KHLSS274	151	152	RAT KHL	1.18	0.029	2.11	40.2
KHLSS274	152	153	RAT KHL	1.26	0.025	3.63	47.6
KHLSS274	153	154	RAT KHL	1.19	0.032	4.73	50.5
KHLSS274	154	155	RAT KHL	1.28	0.043	4.22	43
KHLSS274	155	156	RAT KHL	1.49	0.016	5.16	52.3
KHLSS274	156	157	RAT KHL	1.21	0.026	5.45	48.7
KHLSS274	157	158	RAT KHL	1.04	0.031	5.29	36.5
KHLSS274	158	159	RAT KHL	1.02	0.033	5.88	37.1
KHLSS274	159	160	RAT KHL	1.1	0.039	5.13	33.6
KHLSS274	160	161	RAT KHL	0.9	0.039	5.58	24.7
KTCSS315	351	352	RAT KNS	0.98	0.015	0.47	0.9
KTCSS315	352	353	RAT KNS	0.93	0.015	1.17	6.3
KTCSS315	353	354	RAT KNS	0.86	0.014	1.33	7.4
KTCSS315	354	355	RAT KNS	1.34	0.014	1.61	4.7
KTCSS315	355	355.8	RAT KNS	1.38	0.011	1.68	1.4
KTCSS326	264	265	RAT KNS	1.36	0.008	0.53	3.2
KTCSS326	265	265.9	RAT KNS	1.37	0.009	0.75	5.9
KTCSS326	266.5	267.5	RAT KNS	1.54	0.013	0.75	5.4
KTCSS326	267.5	268.3	RAT KNS	1.47	0.011	0.75	4.6
KTCSS326	268.3	270	RAT KNS	1.3	0.01	0.97	18.9
KTCSS326	270	271	RAT KNS	1.33	0.009	0.78	45.1
KTCSS326	271	272	RAT KNS	1.33	0.008	0.75	42.1
KTCSS326	272	273	RAT KNS	1.21	0.01	0.42	48
KTCSS326	273	274	RAT KNS	1.71	0.01	0.2	53.3
KTCSS326	279	280	RAT KNS	1.36	0.007	0.03	2.1
KTCSS326	280	281	RAT KNS	1.51	0.008	0.02	2.4
KTCSS326	286	287	HBX KNS	8.58	0.033	0.005	32.2
KTCSS326	287	288	DIP KNS	2.16	0.035	0.005	82.6
KTCSS326	294	295	DIP KNS	3.15	0.013	0.04	176.5
KTCSS326	295	296	DIP KNS	4.35	0.015	0.03	197.5
SM59016	20.4	24	DIP SM	1.28	0.081	2.57	40.7
SM59016	24	27.9	DIP SM	0.76	0.089	0.93	21.8
SM59016	30.9	34	DIP SM	0.06	0.021	0.16	1.6

Hole_ID	Depth_From	Depth_To	Strat. Code	Ho_ppm	In_ppm	K2O_%	La_ppm
SM59016	34	38	DIP SM	0.03	0.018	0.17	1.5
SM59016	38	42	DIP SM	0.02	0.02	0.12	0.8
SM59016	42	43.4	DIP SM	0.04	0.016	0.1	0.9
SM59016	44.4	46	DIP SM	0.02	0.018	0.1	0.6
SM59016	46	47.4	DIP SM	0.03	0.014	0.13	1.2
SM59016	52.4	54	DIP SM	0.04	0.017	0.16	1.3
SM59016	54	55	DIP SM	0.03	0.01	0.06	0.6
SM59016	55	56	DIP SM	0.03	0.017	0.09	0.8
SM59016	56	60	HBX SM	0.06	0.008	0.17	1.9
SM59016	60	64	HBX SM	0.68	0.013	1.48	25.2
SM59016	64	67.6	HBX SM	0.61	0.023	0.4	25.8
SM59016	67.6	71	HBX SM	1.07	0.036	0.05	82.2
SM59016	71	75	HBX SM	0.84	0.014	0.01	3.6
SM59016	75	77.4	HBX SM	0.72	0.01	0.005	7.3
SM59016	77.4	81	HBX SM	0.69	0.019	0.21	20.1
SM59016	81	85	HBX SM	0.52	0.019	0.77	3.9
SM59016	85	86.4	HBX SM	1.37	0.085	0.56	72.7
SM59016	86.4	89	HBX SM	0.75	0.023	0.74	28.1
SM59016	89	90.8	HBX SM	1.3	0.012	0.41	45.8
SM59016	90.8	95	HBX SM	0.35	0.005	0.005	2.5
SM59016	95	99	HBX SM	0.35	0.005	0.01	3.3
SM59016	99	103	HBX SM	0.37	0.006	0.01	4.1
SM59016	103	107	HBX SM	2.45	0.0025	0.005	2.6
SM59016	107	111	RAT SM	1.62	0.007	1.23	18.8
SM59016	111	115	RAT SM	1.17	0.008	2.17	57.7
SM59016	115	119	RAT SM	0.97	0.009	1.93	32.1
SM59016	119	123	RAT SM	1.24	0.008	1.5	25.6
SM59016	123	127	RAT SM	1.39	0.012	1.18	47.3
SM59016	127	131	RAT SM	2.5	0.009	0.91	33.8
SM59016	131	135	RAT SM	1.47	0.009	0.74	39.1
SM59016	135	139	RAT SM	1.21	0.01	1.83	51.1
SM59016	139	143	RAT SM	1.4	0.008	2.13	49.5
SM59016	143	144	RAT SM	1.06	0.01	2.18	8.6
SM59016	144	145	RAT SM	1.06	0.01	1.9	21.8
SM59016	145	146	RAT SM	1.04	0.011	1.37	8.4
SM59016	146	147.3	RAT SM	0.86	0.025	0.52	48.8

Hole_ID	Depth_From	Depth_To	Strat. Code	Li_ppm	LOI_%	Lu_ppm	MgO_%
KHLSS274	70	71	DIP KHL	100	8.38	0.4	15.85
KHLSS274	71	72	DIP KHL	100	15.45	0.12	19.25
KHLSS274	72	73	DIP KHL	80	19.8	0.18	19
KHLSS274	73	74	DIP KHL	80	14.75	0.13	18
KHLSS274	74	75	DIP KHL	80	16.85	0.16	19.4
KHLSS274	75	76	DIP KHL	70	16.8	0.18	18.75
KHLSS274	76	77	DIP KHL	90	12.6	0.24	19.35
KHLSS274	77	78	DIP KHL	130	17.7	0.23	15.6
KHLSS274	78	79	DIP KHL	120	13.05	0.31	15.3
KHLSS274	79	80	DIP KHL	110	15.7	0.22	15.75
KHLSS274	80	81	DIP KHL	90	17.4	0.25	16.3

Hole_ID	Depth_From	Depth_To	Strat. Code	Li_ppm	LOI_%	Lu_ppm	MgO_%
KHLSS274	81	82	DIP KHL	100	13.4	0.2	15.1
KHLSS274	82	83	DIP KHL	110	16.8	0.22	15.95
KHLSS274	83	84	DIP KHL	110	15.85	0.23	16.55
KHLSS274	84	85	DIP KHL	110	13.4	0.34	16.25
KHLSS274	85	86	DIP KHL	110	13.5	0.28	15.95
KHLSS274	86	87	DIP KHL	100	14.05	0.24	16.5
KHLSS274	87	88	DIP KHL	120	11.9	0.27	16.65
KHLSS274	88	89	DIP KHL	100	10.2	0.21	15.3
KHLSS274	89	90	DIP KHL	110	11.05	0.34	15.15
KHLSS274	90	91	DIP KHL	120	12.05	0.27	15.8
KHLSS274	91	92	DIP KHL	100	13.3	0.26	15.95
KHLSS274	92	93	DIP KHL	90	9.61	0.26	15.15
KHLSS274	93	94	DIP KHL	100	8.8	0.27	15.6
KHLSS274	94	95	DIP KHL	100	10.3	0.38	15.5
KHLSS274	95	96	DIP KHL	90	14.15	0.47	16
KHLSS274	96	97	DIP KHL	90	14.05	0.43	16.25
KHLSS274	97	98	DIP KHL	100	13.75	0.82	16.4
KHLSS274	98	99	DIP KHL	100	15.8	0.38	16.65
KHLSS274	99	100	DIP KHL	100	15.7	0.32	17.4
KHLSS274	100	101	DIP KHL	80	16.85	0.27	17.75
KHLSS274	101	102	DIP KHL	90	19.15	0.3	18.3
KHLSS274	102	103	DIP KHL	100	16.55	0.25	17.85
KHLSS274	103	104	DIP KHL	90	15.5	0.41	17.5
KHLSS274	104	105	DIP KHL	90	13.5	0.37	17.1
KHLSS274	105	106	DIP KHL	80	19	0.29	17.85
KHLSS274	106	107	DIP KHL	90	16.35	0.39	16.9
KHLSS274	107	108	DIP KHL	80	19.9	0.31	17.95
KHLSS274	108	109	DIP KHL	90	17.55	0.63	17.9
KHLSS274	109	110	DIP KHL	90	13.6	0.57	16.85
KHLSS274	110	111	DIP KHL	90	13.55	0.5	16.9
KHLSS274	111	112	DIP KHL	90	15.5	0.48	17.3
KHLSS274	112	113	DIP KHL	90	15.55	0.41	17.15
KHLSS274	113	114	DIP KHL	90	11.75	0.73	16.55
KHLSS274	114	115	DIP KHL	90	10.55	0.53	16.55
KHLSS274	115	116	DIP KHL	110	14.7	0.66	17.7
KHLSS274	116	117	DIP KHL	90	16	0.42	17.9
KHLSS274	117	118	DIP KHL	90	18.35	0.32	17.75
KHLSS274	118	119	DIP KHL	90	17.7	0.27	17.9
KHLSS274	119	120	DIP KHL	100	17.6	0.24	18.05
KHLSS274	120	121	DIP KHL	90	17.9	0.24	17.85
KHLSS274	121	122	DIP KHL	100	14.7	0.33	17.2
KHLSS274	122	123	DIP KHL	110	14.05	0.41	16.9
KHLSS274	123	124	DIP KHL	90	20.9	0.32	17.8
KHLSS274	124	125	DIP KHL	60	21.1	0.28	16.95
KHLSS274	125	126	HBX KHL	120	23.1	0.52	16.8
KHLSS274	126	127	HBX KHL	130	16.45	0.37	16.3
KHLSS274	127	128	HBX KHL	80	13.45	0.47	8.2
KHLSS274	128	129	HBX KHL	100	16.75	0.36	13
KHLSS274	129	130	HBX KHL	70	9.61	0.38	8.15

Hole_ID	Depth_From	Depth_To	Strat. Code	Li_ppm	LOI_%	Lu_ppm	MgO_%
KHLSS274	130	131	HBX KHL	60	7.58	0.42	6.87
KHLSS274	131	132	HBX KHL	60	13.85	0.36	10.2
KHLSS274	132	133	HBX KHL	130	15.2	0.39	13.65
KHLSS274	133	134	RAT KHL	120	10.25	0.43	11.25
KHLSS274	134	135	RAT KHL	160	10.2	0.43	11.75
KHLSS274	135	136	RAT KHL	140	10.25	0.51	10.85
KHLSS274	136	137	RAT KHL	140	8.31	0.44	9.88
KHLSS274	137	138	RAT KHL	140	7.29	0.48	9.66
KHLSS274	138	139	RAT KHL	170	7.73	0.46	10.8
KHLSS274	139	140	RAT KHL	170	8.09	0.39	11.1
KHLSS274	140	141	RAT KHL	170	6.78	0.46	10.7
KHLSS274	141	142	RAT KHL	170	8.82	0.43	12.6
KHLSS274	142	143	RAT KHL	190	8.27	0.56	13.35
KHLSS274	143	144	RAT KHL	190	10.95	0.5	15
KHLSS274	144	145	RAT KHL	180	10.7	0.37	13.45
KHLSS274	145	146	RAT KHL	210	10.35	0.45	15.85
KHLSS274	146	147	RAT KHL	190	11.7	0.43	15.25
KHLSS274	147	148	RAT KHL	160	13.55	0.77	13.85
KHLSS274	148	149	RAT KHL	170	14.45	0.6	14.8
KHLSS274	149	150	RAT KHL	190	12.6	0.53	15.85
KHLSS274	150	151	RAT KHL	200	10.45	0.65	15
KHLSS274	151	152	RAT KHL	170	12.1	0.47	13.5
KHLSS274	152	153	RAT KHL	130	15	0.49	11.6
KHLSS274	153	154	RAT KHL	130	12.95	0.46	10
KHLSS274	154	155	RAT KHL	130	13.85	0.49	11.45
KHLSS274	155	156	RAT KHL	120	12.05	0.57	9.16
KHLSS274	156	157	RAT KHL	120	13.6	0.48	9.03
KHLSS274	157	158	RAT KHL	100	16.9	0.44	10.45
KHLSS274	158	159	RAT KHL	100	14.9	0.43	9.7
KHLSS274	159	160	RAT KHL	100	17.65	0.4	10.6
KHLSS274	160	161	RAT KHL	120	14.1	0.37	9.31
KTCSS315	351	352	RAT KNS	180	18.55	0.38	18.65
KTCSS315	352	353	RAT KNS	160	14.7	0.4	13.9
KTCSS315	353	354	RAT KNS	160	14.1	0.39	13
KTCSS315	354	355	RAT KNS	160	12.4	0.55	12.85
KTCSS315	355	355.8	RAT KNS	160	11.9	0.56	12.2
KTCSS326	264	265	RAT KNS	220	13.2	0.52	17.45
KTCSS326	265	265.9	RAT KNS	210	11.55	0.57	15.15
KTCSS326	266.5	267.5	RAT KNS	230	12.75	0.61	15.3
KTCSS326	267.5	268.3	RAT KNS	230	13.4	0.54	15.6
KTCSS326	268.3	270	RAT KNS	220	13.05	0.47	15.2
KTCSS326	270	271	RAT KNS	230	14	0.5	15.65
KTCSS326	271	272	RAT KNS	250	11.55	0.46	15.35
KTCSS326	272	273	RAT KNS	240	11.65	0.45	15.65
KTCSS326	273	274	RAT KNS	270	11.3	0.67	17.05
KTCSS326	279	280	RAT KNS	250	12.2	0.49	19.8
KTCSS326	280	281	RAT KNS	250	12	0.57	19.3
KTCSS326	286	287	HBX KNS	210	16.85	2.93	17.95
KTCSS326	287	288	DIP KNS	220	14.85	0.72	17.7

Hole_ID	Depth_From	Depth_To	Strat. Code	Li_ppm	LOI_%	Lu_ppm	MgO_%
KTCSS326	294	295	DIP KNS	160	19.4	0.98	21.8
KTCSS326	295	296	DIP KNS	150	21.1	1.33	26
SM59016	20.4	24	DIP SM	40	9.05	0.49	7.35
SM59016	24	27.9	DIP SM	50	6.76	0.28	16.15
SM59016	30.9	34	DIP SM	60	41.6	0.02	22
SM59016	34	38	DIP SM	50	40.4	0.01	20.1
SM59016	38	42	DIP SM	40	41.9	0.01	20.9
SM59016	42	43.4	DIP SM	40	41.7	0.01	20.6
SM59016	44.4	46	DIP SM	40	42.2	0.01	20.2
SM59016	46	47.4	DIP SM	60	43.3	0.01	21.6
SM59016	52.4	54	DIP SM	80	34	0.02	17.95
SM59016	54	55	DIP SM	40	44.6	0.01	21.5
SM59016	55	56	DIP SM	60	43.1	0.01	21.3
SM59016	56	60	HBX SM	70	40.9	0.02	21.5
SM59016	60	64	HBX SM	100	20.5	0.29	15.25
SM59016	64	67.6	HBX SM	240	16.35	0.29	15.05
SM59016	67.6	71	HBX SM	370	21.1	0.51	16.5
SM59016	71	75	HBX SM	80	13.4	0.4	9.92
SM59016	75	77.4	HBX SM	100	17.55	0.33	9.79
SM59016	77.4	81	HBX SM	130	22.9	0.31	16.15
SM59016	81	85	HBX SM	140	18.3	0.27	16.45
SM59016	85	86.4	HBX SM	210	11.65	0.41	15.2
SM59016	86.4	89	HBX SM	100	22.2	0.31	16.25
SM59016	89	90.8	HBX SM	190	18.75	0.46	15.7
SM59016	90.8	95	HBX SM	140	14.8	0.21	19.5
SM59016	95	99	HBX SM	210	11.95	0.28	20
SM59016	99	103	HBX SM	210	13.8	0.22	19.6
SM59016	103	107	HBX SM	150	17.3	1.02	20.6
SM59016	107	111	RAT SM	200	12.1	0.68	16.25
SM59016	111	115	RAT SM	280	9.89	0.46	12.9
SM59016	115	119	RAT SM	330	9.07	0.43	14
SM59016	119	123	RAT SM	320	10.7	0.49	14.8
SM59016	123	127	RAT SM	320	12.15	0.61	15.9
SM59016	127	131	RAT SM	360	9.59	0.93	15.85
SM59016	131	135	RAT SM	340	13.1	0.55	16.7
SM59016	135	139	RAT SM	290	12.5	0.51	13.75
SM59016	139	143	RAT SM	250	14.65	0.58	13
SM59016	143	144	RAT SM	290	12.8	0.47	12.9
SM59016	144	145	RAT SM	330	12.35	0.49	13.45
SM59016	145	146	RAT SM	340	11.6	0.47	13.8
SM59016	146	147.3	RAT SM	290	18	0.33	16.1

Hole_ID	Depth_From	Depth_To	Strat. Code	MnO_ppm	Mo_ppm	Na2O_ppm	Nb_ppm
KHLSS274	70	71	DIP KHL	100	1	900	14.6
KHLSS274	71	72	DIP KHL	600	0.5	500	10.4
KHLSS274	72	73	DIP KHL	700	1	300	8.3
KHLSS274	73	74	DIP KHL	600	0.5	400	11.6
KHLSS274	74	75	DIP KHL	700	0.5	300	10.7
KHLSS274	75	76	DIP KHL	700	1	400	9.7

Hole_ID	Depth_From	Depth_To	Strat. Code	MnO_ppm	Mo_ppm	Na2O_ppm	Nb_ppm
KHLSS274	76	77	DIP KHL	900	1	500	10.1
KHLSS274	77	78	DIP KHL	2700	1	400	11
KHLSS274	78	79	DIP KHL	1000	1	200	12.2
KHLSS274	79	80	DIP KHL	1800	0.5	300	11.6
KHLSS274	80	81	DIP KHL	2100	1	300	11.4
KHLSS274	81	82	DIP KHL	800	1	200	13.1
KHLSS274	82	83	DIP KHL	1900	0.5	300	11.8
KHLSS274	83	84	DIP KHL	1600	0.5	200	11.9
KHLSS274	84	85	DIP KHL	800	1	300	13.5
KHLSS274	85	86	DIP KHL	900	1	300	13.7
KHLSS274	86	87	DIP KHL	900	1	400	13.4
KHLSS274	87	88	DIP KHL	500	1	400	14.9
KHLSS274	88	89	DIP KHL	200	0.5	400	15.9
KHLSS274	89	90	DIP KHL	400	1	400	15.1
KHLSS274	90	91	DIP KHL	700	1	400	15.6
KHLSS274	91	92	DIP KHL	800	1	400	14.5
KHLSS274	92	93	DIP KHL	100	0.5	400	15.6
KHLSS274	93	94	DIP KHL	300	1	400	15.6
KHLSS274	94	95	DIP KHL	1000	0.5	300	16.2
KHLSS274	95	96	DIP KHL	1200	1	300	13.6
KHLSS274	96	97	DIP KHL	1300	1	300	13.8
KHLSS274	97	98	DIP KHL	1200	1	300	14.7
KHLSS274	98	99	DIP KHL	1700	1	300	13.8
KHLSS274	99	100	DIP KHL	1400	1	200	12.2
KHLSS274	100	101	DIP KHL	1500	1	200	12.2
KHLSS274	101	102	DIP KHL	1800	1	200	11.7
KHLSS274	102	103	DIP KHL	1300	1	200	11.5
KHLSS274	103	104	DIP KHL	1200	0.5	200	15.3
KHLSS274	104	105	DIP KHL	1000	1	200	13.1
KHLSS274	105	106	DIP KHL	1800	1	200	11
KHLSS274	106	107	DIP KHL	1400	1	200	11.3
KHLSS274	107	108	DIP KHL	1900	1	200	10.9
KHLSS274	108	109	DIP KHL	1500	1	200	10.8
KHLSS274	109	110	DIP KHL	800	1	200	12.5
KHLSS274	110	111	DIP KHL	900	0.5	300	13
KHLSS274	111	112	DIP KHL	1300	1	300	13.2
KHLSS274	112	113	DIP KHL	1200	0.5	300	12.7
KHLSS274	113	114	DIP KHL	600	1	200	14
KHLSS274	114	115	DIP KHL	400	1	200	15.1
KHLSS274	115	116	DIP KHL	1100	1	200	13.5
KHLSS274	116	117	DIP KHL	1400	1	100	12.9
KHLSS274	117	118	DIP KHL	1600	1	100	11.3
KHLSS274	118	119	DIP KHL	1500	1	100	12.3
KHLSS274	119	120	DIP KHL	1500	1	100	11.6
KHLSS274	120	121	DIP KHL	1500	0.5	100	11.4
KHLSS274	121	122	DIP KHL	1100	1	100	27.3
KHLSS274	122	123	DIP KHL	900	1	100	29.6
KHLSS274	123	124	DIP KHL	2100	1	100	18.7
KHLSS274	124	125	DIP KHL	2000	0.5	100	11.9

Hole_ID	Depth_From	Depth_To	Strat. Code	MnO_ppm	Mo_ppm	Na2O_ppm	Nb_ppm
KHLSS274	125	126	HBX KHL	2600	1	200	10.3
KHLSS274	126	127	HBX KHL	1800	1	600	14.9
KHLSS274	127	128	HBX KHL	1700	1	1700	21
KHLSS274	128	129	HBX KHL	3100	1	600	17.6
KHLSS274	129	130	HBX KHL	1200	1	600	21.3
KHLSS274	130	131	HBX KHL	700	1	600	24.2
KHLSS274	131	132	HBX KHL	2100	1	700	20.1
KHLSS274	132	133	HBX KHL	1800	0.5	700	17.4
KHLSS274	133	134	RAT KHL	800	1	600	22.7
KHLSS274	134	135	RAT KHL	500	1	800	26.7
KHLSS274	135	136	RAT KHL	500	2	700	25.8
KHLSS274	136	137	RAT KHL	400	1	600	24.7
KHLSS274	137	138	RAT KHL	300	2	600	25.4
KHLSS274	138	139	RAT KHL	300	1	400	26.3
KHLSS274	139	140	RAT KHL	300	0.5	400	24.8
KHLSS274	140	141	RAT KHL	200	1	500	27.6
KHLSS274	141	142	RAT KHL	300	1	400	24
KHLSS274	142	143	RAT KHL	300	0.5	400	36.8
KHLSS274	143	144	RAT KHL	500	0.5	400	29
KHLSS274	144	145	RAT KHL	400	0.5	400	22.1
KHLSS274	145	146	RAT KHL	300	0.5	400	24.1
KHLSS274	146	147	RAT KHL	500	0.5	400	27
KHLSS274	147	148	RAT KHL	800	1	300	46.3
KHLSS274	148	149	RAT KHL	700	0.5	400	38.2
KHLSS274	149	150	RAT KHL	500	1	400	28.3
KHLSS274	150	151	RAT KHL	500	0.5	500	38.9
KHLSS274	151	152	RAT KHL	800	0.5	500	27.2
KHLSS274	152	153	RAT KHL	1100	1	500	27.3
KHLSS274	153	154	RAT KHL	1000	1	600	28.7
KHLSS274	154	155	RAT KHL	1100	1	600	35.4
KHLSS274	155	156	RAT KHL	900	1	700	37.4
KHLSS274	156	157	RAT KHL	1100	1	600	27.6
KHLSS274	157	158	RAT KHL	1500	1	600	22.9
KHLSS274	158	159	RAT KHL	1400	5	600	25.1
KHLSS274	159	160	RAT KHL	2000	9	600	21.6
KHLSS274	160	161	RAT KHL	1600	8	600	21.2
KTCSS315	351	352	RAT KNS	700	13	200	21.3
KTCSS315	352	353	RAT KNS	400	8	400	22.2
KTCSS315	353	354	RAT KNS	500	3	300	22
KTCSS315	354	355	RAT KNS	500	1	400	33.1
KTCSS315	355	355.8	RAT KNS	300	1	400	37.4
KTCSS326	264	265	RAT KNS	200	1	300	31.4
KTCSS326	265	265.9	RAT KNS	100	0.5	400	36
KTCSS326	266.5	267.5	RAT KNS	200	0.5	400	38.6
KTCSS326	267.5	268.3	RAT KNS	200	0.5	400	35.6
KTCSS326	268.3	270	RAT KNS	300	1	400	26.8
KTCSS326	270	271	RAT KNS	400	1	400	30.3
KTCSS326	271	272	RAT KNS	300	1	400	28.1
KTCSS326	272	273	RAT KNS	400	1	400	30.4

Hole_ID	Depth_From	Depth_To	Strat. Code	MnO_ppm	Mo_ppm	Na2O_ppm	Nb_ppm
KTCSS326	273	274	RAT KNS	400	1	300	40.6
KTCSS326	279	280	RAT KNS	200	0.5	300	26.1
KTCSS326	280	281	RAT KNS	200	0.5	300	30.4
KTCSS326	286	287	HBX KNS	2600	1	400	15.5
KTCSS326	287	288	DIP KNS	2500	1	300	12.6
KTCSS326	294	295	DIP KNS	1800	1	200	10.4
KTCSS326	295	296	DIP KNS	1300	1	200	11.6
SM59016	20.4	24	DIP SM	800	1	1000	22.6
SM59016	24	27.9	DIP SM	800	0.5	700	9.4
SM59016	30.9	34	DIP SM	400	1	200	0.9
SM59016	34	38	DIP SM	400	2	300	0.4
SM59016	38	42	DIP SM	600	2	500	0.3
SM59016	42	43.4	DIP SM	800	0.5	400	0.2
SM59016	44.4	46	DIP SM	700	0.5	300	0.1
SM59016	46	47.4	DIP SM	600	0.5	800	0.5
SM59016	52.4	54	DIP SM	600	1	700	0.5
SM59016	54	55	DIP SM	700	0.5	200	0.1
SM59016	55	56	DIP SM	600	1	200	0.1
SM59016	56	60	HBX SM	700	1	1000	0.9
SM59016	60	64	HBX SM	900	1	600	12.5
SM59016	64	67.6	HBX SM	500	1	400	12.1
SM59016	67.6	71	HBX SM	1400	0.5	300	11.8
SM59016	71	75	HBX SM	800	0.5	300	9.7
SM59016	75	77.4	HBX SM	900	0.5	200	8.4
SM59016	77.4	81	HBX SM	1100	1	400	10
SM59016	81	85	HBX SM	900	0.5	500	13.4
SM59016	85	86.4	HBX SM	300	0.5	500	19.1
SM59016	86.4	89	HBX SM	900	1	500	15.1
SM59016	89	90.8	HBX SM	1300	1	500	15
SM59016	90.8	95	HBX SM	900	0.5	300	12.7
SM59016	95	99	HBX SM	500	0.5	400	16
SM59016	99	103	HBX SM	400	0.5	300	14.1
SM59016	103	107	HBX SM	600	0.5	300	12.2
SM59016	107	111	RAT SM	400	0.5	500	20.9
SM59016	111	115	RAT SM	300	0.5	600	27.5
SM59016	115	119	RAT SM	200	0.5	500	26.2
SM59016	119	123	RAT SM	300	0.5	400	29
SM59016	123	127	RAT SM	400	1	400	36.9
SM59016	127	131	RAT SM	200	0.5	400	58.8
SM59016	131	135	RAT SM	400	0.5	400	35.4
SM59016	135	139	RAT SM	400	0.5	500	29.7
SM59016	139	143	RAT SM	500	1	500	34.6
SM59016	143	144	RAT SM	500	0.5	500	29.2
SM59016	144	145	RAT SM	400	1	500	29.3
SM59016	145	146	RAT SM	500	15	600	30
SM59016	146	147.3	RAT SM	1600	21	500	19.1

Hole_ID	Depth_From	Depth_To	Strat. Code	Nd_ppm	Ni_ppm	P2O5_%	Pb_ppm
KHLSS274	70	71	DIP KHL	147	81	0.22	1
KHLSS274	71	72	DIP KHL	3.8	55	0.24	1
KHLSS274	72	73	DIP KHL	4.5	44	0.28	1
KHLSS274	73	74	DIP KHL	2.2	38	0.16	1
KHLSS274	74	75	DIP KHL	3	47	0.3	1
KHLSS274	75	76	DIP KHL	5.2	44	0.31	1
KHLSS274	76	77	DIP KHL	3.1	57	0.2	1
KHLSS274	77	78	DIP KHL	6.4	36	0.44	1
KHLSS274	78	79	DIP KHL	33.4	28	0.19	1
KHLSS274	79	80	DIP KHL	38.8	28	0.15	1
KHLSS274	80	81	DIP KHL	32.5	29	0.13	1
KHLSS274	81	82	DIP KHL	35.5	30	0.15	1
KHLSS274	82	83	DIP KHL	33.1	29	0.17	1
KHLSS274	83	84	DIP KHL	42.4	31	0.12	1
KHLSS274	84	85	DIP KHL	38.8	30	0.12	1
KHLSS274	85	86	DIP KHL	40.1	30	0.13	1
KHLSS274	86	87	DIP KHL	43.8	32	0.15	1
KHLSS274	87	88	DIP KHL	54	33	0.16	1
KHLSS274	88	89	DIP KHL	49.2	31	0.17	1
KHLSS274	89	90	DIP KHL	47.5	28	0.16	1
KHLSS274	90	91	DIP KHL	45.3	30	0.12	1
KHLSS274	91	92	DIP KHL	42.5	29	0.13	1
KHLSS274	92	93	DIP KHL	45.4	31	0.12	1
KHLSS274	93	94	DIP KHL	43.5	30	0.15	1
KHLSS274	94	95	DIP KHL	52.1	31	0.12	1
KHLSS274	95	96	DIP KHL	38.6	27	0.13	1
KHLSS274	96	97	DIP KHL	37.2	29	0.14	1
KHLSS274	97	98	DIP KHL	36	29	0.11	1
KHLSS274	98	99	DIP KHL	33.5	28	0.15	1
KHLSS274	99	100	DIP KHL	39.2	31	0.1	1
KHLSS274	100	101	DIP KHL	38.4	31	0.1	1
KHLSS274	101	102	DIP KHL	39.8	30	0.1	1
KHLSS274	102	103	DIP KHL	43	32	0.13	1
KHLSS274	103	104	DIP KHL	36.6	28	0.09	1
KHLSS274	104	105	DIP KHL	32.2	31	0.1	1
KHLSS274	105	106	DIP KHL	33.8	28	0.1	1
KHLSS274	106	107	DIP KHL	32.3	27	0.09	1
KHLSS274	107	108	DIP KHL	29.1	27	0.09	1
KHLSS274	108	109	DIP KHL	29.6	26	0.09	1
KHLSS274	109	110	DIP KHL	30.8	28	0.09	1
KHLSS274	110	111	DIP KHL	32.1	28	0.11	1
KHLSS274	111	112	DIP KHL	28.4	30	0.09	1
KHLSS274	112	113	DIP KHL	29.5	26	0.08	1
KHLSS274	113	114	DIP KHL	33.6	28	0.09	1
KHLSS274	114	115	DIP KHL	32.5	30	0.08	1
KHLSS274	115	116	DIP KHL	17.4	31	0.11	1
KHLSS274	116	117	DIP KHL	27.1	29	0.1	1
KHLSS274	117	118	DIP KHL	29.3	30	0.08	1
KHLSS274	118	119	DIP KHL	27.1	28	0.07	1

Hole_ID	Depth_From	Depth_To	Strat. Code	Nd_ppm	Ni_ppm	P2O5_%	Pb_ppm
KHLSS274	119	120	DIP KHL	28.3	30	0.08	1
KHLSS274	120	121	DIP KHL	27.3	27	0.08	1
KHLSS274	121	122	DIP KHL	33	31	0.09	1
KHLSS274	122	123	DIP KHL	37.2	33	0.07	1
KHLSS274	123	124	DIP KHL	28.2	29	0.06	1
KHLSS274	124	125	DIP KHL	28.1	29	0.08	1
KHLSS274	125	126	HBX KHL	34.9	27	0.08	1
KHLSS274	126	127	HBX KHL	34	43	0.14	1
KHLSS274	127	128	HBX KHL	47.7	23	0.13	2
KHLSS274	128	129	HBX KHL	28.7	25	0.09	1
KHLSS274	129	130	HBX KHL	37.3	30	0.17	1
KHLSS274	130	131	HBX KHL	45.5	35	0.17	1
KHLSS274	131	132	HBX KHL	43.2	32	0.14	2
KHLSS274	132	133	HBX KHL	34.6	32	0.15	2
KHLSS274	133	134	RAT KHL	34.3	34	0.17	1
KHLSS274	134	135	RAT KHL	42.6	36	0.18	1
KHLSS274	135	136	RAT KHL	40.9	31	0.18	1
KHLSS274	136	137	RAT KHL	42.4	31	0.18	1
KHLSS274	137	138	RAT KHL	39.9	32	0.19	1
KHLSS274	138	139	RAT KHL	46.7	37	0.21	4
KHLSS274	139	140	RAT KHL	42.2	34	0.2	1
KHLSS274	140	141	RAT KHL	44.3	30	0.21	4
KHLSS274	141	142	RAT KHL	41	30	0.16	1
KHLSS274	142	143	RAT KHL	50.1	32	0.17	2
KHLSS274	143	144	RAT KHL	46.1	31	0.15	1
KHLSS274	144	145	RAT KHL	41.5	31	0.17	1
KHLSS274	145	146	RAT KHL	42.2	34	0.17	1
KHLSS274	146	147	RAT KHL	42.9	30	0.16	1
KHLSS274	147	148	RAT KHL	46.4	23	0.14	1
KHLSS274	148	149	RAT KHL	47.6	25	0.13	1
KHLSS274	149	150	RAT KHL	45.9	30	0.16	1
KHLSS274	150	151	RAT KHL	50	32	0.16	2
KHLSS274	151	152	RAT KHL	36.2	27	0.16	3
KHLSS274	152	153	RAT KHL	43.7	23	0.17	1
KHLSS274	153	154	RAT KHL	45.1	23	0.13	2
KHLSS274	154	155	RAT KHL	39	31	0.16	1
KHLSS274	155	156	RAT KHL	47.6	29	0.15	1
KHLSS274	156	157	RAT KHL	43.3	23	0.15	1
KHLSS274	157	158	RAT KHL	33.8	20	0.13	2
KHLSS274	158	159	RAT KHL	33.4	22	0.13	20
KHLSS274	159	160	RAT KHL	29.7	31	0.12	41
KHLSS274	160	161	RAT KHL	23	33	0.13	15
KTCSS315	351	352	RAT KNS	2	95	0.15	22
KTCSS315	352	353	RAT KNS	5.3	62	0.15	15
KTCSS315	353	354	RAT KNS	6.1	53	0.08	7
KTCSS315	354	355	RAT KNS	6	48	0.16	6
KTCSS315	355	355.8	RAT KNS	3.1	47	0.13	1
KTCSS326	264	265	RAT KNS	3.7	47	0.17	3
KTCSS326	265	265.9	RAT KNS	6.2	47	0.18	1

Hole_ID	Depth_From	Depth_To	Strat. Code	Nd_ppm	Ni_ppm	P2O5_%	Pb_ppm
KTCSS326	266.5	267.5	RAT KNS	5.7	51	0.16	1
KTCSS326	267.5	268.3	RAT KNS	4.8	53	0.16	1
KTCSS326	268.3	270	RAT KNS	14	52	0.16	1
KTCSS326	270	271	RAT KNS	31.2	52	0.15	2
KTCSS326	271	272	RAT KNS	29.3	60	0.16	1
KTCSS326	272	273	RAT KNS	41.4	61	0.17	1
KTCSS326	273	274	RAT KNS	45.3	75	0.18	1
KTCSS326	279	280	RAT KNS	3	76	0.19	1
KTCSS326	280	281	RAT KNS	3.3	76	0.16	1
KTCSS326	286	287	HBX KNS	37.6	114	0.13	1
KTCSS326	287	288	DIP KNS	36.7	161	0.14	2
KTCSS326	294	295	DIP KNS	89.8	141	0.12	1
KTCSS326	295	296	DIP KNS	102	142	0.1	1
SM59016	20.4	24	DIP SM	41.3	54	0.1	17
SM59016	24	27.9	DIP SM	23.9	32	0.07	5
SM59016	30.9	34	DIP SM	1.9	1	0.04	1
SM59016	34	38	DIP SM	1.4	0.5	0.14	1
SM59016	38	42	DIP SM	0.8	1	0.03	1
SM59016	42	43.4	DIP SM	1	1	0.04	2
SM59016	44.4	46	DIP SM	0.6	0.5	0.05	2
SM59016	46	47.4	DIP SM	1.2	0.5	0.04	1
SM59016	52.4	54	DIP SM	1.1	4	0.03	1
SM59016	54	55	DIP SM	0.7	0.5	0.01	1
SM59016	55	56	DIP SM	0.8	0.5	0.02	1
SM59016	56	60	HBX SM	1.9	2	0.03	8
SM59016	60	64	HBX SM	22	26	0.1	2
SM59016	64	67.6	HBX SM	17	41	0.17	4
SM59016	67.6	71	HBX SM	27.1	66	0.13	1
SM59016	71	75	HBX SM	6.3	36	0.07	7
SM59016	75	77.4	HBX SM	10	26	0.13	13
SM59016	77.4	81	HBX SM	12.7	43	0.13	2
SM59016	81	85	HBX SM	4.6	37	0.25	2
SM59016	85	86.4	HBX SM	63.3	100	0.27	4
SM59016	86.4	89	HBX SM	27.5	32	0.29	7
SM59016	89	90.8	HBX SM	27.6	35	0.18	4
SM59016	90.8	95	HBX SM	1.8	30	0.09	2
SM59016	95	99	HBX SM	3.4	84	0.16	3
SM59016	99	103	HBX SM	4.1	83	0.13	2
SM59016	103	107	HBX SM	2.6	88	0.1	3
SM59016	107	111	RAT SM	18	59	0.14	4
SM59016	111	115	RAT SM	55.3	36	0.16	4
SM59016	115	119	RAT SM	31	39	0.18	3
SM59016	119	123	RAT SM	25.7	36	0.16	3
SM59016	123	127	RAT SM	45.1	32	0.15	4
SM59016	127	131	RAT SM	33.9	34	0.15	3
SM59016	131	135	RAT SM	38	37	0.16	6
SM59016	135	139	RAT SM	46.4	34	0.14	1
SM59016	139	143	RAT SM	44.4	26	0.13	4
SM59016	143	144	RAT SM	12.4	26	0.12	2

Hole_ID	Depth_From	Depth_To	Strat. Code	Nd_ppm	Ni_ppm	P2O5_%	Pb_ppm
SM59016	144	145	RAT SM	22	34	0.15	6
SM59016	145	146	RAT SM	10.2	42	0.15	27
SM59016	146	147.3	RAT SM	42.9	44	0.12	27

Hole_ID	Depth_From	Depth_To	Strat. Code	Pr_ppm	Rb_ppm	Re_ppm	S_%
KHLSS274	70	71	DIP KHL	40	1.2	0.004	0.02
KHLSS274	71	72	DIP KHL	0.92	0.8	0.002	0.03
KHLSS274	72	73	DIP KHL	0.86	0.4	0.001	0.03
KHLSS274	73	74	DIP KHL	0.56	0.6	0.0005	0.03
KHLSS274	74	75	DIP KHL	0.59	0.4	0.0005	0.03
KHLSS274	75	76	DIP KHL	0.9	0.3	0.0005	0.04
KHLSS274	76	77	DIP KHL	0.64	0.4	0.0005	0.02
KHLSS274	77	78	DIP KHL	1.25	2.3	0.0005	0.01
KHLSS274	78	79	DIP KHL	8.31	1.3	0.0005	0.01
KHLSS274	79	80	DIP KHL	10.4	1	0.0005	0.01
KHLSS274	80	81	DIP KHL	8.38	1	0.0005	0.01
KHLSS274	81	82	DIP KHL	10.65	1.3	0.0005	0.01
KHLSS274	82	83	DIP KHL	8.31	0.8	0.0005	0.01
KHLSS274	83	84	DIP KHL	11.3	0.8	0.0005	0.01
KHLSS274	84	85	DIP KHL	10.9	2.1	0.0005	0.01
KHLSS274	85	86	DIP KHL	10.6	13.6	0.0005	0.01
KHLSS274	86	87	DIP KHL	11.3	11.5	0.0005	0.005
KHLSS274	87	88	DIP KHL	14.15	11.5	0.0005	0.005
KHLSS274	88	89	DIP KHL	13	23.1	0.0005	0.005
KHLSS274	89	90	DIP KHL	12.6	22.4	0.0005	0.005
KHLSS274	90	91	DIP KHL	12.1	18.4	0.0005	0.005
KHLSS274	91	92	DIP KHL	11.45	16.6	0.0005	0.005
KHLSS274	92	93	DIP KHL	11.85	16.5	0.0005	0.005
KHLSS274	93	94	DIP KHL	11.6	14.1	0.0005	0.005
KHLSS274	94	95	DIP KHL	12.55	12.8	0.0005	0.005
KHLSS274	95	96	DIP KHL	9.81	16.7	0.0005	0.005
KHLSS274	96	97	DIP KHL	9.51	16.1	0.0005	0.005
KHLSS274	97	98	DIP KHL	9.96	13.2	0.0005	0.005
KHLSS274	98	99	DIP KHL	9.03	12.9	0.0005	0.005
KHLSS274	99	100	DIP KHL	10.75	2.7	0.0005	0.005
KHLSS274	100	101	DIP KHL	11	0.8	0.0005	0.005
KHLSS274	101	102	DIP KHL	11.15	0.7	0.0005	0.005
KHLSS274	102	103	DIP KHL	11.75	0.4	0.0005	0.005
KHLSS274	103	104	DIP KHL	10.75	0.7	0.0005	0.005
KHLSS274	104	105	DIP KHL	9.55	0.7	0.0005	0.005
KHLSS274	105	106	DIP KHL	10.15	0.5	0.0005	0.005
KHLSS274	106	107	DIP KHL	9.11	0.6	0.0005	0.005
KHLSS274	107	108	DIP KHL	8.05	0.4	0.0005	0.005
KHLSS274	108	109	DIP KHL	8.63	0.9	0.0005	0.005
KHLSS274	109	110	DIP KHL	8.24	4.4	0.0005	0.005
KHLSS274	110	111	DIP KHL	8.51	7.4	0.0005	0.005
KHLSS274	111	112	DIP KHL	7.98	4.6	0.0005	0.02
KHLSS274	112	113	DIP KHL	7.89	4.6	0.0005	0.005
KHLSS274	113	114	DIP KHL	8.91	7.1	0.0005	0.005

Hole_ID	Depth_From	Depth_To	Strat. Code	Pr_ppm	Rb_ppm	Re_ppm	S_%
KHLSS274	114	115	DIP KHL	8.65	5.4	0.0005	0.005
KHLSS274	115	116	DIP KHL	4.56	0.7	0.0005	0.005
KHLSS274	116	117	DIP KHL	7.67	0.5	0.0005	0.005
KHLSS274	117	118	DIP KHL	7.89	0.3	0.0005	0.005
KHLSS274	118	119	DIP KHL	7.75	0.3	0.0005	0.01
KHLSS274	119	120	DIP KHL	8.29	0.3	0.0005	0.01
KHLSS274	120	121	DIP KHL	7.77	0.4	0.0005	0.01
KHLSS274	121	122	DIP KHL	9.38	0.3	0.0005	0.01
KHLSS274	122	123	DIP KHL	10.7	0.4	0.0005	0.01
KHLSS274	123	124	DIP KHL	8.18	0.3	0.0005	0.01
KHLSS274	124	125	DIP KHL	8.01	0.3	0.0005	0.01
KHLSS274	125	126	HBX KHL	10.3	0.6	0.0005	0.01
KHLSS274	126	127	HBX KHL	8.65	35.2	0.0005	0.02
KHLSS274	127	128	HBX KHL	11.5	131.5	0.0005	0.01
KHLSS274	128	129	HBX KHL	7.46	80.9	0.0005	0.01
KHLSS274	129	130	HBX KHL	10.15	105	0.0005	0.03
KHLSS274	130	131	HBX KHL	11.2	136.5	0.0005	0.04
KHLSS274	131	132	HBX KHL	11.05	105	0.0005	0.03
KHLSS274	132	133	HBX KHL	9.31	83.5	0.0005	0.02
KHLSS274	133	134	RAT KHL	9	126	0.0005	0.02
KHLSS274	134	135	RAT KHL	10.85	105.5	0.0005	0.02
KHLSS274	135	136	RAT KHL	10.55	119.5	0.0005	0.02
KHLSS274	136	137	RAT KHL	11.45	124.5	0.0005	0.02
KHLSS274	137	138	RAT KHL	10.35	130.5	0.0005	0.02
KHLSS274	138	139	RAT KHL	12.25	140	0.0005	0.01
KHLSS274	139	140	RAT KHL	11.25	129	0.0005	0.02
KHLSS274	140	141	RAT KHL	11.7	144	0.0005	0.02
KHLSS274	141	142	RAT KHL	10.8	123	0.0005	0.02
KHLSS274	142	143	RAT KHL	12.65	112	0.0005	0.02
KHLSS274	143	144	RAT KHL	12.1	93.4	0.0005	0.02
KHLSS274	144	145	RAT KHL	11	113.5	0.0005	0.02
KHLSS274	145	146	RAT KHL	11.15	85.1	0.0005	0.02
KHLSS274	146	147	RAT KHL	11.05	90.3	0.0005	0.02
KHLSS274	147	148	RAT KHL	12	82.9	0.0005	0.02
KHLSS274	148	149	RAT KHL	12.25	79.1	0.0005	0.03
KHLSS274	149	150	RAT KHL	11.8	71.8	0.0005	0.02
KHLSS274	150	151	RAT KHL	13.05	78.8	0.0005	0.03
KHLSS274	151	152	RAT KHL	9.45	85.1	0.0005	0.02
KHLSS274	152	153	RAT KHL	10.75	120	0.0005	0.02
KHLSS274	153	154	RAT KHL	11.85	146.5	0.0005	0.01
KHLSS274	154	155	RAT KHL	10.05	118	0.0005	0.02
KHLSS274	155	156	RAT KHL	12.1	151.5	0.0005	0.02
KHLSS274	156	157	RAT KHL	11.3	161	0.0005	0.02
KHLSS274	157	158	RAT KHL	8.75	136.5	0.0005	0.02
KHLSS274	158	159	RAT KHL	8.78	133.5	0.001	0.01
KHLSS274	159	160	RAT KHL	7.92	117.5	0.003	0.02
KHLSS274	160	161	RAT KHL	5.91	143	0.001	0.01
KTCSS315	351	352	RAT KNS	0.3	15.6	0.026	1.58
KTCSS315	352	353	RAT KNS	1.24	37.6	0.001	0.12

Hole_ID	Depth_From	Depth_To	Strat. Code	Pr_ppm	Rb_ppm	Re_ppm	S_%
KTCSS315	353	354	RAT KNS	1.5	36.8	0.001	0.05
KTCSS315	354	355	RAT KNS	1.13	48.4	0.001	0.05
KTCSS315	355	355.8	RAT KNS	0.52	53.3	0.0005	0.03
KTCSS326	264	265	RAT KNS	0.85	19.1	0.0005	0.05
KTCSS326	265	265.9	RAT KNS	1.57	27.4	0.001	0.03
KTCSS326	266.5	267.5	RAT KNS	1.42	27.4	0.0005	0.04
KTCSS326	267.5	268.3	RAT KNS	1.19	27.4	0.0005	0.03
KTCSS326	268.3	270	RAT KNS	3.71	36.5	0.0005	0.03
KTCSS326	270	271	RAT KNS	8.63	28.2	0.0005	0.03
KTCSS326	271	272	RAT KNS	8.32	27.7	0.0005	0.05
KTCSS326	272	273	RAT KNS	11.2	15.8	0.0005	0.03
KTCSS326	273	274	RAT KNS	12.2	7.3	0.0005	0.07
KTCSS326	279	280	RAT KNS	0.61	1.1	0.0005	0.03
KTCSS326	280	281	RAT KNS	0.7	1	0.0005	0.03
KTCSS326	286	287	HBX KNS	8.99	0.4	0.001	0.02
KTCSS326	287	288	DIP KNS	9.74	0.2	0.0005	0.02
KTCSS326	294	295	DIP KNS	28.9	1	0.0005	0.01
KTCSS326	295	296	DIP KNS	32.5	0.8	0.0005	0.01
SM59016	20.4	24	DIP SM	10.45	45.4	0.001	0.02
SM59016	24	27.9	DIP SM	6.1	37.9	0.0005	0.005
SM59016	30.9	34	DIP SM	0.4	10.9	0.0005	0.01
SM59016	34	38	DIP SM	0.33	11.7	0.0005	0.02
SM59016	38	42	DIP SM	0.21	8.1	0.002	0.04
SM59016	42	43.4	DIP SM	0.2	6.4	0.0005	0.01
SM59016	44.4	46	DIP SM	0.15	6.4	0.0005	0.01
SM59016	46	47.4	DIP SM	0.32	8.6	0.0005	0.01
SM59016	52.4	54	DIP SM	0.29	10.4	0.0005	0.01
SM59016	54	55	DIP SM	0.17	4.3	0.0005	0.005
SM59016	55	56	DIP SM	0.2	6.3	0.0005	0.01
SM59016	56	60	HBX SM	0.5	8.2	0.0005	0.03
SM59016	60	64	HBX SM	5.88	46.2	0.0005	0.03
SM59016	64	67.6	HBX SM	4.75	14.4	0.0005	0.01
SM59016	67.6	71	HBX SM	9.12	1.7	0.001	0.02
SM59016	71	75	HBX SM	1.4	0.7	0.0005	0.005
SM59016	75	77.4	HBX SM	1.99	0.3	0.0005	0.01
SM59016	77.4	81	HBX SM	3.68	7	0.0005	0.01
SM59016	81	85	HBX SM	1.06	26	0.0005	0.01
SM59016	85	86.4	HBX SM	16.6	19.7	0.0005	0.01
SM59016	86.4	89	HBX SM	7.26	29.2	0.0005	0.02
SM59016	89	90.8	HBX SM	8.15	17.1	0.0005	0.02
SM59016	90.8	95	HBX SM	0.46	0.2	0.0005	0.01
SM59016	95	99	HBX SM	0.86	0.3	0.001	0.01
SM59016	99	103	HBX SM	0.99	0.4	0.0005	0.01
SM59016	103	107	HBX SM	0.63	0.2	0.0005	0.01
SM59016	107	111	RAT SM	4.89	48.8	0.0005	0.04
SM59016	111	115	RAT SM	14.65	88.9	0.0005	0.04
SM59016	115	119	RAT SM	8.18	83.8	0.003	0.02
SM59016	119	123	RAT SM	6.72	68	0.013	0.01
SM59016	123	127	RAT SM	11.7	53.5	0.008	0.03

Hole_ID	Depth_From	Depth_To	Strat. Code	Pr_ppm	Rb_ppm	Re_ppm	S_%
SM59016	127	131	RAT SM	8.96	41.3	0.008	0.04
SM59016	131	135	RAT SM	10	32.8	0.009	0.04
SM59016	135	139	RAT SM	12.7	75.6	0.002	0.01
SM59016	139	143	RAT SM	11.95	81.8	0.001	0.01
SM59016	143	144	RAT SM	2.82	87.2	0.001	0.02
SM59016	144	145	RAT SM	5.64	75.2	0.007	0.12
SM59016	145	146	RAT SM	2.41	57.3	0.012	0.21
SM59016	146	147.3	RAT SM	11.55	23.7	0.027	0.23

Hole_ID	Depth_From	Depth_To	Strat. Code	Sb_ppm	Sc_ppm	Se_ppm	SiO2_%
KHLSS274	70	71	DIP KHL	0.025	21	0.1	55.4
KHLSS274	71	72	DIP KHL	0.025	12	0.2	44.7
KHLSS274	72	73	DIP KHL	0.025	11	0.1	37.6
KHLSS274	73	74	DIP KHL	0.025	8	0.3	46.6
KHLSS274	74	75	DIP KHL	0.025	9	0.1	42
KHLSS274	75	76	DIP KHL	0.025	8	0.1	41.5
KHLSS274	76	77	DIP KHL	0.025	10	0.1	47.5
KHLSS274	77	78	DIP KHL	0.025	10	0.1	40.8
KHLSS274	78	79	DIP KHL	0.025	7	0.1	47.6
KHLSS274	79	80	DIP KHL	0.025	9	0.2	42.7
KHLSS274	80	81	DIP KHL	0.025	9	0.1	41.3
KHLSS274	81	82	DIP KHL	0.025	7	0.1	48.2
KHLSS274	82	83	DIP KHL	0.025	9	0.2	42.4
KHLSS274	83	84	DIP KHL	0.025	9	0.1	43.5
KHLSS274	84	85	DIP KHL	0.025	8	0.1	48.3
KHLSS274	85	86	DIP KHL	0.025	8	0.1	47.8
KHLSS274	86	87	DIP KHL	0.025	7	0.1	47.2
KHLSS274	87	88	DIP KHL	0.025	6	0.1	52.9
KHLSS274	88	89	DIP KHL	0.025	6	0.1	54.4
KHLSS274	89	90	DIP KHL	0.025	8	0.1	53.3
KHLSS274	90	91	DIP KHL	0.025	9	0.1	52.6
KHLSS274	91	92	DIP KHL	0.025	9	0.1	50.9
KHLSS274	92	93	DIP KHL	0.025	5	0.1	57
KHLSS274	93	94	DIP KHL	0.025	6	0.1	57.6
KHLSS274	94	95	DIP KHL	0.025	10	0.1	55.6
KHLSS274	95	96	DIP KHL	0.025	10	0.1	48.2
KHLSS274	96	97	DIP KHL	0.025	9	0.1	48.4
KHLSS274	97	98	DIP KHL	0.025	9	0.1	50
KHLSS274	98	99	DIP KHL	0.025	12	0.1	45.3
KHLSS274	99	100	DIP KHL	0.025	9	0.1	46
KHLSS274	100	101	DIP KHL	0.025	9	0.1	44.9
KHLSS274	101	102	DIP KHL	0.025	12	0.1	40.5
KHLSS274	102	103	DIP KHL	0.025	10	0.1	44.7
KHLSS274	103	104	DIP KHL	0.025	10	0.1	46.1
KHLSS274	104	105	DIP KHL	0.025	8	0.1	47.7
KHLSS274	105	106	DIP KHL	0.025	10	0.1	39.1
KHLSS274	106	107	DIP KHL	0.025	9	0.1	41.2
KHLSS274	107	108	DIP KHL	0.025	10	0.1	38.1
KHLSS274	108	109	DIP KHL	0.025	10	0.1	41

Hole_ID	Depth_From	Depth_To	Strat. Code	Sb_ppm	Sc_ppm	Se_ppm	SiO2_%
KHLSS274	109	110	DIP KHL	0.025	8	0.2	48.5
KHLSS274	110	111	DIP KHL	0.025	8	0.1	47.8
KHLSS274	111	112	DIP KHL	0.025	9	0.3	43.1
KHLSS274	112	113	DIP KHL	0.025	8	0.1	44.8
KHLSS274	113	114	DIP KHL	0.025	7	0.1	49.7
KHLSS274	114	115	DIP KHL	0.025	6	0.1	52
KHLSS274	115	116	DIP KHL	0.025	8	0.1	43.2
KHLSS274	116	117	DIP KHL	0.025	8	0.1	42.5
KHLSS274	117	118	DIP KHL	0.025	11	0.1	38
KHLSS274	118	119	DIP KHL	0.025	10	0.1	39.8
KHLSS274	119	120	DIP KHL	0.025	10	0.1	41
KHLSS274	120	121	DIP KHL	0.025	10	0.1	40.4
KHLSS274	121	122	DIP KHL	0.025	9	0.1	45.9
KHLSS274	122	123	DIP KHL	0.025	9	0.1	47
KHLSS274	123	124	DIP KHL	0.025	13	0.1	37.4
KHLSS274	124	125	DIP KHL	0.025	11	0.1	36.7
KHLSS274	125	126	HBX KHL	0.025	9	0.1	33.5
KHLSS274	126	127	HBX KHL	0.025	13	0.1	40.8
KHLSS274	127	128	HBX KHL	0.05	12	0.1	42.8
KHLSS274	128	129	HBX KHL	0.025	13	0.1	39.1
KHLSS274	129	130	HBX KHL	0.05	12	0.3	49.7
KHLSS274	130	131	HBX KHL	0.025	11	0.1	51.7
KHLSS274	131	132	HBX KHL	0.025	11	0.2	44
KHLSS274	132	133	HBX KHL	0.05	12	0.1	42.4
KHLSS274	133	134	RAT KHL	0.07	14	0.1	50.4
KHLSS274	134	135	RAT KHL	0.07	14	0.1	48.7
KHLSS274	135	136	RAT KHL	0.06	13	0.1	48.8
KHLSS274	136	137	RAT KHL	0.08	13	0.1	53
KHLSS274	137	138	RAT KHL	0.07	13	0.1	54
KHLSS274	138	139	RAT KHL	0.09	14	0.1	52.3
KHLSS274	139	140	RAT KHL	0.08	14	0.1	52.3
KHLSS274	140	141	RAT KHL	0.08	13	0.1	54.4
KHLSS274	141	142	RAT KHL	0.07	12	0.1	50.4
KHLSS274	142	143	RAT KHL	0.08	13	0.1	53.3
KHLSS274	143	144	RAT KHL	0.07	12	0.1	49.8
KHLSS274	144	145	RAT KHL	0.09	13	0.4	48.4
KHLSS274	145	146	RAT KHL	0.07	13	0.1	47.8
KHLSS274	146	147	RAT KHL	0.08	12	0.1	46.6
KHLSS274	147	148	RAT KHL	0.1	10	0.2	47.5
KHLSS274	148	149	RAT KHL	0.09	11	0.1	45.4
KHLSS274	149	150	RAT KHL	0.1	11	0.3	45.5
KHLSS274	150	151	RAT KHL	0.08	11	0.1	49.3
KHLSS274	151	152	RAT KHL	0.09	11	0.1	48.8
KHLSS274	152	153	RAT KHL	0.1	10	0.1	44
KHLSS274	153	154	RAT KHL	0.1	11	0.1	47.2
KHLSS274	154	155	RAT KHL	0.11	11	0.1	45.1
KHLSS274	155	156	RAT KHL	0.08	12	0.1	48.2
KHLSS274	156	157	RAT KHL	0.11	12	0.1	46.1
KHLSS274	157	158	RAT KHL	0.08	11	0.2	42.5

Hole_ID	Depth_From	Depth_To	Strat. Code	Sb_ppm	Sc_ppm	Se_ppm	SiO2_%
KHLSS274	158	159	RAT KHL	0.23	11	0.1	44.5
KHLSS274	159	160	RAT KHL	1.03	11	0.2	39.7
KHLSS274	160	161	RAT KHL	1.86	11	0.4	45.3
KTCSS315	351	352	RAT KNS	0.28	12	2.4	38.4
KTCSS315	352	353	RAT KNS	0.28	13	4.2	46
KTCSS315	353	354	RAT KNS	0.15	12	6.4	45.8
KTCSS315	354	355	RAT KNS	0.08	14	1.4	52.1
KTCSS315	355	355.8	RAT KNS	0.05	14	0.3	53
KTCSS326	264	265	RAT KNS	0.07	11	0.1	50.1
KTCSS326	265	265.9	RAT KNS	0.08	12	0.4	53.9
KTCSS326	266.5	267.5	RAT KNS	0.05	13	0.1	50.5
KTCSS326	267.5	268.3	RAT KNS	0.07	12	0.1	49.3
KTCSS326	268.3	270	RAT KNS	0.06	12	0.1	49.5
KTCSS326	270	271	RAT KNS	0.05	13	0.1	48.3
KTCSS326	271	272	RAT KNS	0.06	13	0.1	50.3
KTCSS326	272	273	RAT KNS	0.07	14	0.1	51.1
KTCSS326	273	274	RAT KNS	0.08	16	0.1	48.8
KTCSS326	279	280	RAT KNS	0.025	12	0.1	49.1
KTCSS326	280	281	RAT KNS	0.06	14	0.1	50.1
KTCSS326	286	287	HBX KNS	0.05	25	0.1	40.5
KTCSS326	287	288	DIP KNS	0.05	13	0.1	43.3
KTCSS326	294	295	DIP KNS	0.05	18	0.1	35.9
KTCSS326	295	296	DIP KNS	0.06	17	0.1	34.1
SM59016	20.4	24	DIP SM	0.46	15	0.1	54
SM59016	24	27.9	DIP SM	0.39	8	0.1	62
SM59016	30.9	34	DIP SM	0.09	1	0.2	8.29
SM59016	34	38	DIP SM	0.5	0.5	0.1	11.75
SM59016	38	42	DIP SM	0.49	0.5	0.1	8.72
SM59016	42	43.4	DIP SM	0.78	0.5	0.1	9.46
SM59016	44.4	46	DIP SM	0.74	0.5	0.2	8.58
SM59016	46	47.4	DIP SM	0.46	0.5	0.1	5.69
SM59016	52.4	54	DIP SM	0.64	0.5	0.1	23.8
SM59016	54	55	DIP SM	0.49	0.5	0.1	3.95
SM59016	55	56	DIP SM	0.7	0.5	0.1	6.7
SM59016	56	60	HBX SM	1.15	1	0.1	9.71
SM59016	60	64	HBX SM	0.1	9	0.4	37.3
SM59016	64	67.6	HBX SM	0.23	11	0.1	44.7
SM59016	67.6	71	HBX SM	0.21	19	0.1	36.3
SM59016	71	75	HBX SM	0.11	16	0.4	30.3
SM59016	75	77.4	HBX SM	0.15	16	4.6	24.6
SM59016	77.4	81	HBX SM	0.14	10	0.8	32.7
SM59016	81	85	HBX SM	0.1	9	0.1	38.8
SM59016	85	86.4	HBX SM	0.11	17	0.7	46.3
SM59016	86.4	89	HBX SM	0.1	11	0.2	34.6
SM59016	89	90.8	HBX SM	0.06	9	0.3	39.7
SM59016	90.8	95	HBX SM	0.025	11	0.6	47.2
SM59016	95	99	HBX SM	0.025	21	0.1	45.6
SM59016	99	103	HBX SM	0.025	18	0.1	40.9
SM59016	103	107	HBX SM	0.025	20	0.3	36.8

Hole_ID	Depth_From	Depth_To	Strat. Code	Sb_ppm	Sc_ppm	Se_ppm	SiO2_%
SM59016	107	111	RAT SM	0.025	13	0.1	47.4
SM59016	111	115	RAT SM	0.025	14	0.1	51.7
SM59016	115	119	RAT SM	0.025	13	0.2	52.8
SM59016	119	123	RAT SM	0.05	11	0.1	49.7
SM59016	123	127	RAT SM	0.06	12	0.1	48
SM59016	127	131	RAT SM	0.07	11	0.1	52.5
SM59016	131	135	RAT SM	0.06	12	0.2	47
SM59016	135	139	RAT SM	0.05	11	0.1	48.3
SM59016	139	143	RAT SM	0.08	12	0.2	46.4
SM59016	143	144	RAT SM	0.06	12	0.3	50.4
SM59016	144	145	RAT SM	0.06	11	5.2	50.3
SM59016	145	146	RAT SM	0.28	12	14.8	49
SM59016	146	147.3	RAT SM	0.5	9	5	37.9

Hole_ID	Depth_From	Depth_To	Strat. Code	Sm_ppm	Sn_ppm	Sr_ppm	SrO_ppm
KHLSS274	70	71	DIP KHL	25.4	3	72.9	0.01
KHLSS274	71	72	DIP KHL	0.92	2	56.4	0.01
KHLSS274	72	73	DIP KHL	1.16	1	76.9	0.01
KHLSS274	73	74	DIP KHL	0.72	1	40.3	0.01
KHLSS274	74	75	DIP KHL	0.61	2	52.4	0.01
KHLSS274	75	76	DIP KHL	1.64	2	37.8	0.005
KHLSS274	76	77	DIP KHL	0.76	2	25.1	0.005
KHLSS274	77	78	DIP KHL	2.24	2	57.5	0.01
KHLSS274	78	79	DIP KHL	7.53	2	51.3	0.005
KHLSS274	79	80	DIP KHL	6.27	2	63	0.01
KHLSS274	80	81	DIP KHL	5.51	2	68.8	0.01
KHLSS274	81	82	DIP KHL	6.08	2	91.5	0.01
KHLSS274	82	83	DIP KHL	6.71	2	62.5	0.01
KHLSS274	83	84	DIP KHL	7.03	2	59.7	0.01
KHLSS274	84	85	DIP KHL	6.13	2	100.5	0.01
KHLSS274	85	86	DIP KHL	6.53	2	131	0.02
KHLSS274	86	87	DIP KHL	8.21	1	160	0.02
KHLSS274	87	88	DIP KHL	9.91	1	221	0.03
KHLSS274	88	89	DIP KHL	7.98	2	152	0.02
KHLSS274	89	90	DIP KHL	7.51	1	134.5	0.02
KHLSS274	90	91	DIP KHL	7.79	1	131.5	0.01
KHLSS274	91	92	DIP KHL	7.15	1	135	0.01
KHLSS274	92	93	DIP KHL	7.57	1	122	0.01
KHLSS274	93	94	DIP KHL	7.41	1	91.4	0.01
KHLSS274	94	95	DIP KHL	10.3	1	113.5	0.02
KHLSS274	95	96	DIP KHL	7.03	1	120	0.02
KHLSS274	96	97	DIP KHL	7.24	1	131	0.02
KHLSS274	97	98	DIP KHL	7.09	1	146	0.02
KHLSS274	98	99	DIP KHL	6.48	1	123	0.02
KHLSS274	99	100	DIP KHL	6.73	1	180.5	0.02
KHLSS274	100	101	DIP KHL	6.22	1	210	0.03
KHLSS274	101	102	DIP KHL	7.06	1	243	0.03
KHLSS274	102	103	DIP KHL	7.63	1	198.5	0.02
KHLSS274	103	104	DIP KHL	6.03	1	169	0.02

Hole_ID	Depth_From	Depth_To	Strat. Code	Sm_ppm	Sn_ppm	Sr_ppm	SrO_ppm
KHLSS274	104	105	DIP KHL	5.35	1	148	0.02
KHLSS274	105	106	DIP KHL	5.75	1	209	0.03
KHLSS274	106	107	DIP KHL	6.95	1	146	0.02
KHLSS274	107	108	DIP KHL	6.22	1	150.5	0.02
KHLSS274	108	109	DIP KHL	6.98	1	119	0.02
KHLSS274	109	110	DIP KHL	6.63	1	86.5	0.01
KHLSS274	110	111	DIP KHL	6.31	1	84.7	0.01
KHLSS274	111	112	DIP KHL	6.58	1	103	0.01
KHLSS274	112	113	DIP KHL	6.15	1	104.5	0.01
KHLSS274	113	114	DIP KHL	6.77	2	84.3	0.01
KHLSS274	114	115	DIP KHL	6.85	1	72	0.01
KHLSS274	115	116	DIP KHL	3.9	2	66.3	0.01
KHLSS274	116	117	DIP KHL	5.02	2	66.2	0.01
KHLSS274	117	118	DIP KHL	5.36	1	77.3	0.01
KHLSS274	118	119	DIP KHL	4.46	1	83.1	0.01
KHLSS274	119	120	DIP KHL	4.9	1	81.7	0.01
KHLSS274	120	121	DIP KHL	4.54	1	85.7	0.01
KHLSS274	121	122	DIP KHL	5.03	1	90.4	0.01
KHLSS274	122	123	DIP KHL	5.67	2	111.5	0.01
KHLSS274	123	124	DIP KHL	4.56	1	113.5	0.02
KHLSS274	124	125	DIP KHL	5.17	1	120	0.02
KHLSS274	125	126	HBX KHL	5.55	2	127	0.02
KHLSS274	126	127	HBX KHL	6.68	3	62.9	0.01
KHLSS274	127	128	HBX KHL	9.98	3	81.9	0.01
KHLSS274	128	129	HBX KHL	5.2	2	69.5	0.01
KHLSS274	129	130	HBX KHL	7.16	3	60.6	0.01
KHLSS274	130	131	HBX KHL	9.12	3	59.2	0.01
KHLSS274	131	132	HBX KHL	10.1	2	126.5	0.01
KHLSS274	132	133	HBX KHL	7.39	2	167.5	0.02
KHLSS274	133	134	RAT KHL	6.91	3	41.7	0.01
KHLSS274	134	135	RAT KHL	8.64	4	57.9	0.01
KHLSS274	135	136	RAT KHL	8	4	59.5	0.01
KHLSS274	136	137	RAT KHL	8.34	4	54.5	0.01
KHLSS274	137	138	RAT KHL	7.61	3	46.4	0.005
KHLSS274	138	139	RAT KHL	8.82	4	38.1	0.005
KHLSS274	139	140	RAT KHL	8.33	3	53.3	0.01
KHLSS274	140	141	RAT KHL	8.17	4	55.4	0.005
KHLSS274	141	142	RAT KHL	7.68	3	44.5	0.01
KHLSS274	142	143	RAT KHL	9.03	4	35.9	0.005
KHLSS274	143	144	RAT KHL	8.63	4	73.2	0.01
KHLSS274	144	145	RAT KHL	7.6	3	47.1	0.005
KHLSS274	145	146	RAT KHL	8.14	3	44.2	0.005
KHLSS274	146	147	RAT KHL	7.74	3	51.2	0.01
KHLSS274	147	148	RAT KHL	9.98	4	64.8	0.01
KHLSS274	148	149	RAT KHL	8.94	4	110.5	0.01
KHLSS274	149	150	RAT KHL	8.57	3	66.2	0.01
KHLSS274	150	151	RAT KHL	9.49	4	60.1	0.01
KHLSS274	151	152	RAT KHL	7.24	3	54.1	0.005
KHLSS274	152	153	RAT KHL	7.95	3	56.6	0.01

Hole_ID	Depth_From	Depth_To	Strat. Code	Sm_ppm	Sn_ppm	Sr_ppm	SrO_ppm
KHLSS274	153	154	RAT KHL	8.26	3	52.7	0.01
KHLSS274	154	155	RAT KHL	7.55	4	94.7	0.01
KHLSS274	155	156	RAT KHL	8.93	4	56.1	0.01
KHLSS274	156	157	RAT KHL	7.94	4	49.7	0.01
KHLSS274	157	158	RAT KHL	6.27	3	59.8	0.01
KHLSS274	158	159	RAT KHL	6.26	3	58.5	0.01
KHLSS274	159	160	RAT KHL	5.91	3	61.6	0.01
KHLSS274	160	161	RAT KHL	4.99	4	71.5	0.01
KTCSS315	351	352	RAT KNS	2.71	2	61.1	0.01
KTCSS315	352	353	RAT KNS	3.34	2	60.9	0.01
KTCSS315	353	354	RAT KNS	3.37	2	46.7	0.005
KTCSS315	354	355	RAT KNS	4.67	5	933	0.11
KTCSS315	355	355.8	RAT KNS	2.95	9	58.3	0.005
KTCSS326	264	265	RAT KNS	2.2	3	49.8	0.005
KTCSS326	265	265.9	RAT KNS	2.86	6	61.5	0.005
KTCSS326	266.5	267.5	RAT KNS	2.31	9	81.9	0.005
KTCSS326	267.5	268.3	RAT KNS	2.19	7	90.7	0.005
KTCSS326	268.3	270	RAT KNS	3.27	7	51.4	0.005
KTCSS326	270	271	RAT KNS	5.99	5	69.2	0.005
KTCSS326	271	272	RAT KNS	5.23	5	66.3	0.005
KTCSS326	272	273	RAT KNS	6.92	4	77.6	0.005
KTCSS326	273	274	RAT KNS	8.77	5	135.5	0.01
KTCSS326	279	280	RAT KNS	1.7	4	35.9	0.005
KTCSS326	280	281	RAT KNS	1.84	5	51.1	0.005
KTCSS326	286	287	HBX KNS	10.05	3	75.4	0.005
KTCSS326	287	288	DIP KNS	7.53	2	90.6	0.005
KTCSS326	294	295	DIP KNS	9.53	5	155	0.01
KTCSS326	295	296	DIP KNS	10.25	5	126.5	0.01
SM59016	20.4	24	DIP SM	8.87	4	25.8	0.005
SM59016	24	27.9	DIP SM	4.88	3	23	0.005
SM59016	30.9	34	DIP SM	0.4	0.5	114	0.01
SM59016	34	38	DIP SM	0.23	0.5	210	0.02
SM59016	38	42	DIP SM	0.16	0.5	404	0.04
SM59016	42	43.4	DIP SM	0.16	0.5	230	0.02
SM59016	44.4	46	DIP SM	0.16	0.5	231	0.02
SM59016	46	47.4	DIP SM	0.34	0.5	274	0.03
SM59016	52.4	54	DIP SM	0.18	0.5	153	0.01
SM59016	54	55	DIP SM	0.16	0.5	264	0.02
SM59016	55	56	DIP SM	0.14	0.5	323	0.03
SM59016	56	60	HBX SM	0.44	0.5	267	0.03
SM59016	60	64	HBX SM	4.22	2	166	0.01
SM59016	64	67.6	HBX SM	2.73	2	369	0.04
SM59016	67.6	71	HBX SM	3.51	1	420	0.04
SM59016	71	75	HBX SM	1.84	7	257	0.03
SM59016	75	77.4	HBX SM	3.06	7	440	0.05
SM59016	77.4	81	HBX SM	2.69	2	192	0.02
SM59016	81	85	HBX SM	1.38	2	72	0.01
SM59016	85	86.4	HBX SM	13.95	2	88.4	0.01
SM59016	86.4	89	HBX SM	5.96	2	641	0.07

Hole_ID	Depth_From	Depth_To	Strat. Code	Sm_ppm	Sn_ppm	Sr_ppm	SrO_ppm
SM59016	89	90.8	HBX SM	4.78	2	538	0.06
SM59016	90.8	95	HBX SM	0.58	1	98.3	0.01
SM59016	95	99	HBX SM	0.65	1	34	0.005
SM59016	99	103	HBX SM	0.95	2	29.4	0.005
SM59016	103	107	HBX SM	1.02	2	18	0.005
SM59016	107	111	RAT SM	4.24	3	40.6	0.005
SM59016	111	115	RAT SM	10.2	5	40.6	0.005
SM59016	115	119	RAT SM	6.43	10	30.4	0.005
SM59016	119	123	RAT SM	5.86	7	30.2	0.005
SM59016	123	127	RAT SM	9.37	4	38.6	0.005
SM59016	127	131	RAT SM	10.25	5	34.4	0.005
SM59016	131	135	RAT SM	8.39	4	38	0.005
SM59016	135	139	RAT SM	8.81	4	34.9	0.005
SM59016	139	143	RAT SM	8.75	6	41.1	0.005
SM59016	143	144	RAT SM	4.1	5	34.3	0.005
SM59016	144	145	RAT SM	5.22	5	36.6	0.005
SM59016	145	146	RAT SM	3.73	4	34	0.005
SM59016	146	147.3	RAT SM	8.69	2	65.7	0.005

Hole_ID	Depth_From	Depth_To	Strat. Code	Ta_ppm	Tb_ppm	Te_ppm	Th_ppm
KHLSS274	70	71	DIP KHL	1.1	2.09	0.005	5.4
KHLSS274	71	72	DIP KHL	0.8	0.14	0.01	6.99
KHLSS274	72	73	DIP KHL	0.7	0.2	0.01	6.41
KHLSS274	73	74	DIP KHL	0.9	0.12	0.01	10.3
KHLSS274	74	75	DIP KHL	0.9	0.11	0.02	11.35
KHLSS274	75	76	DIP KHL	0.8	0.24	0.02	9.09
KHLSS274	76	77	DIP KHL	1	0.19	0.005	11.2
KHLSS274	77	78	DIP KHL	0.9	0.4	0.02	12.35
KHLSS274	78	79	DIP KHL	1	1.06	0.01	15
KHLSS274	79	80	DIP KHL	0.9	0.6	0.01	13.05
KHLSS274	80	81	DIP KHL	0.9	0.42	0.02	11.4
KHLSS274	81	82	DIP KHL	1.1	0.49	0.01	14.6
KHLSS274	82	83	DIP KHL	0.9	0.43	0.02	11.35
KHLSS274	83	84	DIP KHL	0.9	0.36	0.005	11.15
KHLSS274	84	85	DIP KHL	0.9	0.62	0.01	13.75
KHLSS274	85	86	DIP KHL	0.9	0.52	0.005	14.95
KHLSS274	86	87	DIP KHL	0.9	0.36	0.005	14.1
KHLSS274	87	88	DIP KHL	1.1	0.61	0.01	17.5
KHLSS274	88	89	DIP KHL	1	0.41	0.005	16.8
KHLSS274	89	90	DIP KHL	1	0.61	0.01	16
KHLSS274	90	91	DIP KHL	1	0.4	0.005	15
KHLSS274	91	92	DIP KHL	1.1	0.33	0.005	14.4
KHLSS274	92	93	DIP KHL	1.1	0.41	0.01	16.4
KHLSS274	93	94	DIP KHL	1.1	0.35	0.005	15.45
KHLSS274	94	95	DIP KHL	1.1	0.62	0.01	15.05
KHLSS274	95	96	DIP KHL	1	0.73	0.01	13.95
KHLSS274	96	97	DIP KHL	1	0.9	0.005	14.35
KHLSS274	97	98	DIP KHL	0.9	1.06	0.005	13.4
KHLSS274	98	99	DIP KHL	0.9	0.51	0.01	13.85

Hole_ID	Depth_From	Depth_To	Strat. Code	Ta_ppm	Tb_ppm	Te_ppm	Th_ppm
KHLSS274	99	100	DIP KHL	0.9	0.52	0.005	12.6
KHLSS274	100	101	DIP KHL	0.8	0.42	0.02	12.45
KHLSS274	101	102	DIP KHL	0.9	0.54	0.005	12.2
KHLSS274	102	103	DIP KHL	0.8	0.63	0.01	12.15
KHLSS274	103	104	DIP KHL	1.2	0.6	0.01	12.15
KHLSS274	104	105	DIP KHL	1	0.8	0.005	11.25
KHLSS274	105	106	DIP KHL	0.7	0.63	0.005	11.15
KHLSS274	106	107	DIP KHL	0.8	1	0.01	12.95
KHLSS274	107	108	DIP KHL	0.7	0.6	0.005	10.6
KHLSS274	108	109	DIP KHL	0.8	1.31	0.005	12.45
KHLSS274	109	110	DIP KHL	0.8	1.24	0.005	11.3
KHLSS274	110	111	DIP KHL	0.9	1.03	0.01	12.2
KHLSS274	111	112	DIP KHL	0.9	0.87	0.01	13.5
KHLSS274	112	113	DIP KHL	1	0.91	0.01	12.85
KHLSS274	113	114	DIP KHL	1.2	1.44	0.005	13.85
KHLSS274	114	115	DIP KHL	1.4	1.09	0.005	13.25
KHLSS274	115	116	DIP KHL	1.1	1.57	0.01	9.49
KHLSS274	116	117	DIP KHL	1.1	0.95	0.005	12
KHLSS274	117	118	DIP KHL	1	0.78	0.01	12.7
KHLSS274	118	119	DIP KHL	1.1	0.5	0.005	12.35
KHLSS274	119	120	DIP KHL	1	0.45	0.005	13.2
KHLSS274	120	121	DIP KHL	1	0.46	0.005	12.35
KHLSS274	121	122	DIP KHL	2	0.5	0.005	15.55
KHLSS274	122	123	DIP KHL	2.1	0.6	0.01	20
KHLSS274	123	124	DIP KHL	1.4	0.44	0.01	13.7
KHLSS274	124	125	DIP KHL	1	0.45	0.01	13.85
KHLSS274	125	126	HBX KHL	0.9	1.33	0.01	11.45
KHLSS274	126	127	HBX KHL	1.2	0.82	0.02	12.7
KHLSS274	127	128	HBX KHL	1.6	1.25	0.02	19.35
KHLSS274	128	129	HBX KHL	1.4	0.86	0.01	13.9
KHLSS274	129	130	HBX KHL	1.7	0.89	0.01	17.9
KHLSS274	130	131	HBX KHL	1.8	1.11	0.02	18.8
KHLSS274	131	132	HBX KHL	1.3	0.95	0.05	17.1
KHLSS274	132	133	HBX KHL	1.1	0.92	0.02	15.15
KHLSS274	133	134	RAT KHL	1.7	0.98	0.01	14.1
KHLSS274	134	135	RAT KHL	1.9	1.04	0.02	16
KHLSS274	135	136	RAT KHL	1.9	1.06	0.03	16.7
KHLSS274	136	137	RAT KHL	1.8	1.1	0.05	16.4
KHLSS274	137	138	RAT KHL	2	1.13	0.04	17.55
KHLSS274	138	139	RAT KHL	1.9	1.09	0.03	17.3
KHLSS274	139	140	RAT KHL	1.8	1.02	0.04	15.45
KHLSS274	140	141	RAT KHL	2	1.04	0.02	16.8
KHLSS274	141	142	RAT KHL	1.8	0.99	0.01	15.9
KHLSS274	142	143	RAT KHL	2.5	1.24	0.005	15.55
KHLSS274	143	144	RAT KHL	2.1	1.01	0.01	14.4
KHLSS274	144	145	RAT KHL	1.6	0.98	0.02	13.6
KHLSS274	145	146	RAT KHL	1.7	0.97	0.01	12.65
KHLSS274	146	147	RAT KHL	1.9	1	0.01	13.75
KHLSS274	147	148	RAT KHL	3.1	1.6	0.01	15.2

Hole_ID	Depth_From	Depth_To	Strat. Code	Ta_ppm	Tb_ppm	Te_ppm	Th_ppm
KHLSS274	148	149	RAT KHL	2.5	1.27	0.01	13.9
KHLSS274	149	150	RAT KHL	1.9	1.08	0.01	13.15
KHLSS274	150	151	RAT KHL	2.6	1.28	0.005	15.15
KHLSS274	151	152	RAT KHL	1.7	1.09	0.005	13.75
KHLSS274	152	153	RAT KHL	1.9	0.99	0.01	14.3
KHLSS274	153	154	RAT KHL	2	0.93	0.01	13.6
KHLSS274	154	155	RAT KHL	2.3	1.03	0.01	15.65
KHLSS274	155	156	RAT KHL	2.5	1.24	0.02	15.85
KHLSS274	156	157	RAT KHL	1.8	1.01	0.02	13.05
KHLSS274	157	158	RAT KHL	1.7	0.83	0.03	11.2
KHLSS274	158	159	RAT KHL	1.7	0.85	0.07	11.05
KHLSS274	159	160	RAT KHL	1.6	0.83	0.1	10.6
KHLSS274	160	161	RAT KHL	1.6	0.7	0.03	9.76
KTCSS315	351	352	RAT KNS	1.3	1.06	0.03	11
KTCSS315	352	353	RAT KNS	1.3	0.83	0.15	12.4
KTCSS315	353	354	RAT KNS	1.2	0.73	0.44	12.3
KTCSS315	354	355	RAT KNS	2.1	1.24	0.28	18.85
KTCSS315	355	355.8	RAT KNS	2.4	1.2	0.06	16
KTCSS326	264	265	RAT KNS	2.1	1.04	0.01	12.75
KTCSS326	265	265.9	RAT KNS	2.3	1.13	0.01	15.35
KTCSS326	266.5	267.5	RAT KNS	2.5	1.24	0.005	11.25
KTCSS326	267.5	268.3	RAT KNS	2.2	1.14	0.005	12.55
KTCSS326	268.3	270	RAT KNS	1.8	1.08	0.005	15.1
KTCSS326	270	271	RAT KNS	2	1.09	0.005	15.1
KTCSS326	271	272	RAT KNS	1.8	1.04	0.005	16.75
KTCSS326	272	273	RAT KNS	2	0.89	0.005	12.55
KTCSS326	273	274	RAT KNS	2.7	1.46	0.005	16.4
KTCSS326	279	280	RAT KNS	1.7	1.07	0.005	11.8
KTCSS326	280	281	RAT KNS	2	1.18	0.005	16.4
KTCSS326	286	287	HBX KNS	1.1	4.95	0.01	14.6
KTCSS326	287	288	DIP KNS	0.9	1.37	0.005	12.75
KTCSS326	294	295	DIP KNS	0.7	2.17	0.005	10.5
KTCSS326	295	296	DIP KNS	0.8	3.03	0.005	12.7
SM59016	20.4	24	DIP SM	1.6	0.99	0.03	14
SM59016	24	27.9	DIP SM	0.6	0.61	0.01	6.32
SM59016	30.9	34	DIP SM	0.05	0.04	0.005	0.48
SM59016	34	38	DIP SM	0.05	0.03	0.005	0.4
SM59016	38	42	DIP SM	0.05	0.01	0.005	0.21
SM59016	42	43.4	DIP SM	0.05	0.02	0.01	0.23
SM59016	44.4	46	DIP SM	0.05	0.01	0.005	0.18
SM59016	46	47.4	DIP SM	0.05	0.02	0.005	0.36
SM59016	52.4	54	DIP SM	0.05	0.02	0.005	0.36
SM59016	54	55	DIP SM	0.05	0.02	0.005	0.14
SM59016	55	56	DIP SM	0.05	0.01	0.005	0.14
SM59016	56	60	HBX SM	0.05	0.04	0.005	0.76
SM59016	60	64	HBX SM	0.8	0.56	0.01	9.44
SM59016	64	67.6	HBX SM	0.9	0.44	0.02	10.95
SM59016	67.6	71	HBX SM	0.7	0.65	0.02	11.4
SM59016	71	75	HBX SM	0.6	0.51	0.02	12.45

Hole_ID	Depth_From	Depth_To	Strat. Code	Ta_ppm	Tb_ppm	Te_ppm	Th_ppm
SM59016	75	77.4	HBX SM	0.6	0.5	0.03	16.05
SM59016	77.4	81	HBX SM	0.7	0.51	0.03	10.4
SM59016	81	85	HBX SM	0.9	0.38	0.01	9.62
SM59016	85	86.4	HBX SM	1.2	1.62	0.02	5.14
SM59016	86.4	89	HBX SM	1	0.74	0.01	9.42
SM59016	89	90.8	HBX SM	1	1.03	0.01	10.4
SM59016	90.8	95	HBX SM	1	0.19	0.005	10.25
SM59016	95	99	HBX SM	1.1	0.19	0.005	4.86
SM59016	99	103	HBX SM	0.9	0.2	0.005	5.95
SM59016	103	107	HBX SM	0.9	1.01	0.01	10.1
SM59016	107	111	RAT SM	1.4	0.95	0.005	13.25
SM59016	111	115	RAT SM	1.8	1.16	0.005	17.35
SM59016	115	119	RAT SM	1.7	0.92	0.005	17.8
SM59016	119	123	RAT SM	2	1.06	0.005	16.3
SM59016	123	127	RAT SM	2.4	1.38	0.005	17.7
SM59016	127	131	RAT SM	3.8	2.35	0.005	20.3
SM59016	131	135	RAT SM	2.3	1.48	0.01	16.15
SM59016	135	139	RAT SM	1.9	1.15	0.01	16.4
SM59016	139	143	RAT SM	2.2	1.25	0.02	18.05
SM59016	143	144	RAT SM	1.9	0.87	0.01	15.25
SM59016	144	145	RAT SM	1.9	0.92	0.07	15.3
SM59016	145	146	RAT SM	1.8	0.85	0.04	13
SM59016	146	147.3	RAT SM	1.3	0.92	0.03	16.15

Hole_ID	Depth_From	Depth_To	Strat. Code	TiO2_%	Tl_ppm	Tm_ppm	Majors Total %
KHLSS274	70	71	DIP KHL	1.54	0.03	0.41	101.2
KHLSS274	71	72	DIP KHL	0.46	0.01	0.11	99.57
KHLSS274	72	73	DIP KHL	0.4	0.01	0.14	98.28
KHLSS274	73	74	DIP KHL	0.51	0.01	0.07	99.34
KHLSS274	74	75	DIP KHL	0.45	0.01	0.12	99.55
KHLSS274	75	76	DIP KHL	0.4	0.02	0.14	98.02
KHLSS274	76	77	DIP KHL	0.48	0.01	0.17	99.09
KHLSS274	77	78	DIP KHL	0.47	0.01	0.22	98.48
KHLSS274	78	79	DIP KHL	0.53	0.01	0.38	99.43
KHLSS274	79	80	DIP KHL	0.5	0.01	0.26	99.73
KHLSS274	80	81	DIP KHL	0.49	0.01	0.17	100.16
KHLSS274	81	82	DIP KHL	0.56	0.01	0.19	99.71
KHLSS274	82	83	DIP KHL	0.5	0.01	0.15	99.25
KHLSS274	83	84	DIP KHL	0.52	0.01	0.17	99.08
KHLSS274	84	85	DIP KHL	0.55	0.01	0.33	99.73
KHLSS274	85	86	DIP KHL	0.55	0.01	0.29	99.46
KHLSS274	86	87	DIP KHL	0.55	0.01	0.21	99.61
KHLSS274	87	88	DIP KHL	0.6	0.01	0.21	101.2
KHLSS274	88	89	DIP KHL	0.62	0.01	0.19	100.22
KHLSS274	89	90	DIP KHL	0.61	0.01	0.34	100.45
KHLSS274	90	91	DIP KHL	0.59	0.01	0.21	99.64
KHLSS274	91	92	DIP KHL	0.57	0.01	0.17	100.73
KHLSS274	92	93	DIP KHL	0.63	0.01	0.18	101.02
KHLSS274	93	94	DIP KHL	0.63	0.01	0.23	101.1

Hole_ID	Depth_From	Depth_To	Strat. Code	TiO2_%	Tl_ppm	Tm_ppm	Majors Total %
KHLSS274	94	95	DIP KHL	0.63	0.01	0.37	100.09
KHLSS274	95	96	DIP KHL	0.53	0.01	0.52	99.93
KHLSS274	96	97	DIP KHL	0.54	0.01	0.55	100.48
KHLSS274	97	98	DIP KHL	0.56	0.01	0.97	101.03
KHLSS274	98	99	DIP KHL	0.52	0.01	0.33	99.6
KHLSS274	99	100	DIP KHL	0.51	0.01	0.25	99.96
KHLSS274	100	101	DIP KHL	0.5	0.01	0.26	100.21
KHLSS274	101	102	DIP KHL	0.46	0.01	0.27	98.4
KHLSS274	102	103	DIP KHL	0.51	0.01	0.25	99.29
KHLSS274	103	104	DIP KHL	0.51	0.01	0.33	99.64
KHLSS274	104	105	DIP KHL	0.51	0.01	0.41	100.14
KHLSS274	105	106	DIP KHL	0.45	0.01	0.27	99.22
KHLSS274	106	107	DIP KHL	0.46	0.01	0.47	98.71
KHLSS274	107	108	DIP KHL	0.45	0.01	0.28	99.13
KHLSS274	108	109	DIP KHL	0.46	0.01	0.69	99.05
KHLSS274	109	110	DIP KHL	0.52	0.01	0.66	99.75
KHLSS274	110	111	DIP KHL	0.52	0.01	0.59	99.89
KHLSS274	111	112	DIP KHL	0.52	0.01	0.53	99.07
KHLSS274	112	113	DIP KHL	0.51	0.01	0.47	100.26
KHLSS274	113	114	DIP KHL	0.55	0.01	0.88	100.29
KHLSS274	114	115	DIP KHL	0.59	0.01	0.57	99.91
KHLSS274	115	116	DIP KHL	0.51	0.01	0.91	98.74
KHLSS274	116	117	DIP KHL	0.49	0.01	0.55	99.88
KHLSS274	117	118	DIP KHL	0.44	0.01	0.38	99.01
KHLSS274	118	119	DIP KHL	0.45	0.01	0.24	99.01
KHLSS274	119	120	DIP KHL	0.45	0.01	0.2	99.79
KHLSS274	120	121	DIP KHL	0.46	0.01	0.22	99.43
KHLSS274	121	122	DIP KHL	0.49	0.01	0.25	100.04
KHLSS274	122	123	DIP KHL	0.49	0.01	0.38	99.95
KHLSS274	123	124	DIP KHL	0.41	0.01	0.28	98.66
KHLSS274	124	125	DIP KHL	0.43	0.01	0.25	98.96
KHLSS274	125	126	HBX KHL	0.4	0.01	0.69	99.03
KHLSS274	126	127	HBX KHL	0.79	0.03	0.44	98.16
KHLSS274	127	128	HBX KHL	0.71	0.08	0.42	98.22
KHLSS274	128	129	HBX KHL	0.53	0.03	0.38	98.99
KHLSS274	129	130	HBX KHL	0.7	0.02	0.46	100.26
KHLSS274	130	131	HBX KHL	0.8	0.02	0.47	98.71
KHLSS274	131	132	HBX KHL	0.71	0.02	0.39	99.59
KHLSS274	132	133	HBX KHL	0.65	0.02	0.43	99.6
KHLSS274	133	134	RAT KHL	0.76	0.02	0.46	98.58
KHLSS274	134	135	RAT KHL	0.81	0.03	0.5	99.03
KHLSS274	135	136	RAT KHL	0.8	0.04	0.51	99.01
KHLSS274	136	137	RAT KHL	0.82	0.04	0.48	99.5
KHLSS274	137	138	RAT KHL	0.89	0.04	0.53	99.15
KHLSS274	138	139	RAT KHL	0.83	0.04	0.49	99.56
KHLSS274	139	140	RAT KHL	0.78	0.05	0.46	98.53
KHLSS274	140	141	RAT KHL	0.78	0.05	0.48	99.82
KHLSS274	141	142	RAT KHL	0.74	0.04	0.46	99.02
KHLSS274	142	143	RAT KHL	0.7	0.03	0.61	101.2

Hole_ID	Depth_From	Depth_To	Strat. Code	TiO2_%	Tl_ppm	Tm_ppm	Majors Total %
KHLSS274	143	144	RAT KHL	0.66	0.05	0.55	101.84
KHLSS274	144	145	RAT KHL	0.68	0.05	0.4	99.7
KHLSS274	145	146	RAT KHL	0.68	0.05	0.45	100.29
KHLSS274	146	147	RAT KHL	0.66	0.04	0.48	99.63
KHLSS274	147	148	RAT KHL	0.53	0.06	0.87	99.96
KHLSS274	148	149	RAT KHL	0.59	0.04	0.62	100.73
KHLSS274	149	150	RAT KHL	0.69	0.05	0.54	100.32
KHLSS274	150	151	RAT KHL	0.71	0.03	0.61	100.43
KHLSS274	151	152	RAT KHL	0.59	0.05	0.51	99.46
KHLSS274	152	153	RAT KHL	0.58	0.06	0.52	99.18
KHLSS274	153	154	RAT KHL	0.65	0.05	0.45	100.23
KHLSS274	154	155	RAT KHL	0.71	0.06	0.56	100.28
KHLSS274	155	156	RAT KHL	0.7	0.04	0.56	99.14
KHLSS274	156	157	RAT KHL	0.69	0.06	0.54	99.87
KHLSS274	157	158	RAT KHL	0.64	0.07	0.45	99.69
KHLSS274	158	159	RAT KHL	0.66	0.08	0.42	100.22
KHLSS274	159	160	RAT KHL	0.6	0.11	0.43	100.05
KHLSS274	160	161	RAT KHL	0.65	0.12	0.37	99.84
KTCSS315	351	352	RAT KNS	0.6	0.38	0.39	99.5
KTCSS315	352	353	RAT KNS	0.66	0.03	0.4	98.01
KTCSS315	353	354	RAT KNS	0.67	0.02	0.37	94.92
KTCSS315	354	355	RAT KNS	0.72	0.01	0.56	99.72
KTCSS315	355	355.8	RAT KNS	0.71	0.02	0.58	98.47
KTCSS326	264	265	RAT KNS	0.76	0.01	0.56	100.39
KTCSS326	265	265.9	RAT KNS	0.72	0.01	0.58	100.08
KTCSS326	266.5	267.5	RAT KNS	0.77	0.01	0.66	98.58
KTCSS326	267.5	268.3	RAT KNS	0.7	0.01	0.56	98.87
KTCSS326	268.3	270	RAT KNS	0.66	0.01	0.49	98.75
KTCSS326	270	271	RAT KNS	0.62	0.01	0.5	98.98
KTCSS326	271	272	RAT KNS	0.7	0.01	0.5	99
KTCSS326	272	273	RAT KNS	0.63	0.01	0.52	99.44
KTCSS326	273	274	RAT KNS	0.77	0.01	0.67	98.43
KTCSS326	279	280	RAT KNS	0.69	0.01	0.53	100.07
KTCSS326	280	281	RAT KNS	0.67	0.01	0.59	100.35
KTCSS326	286	287	HBX KNS	0.54	0.01	3.25	99.88
KTCSS326	287	288	DIP KNS	0.5	0.01	0.79	100.36
KTCSS326	294	295	DIP KNS	0.42	0.01	1.1	99.95
KTCSS326	295	296	DIP KNS	0.4	0.01	1.54	99.85
SM59016	20.4	24	DIP SM	0.94	0.06	0.55	99.17
SM59016	24	27.9	DIP SM	0.42	0.11	0.29	99.42
SM59016	30.9	34	DIP SM	0.03	0.05	0.01	99.26
SM59016	34	38	DIP SM	0.02	0.04	0.01	99.14
SM59016	38	42	DIP SM	0.01	0.03	0.005	99.03
SM59016	42	43.4	DIP SM	0.01	0.04	0.01	99.54
SM59016	44.4	46	DIP SM	0.01	0.02	0.005	98.58
SM59016	46	47.4	DIP SM	0.01	0.02	0.01	98.98
SM59016	52.4	54	DIP SM	0.02	0.03	0.01	98.43
SM59016	54	55	DIP SM	0.01	0.01	0.01	98.89
SM59016	55	56	DIP SM	0.01	0.01	0.005	99.03

Hole_ID	Depth_From	Depth_To	Strat. Code	TiO2_%	Tl_ppm	Tm_ppm	Majors Total %
SM59016	56	60	HBX SM	0.04	0.01	0.01	99.31
SM59016	60	64	HBX SM	0.44	0.02	0.29	98.71
SM59016	64	67.6	HBX SM	0.45	0.01	0.27	98.67
SM59016	67.6	71	HBX SM	0.42	0.01	0.48	98.12
SM59016	71	75	HBX SM	0.35	0.01	0.4	100.88
SM59016	75	77.4	HBX SM	0.3	0.01	0.34	100.15
SM59016	77.4	81	HBX SM	0.39	0.01	0.3	101.29
SM59016	81	85	HBX SM	0.57	0.01	0.23	100.29
SM59016	85	86.4	HBX SM	2.44	0.01	0.48	100.59
SM59016	86.4	89	HBX SM	0.89	0.01	0.31	100.38
SM59016	89	90.8	HBX SM	0.52	0.01	0.49	99.82
SM59016	90.8	95	HBX SM	0.49	0.01	0.19	100.66
SM59016	95	99	HBX SM	1.58	0.02	0.22	99.74
SM59016	99	103	HBX SM	1.12	0.02	0.19	98.83
SM59016	103	107	HBX SM	0.51	0.01	1.21	99.36
SM59016	107	111	RAT SM	0.67	0.01	0.74	100.42
SM59016	111	115	RAT SM	0.79	0.02	0.48	100.71
SM59016	115	119	RAT SM	0.76	0.03	0.42	99.85
SM59016	119	123	RAT SM	0.67	0.02	0.53	98.83
SM59016	123	127	RAT SM	0.65	0.02	0.67	100.55
SM59016	127	131	RAT SM	0.68	0.02	0.95	100.42
SM59016	131	135	RAT SM	0.7	0.01	0.6	100.28
SM59016	135	139	RAT SM	0.68	0.02	0.52	99.06
SM59016	139	143	RAT SM	0.69	0.03	0.57	99.13
SM59016	143	144	RAT SM	0.76	0.04	0.48	100.5
SM59016	144	145	RAT SM	0.74	0.04	0.52	100.21
SM59016	145	146	RAT SM	0.72	0.04	0.48	99.58
SM59016	146	147.3	RAT SM	0.57	0.07	0.33	99.32

Hole_ID	Depth_From	Depth_To	Strat. Code	U_ppm	V_ppm	W_ppm	Y_ppm
KHLSS274	70	71	DIP KHL	10.1	207	1	42.9
KHLSS274	71	72	DIP KHL	11.3	102	1	7.5
KHLSS274	72	73	DIP KHL	16.85	95	1	9
KHLSS274	73	74	DIP KHL	7.17	71	2	7
KHLSS274	74	75	DIP KHL	11.75	94	2	8.9
KHLSS274	75	76	DIP KHL	7.93	83	2	13.1
KHLSS274	76	77	DIP KHL	12.25	103	4	13.2
KHLSS274	77	78	DIP KHL	15.95	66	2	16.9
KHLSS274	78	79	DIP KHL	3.38	46	2	31.9
KHLSS274	79	80	DIP KHL	2.12	47	2	18
KHLSS274	80	81	DIP KHL	2.27	43	2	10.8
KHLSS274	81	82	DIP KHL	1.92	43	2	11.7
KHLSS274	82	83	DIP KHL	2.22	40	2	9.7
KHLSS274	83	84	DIP KHL	1.47	37	2	10.2
KHLSS274	84	85	DIP KHL	1.58	41	2	24.3
KHLSS274	85	86	DIP KHL	1.37	45	2	17.4
KHLSS274	86	87	DIP KHL	1.33	37	2	12.2
KHLSS274	87	88	DIP KHL	1.24	37	2	11.7
KHLSS274	88	89	DIP KHL	1.09	44	2	10.3

Hole_ID	Depth_From	Depth_To	Strat. Code	U_ppm	V_ppm	W_ppm	Y_ppm
KHLSS274	89	90	DIP KHL	1.22	45	2	23.1
KHLSS274	90	91	DIP KHL	1.19	41	6	11.2
KHLSS274	91	92	DIP KHL	1.12	36	2	10.4
KHLSS274	92	93	DIP KHL	1.13	42	2	11.8
KHLSS274	93	94	DIP KHL	1.24	51	2	12.7
KHLSS274	94	95	DIP KHL	1.22	47	2	21.2
KHLSS274	95	96	DIP KHL	1.21	48	2	34.4
KHLSS274	96	97	DIP KHL	1.31	48	2	38.2
KHLSS274	97	98	DIP KHL	1.16	46	2	68
KHLSS274	98	99	DIP KHL	1.27	57	2	22.3
KHLSS274	99	100	DIP KHL	1.23	24	2	17.1
KHLSS274	100	101	DIP KHL	1.38	20	2	15.4
KHLSS274	101	102	DIP KHL	1.73	15	2	18.2
KHLSS274	102	103	DIP KHL	1.39	20	2	15.7
KHLSS274	103	104	DIP KHL	1.29	24	2	16.6
KHLSS274	104	105	DIP KHL	1.17	28	2	28.3
KHLSS274	105	106	DIP KHL	1.09	29	2	18.5
KHLSS274	106	107	DIP KHL	1.09	74	2	37
KHLSS274	107	108	DIP KHL	1.15	32	3	21.1
KHLSS274	108	109	DIP KHL	1.21	37	2	52.1
KHLSS274	109	110	DIP KHL	1.13	47	2	51.5
KHLSS274	110	111	DIP KHL	1.16	54	2	44.2
KHLSS274	111	112	DIP KHL	1.1	51	2	35.8
KHLSS274	112	113	DIP KHL	1.01	51	2	38.4
KHLSS274	113	114	DIP KHL	1.15	56	3	65.1
KHLSS274	114	115	DIP KHL	1.09	56	2	42.3
KHLSS274	115	116	DIP KHL	1.17	71	2	66.6
KHLSS274	116	117	DIP KHL	1.16	46	2	37.5
KHLSS274	117	118	DIP KHL	0.94	33	2	22.5
KHLSS274	118	119	DIP KHL	1.13	30	2	14.6
KHLSS274	119	120	DIP KHL	1.02	28	2	11.6
KHLSS274	120	121	DIP KHL	1	27	2	12.5
KHLSS274	121	122	DIP KHL	1.15	29	2	14.7
KHLSS274	122	123	DIP KHL	1.09	31	2	19.7
KHLSS274	123	124	DIP KHL	1.01	24	2	14.6
KHLSS274	124	125	DIP KHL	1.03	37	2	15.7
KHLSS274	125	126	HBX KHL	0.89	50	2	51
KHLSS274	126	127	HBX KHL	4.32	106	2	27
KHLSS274	127	128	HBX KHL	7.96	83	2	33.9
KHLSS274	128	129	HBX KHL	2.87	72	2	26.5
KHLSS274	129	130	HBX KHL	3.17	90	2	26.5
KHLSS274	130	131	HBX KHL	3.6	104	2	28.4
KHLSS274	131	132	HBX KHL	3.37	94	2	25.9
KHLSS274	132	133	HBX KHL	2.82	87	2	26.8
KHLSS274	133	134	RAT KHL	4.52	96	2	30
KHLSS274	134	135	RAT KHL	4.72	102	2	31.3
KHLSS274	135	136	RAT KHL	4.5	100	2	32.1
KHLSS274	136	137	RAT KHL	3.95	93	2	30.4
KHLSS274	137	138	RAT KHL	4.24	104	2	31.3

Hole_ID	Depth_From	Depth_To	Strat. Code	U_ppm	V_ppm	W_ppm	Y_ppm
KHLSS274	138	139	RAT KHL	4.04	99	2	31.8
KHLSS274	139	140	RAT KHL	3.9	99	3	29.1
KHLSS274	140	141	RAT KHL	4	104	3	30.9
KHLSS274	141	142	RAT KHL	4.03	97	2	28.8
KHLSS274	142	143	RAT KHL	5.48	94	2	39.6
KHLSS274	143	144	RAT KHL	4.56	91	4	34.4
KHLSS274	144	145	RAT KHL	3.87	93	2	29.1
KHLSS274	145	146	RAT KHL	3.56	87	2	29.8
KHLSS274	146	147	RAT KHL	3.86	86	2	29.7
KHLSS274	147	148	RAT KHL	6.78	76	2	52.3
KHLSS274	148	149	RAT KHL	5.23	78	2	42.4
KHLSS274	149	150	RAT KHL	4.37	82	2	32.7
KHLSS274	150	151	RAT KHL	5.75	94	3	40.8
KHLSS274	151	152	RAT KHL	5.63	87	2	30.6
KHLSS274	152	153	RAT KHL	6.22	85	2	31.6
KHLSS274	153	154	RAT KHL	5.19	89	2	31.3
KHLSS274	154	155	RAT KHL	6.03	83	2	34.6
KHLSS274	155	156	RAT KHL	6.06	89	2	38.6
KHLSS274	156	157	RAT KHL	4.84	86	2	32.2
KHLSS274	157	158	RAT KHL	4.81	81	2	27.4
KHLSS274	158	159	RAT KHL	6.78	109	2	28.1
KHLSS274	159	160	RAT KHL	8.43	118	2	26.9
KHLSS274	160	161	RAT KHL	7.67	90	2	24.6
KTCSS315	351	352	RAT KNS	19.55	92	2	24.2
KTCSS315	352	353	RAT KNS	10.05	121	2	24.3
KTCSS315	353	354	RAT KNS	6.67	151	3	21.6
KTCSS315	354	355	RAT KNS	7.55	173	2	34
KTCSS315	355	355.8	RAT KNS	4.65	83	3	35.7
KTCSS326	264	265	RAT KNS	5.85	129	3	32.7
KTCSS326	265	265.9	RAT KNS	3.76	96	2	35.5
KTCSS326	266.5	267.5	RAT KNS	2.79	60	3	39.1
KTCSS326	267.5	268.3	RAT KNS	2.06	61	2	36
KTCSS326	268.3	270	RAT KNS	1.81	59	6	31.7
KTCSS326	270	271	RAT KNS	2.07	56	3	32.5
KTCSS326	271	272	RAT KNS	1.9	71	3	32.2
KTCSS326	272	273	RAT KNS	1.94	69	2	28.5
KTCSS326	273	274	RAT KNS	2.08	73	4	43.7
KTCSS326	279	280	RAT KNS	2.7	93	2	33.5
KTCSS326	280	281	RAT KNS	3.16	89	2	36.8
KTCSS326	286	287	HBX KNS	1.29	85	2	211
KTCSS326	287	288	DIP KNS	0.76	65	2	52.9
KTCSS326	294	295	DIP KNS	1.32	60	2	78.8
KTCSS326	295	296	DIP KNS	1.05	58	2	108
SM59016	20.4	24	DIP SM	5.08	124	3	32
SM59016	24	27.9	DIP SM	2.6	67	6	19
SM59016	30.9	34	DIP SM	8.76	6	1	1.4
SM59016	34	38	DIP SM	28.5	7	0.5	1
SM59016	38	42	DIP SM	30.3	2.5	1	0.7
SM59016	42	43.4	DIP SM	16.75	5	1	1

Hole_ID	Depth_From	Depth_To	Strat. Code	U_ppm	V_ppm	W_ppm	Y_ppm
SM59016	44.4	46	DIP SM	17.5	2.5	1	0.6
SM59016	46	47.4	DIP SM	16.8	5	1	0.9
SM59016	52.4	54	DIP SM	6.57	2.5	1	0.8
SM59016	54	55	DIP SM	7.94	2.5	4	0.7
SM59016	55	56	DIP SM	7.46	2.5	0.5	0.7
SM59016	56	60	HBX SM	12.1	7	2	1.6
SM59016	60	64	HBX SM	3.45	57	2	18.2
SM59016	64	67.6	HBX SM	2.75	63	2	17.3
SM59016	67.6	71	HBX SM	2.31	63	2	28.5
SM59016	71	75	HBX SM	1.84	406	3	22.2
SM59016	75	77.4	HBX SM	2.99	418	4	19.7
SM59016	77.4	81	HBX SM	4.66	107	2	19.5
SM59016	81	85	HBX SM	5.32	80	3	15.5
SM59016	85	86.4	HBX SM	4.54	287	1	32.8
SM59016	86.4	89	HBX SM	5.57	102	2	20.9
SM59016	89	90.8	HBX SM	3.51	70	2	37.5
SM59016	90.8	95	HBX SM	1.48	41	4	11.3
SM59016	95	99	HBX SM	1.96	209	5	10.3
SM59016	99	103	HBX SM	1.48	153	1	9.7
SM59016	103	107	HBX SM	0.85	97	3	85.5
SM59016	107	111	RAT SM	2.69	89	2	51.5
SM59016	111	115	RAT SM	3.64	105	4	30
SM59016	115	119	RAT SM	3.57	100	3	27
SM59016	119	123	RAT SM	4.06	98	4	32.6
SM59016	123	127	RAT SM	4.43	94	2	39.7
SM59016	127	131	RAT SM	6.24	87	2	68.9
SM59016	131	135	RAT SM	4.15	87	2	37.6
SM59016	135	139	RAT SM	4.18	91	2	32.1
SM59016	139	143	RAT SM	4.38	83	2	36.4
SM59016	143	144	RAT SM	6.25	99	2	29
SM59016	144	145	RAT SM	31.8	96	2	27.8
SM59016	145	146	RAT SM	25	124	2	28.9
SM59016	146	147.3	RAT SM	15.85	85	2	20.9

Hole_ID	Depth_From	Depth_To	Strat. Code	Yb_ppm	Zn_ppm	Zr_ppm
KHLSS274	70	71	DIP KHL	2.38	22	125
KHLSS274	71	72	DIP KHL	1	18	118
KHLSS274	72	73	DIP KHL	1.06	14	118
KHLSS274	73	74	DIP KHL	0.99	14	151
KHLSS274	74	75	DIP KHL	1.07	12	116
KHLSS274	75	76	DIP KHL	0.94	11	88
KHLSS274	76	77	DIP KHL	1.29	12	112
KHLSS274	77	78	DIP KHL	1.72	6	138
KHLSS274	78	79	DIP KHL	2.45	5	127
KHLSS274	79	80	DIP KHL	1.65	5	122
KHLSS274	80	81	DIP KHL	1.32	4	132
KHLSS274	81	82	DIP KHL	1.22	5	136
KHLSS274	82	83	DIP KHL	1.24	4	122
KHLSS274	83	84	DIP KHL	1.19	4	147

Hole_ID	Depth_From	Depth_To	Strat. Code	Yb_ppm	Zn_ppm	Zr_ppm
KHLSS274	84	85	DIP KHL	2.23	4	150
KHLSS274	85	86	DIP KHL	1.67	4	145
KHLSS274	86	87	DIP KHL	1.46	4	136
KHLSS274	87	88	DIP KHL	1.59	6	156
KHLSS274	88	89	DIP KHL	1.23	5	151
KHLSS274	89	90	DIP KHL	2.38	5	148
KHLSS274	90	91	DIP KHL	1.49	5	154
KHLSS274	91	92	DIP KHL	1.45	8	145
KHLSS274	92	93	DIP KHL	1.58	4	159
KHLSS274	93	94	DIP KHL	1.73	4	161
KHLSS274	94	95	DIP KHL	2.37	6	172
KHLSS274	95	96	DIP KHL	3.02	5	135
KHLSS274	96	97	DIP KHL	3.33	5	144
KHLSS274	97	98	DIP KHL	5.74	4	146
KHLSS274	98	99	DIP KHL	2.54	5	130
KHLSS274	99	100	DIP KHL	1.94	4	127
KHLSS274	100	101	DIP KHL	1.83	4	131
KHLSS274	101	102	DIP KHL	1.91	5	124
KHLSS274	102	103	DIP KHL	1.56	4	124
KHLSS274	103	104	DIP KHL	2.48	7	163
KHLSS274	104	105	DIP KHL	2.66	5	126
KHLSS274	105	106	DIP KHL	1.86	5	113
KHLSS274	106	107	DIP KHL	2.88	5	113
KHLSS274	107	108	DIP KHL	1.88	4	122
KHLSS274	108	109	DIP KHL	4.38	6	109
KHLSS274	109	110	DIP KHL	4.25	4	130
KHLSS274	110	111	DIP KHL	3.95	5	124
KHLSS274	111	112	DIP KHL	3.4	4	127
KHLSS274	112	113	DIP KHL	3.04	4	122
KHLSS274	113	114	DIP KHL	5.11	4	140
KHLSS274	114	115	DIP KHL	3.8	4	150
KHLSS274	115	116	DIP KHL	5.12	4	129
KHLSS274	116	117	DIP KHL	3.46	4	128
KHLSS274	117	118	DIP KHL	1.88	4	120
KHLSS274	118	119	DIP KHL	1.61	4	119
KHLSS274	119	120	DIP KHL	1.61	5	112
KHLSS274	120	121	DIP KHL	1.43	4	116
KHLSS274	121	122	DIP KHL	2.18	5	136
KHLSS274	122	123	DIP KHL	2.4	7	145
KHLSS274	123	124	DIP KHL	1.71	7	118
KHLSS274	124	125	DIP KHL	1.83	9	109
KHLSS274	125	126	HBX KHL	4.09	15	100
KHLSS274	126	127	HBX KHL	2.84	127	189
KHLSS274	127	128	HBX KHL	2.85	351	853
KHLSS274	128	129	HBX KHL	2.67	901	187
KHLSS274	129	130	HBX KHL	2.84	56	197
KHLSS274	130	131	HBX KHL	2.85	69	206
KHLSS274	131	132	HBX KHL	2.51	60	185
KHLSS274	132	133	HBX KHL	2.64	45	157

Hole_ID	Depth_From	Depth_To	Strat. Code	Yb_ppm	Zn_ppm	Zr_ppm
KHLSS274	133	134	RAT KHL	2.93	35	191
KHLSS274	134	135	RAT KHL	3.16	32	205
KHLSS274	135	136	RAT KHL	3.22	29	207
KHLSS274	136	137	RAT KHL	2.92	28	202
KHLSS274	137	138	RAT KHL	3.22	30	224
KHLSS274	138	139	RAT KHL	3.05	34	200
KHLSS274	139	140	RAT KHL	3	30	198
KHLSS274	140	141	RAT KHL	3.01	26	206
KHLSS274	141	142	RAT KHL	3.01	28	182
KHLSS274	142	143	RAT KHL	3.98	30	303
KHLSS274	143	144	RAT KHL	3.57	29	245
KHLSS274	144	145	RAT KHL	2.9	28	184
KHLSS274	145	146	RAT KHL	2.96	32	199
KHLSS274	146	147	RAT KHL	3.1	29	207
KHLSS274	147	148	RAT KHL	5.37	24	426
KHLSS274	148	149	RAT KHL	4.25	28	356
KHLSS274	149	150	RAT KHL	3.3	31	249
KHLSS274	150	151	RAT KHL	4.31	33	311
KHLSS274	151	152	RAT KHL	3.18	33	222
KHLSS274	152	153	RAT KHL	3.23	21	224
KHLSS274	153	154	RAT KHL	3.19	21	235
KHLSS274	154	155	RAT KHL	3.84	26	277
KHLSS274	155	156	RAT KHL	4.26	23	331
KHLSS274	156	157	RAT KHL	3.12	20	261
KHLSS274	157	158	RAT KHL	2.99	19	222
KHLSS274	158	159	RAT KHL	2.85	20	220
KHLSS274	159	160	RAT KHL	2.96	26	190
KHLSS274	160	161	RAT KHL	2.66	24	187
KTCSS315	351	352	RAT KNS	2.42	6	208
KTCSS315	352	353	RAT KNS	2.56	8	209
KTCSS315	353	354	RAT KNS	2.33	8	205
KTCSS315	354	355	RAT KNS	3.62	7	294
KTCSS315	355	355.8	RAT KNS	3.73	5	324
KTCSS326	264	265	RAT KNS	3.43	6	292
KTCSS326	265	265.9	RAT KNS	3.55	6	303
KTCSS326	266.5	267.5	RAT KNS	3.71	5	330
KTCSS326	267.5	268.3	RAT KNS	3.58	5	270
KTCSS326	268.3	270	RAT KNS	3.39	7	223
KTCSS326	270	271	RAT KNS	3.38	7	264
KTCSS326	271	272	RAT KNS	3.25	9	256
KTCSS326	272	273	RAT KNS	3.22	9	262
KTCSS326	273	274	RAT KNS	4.22	13	358
KTCSS326	279	280	RAT KNS	3.38	6	224
KTCSS326	280	281	RAT KNS	3.85	6	260
KTCSS326	286	287	HBX KNS	19.9	14	156
KTCSS326	287	288	DIP KNS	5.15	18	129
KTCSS326	294	295	DIP KNS	6.97	7	122
KTCSS326	295	296	DIP KNS	9.11	6	111
SM59016	20.4	24	DIP SM	3.43	138	279

Hole_ID	Depth_From	Depth_To	Strat. Code	Yb_ppm	Zn_ppm	Zr_ppm
SM59016	24	27.9	DIP SM	1.85	177	136
SM59016	30.9	34	DIP SM	0.12	39	15
SM59016	34	38	DIP SM	0.06	48	24
SM59016	38	42	DIP SM	0.03	56	21
SM59016	42	43.4	DIP SM	0.11	49	37
SM59016	44.4	46	DIP SM	0.015	41	31
SM59016	46	47.4	DIP SM	0.07	44	23
SM59016	52.4	54	DIP SM	0.06	52	16
SM59016	54	55	DIP SM	0.04	46	19
SM59016	55	56	DIP SM	0.04	128	17
SM59016	56	60	HBX SM	0.17	293	24
SM59016	60	64	HBX SM	1.85	26	131
SM59016	64	67.6	HBX SM	1.8	36	125
SM59016	67.6	71	HBX SM	3.12	46	125
SM59016	71	75	HBX SM	2.58	22	102
SM59016	75	77.4	HBX SM	2.15	18	110
SM59016	77.4	81	HBX SM	1.89	19	129
SM59016	81	85	HBX SM	1.54	9	141
SM59016	85	86.4	HBX SM	3	12	167
SM59016	86.4	89	HBX SM	2.19	10	142
SM59016	89	90.8	HBX SM	3.18	18	149
SM59016	90.8	95	HBX SM	1.19	25	139
SM59016	95	99	HBX SM	1.69	11	117
SM59016	99	103	HBX SM	1.37	6	111
SM59016	103	107	HBX SM	7.05	7	118
SM59016	107	111	RAT SM	4.84	8	186
SM59016	111	115	RAT SM	3.04	12	219
SM59016	115	119	RAT SM	2.98	11	206
SM59016	119	123	RAT SM	3.52	11	240
SM59016	123	127	RAT SM	3.83	11	335
SM59016	127	131	RAT SM	6.01	11	522
SM59016	131	135	RAT SM	3.58	10	310
SM59016	135	139	RAT SM	3.41	17	261
SM59016	139	143	RAT SM	3.77	18	293
SM59016	143	144	RAT SM	3.29	22	265
SM59016	144	145	RAT SM	3.09	30	261
SM59016	145	146	RAT SM	3.27	44	254
SM59016	146	147.3	RAT SM	2.16	102	169

6. **Appendix 6: Analysis of elements versus thickness of R.A.T. and Dipeta units.**

Subgroup	SM 59016	KTC SS315	KHL SS274	KTCSS326
Dipeta	U: >25ppm Ca: >15 wt.% Al: low (<1 wt.%) Th: low (<1ppm) Cr: low but erratic Fe: low (<1 wt.%) Ga: low detection limit. Basal interval: 25m	No data	U: <detection limit Ca: erratic; 3-8 wt.% Al: 5-7wt% Th: erratic, mostly <detection limit Cr: 20-40 ppm Fe: <3 wt% Ga: <10 ppm Ti: <1.25 wt.% Basal interval: 25m	U: 2-3 ppm Ca: <7wt.% Al: 12-13wt% Th: 12-15wt% Cr: 50-60ppm Fe: <5wt% Ga: 15-25ppm Ti: >0.5wt.% Basal interval: 10m
HBX breccia				
R.A.T.	U: <5 ppm Ca: <5 wt.% Al: >5 wt.% Th: >15 ppm Cr: >50 ppm Fe: >3 wt.% Ga: >20 ppm	U:>15 ppm Ca: <5 to >7 wt.% Al: 10-13 wt.% Th: 2 or 17 ppm Cr: 50-60 ppm Fe: >5 wt.% Ga: <23 ppm	U: 0-10 ppm, erratic. Ca: <3 wt.% in FW, higher below Al: >7 wt.% Th: 20 ppm , then erratic/lower below Cr: 45-55ppm in FW, then lower. Fe: consistent ~4 wt.% Ga: 20 ppm Ti: >1.25 wt%	U: Ca: 4wt.% Al: 13-14wt% Th: 10-15ppm Cr: 70ppm Fe: 1 – 4% Ga: <25ppm Ti: >0.6ppm Basal
Nature of Breccia zone	HW: 30m; HBX: 35m; FW >30m	FW 5 m; 10m more m below	HW: 20m; HBX: 10m; FW: 5-10m	HW:10m; HBX:5m; FW: 20m’